Durham E-Theses

The nature and timing of Late Quaternary glaciation in southernmost South America

DARVILL, CHRISTOPHER

How to cite:

Use policy

The nature and timing of Late Quaternary glaciation in southernmost South America

Christopher Michael Darvill

Department of Geography
Durham University

February 2015

The nature and timing of glaciation in southernmost South America

Christopher Michael Darvill

Abstract

The timing and extent of former ice sheet fluctuations can demonstrate leads and lags during periods of climatic change and the forcing factors responsible, but this requires robust glacial chronologies. Patagonia, in southern South America, offers a well preserved record of glacial geomorphology over a large latitudinal range that is affected by key climatic systems in the Southern Hemisphere, but establishing the timing of ice advances has proven problematic.

This thesis targets five southernmost ice lobes that extended from the former Patagonian Ice Sheet during the Quaternary; from north to south: the Río Gallegos, Skyring, Otway, Magellan and Bahía Inútil – San Sebastián (BI-SSb) ice lobes. The region is chosen because there is ambiguity over the age of glacial limits, which have been hypothesised to relate to different glacial cycles over hundreds of thousands of years but yield cosmogenic nuclide exposure data dominantly < 50 ka. This contradiction is the focus of the thesis: was the sequence of glacial limits deposited over multiple glacial cycles, or during the last glacial cycle?

A new geomorphological map is used to reconstruct glacial limits and to help target new dating. Cosmogenic nuclide depth-profiles through glacial outwash are used to date glacial limits whilst accounting for post-depositional processes. These reveal that limits of the BI-SSb lobe hypothesized to date from MIS 12 (*ca*. 450 ka) and 10 (*ca*. 350 ka) were actually deposited during the last glacial cycle, with the best-dated profile giving an MIS 3 age of *ca*. 30 ka, indicating an extensive advance prior to the global Last Glacial Maximum (gLGM). A glacial reconstruction indicates that this may not have been unique to the BI-SSb lobe, and a compilation of published dates reveals that similar advances during the last glacial cycle indicate related forcing factors operating across Patagonia and New Zealand.

Resumen

La datación y extensión de antiguas capas de hielo puede demostrar avances y retrocesos durante cambios climáticos así como factores responsables de esos cambios. Sin embargo, esto requiere de robustas cronologías glaciares. Patagonia, en el pico sur de Sudamérica, ofrece una buena preservación de la historia geomorfológica glaciar durante largas extensiones latitudinales, la cual es afectada por sistemas climáticos claves en el Hemisferio Sur, aunque el establecimiento de avances en las capas de hielo es problemático.

Esta tesis tiene como objetivo estudiar cinco lenguas glaciares meridionales que se extendieron más allá de la capa de hielo que se formó en la Patagonia durante el Cuaternario. Estas son de norte a sur: El Río Gallegos, Skyring, Otway, Magellan y Bahía Inútil – San Sebastián (BI-SSb). Esta región fue escogida debido a la ambigüedad sobre la datación de los límites del glacial hasta la fecha. Hipótesis señalan que estos límites pertenecen a diferentes ciclos glaciares durante cientos de miles de años pero a los que se les ha establecido una edad dominante de <50 Ka por medio de isótopos cosmogénicos. Esta contradicción es el centro de la tesis: ¿fue la secuencia de límites glaciares depositada durante múltiples ciclos glaciares o durante el último ciclo glaciar?

Un nuevo mapa geomorfológico ha sido elaborado para reconstruir límites glaciares y ayudar a establecer una nueva datación. Perfiles de los isótopos cosmogénicos a través de depósitos glaciares han sido utilizados para datar los límites del glaciar teniendo en cuenta procesos post-deposicionales. Estos revelan que los límites de la lengua glacial BI-SSb de supuesta edad de entre MIS 12 (ca. 450 ka) y 10 (ca. 350 ka) son en realidad depósitos del último ciclo glacial, donde la edad mejor definida se sitúa en el estadio isotópico MIS 3 (30 ka). Esto indica que antes del último periodo glacial máximo global hubo un extenso avance. La reconstrucción glacial indica que esta datación no es única de la lengua glacial BI-SSb, y una compilación de dataciones publicadas revela que similares avances durante el último ciclo glacial indican factores responsables de los cambios climáticos similares a través de Patagonia y Nueva Zelanda.

Contents

List of figures

List of tables

List of abbreviations

AIM	Antarctic Isotope Maximum
BI-SSb	The Bahía Inútil – San Sebastián ice lobe
D-O	Dansgaard-Oeschger event
EBT	Erratic Boulder Train
EDC	EPICA Dome C ice core
EDML	EPICA Dronning Maud Land ice core
GLFC	Global Land Cover Facility
gLGM/LGM	(global) Last Glacial Maximum
GPG	Greatest Patagonian Glaciation
IDR	Irregular Dissected Ridges
IRD	Ice Rafted Debris
ITCZ	Inter-Tropical Convergence Zone
m.a.s.l.	metres above sea level
MIS	Marine Isotope Stage
NGRIP	North Greenland Ice Core Project
PDF	Probability Density Function
SAF	Sub-Antarctic Front
SRTM	Shuttle Radar Topography Mission
SST	Sea Surface Temperature
STF	Sub-Tropical Front

Declaration and statement of copyright

The copyright of this thesis rests with the author. No quotation from it should be published without the author's prior written consent and information derived from it should be acknowledged.

I confirm that no part of the material presented in this thesis has previously been submitted by me or any other person for a degree in this or any other university. In all cases, where is relevant, material from the work of others has been acknowledged.

Christopher Michael Darvill

Department of Geography

Durham University

Submitted February 2015

Final version May 2015

Acknowledgements

I am very grateful to my supervisors, Mike Bentley and Chris Stokes, whose guidance, patience and enthusiasm have helped me through my Ph.D., and whose insightful comments and accompaniment on fieldwork have contributed greatly to this thesis. Their equally good humour has also made the whole process great fun.

I also owe a debt of gratitude to four friends who helped me as field assistants in Patagonia: Will Christiansen, Paul Lincoln, Harold Lovell and Mark Hulbert, the latter of whom also patiently helped me through much of the last three years. Thankyou all for your hard work and good company, and for putting up with me in the field!

Many of the Durham Geography staff and postgraduate community have become good friends and provided a supportive community in which to conduct my research. There are too many people to name individually, but thanks to all those who have helped, listened or provided comic value in the office, GIS lab and coffee room.

Ángel Rodés, Delia Gheorghiu, Alan Davidson and Andy Hein all gave up a lot of their time guiding me through the cosmogenic nuclide dating process and helping me to analyse my samples. Stefan Wastegård also kindly analysed some tephra samples for me, though I am sorry that they did not make the final thesis! Juan Carlos Aravena, Jorge Rabassa and Andrea Coronato were very generous with their time and assistance in Patagonia.

Finally, to all of my great friends outside of Durham, to the Quatskis, and to my wonderful family – Mum, Dad, Louise and Nick – who have been so supportive and encouraging over the years, I thank my lucky stars you're all so brilliant.

Chapter 1. Introduction

1.1 Rationale

Southernmost South America is in a unique geographical position, heavily influenced by globally-important atmospheric and oceanic systems in the most southerly continental setting outside of Antarctica. However, despite the potential to improve our understanding of Southern Hemisphere and global climatic changes over multiple glacial cycles, the age constraints on the timing of pre-global Last Glacial Maximum (gLGM) advances of former ice-lobes in the region remain poorly constrained. An improved chronology for the southernmost ice lobes of the former Patagonian Ice Sheet could yield important insights into climate variability at southernmost latitudes as well as processes governing long-term glacial dynamics.

Just 2% of the earth's surface between 40°S and 60°S is land, mostly in southernmost South America (Zolitschka, 2009). These latitudes are dominated by the Southern Westerly Wind system (Figure 1.1), the strongest time-averaged oceanic winds in the world (Hodgson & Sime, 2010), which otherwise pass unhindered around the Southern Hemisphere. Southern South America is also fully exposed to changes in the Antarctic Circumpolar Current, a key component in the global oceanic circulation system. Both of these systems are thought to have a major influence on global climate: the Antarctic Circumpolar Current on the production of global deep-water (Corliss, 1983; Carter *et al.*, 2008); and the Southern Westerly Winds on Southern Hemisphere precipitation, dust-fluxes and ocean-circulation (Kohfeld *et al.*, 2013; Sime *et al.*, 2013). Moreover, both are intrinsically linked by Antarctic (sea) ice extent and the positions of the oceanic frontal systems. Consequently, they are likely linked in their responses to climatic change (Boning *et al.*, 2008; Wang *et al.*, 2011).

Terrestrial records at these latitudes can act as monitors of the strength of the Antarctic Circumpolar Current and latitudinal fluctuations of the Southern Westerly Winds and, by extension, changes within the Antarctic subcontinent and wider Southern Hemisphere (Sugden *et al.*, 2005; Kaplan *et al.*, 2008a). The location of southernmost South America, adjacent to the southern parts of the Atlantic and Pacific Oceans, means that the region may yield important insights into the contentious issue of inter-hemispheric climatic/glacial (a)synchrony (Broecker, 2003; Barker *et al.*, 2009). Importantly, Patagonia is situated at the southernmost reaches of the former thermal bi-polar seesaw that may have operated in the Atlantic Ocean during periods of past climatic change.
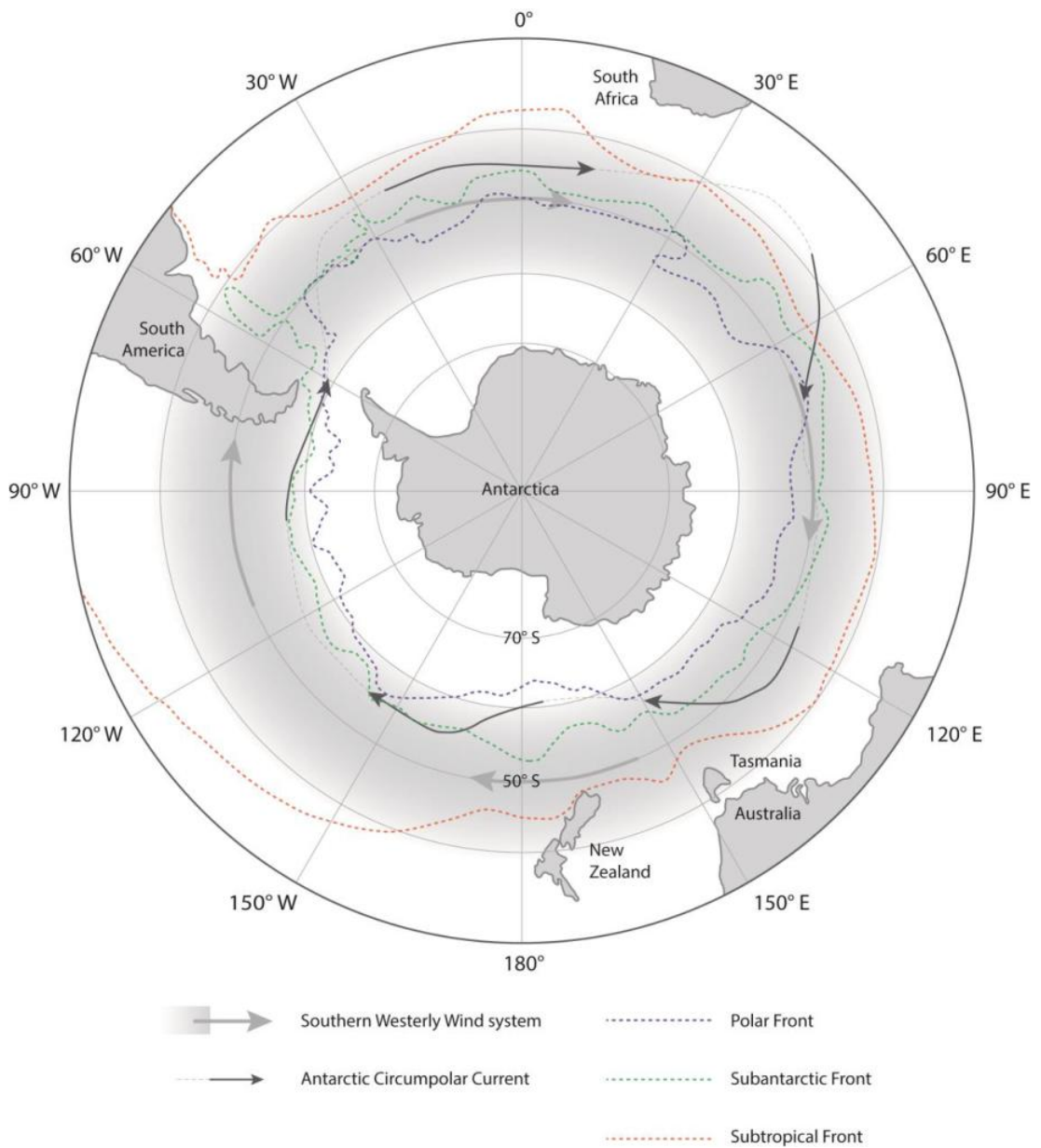
Figure 1.1. Map of the southernmost Southern Hemisphere showing the Southern Westerly Wind System and Antarctic Circumpolar Current as well as oceanic frontal zones. Compiled from Carter (2009) and McGlone *et al.* (2010).

There is a rich terrestrial record in Patagonia, with Clapperton (1993) stating that:

'…the combination of arid climate, successively less ice extent in each glaciation, and the large scale of the deposits, has preserved what is probably the most complete and intact sequence of Quaternary moraines anywhere in the world.' (p. 352)

However, there remains ambiguity regarding the timing of ice advances from what was once the southernmost part of the Patagonian Ice Sheet. In particular, the timing and nature of pre-gLGM glacial advances is poorly understood. Without a comprehensive chronology of ice advances, it is difficult to appreciate how the different components of the land-ocean-atmosphere system fully interact during periods of climatic change (Lamy *et al.*, 2007; Kaiser & Lamy, 2010). Significantly, if we are unsure of when glacial stages occurred in southernmost South America (e.g. at 30 ka or 1.1 Ma?), we cannot hope to properly calibrate regional and global models of climate, an essential step in effectively predicting future climate change. This problem is becoming more acute as longer ice core records are retrieved from Antarctica, spanning multiple glacial cycles (EPICA, 2004; 2006; 2010), that cannot be compared to terrestrial changes in Patagonia because of a lack of firm chronological control. This thesis focuses on constraining the timing of advances of five large ice lobes in the southernmost part of the former Patagonian Ice Sheet, from north to south: the Río Gallegos, Skyring, Otway, Magellan, and Bahía Inútil – San Sebastián (BI-SSb) lobes.

1.2 Aims

1. To reconstruct glacial changes of the southernmost ice lobes of the Patagonian Ice Sheet, with a particular emphasis on glacial chronology, to determine whether ice advances occurred over timescales of 10^4, 10^5 or 10^6 years.

2. To use this new chronological framework to examine the controls on glacial change in southernmost South America.

1.3   Research objectives

To address these aims, this work will be conducted through completion of five specific objectives:

1. Map the glacial geomorphology of southernmost South America from remote imagery and field-checking.
2. Examine the nature and weathering of erratic boulders that have yielded ambiguous cosmogenic nuclide dates on Tierra del Fuego.
3. Test the reliability of moraine boulder ages using a cosmogenic outwash depth-profiling approach.
4. Derive a glacial history for the region and assess the likely timing of glacial advances using previously published chronological information and new outwash depth-profile results.
5. Examine the trends in southern mid-latitude glaciation in order to explore ice sheet response to local, regional and hemispheric forcing.

1.4   Thesis structure and results

Chapter 2 outlines previous work on the southernmost ice lobes of South America. Following this, Chapters 3-7 of this thesis are composed of a series of research papers that have been published, submitted, or prepared for peer-reviewed journals. An introduction to each chapter is given below. The papers have been edited for consistency within the thesis: introductory material has been reduced where necessary to avoid excessive repetition and supplementary information has been incorporated into the chapters where applicable. Because the methods used are specific to each chapter, they are included throughout the thesis rather than as a separate section. Chapters 3-6 present the analytical results and accompanying discussion of research conducted for this thesis to address Objectives 1-4 above. Chapter 7 incorporates this new research into a wider review and synthesis, discussing the likely climatic forcing mechanisms of southern mid-latitude glaciation and addresses Objective 5. Finally, Chapter 8 draws together the main conclusions of the thesis and explains how these address the aims outlined at the start.

1.4.1 Chapter 3

Darvill, C.M., Stokes, C.R., Bentley, M.J. & Lovell, H. (2014) A glacial geomorphological map of the southernmost ice lobes of Patagonia: the Bahía Inútil - San Sebastián, Magellan, Otway, Skyring and Río Gallegos lobes. *Journal of Maps*, 10, 500-520.

This paper outlines the methods and results of geomorphological mapping for the five southernmost ice lobes of the former Patagonian Ice Sheet. The centrepiece of the paper is a map that forms the basis for detailed analysis in subsequent chapters: contextualising the erratic boulder trains in Chapter 4; allowing targeted sampling of glacial limits in Chapters 5; and supporting the glacial reconstruction in Chapter 6. The map shows that meltwater landforms feature heavily in the region and reveals that limits associated with the Otway, Skyring and Río Gallegos lobes are marked by numerous clear moraine ridges, whereas the BI-SSb and Magellan lobes are marked by hummocky terrain and drift limits. The map also highlights cross-cutting landform relationships, suggesting multiple ice advances in those locations.

In this paper, I undertook the mapping, wrote the manuscript and drew the figures. The map extended earlier work by Lovell for the Skyring and Otway area. All authors assisted with fieldwork, contributed ideas and edited the text. The paper has been published in *Journal of Maps* and the introduction has been edited for consistency.

1.4.2 Chapter 4

Darvill, C.M., Bentley, M.J. & Stokes, C.R. (2015) Geomorphology and weathering characteristics of erratic boulder trains on Tierra del Fuego, southernmost South America: implications for dating of glacial deposits. *Geomorphology*, 228, 382-397.

The interpretation of cosmogenic nuclide exposure dates from boulders associated with erratic boulder trains on Tierra del Fuego is a critical component in the argument for the age of glacial limits in the region. Previously reported ages have consisted of lots of younger ages (< 50 ka) with occasional older ages (> 50 ka), with the latter interpreted as closer to the true age, and the former attributed to erosion and exhumation. This paper conducts the first comprehensive study of these boulder trains, analysing their distribution, likely formation, and weathering characteristics to help contextualise the dating. The boulder trains are consistent with one or more supraglacial rock avalanches and weathering indices show little difference between them, suggesting that they could be much closer in age than previously thought. With this in mind, it is possible that occasional older cosmogenic

nuclide exposure dates result from an inheritance signature that was not removed by erosion during supraglacial transport, in which case the majority of younger dates are closer to the true age of deposition.

In this paper, I undertook the fieldwork and analysis; wrote the manuscript; and drew the figures. All authors contributed ideas and edited the text. The paper has been published in *Geomorphology* and the supplementary information from that paper has been incorporated into the main text of this thesis.

1.4.3   Chapter 5

Darvill, C.M., Bentley, M.J., Stokes, C.R., Hein, A.S. & Rodés, Á. (in prep.) Extensive MIS 3 glaciation in southernmost Patagonia revealed by cosmogenic nuclide dating of outwash sediments. *Earth and Planetary Science Letters*.

In the light of the hypothesis raised in Chapter 4, this paper provides the first age constraints for the San Sebastián and Río Cullen limits of the BI-SSb lobe in a way that is not compromised by exhumation and erosion processes. These pre-gLGM glacial limits were previously hypothesised to date from Marine Isotope Stages (MIS) 12 and 10, but we demonstrate that they were deposited much more recently, during the last glacial cycle (MIS 4-2), including one clear MIS 3 advance. With this major reinterpretation of age, we suggest that the cause of such an extensive MIS 3 advance was most likely a southward shift of the Southern Westerly Winds, delivering greater precipitation to the ice lobe at a time of cooler summers and warmer, wetter winters.

In this paper, I undertook the fieldwork, including sampling; much of the laboratory analysis; and most of the depth-profile modelling. I wrote the manuscript and drew the figures. All authors contributed ideas and edited the text. Bentley and Stokes assisted with fieldwork; Hein and Rodés assisted with depth-profile modelling; and Rodés assisted with laboratory analysis. The paper has been prepared for *Earth and Planetary Science Letters*, but the supplementary information has been incorporated into the main text and the introduction has been edited for consistency in this thesis.

1.4.4   Chapter 6

Darvill, C.M., Stokes, C.R. & Bentley, M.J. (in prep.) The glacial history of five ice lobes in southernmost Patagonia. *Journal of Quaternary Science*.

This paper brings together new mapping of glacial geomorphology in southernmost South America from Chapter 3 with new age constraints on glacial limits from

Chapter 5 to present a new reconstruction of the timing and nature of glaciation in the region. We present a series of relative time steps based on our reconstructed glacial limits and, where possible, constrain the timing of glacial advances. In particular, we reinterpret previous chronological information in the light of our depth-profile dating campaign. All of the ice lobes are found to have displayed dynamic behaviour at times, with evidence for re-advances and the development of proglacial lakes that likely affected rates of advance and retreat. It is suggested that the Skyring, Otway and Magellan lobes were likely more extensive prior to the gLGM, similar to findings in Chapter 5 for the BI-SSb lobe.

In this paper, I undertook the analysis, wrote the manuscript and drew the figures. Stokes and Bentley contributed ideas, edited the text and assisted with fieldwork. The paper has been prepared for *Journal of Quaternary Science*.

1.4.5   Chapter 7

Darvill, C.M., Bentley, M.J. & Stokes, C.R. (in prep.) Evaluating the timing and cause of glacial advances in the southern mid-latitudes during the last glacial cycle based on compiled exposure ages from Patagonia and New Zealand. *Quaternary Science Reviews*.

Chapters 5 and 6 demonstrated that southern ice lobes in Patagonia advanced prior to the gLGM, and we argued that a similar pattern has emerged in other recent Southern Hemisphere studies, although it has not been widely discussed. In this paper, we compiled a large chronological dataset for Patagonia and New Zealand to compare the timing of regional ice advances and in so doing discuss the possible forcing factors behind Southern Hemisphere glacial advances during the last glacial cycle. We suggest that orbital parameters may underlie mid-latitude glacial activity, but that the migration of coupled ocean-atmosphere fronts, as part of a wider climatic feedback system, ultimately determines the timing of advances.

In this paper, I undertook the analysis, wrote the manuscript and drew the figures. Bentley and Stokes contributed ideas and edited the text. The paper has been prepared for *Quaternary Science Reviews*.

Chapter 2.   Study area and previous work

2.1 Study area

The study area of this thesis focuses on the southernmost part of the former Patagonian Ice Sheet (Figures 2.1 and 2.2), specifically five ice lobes that extended eastward from the Andean Cordillera at times during the Quaternary period between around 51-54°S. From north to south, these were the Río Gallegos, Skyring, Otway, Magellan and BI-SSb lobes. At present, only a handful of ice caps or small valley glaciers remain, principally the North Patagonian, South Patagonian and Darwin Cordilleran icefields (Figure 2.1). However, the glacial geomorphology of the former ice lobes is exceptionally well preserved by the relatively dry, arid climate and by the preservation of older geomorphology due to decreasing ice extents over time.

Numerous up-to-date reviews exist which summarise the previous literature on glaciations in this region (Rabassa & Clapperton, 1990; Meglioli, 1992; Rabassa, 1992; Rabassa *et al.*, 2000; Coronato *et al.*, 2004; Rabassa *et al.*, 2005; Rabassa, 2008; Rabassa *et al.*, 2009; Rodbell *et al.*, 2009; Coronato & Rabassa, 2011; Harrison & Glasser, 2011; Martínez *et al.*, 2011; Rabassa *et al.*, 2011; Kilian & Lamy, 2012). However, a critical assessment of the evidence for the timing of glaciations in southernmost South America is useful to highlight gaps in knowledge and issues associated with previous attempts at chronology.

Early observations of the presence of glacial deposits in southernmost South America were made by Darwin (1841; 1845; 1848). Subsequently, Nordenskjöld (1899) was the first to accurately map glacial deposits in Patagonia, but it was Caldenius' (1932) seminal work that defined the four glacial limits for Patagonia that are still broadly referred-to today (Figure 2.3). He named these deposits *Initioglacial*, *Daniglacial*, *Gotiglacial* and *Finiglacial* after the Swedish/European system, which implied that they were all of the last glaciation. It has since been shown that the older glacial limits were deposited more than a million years old (Meglioli, 1992; Ton-That *et al.*, 1999; Singer *et al.*, 2004a; Singer *et al.*, 2004b; Hein *et al.*, 2011). However, the original geomorphological characteristics of Caldenius' system were built upon by Meglioli (1992) to establish the current conceptual model of glaciations for southernmost South America (Figure 2.2). This Regional Stratigraphic Model has since been used widely (Coronato *et al.*, 2004; Rabassa, 2008; Coronato & Rabassa, 2011; Rabassa *et al.*, 2011), although few of the glacial deposits have any absolute age controls.
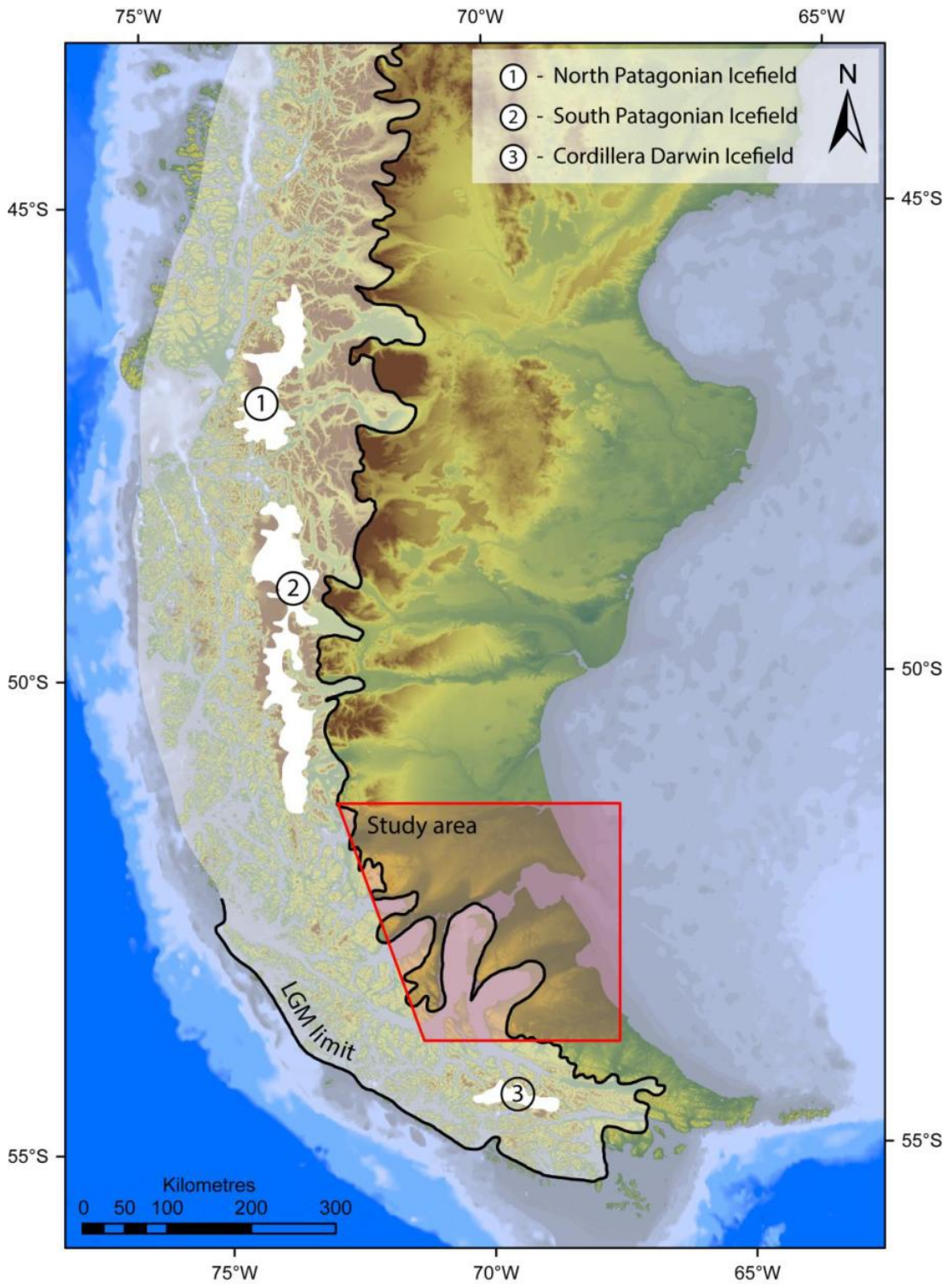
Figure 2.1. Location of the study area in southernmost Patagonia, South America. The present day icefields (numbered) are shown as well as the hypothesised gLGM, adapted from Singer *et al.* (2004a).
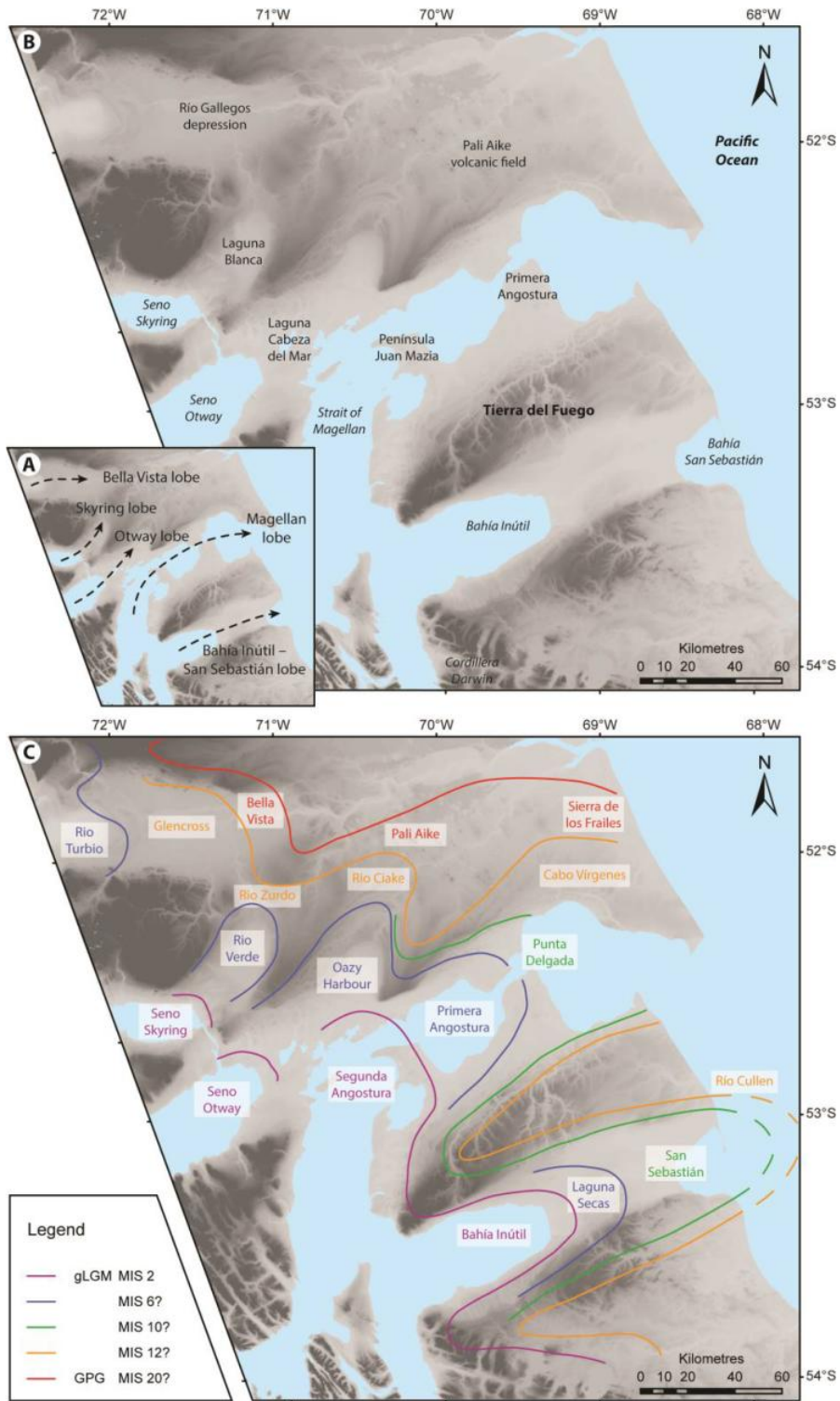
Figure 2.2. (A) Illustration of the flow paths of the five former ice lobes in the study area. (B) An overview of the place names mentioned in this chapter. (C) A conceptual diagram of the Regional Stratigraphic Model proposed by Meglioli (1992) showing the drift limits and their respective names for each lobe, as well as hypothesised age. See Table 2.1 for an overview of these drift deposits.

12

2.2 Previous work

2.2.1 Nature of ice dynamics

2.2.1.1 Glacial erosion and nested limits

A decreasing extent of glacial limits over successive glaciations has been recorded at numerous locations in southern South America (the "nested" moraine formations observed in many glacial valleys; Caldenius, 1932; Figures 2.2 and 2.3). Kaplan *et al.* (2009) inferred that because these sequences do not match global climate variability, the decreasing ice extents cannot be linked to climate, and perhaps partly owe their origin to long-term erosional patterns, later modelled by Anderson *et al.* (2012). However, this hypothesis does not consider that the trends could be related to a regional (e.g. southern mid-latitude) climate trigger, which is not displayed by global climate records dominated by Northern Hemisphere signals.
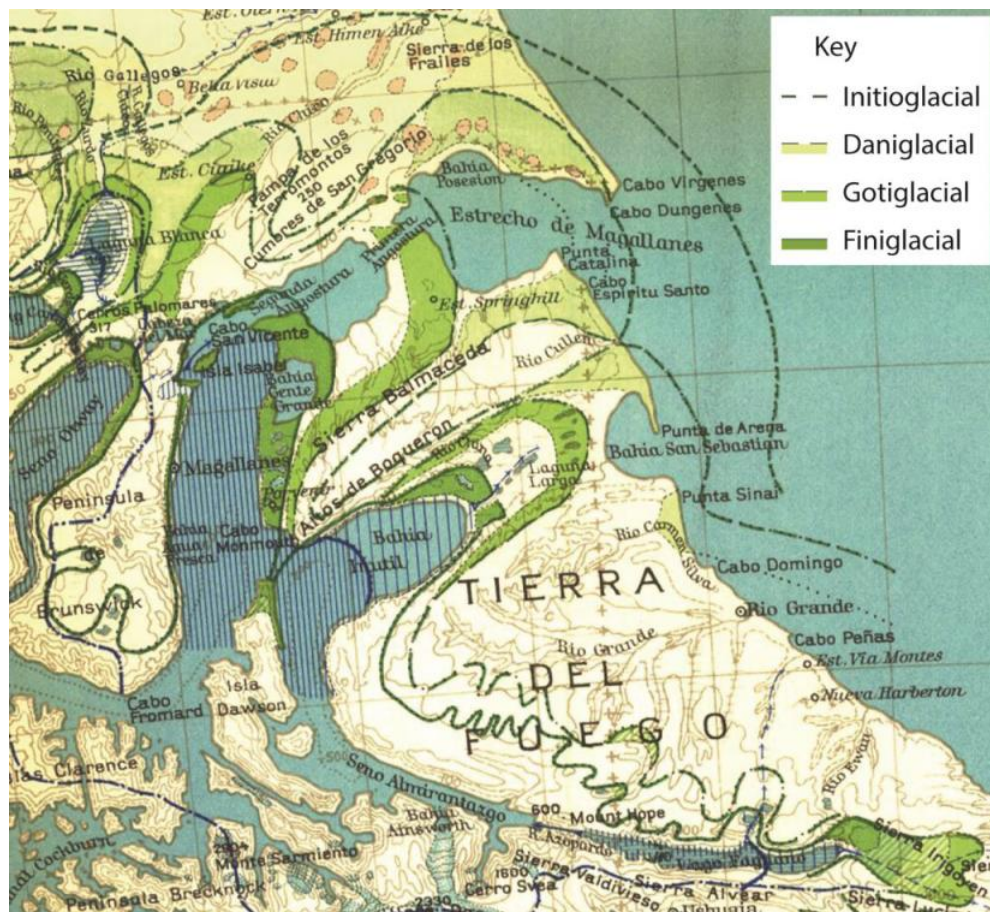
Figure 2.3. A section of the original glacial map of Patagonia by Caldenius (1932), cropped to the study area and with a key added to show his four proposed glacial stages.

Kaplan *et al.* (2009) suggested that over time, topographic changes (e.g. Jamieson *et al.*, 2008) and changes in bedrock elevations (e.g. Montgomery, 2002) could jointly cause more negative glacier mass balances given a constant climatic forcing. In this way, the relationship between topography and Patagonian glacial extent is important to understand (Herman *et al.*, 2013; Barr & Lovell, 2014), and may mask a climatic effect. To establish whether climate played a role, independent evidence is required to demonstrate that climatic changes occurred at the same time as glacier changes. For example, evidence of similar trends in glacial advances in other, distal locations at roughly the same latitudes would suggest that an external climatic forcing was responsible. These locations would need to be affected by similar atmospheric and oceanic systems for the argument to hold; ideal locations would be the glacier records of Patagonia and southern New Zealand (Figure 1.1).

2.2.1.2   *Ice flow dynamics*

There has been some work investigating the dynamics of ice advances and retreat in the study area. For example, numerous authors have mapped and commented on the spectacular drumlin field within the Otway lobe, around Laguna Cabeza del Mar (Clapperton, 1989; Clapperton *et al.*, 1995; Benn & Clapperton, 2000b; Lovell *et al.*, 2012; Figure 2.2), with Benn & Clapperton (2000b) suggesting it may have been formed by ice streaming. More recently, Lovell *et al.* (2012) presented a detailed reconstruction for parts of the Skyring, Otway and Magellan lobes, and found evidence for possible ice-streaming and surge-like behaviour. Although Benn & Clapperton (2000b) inferred a cold-based margin for the Magellan lobe, Bentley *et al.* (2005) and Lovell *et al.* (2012) suggested that this was unlikely. Recent bathymetric work has suggested that basal morphology, including tectonic controls, could have also played a role in defining ice extent in at least the Otway and Magellan lobes (Breuer *et al.*, 2013).

2.2.1.3   *Proglacial lakes*

Numerous raised shorelines have been mapped in the study area, corresponding to all five southern ice lobes (Clapperton *et al.*, 1995; McCulloch & Bentley, 1998; Bentley *et al.*, 2005; McCulloch *et al.*, 2005a; Glasser & Jansson, 2008; Lovell *et al.*, 2011; Sagredo *et al.*, 2011; Stern *et al.*, 2011; Breuer *et al.*, 2013; Kilian *et al.*, 2013; De Muro *et al.*, 2014; García *et al.*, 2014). McCulloch *et al.* (2005a) and García *et al.* (2014) also presented detailed geomorphological and sedimentological evidence for proglacial lakes, as well as demonstrating post-glacial uplift of mapped shorelines due to isostatic and/or tectonic uplift. Recent work combining this evidence with

analysis of digital elevation models has provided some reconstructions of proglacial lake evolution that can supplement investigations into glacial advance and retreat (Lovell *et al.*, 2012; Kilian *et al.*, 2013; García *et al.*, 2014).

Porter *et al.* (1992), Clapperton *et al.* (1995), Bentley *et al.* (2005), McCulloch *et al.* (2005a), Lovell *et al.* (2012) and García *et al.* (2014) have commented on the formation and drainage of proglacial lakes in the region and the possible effects these had on ice dynamics. Porter *et al.* (1992) suggested that lakes in front of the Magellan and BI-SSb lobes may have increased the ice flow rate during recession, possibly even resulting in collapse. Similarly, Lovell *et al.* (2012) hypothesised that rapid flow of the Otway and Magellan lobes could have been linked to proglacial calving. However, the absence of evidence for ice-streaming in the Skyring lobe and for lake development in the Otway lobe makes it difficult to develop this argument further (Lovell *et al.*, 2012).

2.2.1.4 Ice sheet modelling

Hulton *et al.* (1994) and Hulton *et al.* (2002) are the only studies to have modelled the entire Patagonian Ice Sheet, and this has provided useful insights into ice sheet dynamics and climatic forcing. For example, the modelling highlighted the marked contrast between the east and west of the ice sheet. However, this ice sheet-scale modelling has not been updated to include more recent insights into chronology and modelling power (e.g. compared to Golledge *et al.* (2012) for New Zealand). One of the reasons for this is the challenging nature of modelling the Patagonian Ice Sheet. It covered a long latitudinal range (and therefore north-south temperature gradient) and experienced differing regimes from west to east (Hulton *et al.*, 2002; Sugden *et al.*, 2002). On the western side of the ice sheet, glaciers were dominantly marine-terminating, not reaching far from the Andean range but receiving high rates of precipitation carried by westerly winds from the Pacific Ocean. In contrast, the eastern side was relatively drier but was terrestrial terminating, with large ice lobes travelling far from the mountains (Coronato *et al.*, 2008; Rabassa, 2008). Furthermore, Kerr & Sugden (1994) demonstrated a strong dependence of former glaciers on temperature changes, but also that the southern part of the ice sheet was particularly sensitive to precipitation. Uncertainty in changes in the delivery of precipitation by the Southern Westerly Winds, which may have migrated or expanded north and southward over time, makes it challenging to model the former ice sheet. Finally, Glasser & Jansson (2005) also noted that ice streaming within

parts of the ice sheet may help to explain why matching model outputs to the geomorphological record has proven so challenging.

Nonetheless, modelling the whole ice sheet is important because more localised studies of individual glacier systems become limited by assumptions about ice-flow dynamics or chronological constraints that are ultimately difficult to answer without taking a broader, ice sheet-scale view. For example, studies such as Hubbard *et al.* (2005) for northern Patagonia and Fernandez *et al.* (2011) for the Marinelli glacier system in Cordillera Darwin offer a level of detail that may be missed by a coarser model, but struggle to ascertain whether glacier fluctuations are linked to external climate forcing or internal flow dynamics. There is great capacity for further modelling of the Patagonian Ice Sheet, though it is beyond the scope of this thesis.

2.2.2   Timing of ice advances

For this introductory chapter, previous dating of glacial limits is reviewed using the data and interpretations as originally stated in the published works. However, for techniques such as radiocarbon dating and cosmogenic nuclide exposure dating, there have been recent advances in age calibration and so, on subsequent use in the rest of the thesis, dates are re-calibrated where relevant.

Whilst a range of dating techniques have been applied to glacial limits in the study area, these have been conducted and interpreted according to the Regional Stratigraphic Model by Meglioli (1992; Table 2.1). Numerous glacial drift deposits have been assigned relative stratigraphic ages in the region, which are thought to broadly correspond between ice lobes (Coronato *et al.*, 2004). This is supported by relative weathering ages and a few absolute ages from intervening volcanic deposits (Meglioli, 1992). There has been lots of subsequent work on the younger, inner drifts, which date from around the gLGM (Coronato *et al.*, 2004; Coronato & Rabassa, 2011; Rabassa *et al.*, 2011), but little work on the older, outer drifts. An important argument in the age of the older drifts is that marine terraces can be linked to glacial limits (Bujalesky *et al.*, 2001). However, a key geomorphic relationship has not been evidenced and dates on the marine terraces are themselves problematic. Most recently, work using cosmogenic nuclide exposure dating of boulders gave a spread of ages that were interpreted in light of the Regional Stratigraphic Model, such that a small number of relatively old ages were taken as closest ages for the drifts (Kaplan *et al.*, 2007; Evenson *et al.*, 2009). Given the complexity in these arguments, it is worth examining the evidence in detail.
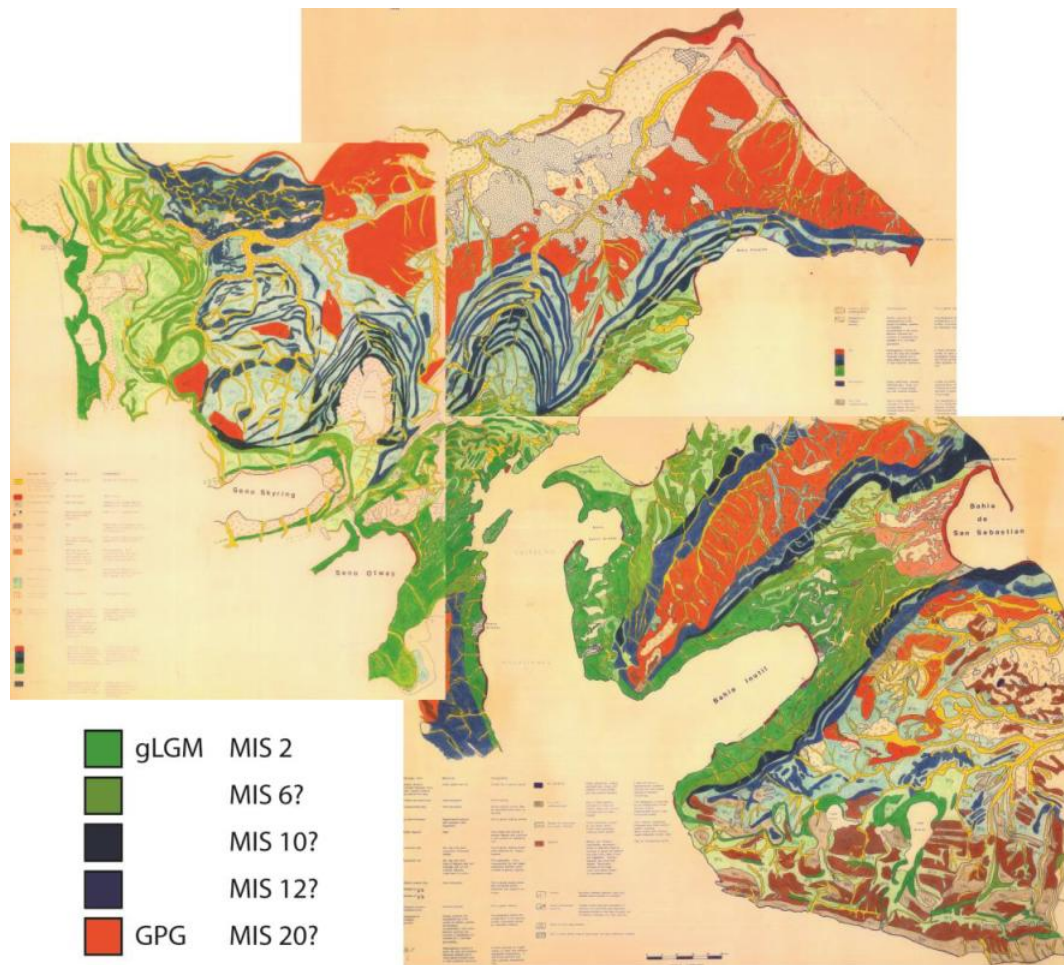
Figure 2.4. Three of the original maps produced by Meglioli (1992) to illustrate his characterisation of drifts across the study area, with a key added to show his hypothesised age model.

2.2.2.1 Drift characterisation

The Regional Stratigraphic Model for southernmost South America proposed by Meglioli (1992) is based upon drift characterisation (Figure 2.4) and consists of isolated examples of the Rio Grande drift followed by local representations of the Greatest Patagonian Glaciation (GPG, ca. 1.1 Ma; Mercer, 1976), then three subsequent glaciations (Coronato *et al.*, 2004) before the gLGM (Clapperton *et al.*, 1995; McCulloch *et al.*, 2005b; Table 2.1). The drifts were defined by Meglioli (1992) based on the relationship of outwash deposits to moraines; moraine morphology; boulder frequency and weathering; presence or absence of cryogenic features; and some were also dated using weathering rind analysis and ^{40}Ar/^{39}Ar dating of basalts. For simplicity, these drifts are referred to as 'glacial limits' throughout the following Chapters and local names are used where necessary to avoid correlation without actual age constraints.

Table 2.1. An overview of the drift deposits described and correlated by Meglioli (1992), along with glaciation names, weathering rind ages, robust argon dates (where available) and hypothesised MIS chronology, whereby MIS 2 corresponds to the gLGM. Grey shading indicates the GPG drifts.

Río Gallegos lobe drifts	Skyring lobe drifts	Otway lobe drifts	Magellan lobe drifts	BI-SSb lobe drifts	Glaciation	Weathering rind age (ka)	$^{40}Ar/^{39}Ar$ ages (ka)	MIS
				Río Grande?	?			?
Bella Vista	*Pali Aike*	*Pali Aike*	*Sierra de los Frailes*	*Pampa de Beta*	Sierra de los Frailes	1200 ± 200	*ca.* 1100	20?
Glencross	*Rio Zurdo*	*Rio Ciake*	*Cabo Vírgenes*	*Río Cullen*	Cabo Virgenes	450 ± 0.1		12
	Laguna Blanca	*Dinamarquero*	*Punta Delgada*	*San Sebastián*	Punta Delgada			10
Rio Turbio	*Rio Verde*	*Oazy Harbour*	*Primera Angostura*	*Lagunas Secas*	Primera Angostura	140 ± 0.1		6
Seno Almirante Montt	*Seno Skyring*	*Seno Otway*	*Segunda Angostura*	*Bahía Inútil*	Segunda Angostura	15.8 ± 0.2		2

2.2.2.2 Weathering analysis

Meglioli (1992) conducted weathering analysis at 87 sites across the study area, which was used as the principal justification for assigning the different drifts to separate glacial cycles. Some important points should be made regarding the spatial distribution of these analyses. First, the Río Gallegos, Skyring and Otway lobes are distinctly underrepresented by analyses, with only 18 of the total 87 sites within these lobes. Secondly, within the Magellan and BI-SSb lobes, the distribution of sites between drifts is unequal. For example, the Lagunas Secas drift is only represented by one sampling location (correlated with a further fifteen on the Primera Angostura drift). While Caldenius (1932) also recorded a distinct glacial limit ('Las Morenas de Filaret', assigned to the Gotiglacial), this is the only 'dated' sample from the Lagunas Secas drift. Finally, the precise positioning of some of the drift limits has large implications for the weathering results, even though Meglioli (1992) observed that the separation of some drifts was unclear. These issues are necessarily guided by the availability of suitable sampling sites, and are not problematic if one assumes that the correlation between lobes can be made. However, Meglioli (1992) also made it clear that calibration of the weathering rind age model was highly tentative. Of the four points that were used in the construction of a weathering rind calibration curve, one had an age range based on a distal argon date from northern Patagonia assumed to be equivalent in age (140 ka in Table 2.1) and two have large age ranges dictated by argon dates from capping lava flows (450 and 1200 ka in Table 2.1). Thus, the calibration curve has large age errors, though these are not necessarily clear from the age estimates presented in the Regional Stratigraphic Model.

2.2.2.3 Argon-dating of basalts

Argon-dating (including K-Ar and ^{40}Ar/^{39}Ar dating) of volcanic deposits capping drift sediments underpins much of the Regional Stratigraphic Model. Meglioli (1992) used ^{40}Ar/^{39}Ar dating of lava flows to constrain the ages of drifts north of the Magellan Straits and improve the chronology of Mercer (1976). The age of the Sierra de los Frailes drift (Figure 2.2 and Table 2.1) was constrained to between 1.4 ± 0.1 and 1.07 ± 0.03 Ma based on basalt flows below and above the drift, respectively. Furthermore, the Cabo Vírgenes drift (Figure 2.2 and Table 2.1) was bracketed by the second basalt flow at 1.07 ± 0.03 Ma and a further overlying flow dated to 450 ± 10 ka. However, relating the dated tills to glacial limits is not necessarily straightforward.

Subsequent studies by Ton-That *et al.* (1999) and Singer *et al.* (2004a) improved the dating of Meglioli (1992) for the Bella Vista drift in the Río Gallegos depression. The accepted age for this drift is now 1.168 ± 0.014 Ma (Singer *et al.*, 2004a), confirming mapping of the greatest glacial extent in Patagonia by Caldenius (1932) and the GPG proposed by Mercer (1976), now regionally bracketed to between 1.168 and 1.016 Ma Singer *et al.* (2004a). The exact relationship between the Río Gallegos lobe, the Skyring lobe and the Bella Vista drift is less clear, although it is usually presumed that the two ice lobes coalesced, such that the drift date corresponds to both (Rabassa, 2008). There are no argon dates relating specifically to the BI-SSb lobe.

2.2.2.4 Amino-acid racemisation

Amino-acid racemisation analysis has been conducted on marine shells in the study area, although no analyses have been conducted in the Río Gallegos, Skyring or Otway lobes. Work by Rutter *et al.* (1989) and Meglioli (1992) has been cited as providing age constraint on glacial drifts of the BI-SSb lobe, but is actually related to raised marine terraces, and the former makes no connection between these and drift deposits. In contrast, Clapperton *et al.* (1995) and McCulloch *et al.* (2005b) presented analyses of shells from tills within moraines of the Magellan lobe relating to their Advances A (pre-Segunda Angostura drift) and B/C (Segunda Angostura drift). Combined with radiocarbon dates, shells from the Segunda Angostura drift imply a marine incursion occurred in the Magellan Strait around 35 ka, linked to considerable deglaciation and implying that the Magellan lobe could have advanced during MIS 4 or earlier (Clapperton *et al.*, 1995). However, there are a number of assumptions associated with the calibration of the amino-acid racemisation analyses and they do not provide absolute ages (Clapperton *et al.*, 1995).

2.2.2.5 Radiocarbon dating

Radiocarbon dating has been applied across the study area. Due to its limited applicable age span, the technique has been most useful in constraining ice fluctuations from the gLGM onwards. For example, Sagredo *et al.* (2011) and Stern *et al.* (2011) recorded ice recession and proglacial lake development from at least *ca.* 17.5 cal ka BP in the Río Gallegos lobe, following deposition of the Seno Almirante Montt drift. Subsequent re-advances may then have occurred before 16.2 cal ka BP and around 14.8-12.8 cal ka BP (Sagredo *et al.*, 2011).

The Skyring and Otway lobes contain few radiocarbon dates, dominantly from marine cores within their respective sounds. In Seno Skyring, the oldest radiocarbon

age of 12.9 cal ka BP and the Reclus tephra age of *ca.* 14.8 cal ka BP support an age model that implies ice retreat before *ca.* 18 ka. Similarly, the oldest age from Seno Otway is *ca.* 14.8 cal ka BP, with an accompanying age model suggesting ice retreat before *ca.* 17 ka. This is consistent with a date of >14.2 cal ka BP for the abandonment of an overspill channel from the Otway proglacial lake into the Strait of Magellan (Mercer, 1976; McCulloch *et al.*, 2005a; Kilian *et al.*, 2013).

The Magellan and BI-SSb lobes have been analysed extensively using radiocarbon dating of the Segunda Angostura and Bahía Inútil drifts. Shell samples from beyond the Segunda Angostura drift limit in the Magellan lobe, likely relating to Primera Angostura and Punta Delgada drift, were dated by Porter (1990) and Clapperton *et al.* (1995). The infinite ages were suggested to show that these drifts were deposited > 47 ka, and possibly during MIS 4 or earlier. However, McCulloch *et al.* (2005b) later suggested that the dates indicated a prolonged opening of the Strait of Magellan to the Pacific Ocean, and therefore any MIS 4 advance would have been less extensive than the gLGM.

McCulloch *et al.* (2005b) also synthesised a large number of radiocarbon dates from shells and organic material within moraines and lacustrine sediments from the Magellan and BI-SSb lobes, along with cosmogenic nuclide exposure dates, and suggested three ice advances using their glacial stages: at *ca.* 25.2-23.1 cal ka BP (Stage B), before *ca.* 21.7-20.3 cal ka BP (Stage C) and before *ca.* 17.5 cal ka BP (Stage D). The compilation also reconstructed relatively rapid deglaciation following these advances and a re-advance during the Antarctic Cold Reversal. However, recent radiocarbon dating by Hall *et al.* (2013) implies ice retreat well into Cordillera Darwin by *ca.* 16.8 cal ka BP, significantly earlier than proposed by McCulloch *et al.* (2005b). These dates seem to be supported by a marine core from the Marinelli Fjord within the Cordillera (Boyd *et al.*, 2008), but are controversial because radiocarbon dating and tephrochrological analyses indicate that proglacial lakes existed in the Strait of Magellan and Bahía Inútil until *ca.* 11.8-12.6 cal ka BP (McCulloch & Bentley, 1998; McCulloch *et al.*, 2000; McCulloch & Davies, 2001; McCulloch *et al.*, 2005a; McCulloch *et al.*, 2005b).

2.2.2.6 Uranium-series dating of marine terraces and glaciofluvial fans

A key piece of evidence for the ages of BI-SSb lobe drifts is the relationship between marine terraces and glaciofluvial fans on the east coast of Tierra del Fuego (Coronato *et al.*, 2004; Rabassa, 2008; Coronato & Rabassa, 2011; Rabassa *et al.*, 2011). Bujalesky *et al.* (2001) analysed three raised beach formations, and dated

them using Uranium-series analysis on shells within the terraces (Figure 2.5). These marine terraces are inferred to represent three marine transgressions, strongly implying that they were formed during (at least) three successive interglacials. If they can be linked geomorphologically to any of the drifts, therefore, they can be used as evidence for the separation of the drifts into different glaciations.
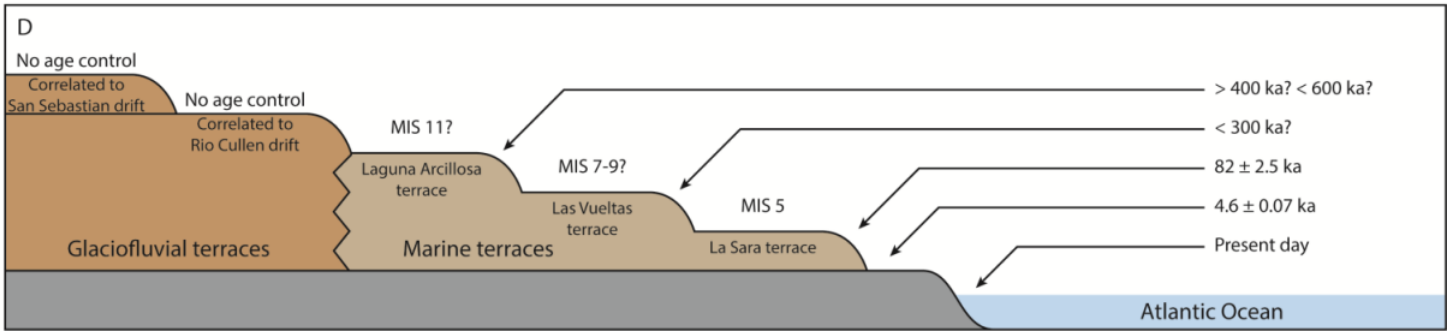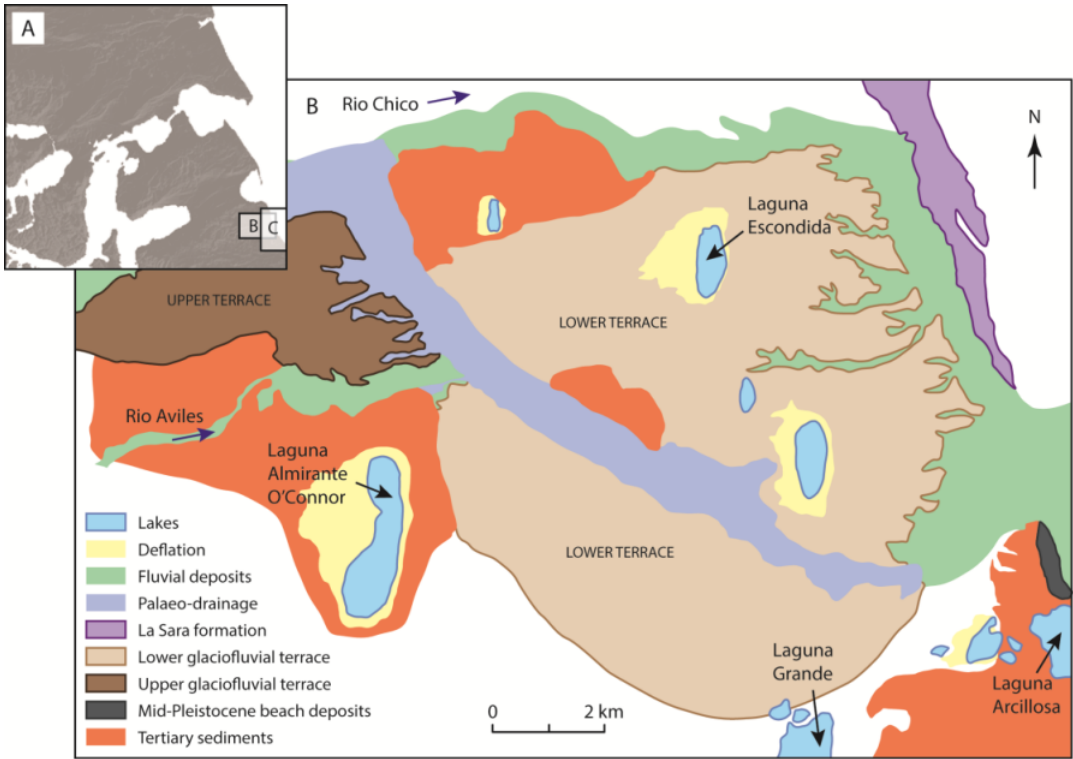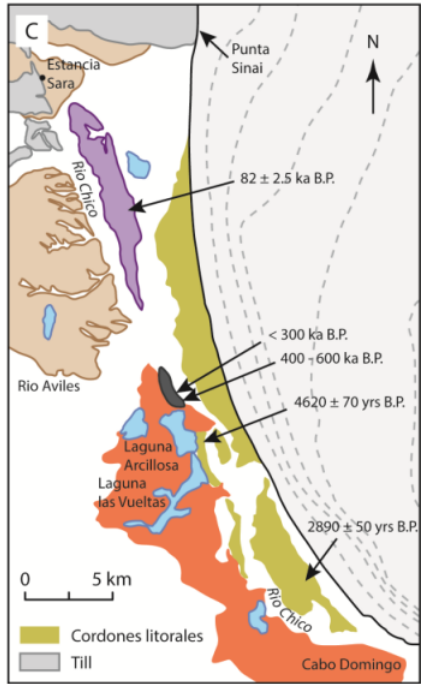
Figure 2.5. (A) Location of the area studied by Bujalesky *et al.* (2001), with their mapping shown in (B) and (C), adapted from the original figures. The lower glaciofluvial terrace is shown in brown in both (B) and (C). (D) is a conceptual diagram to illustrate the relationship between dated marine terraces, glaciofluvial terraces and drifts proposed by Bujalesky *et al.* (2001).

23

Two glaciofluvial terraces were also described by Bujalesky *et al.* (2001) as corresponding to the Río Cullen and San Sebastián drift limits (Figure 2.5), although there is no direct chronological evidence for their ages. The lower terrace has been eroded by the three marine terrace formations, suggesting that it formed prior to three marine transgressions. Crucially, the geomorphic link to the glacial limits was not described by the authors.

The dating on the Las Vueltas and Laguna Arcillosa marine terraces (Figure 2.5) is uncertain given that a portion of the Uranium-signature of both samples implied terrestrial rather than marine origin. Weathering had occurred so that lack of contamination and a closed-system could not be guaranteed, particularly for the Las Vueltas sample. Bujalesky *et al.* (2001) suggested that issues of weathering and contamination affecting the Laguna Arcillosa samples would most likely lead to an age of >400 ka and <600 ka; and that the Las Vueltas age is probably unreliable given weathering and terrestrial contamination. The Las Vueltas terrace was only assigned an age of <300 ka based on dating and the stratigraphic position of the terrace.

Coronato & Rabassa (2011; p.723) stated that "based on the stratigraphical position of paraglacial fans and raised marine beaches, Bujalesky *et al.* (2001) postulated that the Sierras de San Sebastián and Lagunas Secas glacial limits should correspond to MIS 10 and 6, respectively". However, this link is not straightforward because:

1. There is no independent dating of the Lagunas Secas drift and there is no definitive evidence to show that it formed in a separate glacial stage.
2. There is no geomorphic link between the raised marine terraces and the Bahía Inútil or Lagunas Secas drifts with the raised beach formations.
3. The correlation of the San Sebastián drift with MIS 10 is based on the assumption that it was a separate glacial stage, older than the Lagunas Secas drift (presumed MIS 6) and younger than the Río Cullen drift. MIS 10 was selected by Coronato *et al.* (2004) and Coronato & Rabassa (2011) based on Uranium-series dating of the Las Vueltas formation, despite the fact that this dating is stated as being uncertain (Bujalesky *et al.*, 2001). Given that the age of the Lagunas Secas drift is unknown, there is no reason why the San Sebastián drift cannot be of MIS 6 age or younger.

4.   The system of three raised beach formations only incise the lower glaciofluvial fan, hypothesised to link to the Río Cullen drift (Bujalesky *et al.*, 2001). This suggests that deposition of the Río Cullen drift was followed by three interglacial marine transgressions, the oldest of which was likely >400 ka and the youngest of which was at *ca.* 82 ka (MIS 5). However, this does not provide an absolute age for the Río Cullen drift, or any ages for the San Sebastián and Lagunas Secas drifts. Crucially, there is no evidence given to demonstrate that the glaciofluvial fans relate to the San Sebastián and Río Cullen drifts.

2.2.2.7   Palaeomagnetism

Walther *et al.* (2007) presented palaeomagnetic results from glacial sediments from northern Tierra del Fuego. Analysis of basal till from the Río Cullen drift exposed at Bahia San Sebastián demonstrated that it formed during the normally-polarised Brunhes chron and that the Río Cullen, San Sebastián and Lagunas Secas drifts formed after 760 ka (Walther *et al.*, 2007; Rabassa *et al.*, 2011). No similar palaeomagnetic studies have been conducted for the Río Gallegos, Skyring, Otway or Magellan lobes.

2.2.2.8   Luminescence dating

Luminescence dating has only been successfully used once in the study area, with Blomdin *et al.* (2012) obtaining an age of around 22 ka for the deglaciation of the Brunswick Peninsula area west of the Strait of Magellan, supporting the radiocarbon dating chronology in that location (McCulloch *et al.*, 2005b). More important than the age estimates, their study, like that of Harrison *et al.* (2008) in northern Patagonia, highlighted the need to use alternative techniques to Optically Stimulated Luminescence (OSL) dating of glacial sediments in Patagonia. Blomdin *et al.* (2012) utilised K-Feldspar Infrared Stimulated Luminesce (IRSL), whereas Glasser *et al.* (2006) and Harrison *et al.* (2012) used single grain OSL dating. No luminescence dating has been conducted on the Río Gallegos, Skyring and Otway lobes, but the technique has great potential to help constrain glacial limits in the study area in the future.

2.2.2.9   Cosmogenic nuclide exposure dating

No cosmogenic nuclide dating has been published on deposits relating to the Otway or Skyring lobes, but the Río Gallegos lobe has been dated using ^{10}Be and ^{36}Cl analysis of erratic boulders. The Bella Vista drift was dated to 47 ka and 106 ka, with

both ages substantially younger than expected (Kaplan *et al.*, 2007). Likewise, the Rio Turbio and/or Glencross drifts yielded five dates of 38-74 ka (Evenson *et al.*, 2009; the exact sampling strategy is unclear from their work). Sagredo *et al.* (2011) dated younger limits of the Río Gallegos lobe (which they refer to as the Última Esperanza lobe) using four boulders which yielded ages of 38-61 ka. There are issues of stratigraphic consistency within the combined cosmogenic nuclide exposure ages for the Río Gallegos lobe, and tying these ages to glacial drifts or limits is challenging.

The Magellan lobe has been dated using ^{10}Be and ^{26}Al analysis. For the Segunda Angostura drift, the ages are consistent with the gLGM, as previously hypothesised (Meglioli, 1992; McCulloch *et al.*, 2005b; Kaplan *et al.*, 2007; Kaplan *et al.*, 2008a). However, eight dates from the Primera Angostura, Punta Delgada and Cabo Vírgenes drifts yielded young ages <133 ka, with the six dates from the Primera Angostura drift yielding ages of 21-27 ka. This is a similar situation to cosmogenic nuclide exposure dating of the BI-SSb lobe.

Erratics boulder trains within the southern margin of the BI-SSb lobe have been dated extensively by a number of studies, with those on the southern side of Bahía Inútil supporting other dating techniques and assigning the Bahía Inútil drift to the gLGM (McCulloch *et al.*, 2005b; Kaplan *et al.*, 2007; Kaplan *et al.*, 2008a; Evenson *et al.*, 2009). Kaplan *et al.* (2007) also measured combinations of ^{10}Be, ^{26}Al and ^{36}Cl nuclides on erratic boulder trains from pre-gLGM limits within the BI-SSb lobe. They found that on the Rio Cullen and San Sebastián drifts (assumed to be >350 ka) erratics showed relatively young exposure ages (generally <50 ka; Figure 2.6). In light of the Regional Stratigraphic Model (Meglioli, 1992; Coronato *et al.*, 2004), Kaplan *et al.* (2007) proposed that episodic exhumation and erosion of the vast majority of the boulders during the gLGM had caused anomalously young ages, and that the oldest ages were closest to the true age of glacial advance. This was supported by the large range of cosmogenic nuclide exposure ages compared to other ice lobes in northern Patagonia (Kaplan *et al.*, 2004; Douglass *et al.*, 2005; Kaplan *et al.*, 2005; Douglass *et al.*, 2006). Evenson *et al.* (2009) presented a further twenty ^{10}Be and ^{36}Cl cosmogenic samples for the BI-SSb lobe. There is little discussion of the analyses, but they suggested that the Laguna Secas drift may have been deposited during MIS 4, rather than MIS 6, and that wave-washing may have occurred during isostatic depression following MIS 4. Conversely, Evenson *et al.* (2009) also pointed out that excessive boulder erosion is unlikely to have occurred at the same rate on all boulders over hundreds of thousands of years, thus

producing relatively tightly clustered ages. Kaplan *et al.*'s (2007) explanation for the spread of cosmogenic ages is logical and is not contradicted by the Evenson *et al.* (2009) results. However, it is based on fitting to the Regional Stratigraphic Model, which presumes that dating prior to cosmogenic nuclide exposure analysis was robust and the ages of the limits were relatively well known.

This chapter has highlighted that independent age-constraint of the drifts prior to cosmogenic nuclide exposure dating was not as robust as suggested and that the interpretation of the cosmogenic ages may be worth revisiting.
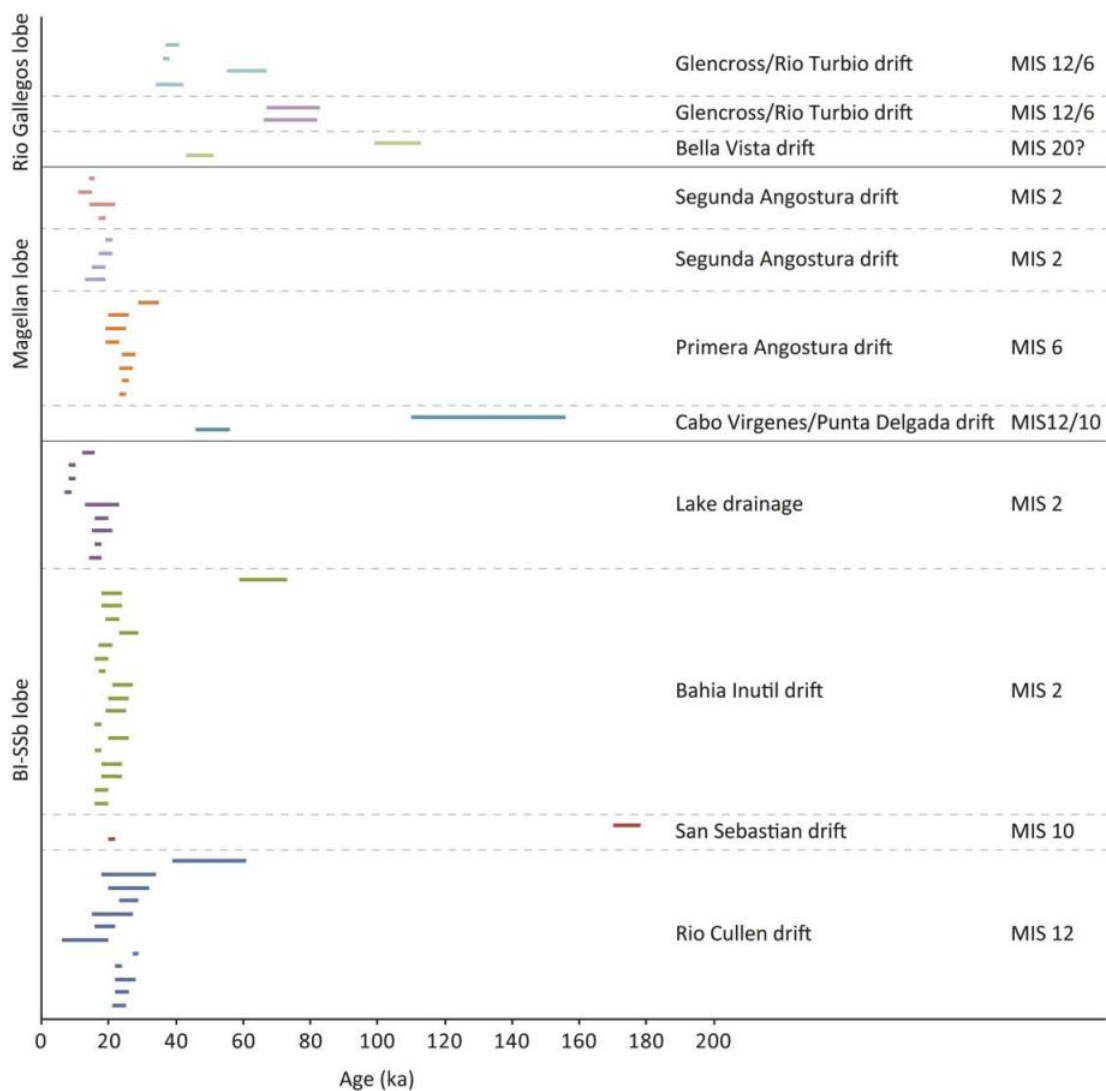
Figure 2.6. The age ranges of all [10]Be analyses previously published for the study area (see text for details). Dates are labelled according to the drifts (and hypothesised ages according to the Regional Stratigraphic Model) to which they relate.

2.2.3 Terrestrial palaeoenvironmental reconstructions

Previous studies have demonstrated links between glacial activity in southern South America and wider past environmental changes. This section briefly outlines a selection of the terrestrial reconstructions from the study area, focussing on pre-Holocene records. These can be used to help interpret glacial activity, but may also be affected by new insights into the timing of glacial activity in the area.

2.2.3.1 Vegetative reconstructions

Markgraf (1993) used pollen records from across southernmost South America to show the succession of vegetation change towards *Nothofagus* forest into the Holocene. This was later supplemented by D/H stable isotopic analyses to improve the temperature and moisture reconstructions, suggesting increased precipitation after *ca.* 15 cal ka BP (Pendall *et al.*, 2001). Heusser (1993; 1995; 2003) and Heusser *et al.* (2000) also reconstructed vegetation changes along the Strait of Magellan, demonstrating that tundra-like vegetation (e.g. *Empetrum* and *Acaena*) existed during the late glacial, consistent with a cooler, drier climate. The pollen record of McCulloch & Davies (2001) supported this, suggesting warming and retreat of the Magellan lobe from *ca.* 17.3 cal ka BP but cooler temperatures until *ca.* 12.3-12.1 cal ka BP. They also suggested that a period of cooler and drier climate during *ca.* 15.3-12.1 cal ka BP altered vegetation composition at the same time as an ice re-advance during the Antarctic Cold Reversal. In the Skyring lobe, Kilian *et al.* (2007) showed a shift towards Magellanic Rainforest in the region after *ca.* 11 cal ka BP, possibly indicative of the end of a similar Antarctic Cold Reversal in this ice lobe.

Markgraf (1993), Heusser (1995) and Pendall *et al.* (2001) all noted the importance of the Southern Westerly Winds in determining vegetation spread. More recent work on post-late glacial pollen records has also suggested a link between environmental changes and the wind system, possibly invoking the Southern Annular Mode (Moreno *et al.*, 2009a; Moreno *et al.*, 2010; Moreno *et al.*, 2012; Moreno *et al.*, 2014), but using pollen records in this way to reconstruct changes in winds intensity may be problematic (Kohfeld *et al.*, 2013).

2.2.3.2 Dust records

Patagonia is one of the dominant sources of southern hemispheric dust found in Antarctic ice-core records (Kaiser & Lamy, 2010; McGee *et al.*, 2010; Wolff *et al.*, 2010a; Martinez-Garcia *et al.*, 2011). Sugden *et al.* (2009) demonstrated a

theoretical and geochemical link between glacial activity in southern South America (including the Magellan lobe), dust availability, and pre-warming dust deposition in Antarctic ice-cores. They suggested that as glaciers retreated in Patagonia, large outwash plains were exposed, and became sources of atmospheric dust which is preserved in Antarctic ice cores (Fischer *et al.*, 2007). Importantly, as ice retreated into proglacial lakes, the dust source was effectively switched-off, explaining an early reduction in Antarctic dust compared to global temperature rise after *ca.* 20 ka (Sugden *et al.*, 2009). It is possible that dust resulting from fluctuations of Patagonian glaciers was one of the major drivers of Quaternary global climatic change (Lambert et al., 2008).

2.2.3.3 The Potrok Aike record

The Potrok Aike Maar lake is situated within the study area, to the east of the Río Gallegos lobe and north of the Skyring lobe, and deserves special mention because it has been the subject of intense study over the last five years (Zolitschka, 2009; Recasens *et al.*, 2012; Zolitschka *et al.*, 2013). The lake is suggested to have remained stable and relatively free of glacial and glaciofluvial activity over the last *ca.* 800 ka (Coronato *et al.*, 2013), though a core record has been shown to cover only *ca.* 51 ka (Buylaert *et al.*, 2013; Kliem *et al.*, 2013b; Lisé-Pronovost *et al.*, 2013; Wastegård *et al.*, 2013). Nonetheless, this record has been used to reconstruct changes in a variety of palaeoevironmental parameters, including lake level (Kliem *et al.*, 2013a) and Southern Westerly Wind intensity (Lisé-Pronovost *et al.*, 2014; Zhu *et al.*, 2014; Lisé-Pronovost *et al.*, 2015), and transfer functions for pollen and diatoms have been developed from around 16 ka to aid palaeoenvironmental and climatic reconstructions (Massaferro & Larocque-Tobler, 2013; Schäbitz *et al.*, 2013). Many of these proxies are still in the developmental stages, but recent work using stable isotopes (Zhu *et al.*, 2014) and mineral magnetic properties (Lisé-Pronovost *et al.*, 2015) over the last 51 ka may help to show how the Southern Westlery Wind system operated during periods of significant climatic change. It is likely that the Potrok Aike site will yield further invaluable environmental and climatic information for the study area in the future.

2.3 Summary

There has been much work on the reconstruction of glacial dynamics in southernmost South America, but there remain several key issues that would benefit from further investigation. Of particular interest are the causes for reduced glacial extent over time (Kaplan *et al.*, 2009; Anderson *et al.*, 2012) and the possibility of

highly dynamic ice lobes (Lovell *et al.*, 2012). However, without understanding the time frame within which the ice lobes advanced, it is difficult to fully assess the nature of glacial change.

There is significant uncertainty in the age of glacial limits in the study area. Meglioli (1992) proposed the Regional Stratigraphic Model of four drifts deposited after the GPG (Caldenius, 1932; Singer *et al.*, 2004a). Weathering rind data was used to separate these drift deposits into four different glacial cycles (Meglioli, 1992). The age of the GPG has been well constrained by Meglioli (1992), Ton-That *et al.* (1999) and Singer *et al.* (2004a) using argon-dating of basalts capping the Bella Vista drift of the Río Gallegos lobe to *ca.* 1.1 Ma. Porter (1990) and Clapperton *et al.* (1995) provided infinite radiocarbon ages for the Punta Delgada and Primera Angostura drifts of the Magellan lobe and Rutter *et al.* (1989), Meglioli (1992), Clapperton *et al.* (1995) and McCulloch *et al.* (2005b) used amino acid racemisation analysis to suggest that the Primera Angostura drift of the Magellan lobe formed prior to the gLGM. The gLGM is well constrained for the Magellan and BI-SSb lobes (and, to an extent the Río Gallegos lobe) by a variety of chronological techniques.

There are few, if any, firm age constraints for pre-gLGM limits in the region, and large uncertainty surrounds those of the BI-SSb lobe. Bujalesky *et al.* (2001) suggested that the Rio Cullen drift of the BI-SSb lobe may have formed the lower of two glaciofluvial terraces eroded by three raised marine terraces, which would imply that the Rio Cullen drift was followed by at least three interglacial cycles, although this link is ambiguous. Cosmogenic nuclide exposure dating by Kaplan *et al.* (2007) and Evenson *et al.* (2009) produced scattered dates, but dominantly < 50 ka. However, dates from limits older than the gLGM limit were called into question because they did not fit the Regional Stratigraphic Model.

This leads to an important, but not previously discussed observation. Specifically, there is at least as much chronological evidence to suggest that the glacial limits deposited after the GPG, but before the gLGM, were part of an earlier advance during the last glacial cycle, as there is to suggest that they were from several previous glacial cycles. Clearly, robust age constraints from these limits are required, and this is a key motivation for this thesis. These may then have important implications for the interpretation of other palaeoenvironmental and climatic records in southernmost South America.

Chapter 3. A glacial geomorphological map of the southernmost ice lobes of Patagonia: the Bahía Inútil - San Sebastián, Magellan, Otway, Skyring and Río Gallegos lobes

Darvill, C.M., Stokes, C.R., Bentley, M.J. & Lovell, H. (2014) 'A glacial geomorphological map of the southernmost ice lobes of Patagonia: the Bahía Inútil - San Sebastián, Magellan, Otway, Skyring and Río Gallegos lobes', *Journal of Maps*, 10, 500-520.

Abstract

This paper presents a glacial geomorphological map of the landforms created by five large ice lobes that extended eastwards from the southernmost reaches of the Patagonian Ice Sheet during the Quaternary period. The study is focussed on Tierra del Fuego, but also updates previous mapping of the Skyring and Otway lobes, and the resulting level of detail and extent is a significant advance on previous work in the region. The map has been created as the necessary precursor for an improved understanding of the glacial history of the region, and to underpin a programme of dating glacial limits in the region. It was produced using Landsat ETM+ and ASTER satellite imagery and vertical aerial photography, supplemented by Google Earth™ imagery and field-checking. Eleven landform types were mapped: moraine ridges, subdued moraine topography, kettle-kame topography, glacial lineations, irregular and regular hummocky terrain, irregular dissected ridges, eskers, meltwater channels, former shorelines and outwash plains. The map reveals three important characteristics of the glacial geomorphology. First, the geomorphic systems are largely dominated by landforms associated with meltwater (channels, outwash plains and kettle-kame topography). Second, there is a difference in the nature of landforms associated with the northern three ice lobes, where limits are generally marked by numerous clear moraine ridges, compared to those to the south, where hummocky terrain and drift limits prevail. Finally, cross-cutting landforms offer evidence of multiple advances, in places, which has implications for the timing of limit deposition, and thus for the design and interpretation of a dating programme.

3.1 Introduction

Patagonia contains some of the longest and best-preserved records of glaciation in the world (Clapperton, 1993). Contemporary glaciation in the region is restricted to three ice caps: the North and South Patagonian and Cordillera Darwin Icefields (Figure 3.1). However, it has been demonstrated that these advanced and coalesced at various times during the Quaternary, as part of an extensive Patagonian Ice Sheet centred on the southern Andes (Caldenius, 1932; Meglioli, 1992; Coronato *et al.*, 2004; Glasser *et al.*, 2008; Rabassa, 2008). Given its location in a region heavily influenced by important atmospheric and oceanic circulation systems, such as the Southern Westerly Winds and the Antarctic Circumpolar Current, Patagonia has received increasing attention in recent decades because it may yield insight into the mechanisms of climatic change in the Southern Hemisphere (Ackert *et al.*, 2008; Kaplan *et al.*, 2008a; Moreno *et al.*, 2009b; Strelin *et al.*, 2011; Murray *et al.*, 2012; Boex *et al.*, 2013) and help in understanding interhemispheric glacial (a)synchrony (Moreno *et al.*, 2001; Sugden *et al.*, 2005; García *et al.*, 2012). Combined with the numerous palaeoenvironmental records that now exist across Patagonia, the timing and pattern of glacial changes may be used to infer changes in past climate (Sugden *et al.*, 2005; Kilian & Lamy, 2012; Moreno *et al.*, 2012).

Extending these investigations beyond the gLGM, however, has thus far proven problematic for the southernmost parts of the region. This is partly due to the lack of a comprehensive mapping of glacial landforms at an appropriate scale (> 30 m resolution) and coverage (regional rather than local), and partly due to uncertainties in existing chronological data (Kaplan *et al.*, 2007). As such, the aim of this paper is to produce a comprehensive map of the glacial geomorphology deposited by the southernmost ice lobes of the Patagonian Ice Sheet that builds on and extends previous work in terms of detail and coverage (Section 3.1.1.1). The map is designed to enable a refined reconstruction of the glacial history of the region using glacial inversion techniques (Kleman *et al.*, 2006) and will be used as the foundation for dating glacial limits in the area, particularly the enigmatic pre-gLGM limits that have thus far proven contentious.
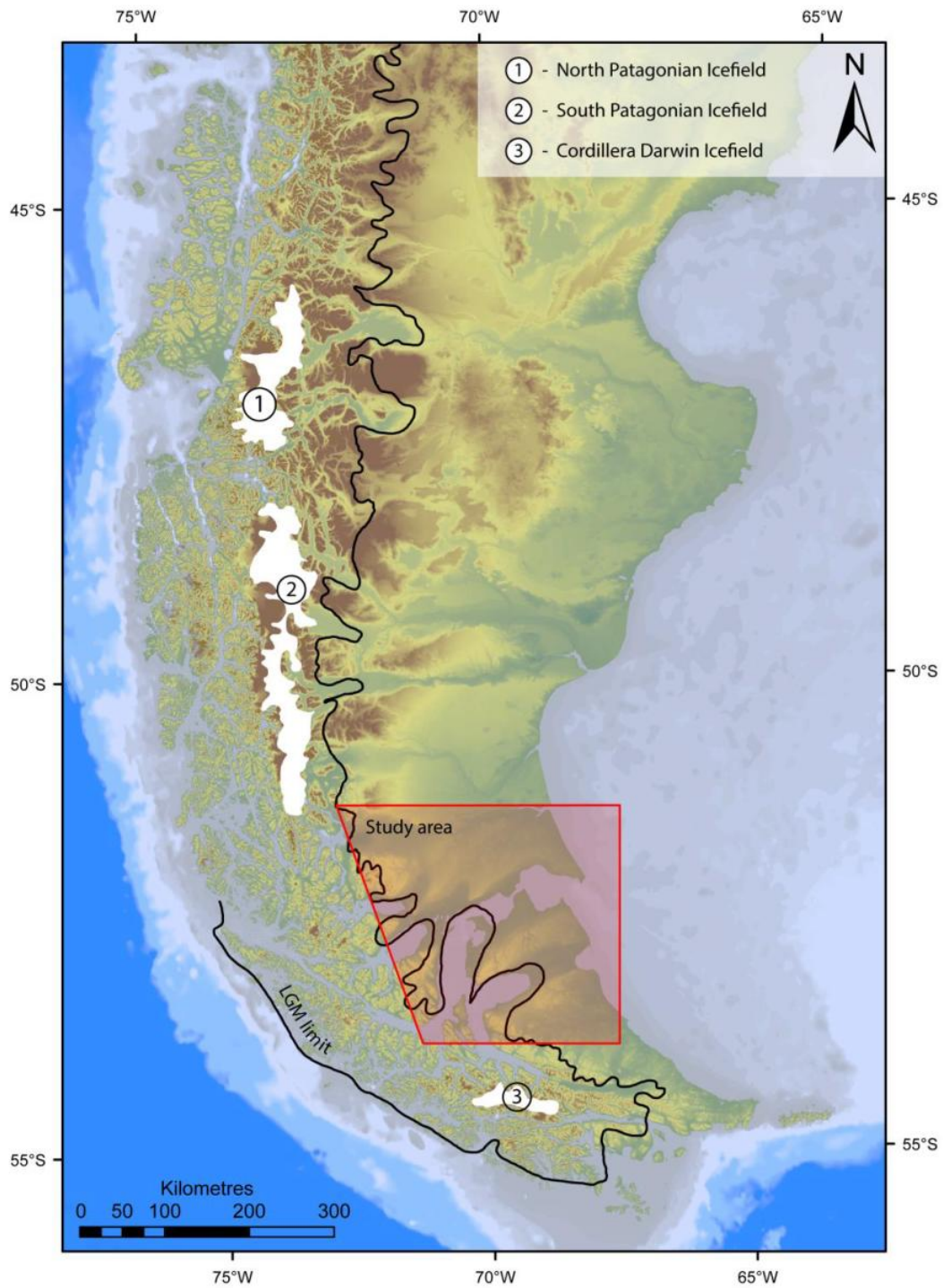
Figure 3.1. Location of the study area in southernmost Patagonia (topography shown using shaded SRTM and ETOPO data). Also shown are the present day icefields (numbered) and the Last Glacial Maximum (gLGM) limit according to Caldenius (1932); adapted from Singer *et al.* (2004a).

3.1.1   Study Area and Previous Work

3.1.1.1   Previous Mapping

This mapping focuses on an area into which the five southernmost ice lobes (the BI-SSb, Magellan, Otway, Skyring and Río Gallegos lobes; Figure 3.2) advanced from the main Patagonian Ice Sheet. Previous work suggests that these lobes were substantially more extensive compared to others in Patagonia (Caldenius, 1932). Early work by Nordenskjöld (1899) and Bonarelli (1917) suggested that Patagonia had been previously glaciated – possibly several times – but it was the seminal work of Caldenius (1932) that first extensively mapped the glacial geomorphology of the region and suggested that several different stages of glaciation were recorded by the nested nature of the geomorphological limits.

Subsequently, there have been several studies that have built upon this early mapping. Raedecke (1978) produced a geomorphological map of the Chilean side of the BI-SSb lobe. It highlighted the complex nature of the geomorphology, describing thrust and *en echelon* moraines as well as bands of drift deposits, but the extent of mapping was limited to the central depression of the BI-SSb lobe. In contrast, Meglioli (1992) mapped the surface features of the southernmost ice lobes at a much broader scale. The study focussed on drift and soil characterisation rather than glacial landforms, resulting in a map which could be considered a representation of surficial properties, rather than depicting glacial landforms. Nonetheless, this work established the current conceptual model for the pattern and timing of glaciations in the region using both relative and absolute dating techniques (Figure 3.2) and was summarised in Coronato *et al.* (2004). More recently, Glasser & Jansson (2008) produced an extensive geomorphological map of the whole Patagonian region. However, the nature of such large-scale mapping meant that the resolution was necessarily coarse and some of the subtle complexity in the geomorphology of individual ice lobes was not recorded.

In contrast to Glasser & Jansson's (2008) map, small regions of the hypothesised gLGM geomorphology in the study area have been mapped in detail by Clapperton *et al.* (1995), McCulloch & Bentley (1998), Benn & Clapperton (2000b), Bentley *et al.* (2005) and Sagredo *et al.* (2011). Bujalesky *et al.* (2001) also mapped an area of older glaciofluvial fans to the south of Bahía San Sebastián and Coronato *et al.* described the geomorphology surrounding the Aike maar, east of the Río Gallegos lobe. Additionally, Ercolano *et al.* (2004) described a drumlinised area within the Río Gallegos valley of the Río Gallegos lobe.

Lovell *et al.* (2011) produced a map of the glacial geomorphology within the Otway and Skyring lobes region (area shown in Figure 3.3). It was the most detailed map produced of the area and was subsequently used to interpret the glacial dynamics of the ice lobes, including surge-like advances and the development of pro-glacial lakes during retreat (Lovell *et al.*, 2012).
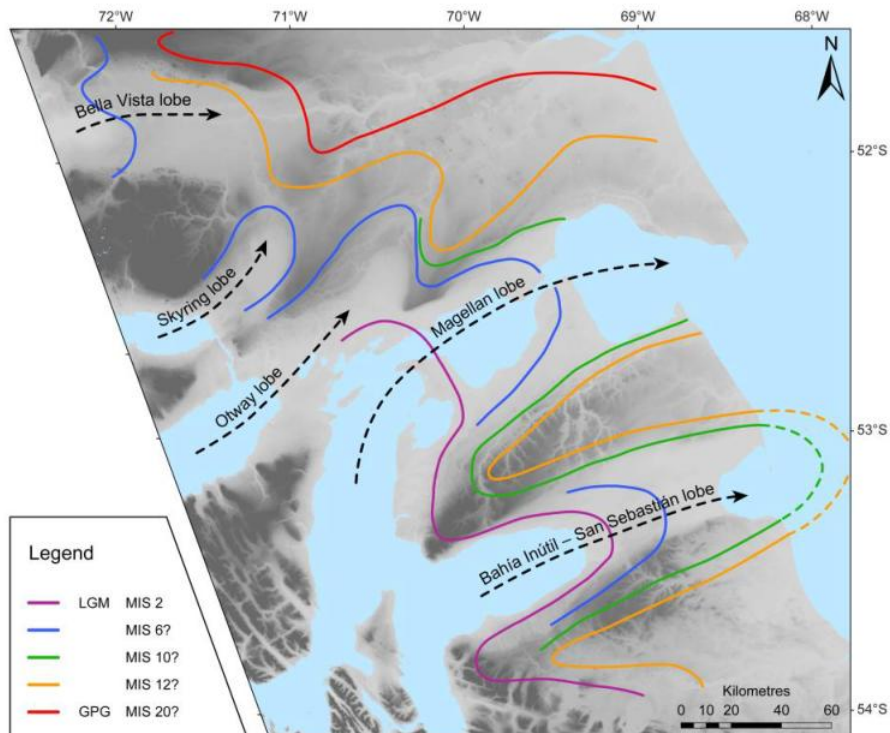
Figure 3.2. The location and previously hypothesised Marine Isotope Stage (MIS) chronology of drift limits within the study area (Meglioli, 1992; Rabassa *et al.*, 2000; Singer *et al.*, 2004a).
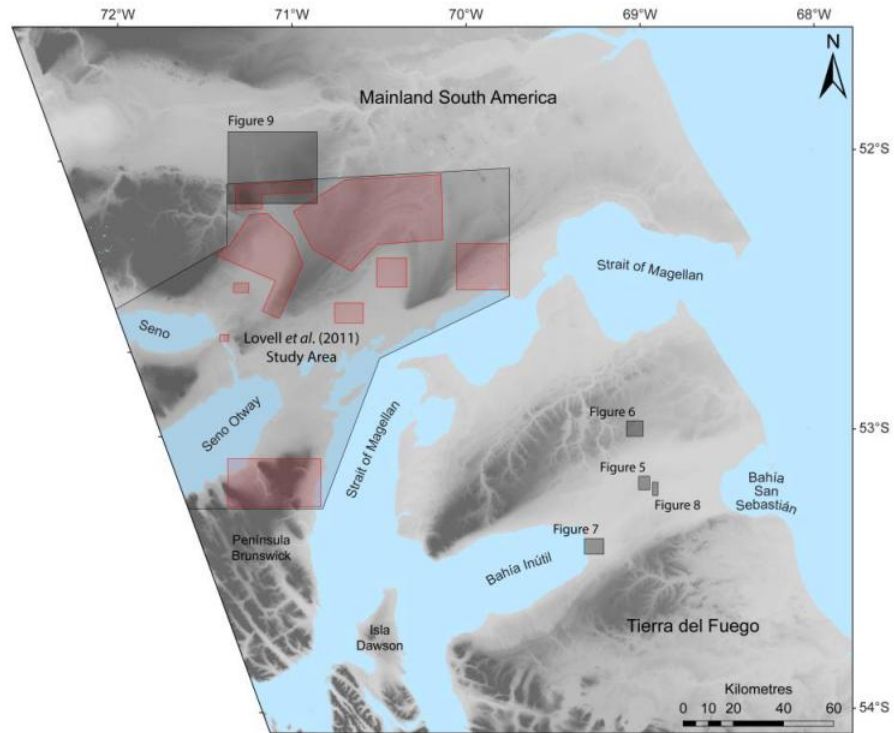
Figure 3.3. Overview of the study area showing the locations of other figures. Also shown is the area mapped by Lovell *et al.* (2011), with red boxes highlighting the key areas that have been updated.

3.2 Map production

The map was produced using a combination of remote sensing analysis and field-checking, with multiple types (and resolutions) of imagery consulted to provide a rigorous interpretation of the glacial geomorphology (Figure 3.4). The central BI-SSb area is shown in an enlarged inset to help improve the clarity of the geomorphology in this lobe, which is substantially more complex than in the other lobes. A copy of this map can be found in the Appendix.

3.2.1 Imagery

Across the region, Landsat ETM+ scenes from the Global Land Cover Facility (GLFC; http://www.landcover.org) were used for mapping. These cover an area of 185 × 185 km and have a spatial resolution of 30 m (or 15 m in band 8). Landsat imagery was supplemented by Google Earth™ imagery (version 7, available from http://www.earth.google.com), consisting of 2013 Cnes/SPOT images and 2013 DigitalGlobe images (up to ~5-15 m resolution). ASTER images from the NASA

Land Processes Distributed Active Archive Centre (http://lpdaac.usgs.gov) were also used. These cover an area of 60 × 60 km, with a spatial resolution of 15 m.

Aerial photographs were used in preference to satellite imagery, where available, and revealed significant complexity that had been missed from some previous maps. A total of 76 vertical aerial photographs were used (12 digital with ~5 m resolution; and 64 scanned hard copies with ~8 m resolution; both from the Servicio Aerofotométrico del la Fuerza Aérea de Chile; Figure 3.4). Where aerial photographs were not available, Google Earth™ often provided imagery of only slightly lower resolution.

Shuttle Radar Topographic Mission (SRTM) data (3 arcsec data, 90 m resolution) from the GLFC depository were used to identify some features only visible as subtle changes in topography and to provide topographic context as a shaded relief greyscale background to the map.

Field seasons during 2012 and 2013 allowed cross-checking of features mapped from remote imagery, although it was not possible to cover the entire area in detail (~80,000 km^2) so fieldwork focused on key mapping elements (Figure 3.4).

The study area includes an area around Seno Skyring and Seno Otway that was previously mapped by Lovell *et al.* (2011; Figure 3.3), and their mapping is included and updated here for two reasons. Firstly, not doing so would leave a large gap in the final geomorphological map, making it difficult to assess the complete geomorphology across the region. Similar mapping criteria and styles have been adopted here as in Lovell *et al.* (2011) to maintain consistency across the entire area. Secondly, extensive field-seasons in 2012 and 2013 have allowed field-checking of the previous work for the first time, and we have updated the mapping based on this (Figure 3.3).
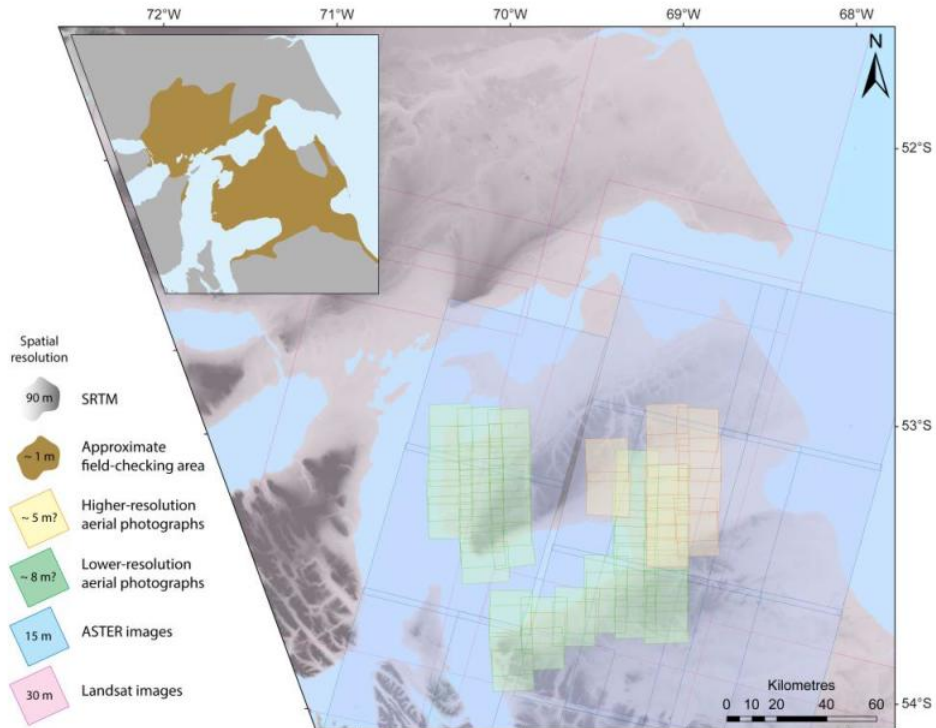
Figure 3.4. The spatial coverage of different imagery used during mapping. Inset shows the approximate area in which field-checking was conducted. Spatial (pixel) resolution of the different imagery is given in the key.

Table 3.1. Summary of the morphology, appearance and possible errors in mapping geomorphological features. The visibility of features on different imagery is also indicated: plus signs mean that features are normally visible; minus signs mean that features may sometimes be visible; and no sign indicates that features are not normally visible on the imagery.

Landform	Identification criteria			Visibility Incr. resolution →					
	Morphology	Appearance	Uncertainties	SRTM	Landsat	ASTER	Aerial scans	Aerial photos	Field
Moraine ridges	Distinctive linear or curvilinear ridges deposited at the ice margin or in medial positions.	Arcuate ridges of positive relief (indicated by darker/lighter shading on opposing sides). Often, following the direction of fragmentary ridges leads to the identification of further features.	Medial moraines could have been missed as they would be particularly difficult to identify under these criteria. Ridges and shorelines could potentially be confused. Often only visible in aerial photos.	-	-	-	+	+	+
Subdued moraine topography	Similar to ridges but much wider and with lower elevations, and break-of-slope not as clear.	Subtle changes in topography, with or without change in surface texture, which may be overprinted by more distinct features. Sometimes visible in the field and on SRTM data, very occasionally visible on aerial photographs or Landsat imagery.	Almost certainly missed where ground-truthing was not possible or where they were not visible on SRTM. Difficult to pick-out on the ground and very difficult to identify from imagery.	-	-		-	-	+
Kettle-kame topography	Large belts consisting of disorganised hills and hollows.	Distinctive areas with a pock-marked appearance, consisting of hills and sometimes small lakes. May contain ridges.	Can become discontinuous in lower areas associated with outwash. Sometimes difficult to distinguish drift from terrain that has simply avoided meltwater. Texture can vary significantly (with the presence of kettle lakes, the shape of hills).	-	+	+	+	+	-
Glacial lineations	Linear, parallel landforms aligned to the direction of ice-flow.	Linear features following the inferred direction of ice-flow and generally perpendicular to moraines, often occurring in groups. Not specifically associated with breaks in vegetation and often appear dark on one side and light on the other, indicating positive relief.	Can be short and consequently difficult to identify, even on aerial photos (often invisible on Landsat/ASTER). Fence lines could be mistaken for lineations, and the features are often disrupted by small lakes or (melt)water drainage.		-	-	+	+	-
Irregular hummocky terrain	Areas of small, disorganised hills.	Subtle patches of hills showing no obvious order and only visible in aerial photography.	Only visible on aerial photographs, and therefore could have been missed in areas with no coverage. The boundaries of the hummocky areas can be difficult to discern.				-	+	+

	Description	Appearance in imagery	Difficulties						
Regular hummocky terrain	Groups of small hills, elongated into small ridges and mirroring patches of small moraine ridges.	Extremely subtle and only visible on high-resolution aerial photography. 'Order' is in the apparent form of several hummocks joined into a small ridge. These very short ridges are difficult to discern in the field without the aid of the aerial photography.	Will be missed in areas not covered by high-resolution aerial photography. The organised nature frequently becomes apparent only once numerous ridges have been mapped.					-	+
Irregular dissected ridges	Groups of larger hills or constrained areas of higher relief, sometimes delineated by minor meltwater channels.	Patches of raised topography, often marked by changes in surface texture or vegetation. Sometimes show a mosaic-like pattern, divided by meltwater channels.	Drainage can sometimes give the illusion of ridges. Actual changes in topography are often difficult to see in imagery, so identification can become over-reliant on vegetation changes.	+	+	-	-	-	
Eskers	Sinuous ridges, generally running sub-parallel to former ice flow.	Sinuous ridges showing a change in colour due to the shadowing caused by positive relief.	Difficult to identify. Moraine ridges, lineations (especially when deformed) or meltwater channels could be mistaken for eskers.			-	-	-	-
Meltwater channels	Channels formed by large amounts of water from melting ice, often not containing contemporary drainage.	Generally sinuous in form and often occurring in combination with moraine ridges, running against contemporary slope. Frequently do not follow modern drainage routes or contain modern drainage, though this is not universal.	Often filled with contemporary drainage even though fieldwork has demonstrated they are over-sized and were once filled with – or created by – meltwater.	-	-	-	+	+	-
Former shorelines	Raised terraces marking the previous level of a body of water (either sea-level or a lake).	Normally parallel to the coast or an area occupied by a lake and forming concentric lines without relief on one side (shown by shading). Shoreline level is either flat or grades evenly along its length.	Often discontinuous and may become difficult to see when their direction changes, particularly in satellite imagery. May be missed where the location of a palaeo-lake is unknown, and difficult to distinguish from moraine ridges.	-	-	-	-	-	
Outwash plains	Large areas of material deposited by meltwater in a flattened, grading plain.	Large, open, approximately flat surfaces, grading to a previous ice limit (marked by moraine ridges, drift, etc), and often dissected by meltwater channels. Generally distinguished by a clear block change in colour and texture on Landsat imagery.	Exact limits of outwash are often difficult to define. Surface grading is often only apparent in the field or over large distances on SRTM. Often form narrow corridors, so can be difficult to distinguish from channels.	+	-	+	+	+	
Lakes	Bodies of water surrounded by land (with no link to the sea).	Blue, black or white in colour imagery; white or black in monochrome. Clearly delimited areas often linked to local drainage. Where transient, can show eastward migration patterns linked to westerly winds.	Not always obvious in aerial photos (a counterpart photo is sometimes necessary). Extent of many lakes is very seasonally variable – so their size can vary in different imagery and in the field.	+	+	+	+	+	
Volcanic craters	Hollows formed by volcanic eruptions.	Rounded or elliptical and generally creating linear fields.	Unlikely to be mistaken for glacial geomorphology.	-	+	+	+	+	-

3.2.2   Geomorphological mapping

In total, eleven different glacial features were mapped as line and/or polygon symbols using ArcMap 10 software: moraine ridges, subdued moraine topography, kettle-kame topography, glacial lineations, irregular hummocky terrain, regular hummocky terrain, irregular dissected ridges, eskers, meltwater channels, former shorelines, and outwash plains. Lakes and prominent volcanic craters were also mapped to provide landscape context and because these systems have been used in previous dating studies in the region.

3.3   Glacial geomorphology

The glacial geomorphological features mapped in this study are summarised in Table 3.1 in terms of their morphology, appearance and any uncertainties in their identification.

3.3.1   Moraine ridges

Moraine ridges are linear or curvilinear, elongate features exhibiting positive relief. They may be level-crested or undulating, continuous or fragmentary, but are distinguished by their linearity and consistency with formerly expanded ice margins. In places, they may overprint lineations (Section 3.3.4) and subdued moraine topography (Section 3.3.2; Figure 3.5), and can coincide with areas of kettle-kame topography (Section 3.3.3) and irregular hummocky terrain (Section 3.3.5). Ridges are often discontinuous, and it is rare to find complete lateral-terminal moraine systems, with the exception of the Otway lobe, where continuous ridges run for tens of kilometres. These features range from small, fragmentary crested ridges, often up to a few hundred metres long and less than 10 metres high (only visible on aerial photography and in the field in the BI-SSb and Magellan lobes; Figure 3.5), up to larger, continuous or semi-continuous hilly ridges, which are up to tens of kilometres long and tens of metres high, such as those delineating the Skyring and Otway lobes.

Much of what Glasser & Jansson (2008) mapped as moraine ridges in the BI-SSb and Magellan lobes, we map as hummocky terrain or kettle-kame topography because they form wide areas of hilly terrain rather than narrow elongate ridges. This is likely due to a difference in mapping criteria and resolution of imagery used, which may also help explain differences in mapping between Glasser & Jansson (2008) and Lovell *et al.* (2011). There is generally good agreement between our mapping and that of Clapperton (1995), McCulloch & Bentley (1998), Benn &

Clapperton (2000b), Bentley *et al.* (2005) and Coronato *et al.* (2013) who all worked at a higher spatial resolution.

3.3.2   Subdued moraine topography

These are somewhat elusive features, occurring mainly in the BI-SSb lobe, but also in the Río Gallegos lobe. They exist as subtle changes in relief, generally not more than 10 metres high and up to a kilometre wide, which are parallel to the orientation of moraine ridges. The features are distinguished as vegetation changes in some places on Landsat imagery and/or very low-relief changes on SRTM data and field-observations helped to confirm their existence. North of Laguna Larga, in the BI-SSb lobe, the moraines exhibit regular fragmentation (Figure 3.5).

The subdued moraines are significantly broader than moraine ridges and are not sharp-crested. Likewise, they are very low relief and low gradient, and are thus unlike hummocky terrain. It is suggested that both moraine ridges and hummocky terrain may be overprinted on the subdued moraines (Figure 3.5). These features do not seem to have been mapped previously.

3.3.3   Kettle-kame topography

Kettle-kame topography is common within the BI-SSb and Magellan lobes. Unlike moraine ridges, the drift constitutes wide bands (often > 2 km) of an irregular mixture of hills and hollows, some containing small kettle-lakes. The kame hills can be greater than 10 m high and rarely show any regularity in their arrangement. Other studies have depicted these deposits as moraine ridges (Clapperton *et al.*, 1995; McCulloch & Bentley, 1998; Bentley *et al.*, 2005; Glasser & Jansson, 2008), which is understandable given that the drift and ridges both record ice advance limits. However, we here follow Raedecke (1978) and Benn & Clapperton (2000b) in mapping the drift as a distinct feature given its clarity in imagery and on the ground. It is particularly prominent as two large, distinctive belts within the BI-SSb lobe (Figure 3.6), forming the Rio Cullen and San Sebastian drift limits of Meglioli (1992; previously mapped by Caldenius, 1932).
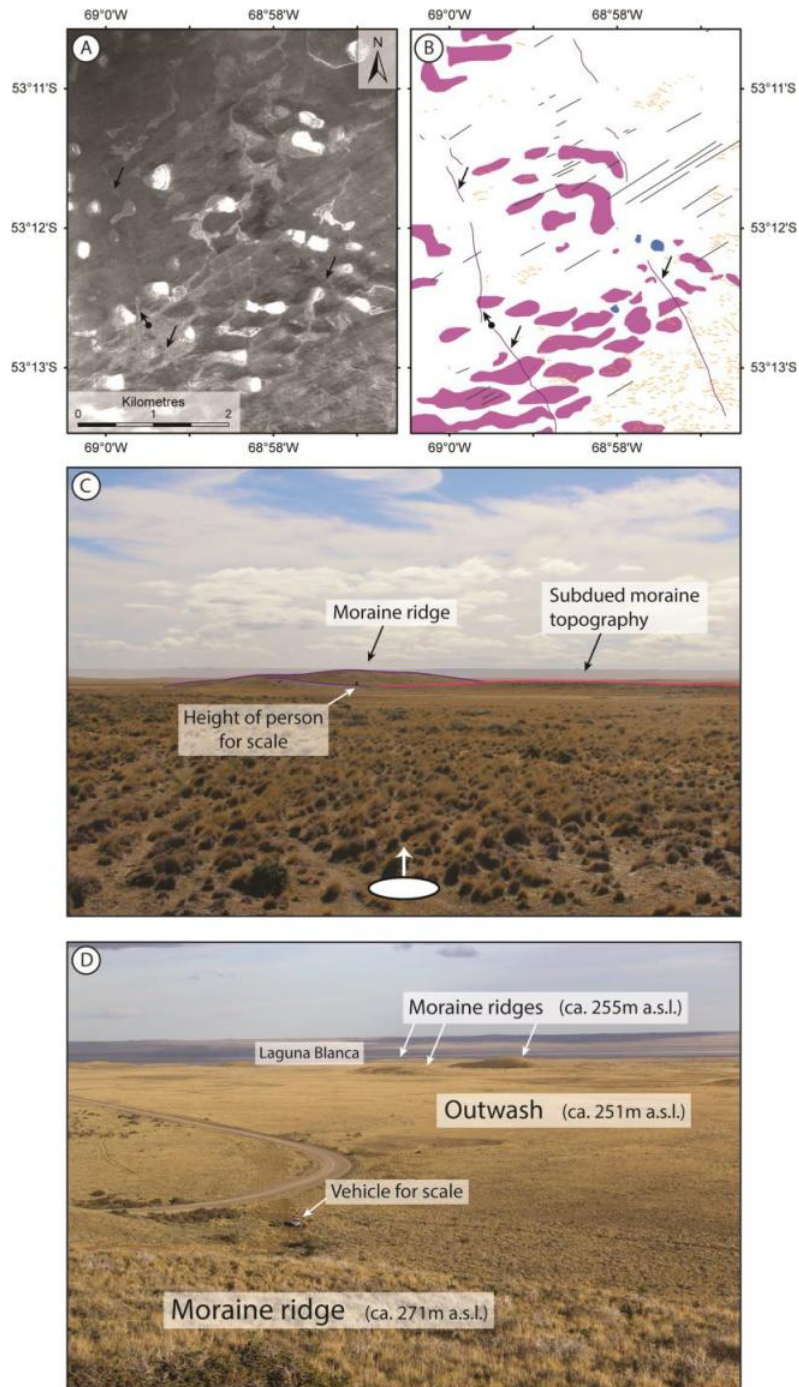
Figure 3.5. (A) Aerial photograph and (B) the mapped features in the central depression of the BI-SSb lobe. Thin, low moraine ridges (mapped as purple lines) are indicated by the black arrows and drape across the subdued moraine topography (mapped as pink polygons) and lineations (black lines). Locations shown in Figure 3.3. (C) Field photograph of one of these moraine ridges draped over subdued moraine topography; location shown in (A) and (B) by black circle with arrow. (D) Field photograph of the larger moraines in the Skyring lobe, separated by expansive outwash. Heights in metres above sea level (m.a.s.l.) are shown for the moraines and outwash plain.
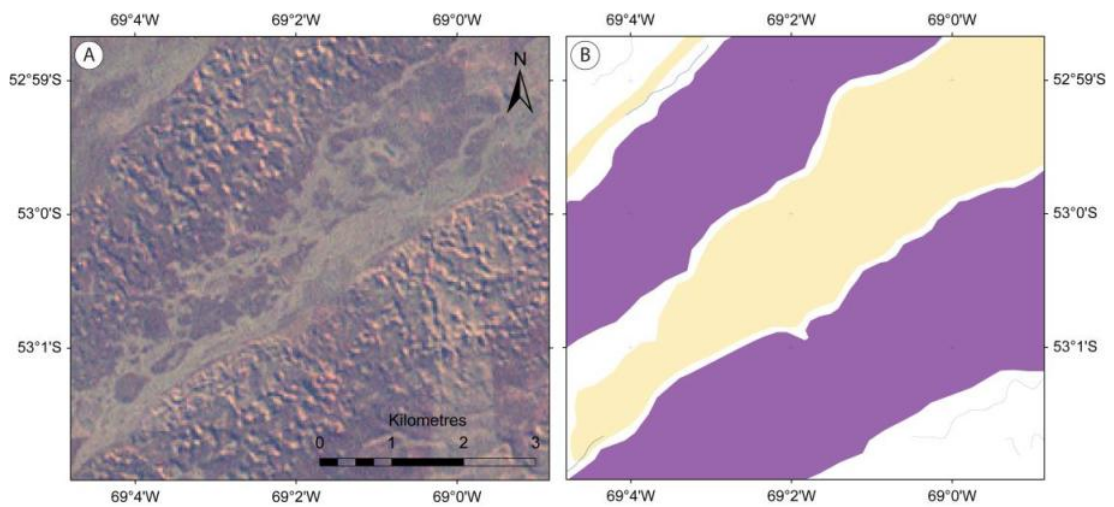
Figure 3.6. Kettle-kame topography on the northern edge of the BI-SSb lobe. (A) Landsat ETM+ (bands 4, 3, 1) showing the characteristic pock-marked appearance of the drift. (B) Mapped bands of drift (purple polygons), separated by outwash surfaces (yellow polygons). Location shown in Figure 3.3.

3.3.4 Glacial lineations

Glacial lineations form beneath an ice sheet and are aligned with ice flow direction (Clarhäll & Jansson, 2003). They occur frequently throughout the study area, from scattered and subdued flutings (< 1m high) to tightly constrained clusters of classic oval-shaped drumlins tens of metres high (Figure 3.7). Where the break of slope could be readily identified, lineations were mapped as polygons, but this was only possible in localised, well-defined drumlinised areas, centred around the Skyring and Otway lobes (Lovell *et al.*, 2011). Elsewhere, and particularly in the BI-SSb lobe, the lineations are mapped as lines.

Raedecke (1978), Benn & Clapperton (2000b), and Glasser & Jansson (2008) also mapped lineations but identified fewer features. For example, we map a significant number of lineations within the BI-SSb lobe, which overlie subdued moraine topography and are cross-cut by moraine ridges. Ercolano *et al.* (2004) noted a swath of elongated drumlins within the Río Gallegos lobe geomormorphology, but did not map them individually.

45
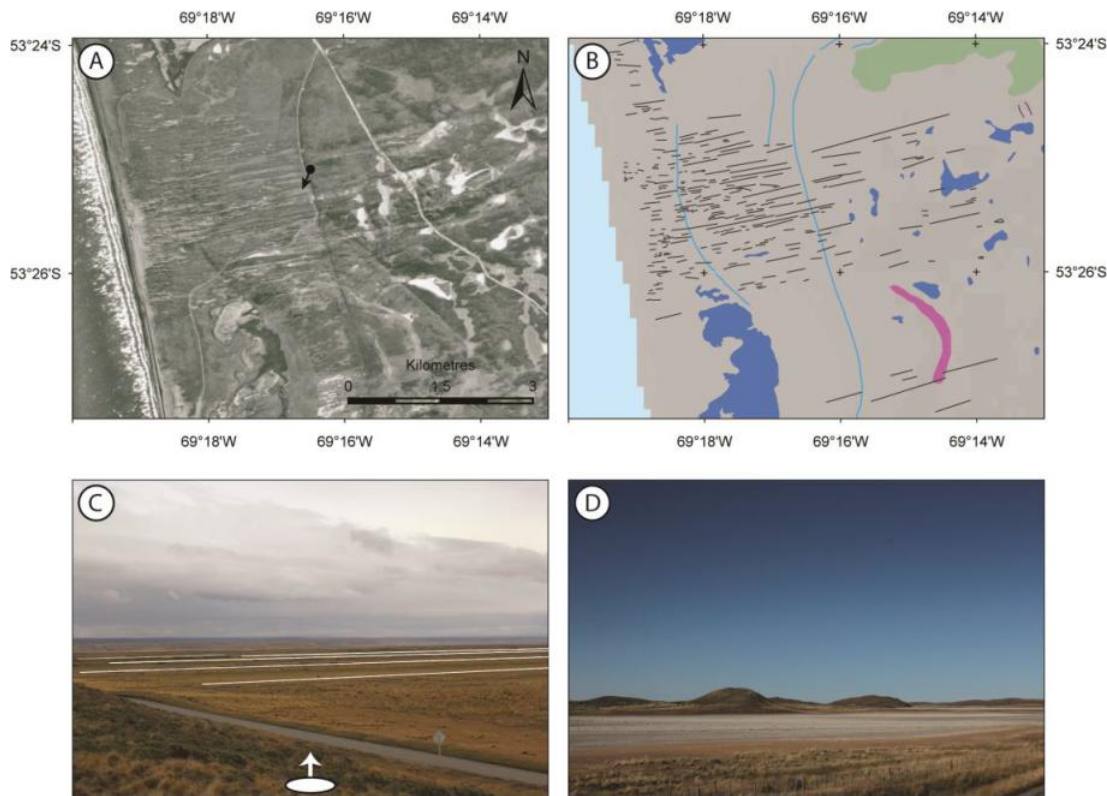
Figure 3.7. Glacial lineations in the study area. (A) Aerial photograph showing a tightly clustered field of low-relief flutings on the coast of Bahía Inútil and (B) the flutings mapped as black lines. Shorelines are also shown running parallel to the coast (light blue lines). The circle and arrow in (A) show the direction of the field photograph in (C), looking across the flutings which have been highlighted with white lines; locations shown in Figure 3.3. At the other end of the scale, (D) shows a field photograph of the much larger, sharp-crested drumlins in the Laguna Cabeza del Mar field of the Otway lobe (see map).

3.3.5   *Irregular hummocky terrain*

We present two forms of hummocky terrain in the study area (irregular and regular), and opt for this nomenclature rather than hummocky moraine (Lukas, 2005; Graham *et al.*, 2007; Lukas, 2007) or controlled moraine (Evans, 2009) to avoid genetic inference. In the field, the hummocky terrain appears as patches of small, semi-rounded hills, rarely more than five metres high (and often less) and ten metres across. Irregular hummocky terrain is significantly more extensive than the regular version (Section 3.3.6) and lacks an organised pattern (Figure 3.8). Raedecke (1978) mapped these features in some parts of the BI-SSb lobe as kettle-kame deposits, forming semi-lobate areas in the centre of the depression. We distinguish hummocky terrain from kettle-kame topography (Section 3.3.3) on the basis of a significant difference in scale, highlighted by the difference in visible resolution (Table 3.1) and a general lack of obvious kettle-holes. Similarly to Raedecke (1978),

46

we also mapped a semi-lobate pattern, and we also note that the feature is exclusive to the BI-SSb lobe.

3.3.6 Regular hummocky terrain

Regular hummocky terrain is rare in the study area and consists of two or three small interconnected hills, forming ridges transverse to ice-flow (Figure 3.8). These features are distinguished from irregular hummocky terrain on the basis of their ridge-like nature and clear orientation. They differ from moraine ridges because the interconnected hills are very short and discontinuous, not marking a clear ice-marginal limit. The main location of the features is north of Laguna Larga (Figure 3.8). It should be noted that both forms of hummocky terrain could only be mapped from aerial photographs, and may have been missed in areas where aerial photography was unavailable (Figure 3.4). This makes it difficult to ascertain whether the features are inherently related to the dynamics of the BI-SSb lobe, explaining its prevalence there, or whether this is due to differences in imagery coverage. This may also explain why these features have not been mapped previously.

3.3.7 Irregular dissected ridges

Lovell *et al.* (2011) mapped features to the north of the Skyring lobe which they described as irregular dissected ridges (IDR), similar to features mapped by Storrar & Stokes (2007) and Greenwood & Clark (2008). Lovell *et al.* (2011) noted that these features tend to be characterised by interweaving meltwater channels. This is clearly the case in some settings, but extended mapping of the IDR reveals that channels are not always present (Figure 3.9). Like the subdued moraine ridges (Section 3.3.2), the IDR are identifiable on Landsat and Google Earth™ imagery due to changes in vegetation, but their low relief means that, in the field, they are clearest where meltwater channels are cut between them.

Mapping of the Río Gallegos geomorphology highlights the presence of a large swath of lineations to the north of the IDR, oriented south-easterly, which were just beyond the mapping limit of Lovell *et al.* (2011). Consequently, it is now clear that the IDR sit in the junction between lineations of the Río Gallegos lobe and moraines of the Skyring lobe (Figure 3.9).

3.3.8 Esker

We found no further evidence of eskers in the study site beyond the one mapped by Clapperton (1989) and Lovell *et al.* (2011) to the north east of Laguna Cabeza del

Mar. In the field, this feature was consistent with the sinuous ridge-like form of an esker, but a lack of sedimentary exposures prevented further investigation.

3.3.9 Meltwater channels

A large number of meltwater channels are mapped in the study area. We identify these features as routes following previous ice-marginal positions, and sometimes flowing across the topographic slope, or issuing from a former ice margin and often – though not exclusively – containing no contemporary drainage. Some of these, particularly in northern Tierra del Fuego, are more than 600 m wide and contain narrow outwash corridors. It is suggested that much of the meltwater associated with the BI-SSb lobe occupied pre-existing drainage channels, probably re-shaping them to some degree. Throughout the study area, much of the contemporary drainage naturally follows the numerous larger meltwater channels, which do not exclusively run laterally, appearing as meandering mis-fit streams. Like Bentley *et al.* (2005), we also find that meltwater channels are clearer and better-preserved than much of the other geomorphology, often forming better indications of former ice-limits than moraines.

3.3.10 Former shorelines

Shorelines show a stepped, terrace-like change in relief and often run parallel to contemporary coastlines and lakes (Figure 3.7). Though roads or moraine ridges may be misidentified as shorelines from remote imagery, particularly where resolution is poor, they are generally clear in the field. In addition to shorelines within the Skyring lobe (Lovell *et al.*, 2011), further examples of this feature have been mapped within the Río Gallegos lobe and around the coast of Bahía Inútil, supporting previous mapping (Bentley *et al.*, 2005; Glasser & Jansson, 2008; Sagredo *et al.*, 2011).

3.3.11 Outwash plains

The eastern part of the study area is dominated by glaciofluvial outwash plains. These are expansive surfaces of sands and gravels which gently grade away from former ice limits. The plains are identifiable on Landsat imagery as smooth, featureless surfaces, often emerging from the downstream ends of large meltwater channels (Figure 3.6). Coronato *et al.* (2013) highlighted the presence of differing terrace levels in outwash associated with the Río Gallegos lobe, and our fieldwork suggests that similar terraces, indicating multiple stages of outwash development, exist in parts of all four other lobes. However, given the difficulty in mapping different

outwash terraces from imagery, the features have been mapped as single units. This has the benefit of simplifying the representation of outwash, but should be taken into consideration when using the mapping to reconstruct glacial history. Where clear meltwater channels can be identified within the outwash, these have been mapped separately.
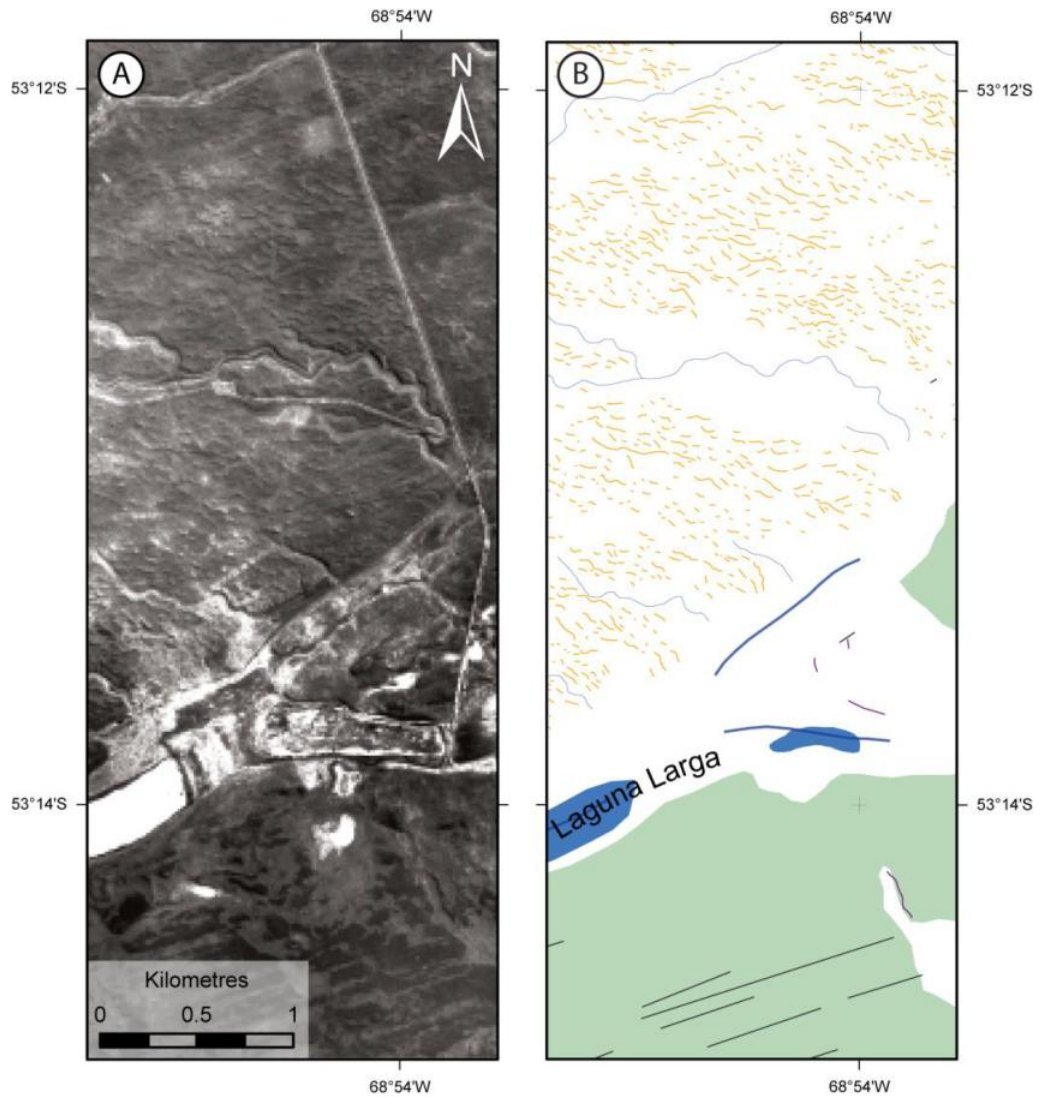
Figure 3.8. (A) Aerial photograph and (B) mapped equivalent of the regular (yellow lines) and irregular (green polygons) hummocky terrain. Due to their ordered-nature and visibility on higher resolution aerial photographs, the regular hummocky terrain can be mapped as individual line features rather than grouped polygons. Location shown in Figure 3.3.
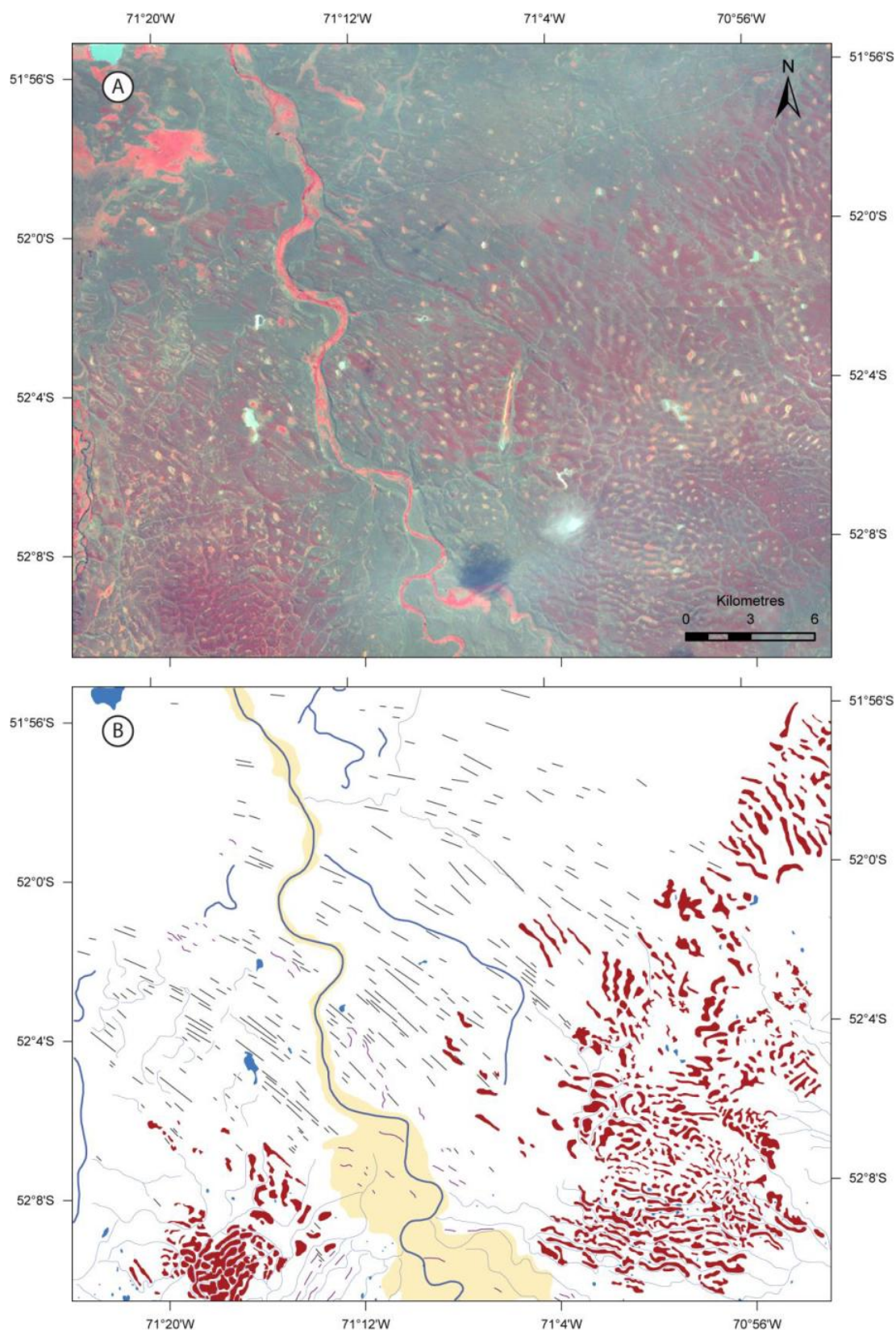
Figure 3.9. (A) Landsat ETM+ image (bands 4, 3, 1) and (B) mapped equivalent showing the intersection between lineations (black lines) and irregular dissected ridges (brown polygons) between the Skyring (to the south) and Río Gallegos (to the north and west) lobes. Also shown are moraine ridges as purple lines, meltwater channels as blue lines and outwash as yellow polygons. Location shown in Figure 3.3.

50

3.4 Summary and conclusions

This paper presents a new, comprehensive map of unprecedented detail of the glacial geomorphology in an area once covered by the five southernmost ice lobes of the former Patagonian Ice Sheet. Mapped features include moraine ridges, subdued moraine topography, kettle-kame topography, glacial lineations, irregular hummocky terrain, regular hummocky terrain, irregular dissected ridges, an esker, meltwater channels, former shorelines, and outwash plains, many of which have not been previously recorded. This map will underpin further work on the glacial history of the ice lobes and will provide the necessary context for robust dating of the glacial limits. It also provides a useful test for numerical ice-sheet modelling in the region.

Preliminary conclusions highlight three important characteristics of the glacial geomorphology:

1. The glacial geomorphology is dominated by landforms associated with meltwater (channels and outwash plains) and possibly indicative of deposition in a slow-moving or stagnant outlet (kettle-kame topography and hummocky terrain). This contrasts with discrete areas of large, well-defined lineations within the inner reaches of the Magellan and Otway lobes, hypothesised to result from more active ice-streaming (Lovell *et al.*, 2012).
2. Moraines to the north differ markedly from those to the south. In the Otway, Skyring and Río Gallegos lobes, limits are generally marked by numerous clear moraine ridges, which are continuous or semi-continuous and relatively sharp-crested. By contrast, the BI-SSb and Magellan lobes are characterised and delimited by hummocky terrain and kettle-kame topography.
3. Cross-cutting landforms offer clear evidence of multiple advances in places, which may have implications for the timing of limit deposition, and thus the dating programme. This is clearest in the BI-SSb lobe, where lineations and moraine ridges overlie and cross-cut subdued moraine topography; indicating at least two stages of advance at that location.

3.5 Software

Image processing and mapping was carried out using ESRI ArcMap 10. Some image processing, such as layer-stacking and mosaicking, was conducted using ERDAS Imagine 9.3. The final geomorphological map was produced in Adobe Illustrator CS4.

Chapter 4.   Geomorphology and weathering characteristics of Erratic Boulder Trains on Tierra del Fuego, southernmost South America: Implications for dating of glacial deposits

Abstract

Erratic boulder trains (EBTs) are a useful glacial geomorphological feature because they reveal former ice flow trajectories and can be targeted for cosmogenic nuclide exposure dating. However, understanding how they are transported and deposited is important because this has implications for palaeoglaciological reconstructions and the pre-exposure and/or erosion of the boulders. In this study, we review previous work on EBTs, which indicates that they may form subglacially or supraglacially but that large angular boulders transported long distances generally reflect supraglacial transport. We then report detailed observations of EBTs from Tierra del Fuego, southernmost South America, where their characteristics provide a useful framework for the interpretation of previously published cosmogenic nuclide exposure dates. We present the first comprehensive map of the EBTs and analyse their spatial distribution, size, and physical appearance. Results suggest that they were produced by one or more supraglacial rock avalanches in the Cordillera Darwin and were then transported supraglacially for 100s of kilometres before being deposited. Rock surface weathering analysis shows no significant difference in the weathering characteristics of a sequence of EBTs, previously hypothesized to be of significantly different age (i.e., different glacial cycles). We interpret this to indicate that the EBTs are much closer in age than previous work has implied. This emphasises the importance of understanding EBT formation when using them for cosmogenic nuclide exposure dating.

4.1 Introduction

Erratic boulder trains (EBTs) are a poorly understood glacial geomorphological feature. These linear clusters of erratic boulders record the flow lines of former glaciers by pinpointing the parent rock from which they have originated (Kujansuu & Saarnisto, 1990; Evans, 2007) and have frequently been targeted for cosmogenic nuclide exposure dating (Jackson *et al.*, 1997; Jackson *et al.*, 1999; McCulloch *et al.*, 2005b; Kaplan *et al.*, 2007; Ward *et al.*, 2007; Kaplan *et al.*, 2008a; Evenson *et al.*, 2009; Vincent *et al.*, 2010; Wilson *et al.*, 2012). Consequently, they offer a valuable tool for reconstructing the nature and timing of former glacial advances.

Despite their importance to palaeoglaciology, these features are rarely reported in detail, and understanding their formation will help contextualise dating studies. This paper brings together previous literature on EBTs to assess how they form and presents detailed observations of examples from Tierra del Fuego, southernmost South America. The Tierra del Fuego EBTs make an excellent case study because they are well preserved and easily distinguishable. They have also been investigated using cosmogenic nuclide exposure dating, but the resultant ages can be interpreted in two quite different ways (McCulloch *et al.*, 2005b; Kaplan *et al.*, 2007; Evenson *et al.*, 2009). This study aims to test between these two opposing hypotheses by combining spatial and volumetric measurements with weathering proxies to gain a better understanding of EBT formation. In this way, we test the interpretation of cosmogenic nuclide exposure dates.

4.2 Definition and previous work on erratic boulder trains

The EBTs are a subset of dispersal trains, which includes any dispersal of a particular lithology by former ice flow (DiLabio, 1981; Dyke & Morris, 1988; DiLabio, 1990; Evans, 2007). However, whilst EBTs are linear clusters of boulders, other dispersal trains are not necessarily linear or clustered and can include a wide range of grain sizes: surficial and within glacial deposits. Given the lack of any previous compilation in the literature, we begin by providing a brief review of the limited number of detailed studies of EBTs, summarised in Figure 4.1 and Table 4.1, focusing on their formation and dating. It is likely that other EBTs exist, but they are rarely reported in the literature and are often only given cursory mention in wider studies.

Table 4.1. Summary of the key characteristics of EBTs based on a review of the literature (NR = Not Reported).

EBT name	Location	Length of train(s)	Max. distance from source	Boulder diameter	Lithology	Suggested transport pathway	CNE dated?	Age	References
Foothills	Canada	> 580 km	>580 km	1 - 41 m	Quartzite and pebbly quartzite	Supraglacial	^{36}Cl	18 - 12 ka	Stalker (1956); Mountjoy (1958); Stalker (1976); Jackson *et al.* (1997); Jackson *et al.* (1999); Jackson & Little (2004)
Athabasca valley	Canada	*ca.* 70 km	*ca.* 120 km	Up to 1 m	Metamorphic schist	Supraglacial	-	-	Roed *et al.* (1967)
Ruby Range	Canada	*ca.* 5 km	*ca.* 5 km	Some > 1.5 m	NR	NR	^{10}Be	54 - 51 ka	Ward *et al.* (2007)
Snake Butte	USA	*ca.* 79 km	*ca.* 80 km	Up to 23 m	Shonkinite	Subglacial?	-	-	Knechtel (1942)
Assynt	Scotland	9 - 14 km (4 trains)	>9 km	NR	Sandstone	NR	-	-	Lawson (1990); Lawson (1995)
Norber	England	> 1 km	>1 km	Up to 4 m	Greywacke	Likely subglacial over a short distance	^{36}Cl	22 - 17 ka	Davis (1880); Goldie (2005); Huddart (2002); Vincent *et al.* (2010); Wilson *et al.* (2012)
Foxdale	Isle of Man	Up to 1 km	≤2 km	Up to 1 m	Granite	Subglacial	-	-	Roberts *et al.* (2007); Roberts (*pers. comm.*)
Bunger Hills	Antarctica	Up to 4 km?	≤4 km	NR	Dolerite	Subglacial but only a short distance	-	-	Adamson & Colhoun (1992); Augustinus *et al.* (1997)
Allan Hills	Antarctica	Up to 3km?	≤3 km	Up to 3 m	Sandstone	Subglacial	-	-	Atkins *et al.* (2002)
Monolith Lake	Antarctica	*ca.* 9 km	*ca.* 12 km	Up to 5 m	Hyaloclastite	Likely supraglacial	-	-	Davies *et al.* (2013)
Tierra del Fuego	Chile / Argentina	4 - 15 km (4 trains) 95 km total	*ca.* 250 km	Up to 21 m	Granodiorite	Supraglacial	^{10}Be ^{26}Al ^{36}Cl	222 - 15 ka	Darwin (1841); Meglioli (1992); Coronato (1999); Bentley *et al.* (2005); McCulloch *et al.* (2005b); Kaplan *et al.* (2007); Kaplan *et al.* (2008a); Evenson *et al.* (2009); This study
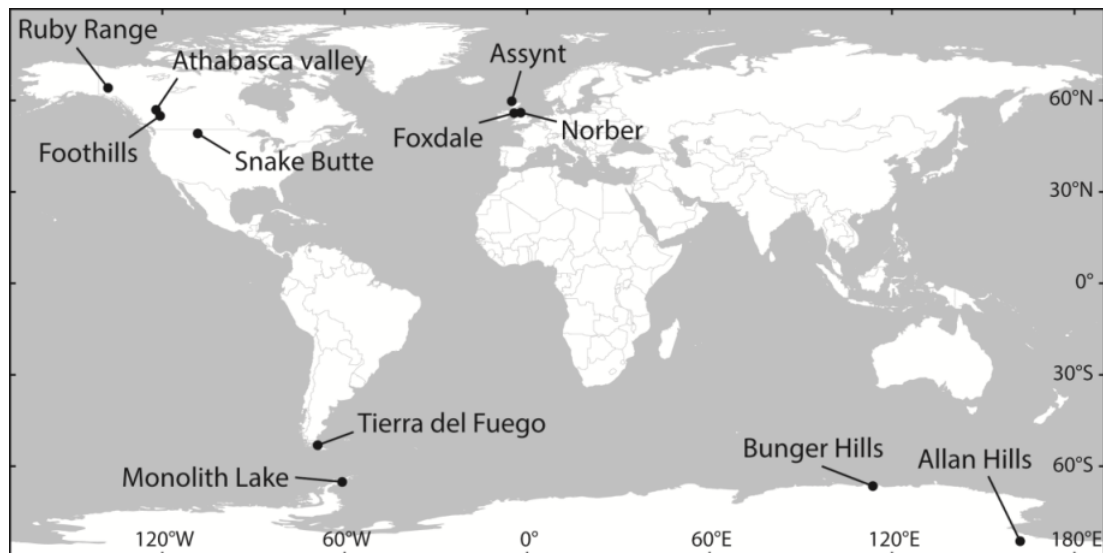
Figure 4.1. Map showing the locations of erratic boulder trains reviewed in this paper (see Section 4.2).

4.2.1 Formation: subglacial versus supraglacial

No single model for the formation of EBTs exists, and it is possible that they can be formed in a variety of ways. This is not surprising given the reported variety in boulder size, train length, number of boulders, transport distance, and lithology (Table 4.1). Two hypotheses prevail: (i) subglacial entrainment and (ii) supraglacial debris.

The Norber EBT in England, Foxdale EBTs on the Isle of Man, Bunger Hills EBT and Allan Hills EBT in Antarctica, and Snake Butte EBT in the USA (see Figure 4.1 and Table 4.1) are all interpreted to have formed subglacially. The Norber boulders have been transported laterally more than 1 km and 120 m vertically upward from their source lithology (Huddart, 2002; Wilson *et al.*, 2012). Given that the ice flowed over the source outcrop (Vincent *et al.*, 2010), we suggest that subglacial transport of the boulders is most probable (although the formation mechanism has not been investigated further). The two Foxdale boulder trains were interpreted to have been initially transported and deposited subglacially by ice flowing southeastward, but with subsequent ice flowing southwestward and dispersing the larger train subglacially across a broader area of the southern part of the island (Roberts *et al.*, 2007). In the Bunger Hills, Augustinus *et al.* (1997) suggested that a lack of glacial polish or facetting on the boulders implied subglacial transport over only a very short distance, thereby explaining the limited extent of the EBT. Likewise, Atkins *et al.* (2002) considered the boulders of the Allan Hills EBT to have been eroded by

plucking of the Beacon sandstone bedrock prior to subglacial dragging and deposition on the stoss side of a bedrock ridge. Knechtel (1942) suggested that striations and polished surfaces of boulders of the Snake Butte EBT resulted from transport at the base of ice flowing southeastward and that they were then deposited with ground moraine.

In contrast, the Foothills EBT and Athabasca Valley EBT in Canada, Monolith Lake EBT in Antarctica, and Tierra del Fuego EBTs in Chile/Argentina, are all suggested to have formed from material being deposited onto ice and then transported supraglacially. The Foothills boulder train formed in a medial ice position as two lobes converged around a nunatak and show no signs of subglacial transport (Jackson & Little, 2004). Similarly, the friable nature of the Monolith Lake boulders means that they are only likely to have survived if transported supraglacially (Davies *et al.*, 2013). Meglioli (1992), Bentley *et al.* (2005), McCulloch *et al.* (2005b), and Evenson *et al.* (2009) all noted the tight distribution, large size, angularity, and monolithology of the boulders on Tierra del Fuego, which are unlikely to have survived subglacial erosion and are instead indicative of supraglacial transport (Evenson *et al.*, 2009).

The transport pathway has important implications for the likely exposure and depositional history of a boulder train. Few detailed studies of EBTs exist to be able to clearly define their formation based on physical characteristics. However, our synthesis of previously published data suggests an apparent trend between transport distance, boulder size, and the proposed transport pathway (Figure 4.2), with those moved greater distances (e.g. > ~10 km) more likely to have been transported supraglacially. The relationship with boulder size is unsurprising given the association between transport pathway and boulder erosion (Boulton, 1978), but it is important in the context of erratic dispersal more generally. For example, the principles of 'half-distance' transport (Salonen, 1986) and concentration peaks (DiLabio, 1981; 1990; Boulton, 1996) may better relate to subglacial EBTs, whereas supraglacial EBTs are also controlled by the maximum transport distance and the preservation potential of the boulders.
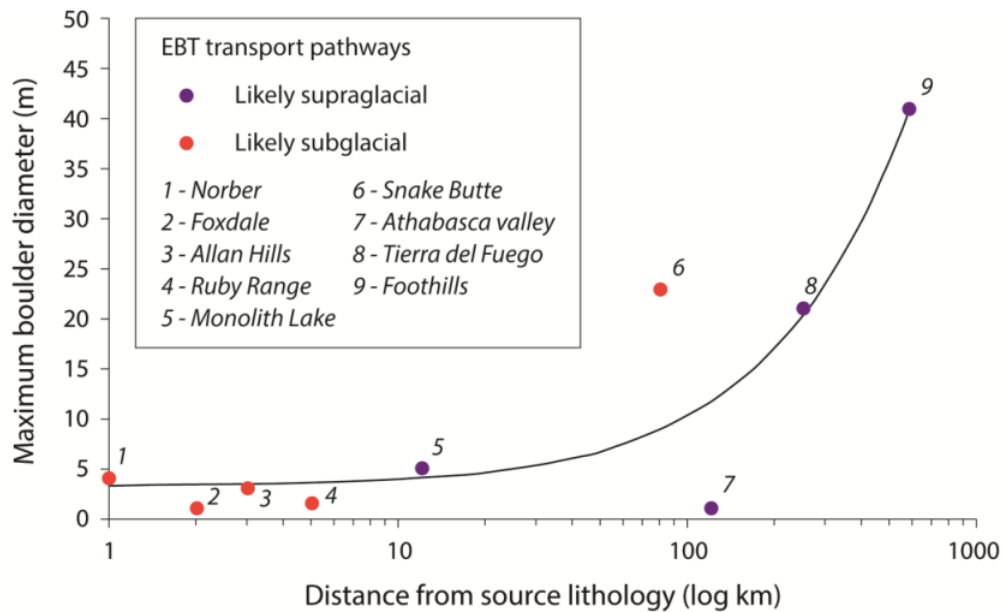
Figure 4.2. Maximum boulder diameter plotted against the maximum distance of boulders from their source lithology (note the log scale), as reported in studies of EBTs (labelled as per Table 4.1). Our review of the literature suggests that EBTs consisting of larger boulders (> 5 m) transported greater distances (> 10 km) are more likely to have been transported supraglacially. The Snake Butte EBT is an exception to this pattern; Knechtel (1942) inferred subglacial transport of these boulders. Of the reported studies, lithology does not appear to play a key role in determining the preservation of boulder trains through supraglacial or subglacial transport.

4.2.2 Cosmogenic nuclide exposure dating

The EBTs are useful targets for cosmogenic nuclide exposure dating, with the added benefit of being able to trace the source and transport pathway of the samples. The Foothills boulder train in Canada was dated using [36]Cl by Jackson *et al.* (1997; 1999), yielding dates of 18-12 ka and demonstrating the limits of the Laurentide Ice Sheet during its LGM. The dates implied a maximum transport time of *ca.* 3 ka (< 17% of the total exposure time; Jackson & Duk-Rodkin, 1996; Jackson *et al.*, 1997) and yielded one anomalously old age of *ca.* 53.3 ka, which Jackson *et al.* (1997) ascribed to pre-exposure.

The Norber boulder train in England was also dated to around 22-17 ka using [36]Cl, which helped establish the timing of deglaciation in the region (Vincent *et al.*, 2010; Wilson *et al.*, 2012). The [10]Be dates from the Ruby Range boulder train in Canada were clustered and suggested that the train was deposited during the penultimate glacial episode, with dates of 54-51 ka (Ward *et al.*, 2007). The authors suggested no significant influence of inheritance given that the same pre-exposure prior to deposition of all four samples is unlikely (Ward *et al.*, 2007), and subglacial transport

of the Norber and Ruby Range boulders may have removed any inheritance signal. Statistical modelling of supraglacial erosion and transport of boulders has also suggested that these processes can yield dateable inheritance signatures in erratic boulders (Applegate *et al.*, 2010; Heyman *et al.*, 2011; Applegate *et al.*, 2012).

As noted above, the Tierra del Fuego EBTs have been targeted for cosmogenic nuclide exposure dating (McCulloch *et al.*, 2005b; Kaplan *et al.*, 2007; Kaplan *et al.*, 2008a; Evenson *et al.*, 2009). The established regional age model for the timing of glaciations implies that a series of four glacial limits are successively less extensive (i.e., 'nested') and correspond to different glacial cycles: MIS 12, 10, 6, and 2 (Figure 4.3). This is based on palaeomagnetism, uranium-series dating, correlation between marine terraces, and relative weathering indices and augmented by radiocarbon, amino acid racemization, and tephra dating of the younger limits (Meglioli, 1992; Coronato *et al.*, 2004; Rabassa, 2008; Rabassa *et al.*, 2011; and references therein). Published cosmogenic nuclide exposure dates from two EBTs on the MIS 2 gLGM limit close to Bahía Inútil cluster around 20 ka (Figures 4.3, 4.4 and 4.5) and agree well with radiocarbon dates of deglaciation in the region (Heusser, 2003; McCulloch *et al.*, 2005b; Kaplan *et al.*, 2008a; Hall *et al.*, 2013). However, two EBTs on the outer two limits yielded dates significantly younger than expected, dominantly between 30 and 15 ka for the putative MIS 12 limit ($n = 7$) and two dates of 24 and 222 ka for the putative MIS 10 limit (Kaplan *et al.*, 2007; Evenson *et al.*, 2009).

Our review of the literature highlights that EBTs can form in different ways, with different erosion, transport, and depositional histories. For supraglacial EBTs, this can result in incomplete erosion of inherited nuclide concentrations, which is important to understand if using the features for cosmogenic nuclide exposure dating.
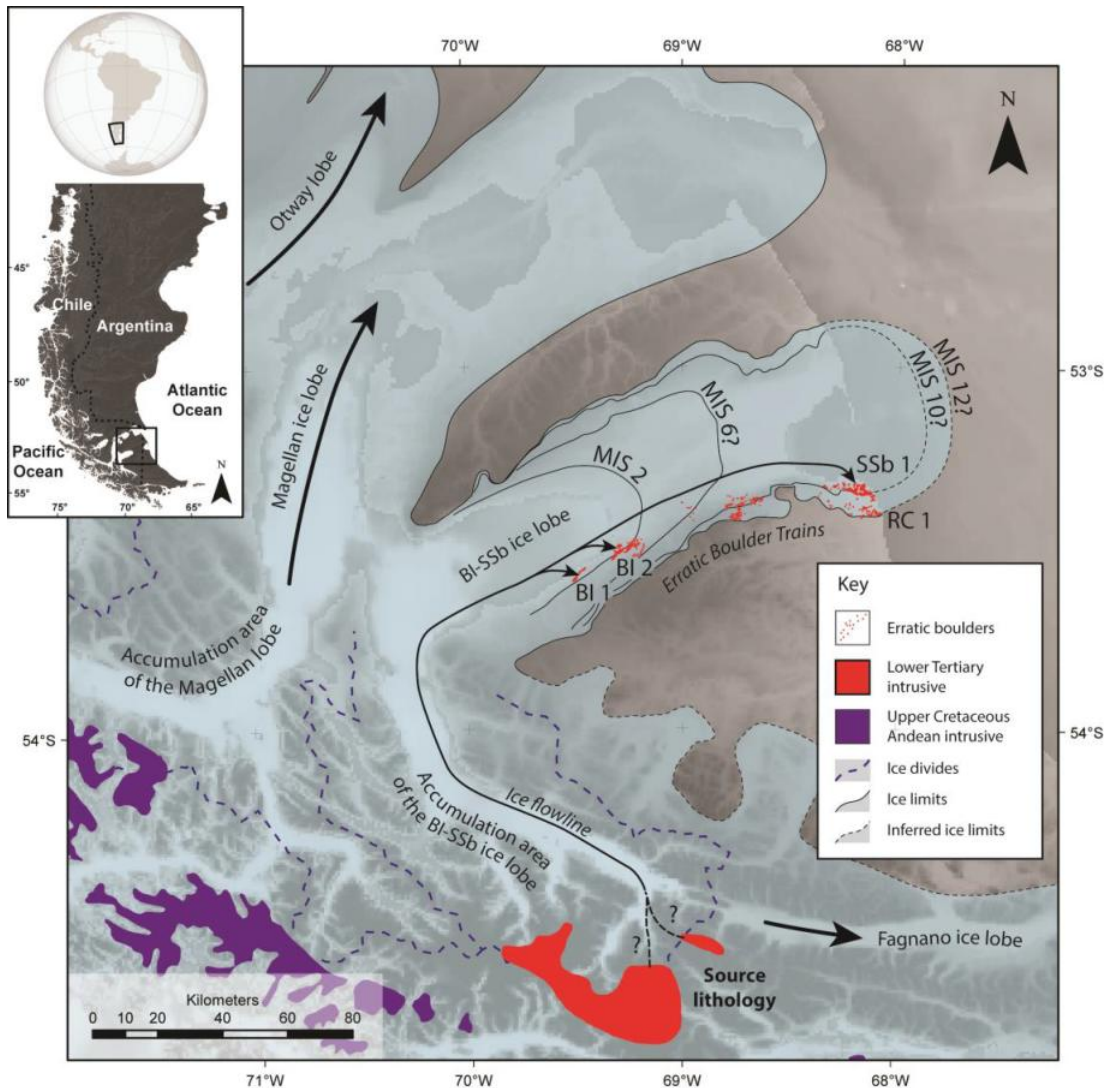
Figure 4.3. The location of the study area, showing the extent of former ice lobes in southernmost South America. Thick dashed lines indicate inferred ice divides, and thin lines show the outermost limit of ice lobes based on geomorphology mapped in Chapter 3 or inferred (dashed) from the literature. For the BI–SSb ice lobe, the hypothesised limits and their ages are shown to illustrate how the EBTs relate to them. All other ice lobes are shown at maximum extent, although this does not imply that they advanced or retreated to these limits at the same time. A former flow line from the source lithology in the Darwin Cordillera to the EBTs on Tierra del Fuego is illustrated. The two possible origins of the granodiorite lithology are shown (from Natland *et al.*, 1974), but only the lower Tertiary intrusive unit outcrops in the former accumulation area of the BI–SSb ice lobe.

Figure 4.4. (A) Simplified overview of the glacial geomorphology from Chapter 3 for Tierra del Fuego. (B) Detailed glacial geomorphological maps showing the boulders mapped in this study on Tierra del Fuego. From our mapping, the boulders clearly form EBTs (rather than simply being boulders on moraines): the trains cut across the moraine morphology, form isolated discrete clusters, and are not found on equivalent moraines to the north. Boxes in the overview map are shown enlarged below — these three boulder trains are examined in this study. The sampled boulders are highlighted within each respective EBT.

60
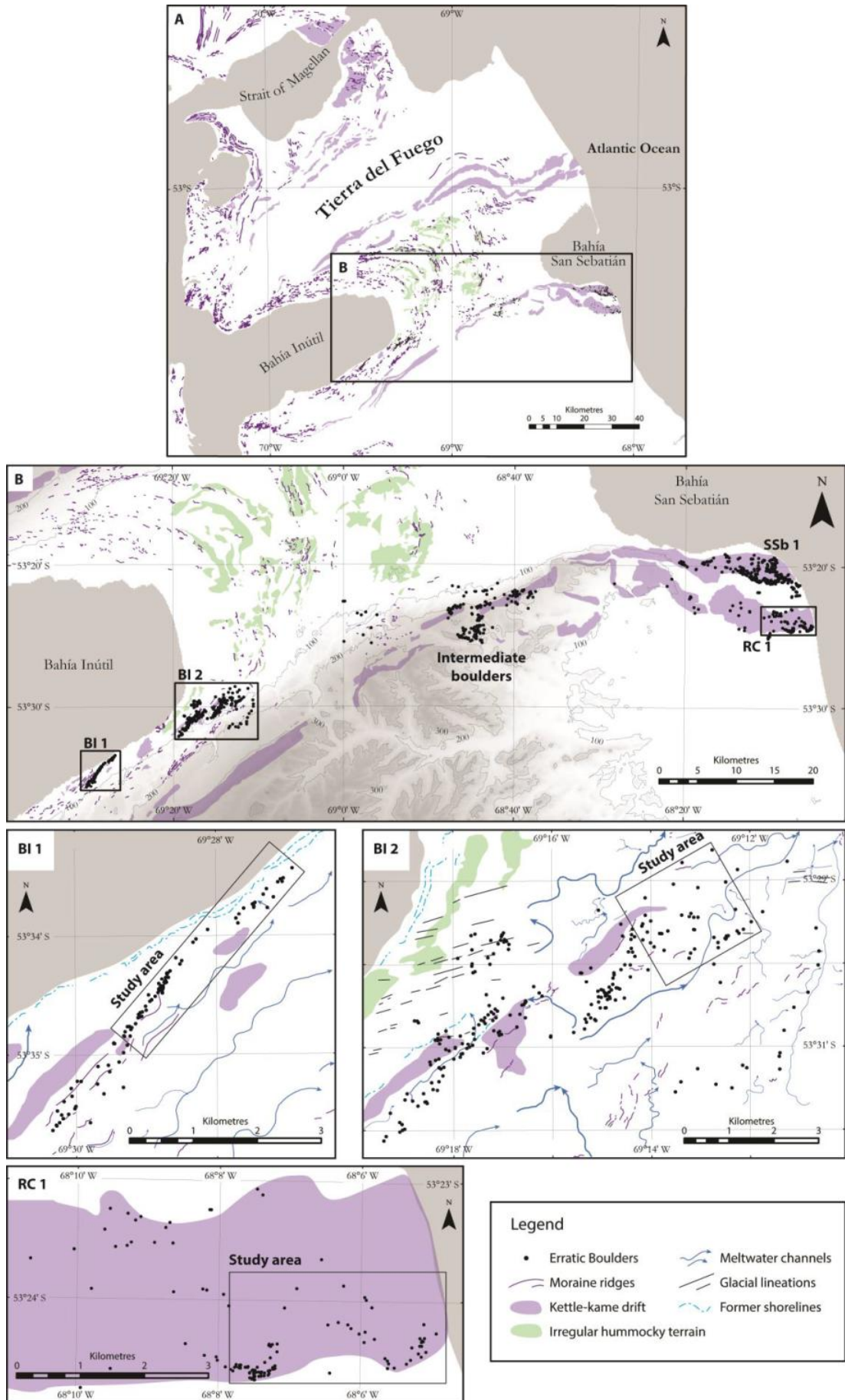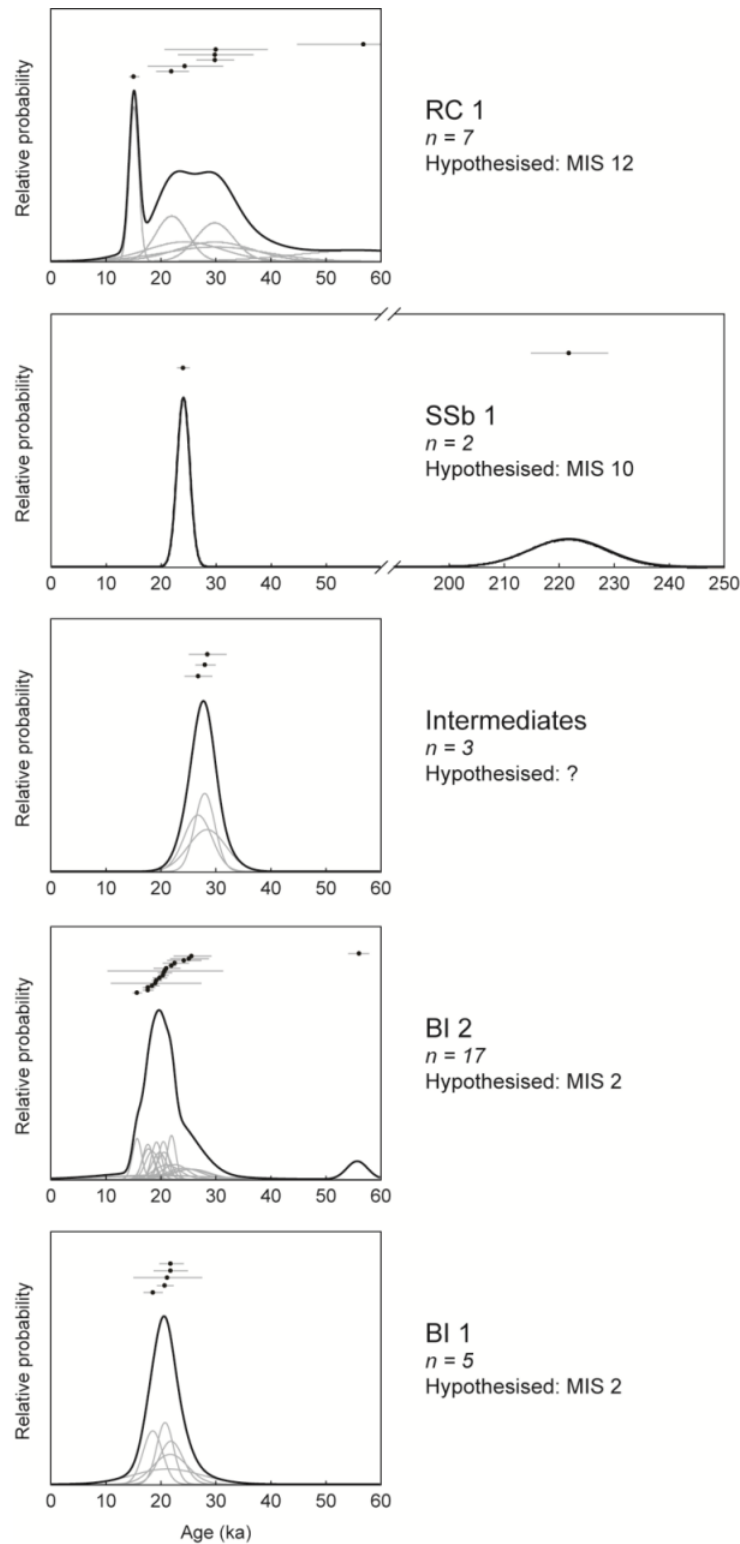
Figure 4.5. Previous [10]Be cosmogenic nuclide exposure dates from the boulder trains, as mean ages with standard errors (plotted in age order) and as probability plots; recalculated from the original data of McCulloch *et al.* (2005b), Kaplan *et al.* (2007), Kaplan *et al.* (2008a), and Evenson *et al.* (2009); and using the production rate of Putnam *et al.* (2010b) and the scaling model of Lal (1991) and Stone (2000). Note the substantial difference between the cosmogenic nuclide exposure dates and the hypothesised ages for RC 1 and SSb 1.

4.2.3   This study

Kaplan *et al.* (2007) suggested that the occasional older dates for the EBTs on Tierra del Fuego were closer to the true age of the glacial limits and proposed that intense, episodic exhumation and/or erosion of the EBTs resulted in the samples yielding anomalously young ages (i.e., they are 'old' boulders that were exhumed; Figure 4.6). However, an alternative hypothesis, not previously considered, is that all of the EBTs in Tierra del Fuego were deposited during the last glacial cycle (i.e., they are 'young' boulders; Figure 4.6), and occasional samples are anomalously old owing to inheritance. The 'old' hypothesis fits with the established age model but requires intense physical exhumation and erosion to explain the dates (Kaplan *et al.*, 2007). The 'young' hypothesis does not require such extreme processes, but questions the established age model and implies that ice was much more extensive during the last glacial cycle. This study tests between these two opposing hypotheses, and a summary of the expected weathering characteristics that might be found under these two different scenarios is given in Table 4.2.
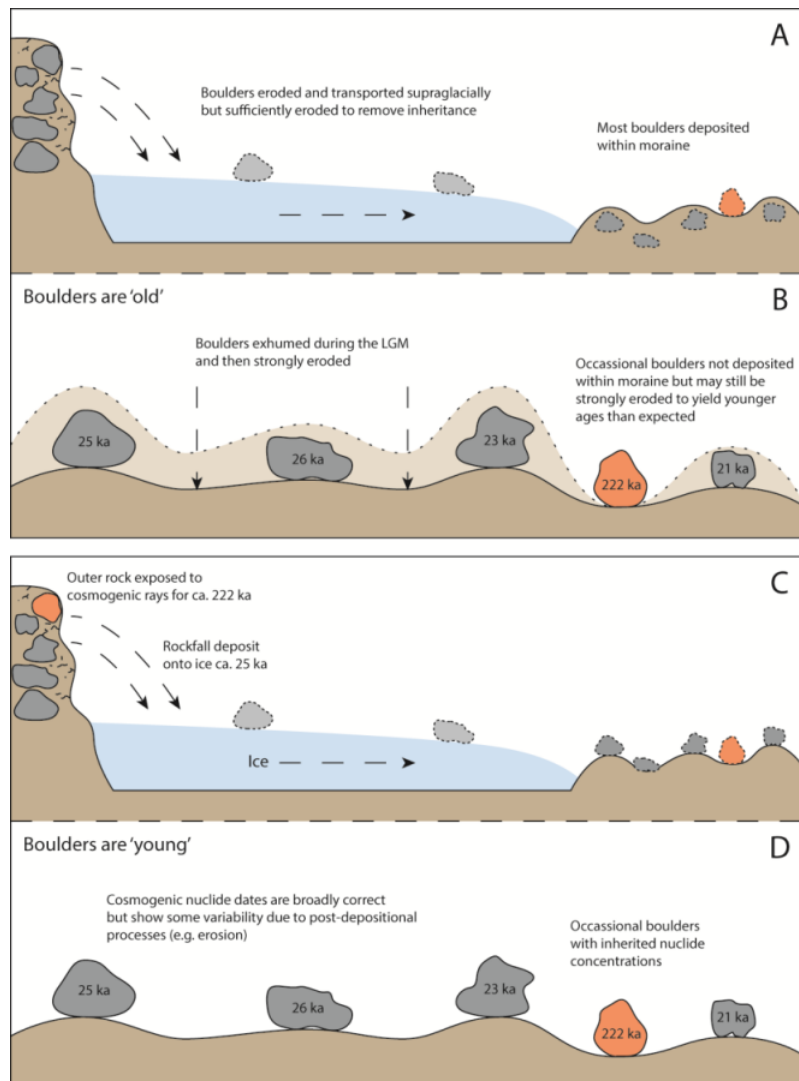
Figure 4.6. The different cosmogenic nuclide exposure dates from the RC 1 and SSb 1 boulders on Tierra del Fuego can be explained by two different hypotheses. (A) and (B) Illustrate the first hypothesis, proposed by Kaplan *et al.* (2007), which suggests that the majority of the boulders were exhumed and eroded subsequent to deposition, yielding anomalously young ages. (C) and (D) Illustrate the second hypothesis, proposed in this study, which suggests that occasional boulders may be anomalously old owing to inheritance because they were not sufficiently eroded by supraglacial transport. In this case, the majority of the cosmogenic nuclide exposure dates are a better representative of the age of the EBTs.

Table 4.2. Age and likely weathering characteristics for the Tierra del Fuego EBTs.

Properties	Boulder train		
	BI 1 / BI 2	RC 1 if 'old' [a]	RC 1 if 'young' [b]
Hypothesised age	20 ka [c]	*ca.* 450 ka [c]	30 - 20 ka [c]
Cosmogenic ages	*ca.* 20 ka [d]	*ca.* 30 - 15 ka [e]	*ca.* 30 - 15 ka [e]
Nature of erosion	Possibly some erosion	Intense exhumation and erosion [f]	Possibly some erosion
Likely agents of erosion	Wind erosion, frost action, dissolution, mild salt-spray weathering	Wind erosion, frost action, dissolution, salt-spray weathering	Wind erosion, frost action, dissolution, salt-spray weathering
Possible weathering rates	0.5 - 12 mm ka^{-1} [g]	> 25 mm ka^{-1} [h]	0.5 - 12 mm ka^{-1} [g]
Likely surface erosion	≤ 240 mm [i]	500 - > 11,250 mm [j]	≤ 360 mm [k]
Likely erosional difference compared to BI 1 / BI 2	0 mm	260 - > 11,010 mm	≤ 120 mm
Roughness compared to BI 1 / BI 2	N/A	Significantly rougher	Possibly slightly rougher or the same
Hardness compared to BI 1 / BI 2	N/A	Significantly weaker	Possibly slightly weaker or the same

[a] As hypothesised by Kaplan *et al.* (2007).

[b] As hypothesised in this study.

[c] Approximate ages, based on Meglioli (1992); Kaplan *et al.* (2007); Kaplan *et al.* (2008a).

[d] McCulloch *et al.* (2005b); Kaplan *et al.* (2008a); Evenson *et al.* (2009).

[e] Kaplan *et al.* (2007); Evenson *et al.* (2009).

[g] Kaplan *et al.* (2005) calculated apparent erosion rates of roughly 0.5 to 2.5 mm ka^{-1} over > 760 ka for boulders deposited by the Lago Buenos Aires lobe in northern Patagonia. Kaplan *et al.* (2007) calculated apparent erosion rates of roughly 5 to 12 mm ka^{-1} over *ca.* 50-120 ka for boulders deposited by the Río Gallegos lobe in southern Patagonia.

[h] Apparent erosion rate estimated by Kaplan *et al.* (2007).

[i] Assuming up to 12 mm ka^{-1} erosion over 20 ka.

[j] Assuming > 25 mm ka^{-1} erosion following rapid exhumation at 20 ka or continuous erosion at > 25 mm ka^{-1} over 450 ka. Kaplan *et al.* (2007) suggested that continuous erosion is unlikely given preservation of original surface geomorphology, so the amount of erosion is probably between these two end members.

[k] Assuming up to 12 mm ka^{-1} erosion over up to 30 ka.

4.3 Methods

4.3.1 Mapping and sampling

We began by mapping all erratic boulders in the study area and then selected a sample of 150 boulders from three of the EBTs to compare trains hypothesised to be of similar and differing ages (Figure 4.3). Many of the boulders are sufficiently large and clear against the surrounding landscape for them to be mapped from remote imagery, so a map was produced to show their distribution using a combination of remote sensing analysis and field-checking. Aerial photographs from the Servicio Aerofotométrico de la Fuerza Aérea de Chile were used where possible as well as Google Earth™ imagery (version 7). Field-checking verified the broad spread of mapped boulders, and the locations of the 150 sampled boulders were recorded using a handheld Magellan eXplorist 610 GPS device. All boulders within a given area were sampled provided they were > 2 m in height. This was to avoid the effects of snow/vegetation cover and variable erosion on smaller boulders, and to avoid the chances of sampling fragments that may have broken off subsequent to deposition. Boulders were described in terms of basic lithology, surface appearance, and setting.

4.3.2 Size approximation, angularity, and appearance

Boulders varied in size and accessibility, so boulder dimensions and volume were estimated using eight photographs taken around each boulder at roughly equal bearings. All photographs included a 1-m measuring-staff that was later used to gauge boulder height, width, and depth. The greatest measurement of height and width was used for each boulder as well as the corresponding largest depth measurement (perpendicular to greatest width). Volume was then calculated in three ways to give approximate upper, middle, and lower values, respectively:

Cubic volume, calculated as:

$$cubic\ volume\ = H\ \times W\ \times D$$

Maximum inscribed cubic volume in a sphere, calculated as:

$$max.\,inscr.\,volume\ = \left(\frac{8}{3^{1/3}}\right) \times {}^{H}\!/_{2} \times {}^{W}\!/_{2} \times {}^{D}\!/_{2}$$

Octahedral volume, calculated as:

$$octahedral\ volume\ = {}^{1}\!/_{3} \times \sqrt{2} \times (H\ \times W\ \times D)$$

Where *H* is boulder height, *W* is boulder width and *D* is boulder depth (Figure 4.7).
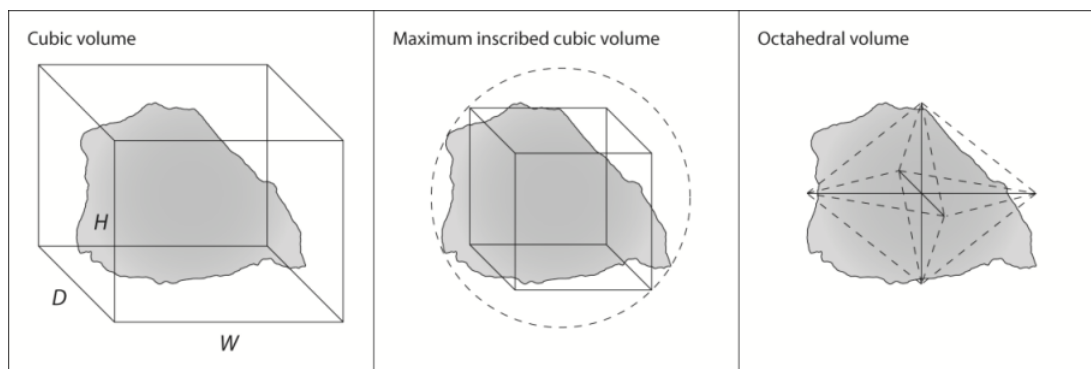
Figure 4.7. Visualisation of the three methods used to calculate boulder volume from the same measurements of Height (H), Width (W) and Depth (D). Volumes are approximations given the use of photographic analysis and that boulders are not regular shapes.

Given the use of photographic analysis, measurements are given to the nearest 1 m. Volumes are still approximations given that boulders are not regular hexahedrons or spheres, but the cubic and octahedral volumes do provide likely maximum and minimum values from the field measurements. For boulders resting on the surface, volumetric values are likely to be correct, but many appear to be at least partially embedded, so that their height, and possibly width and depth, may be greater than was recorded. For the reasons given above, we suggest that our boulder volumes and boulder train volumes are only minimum estimates.

Table 4.3. Criteria used to visually assess boulder roundness (Benn, 2004).

Abbreviation	Class	Description
VA	Very Angular	Edges and faces unworn; sharp, delicate protuberances
A	Angular	Edges and faces unworn
SA	Sub Angular	Faces unworn, edges worn
SR	Sub Rounded	Edges and faces worn but clearly distinguishable
R	Rounded	Edges and faces worn and barely distinguishable
WR	Well Rounded	No edges or faces distinguishable

We measured angularity in two ways. Firstly, we assessed the roundness of each boulder according to a visual scale (Table 4.3). From this, we could calculate RA values (the percentage of angular and very angular boulders) as a measure of angularity (Benn & Ballantyne, 1994). We did not create corresponding C_{40} values for the boulders because these would be biased by partial burial of some of the boulders. Secondly, we recorded the angularity of the most angular edge for each boulder in two of the boulder trains (BI 1 and RC 1; Figure 4.8). For this, we used an adapted version of the method of Kirkbride (2005). We used this technique in a simplistic way to compare relative differences in angularity between the boulder trains and did not manipulate the data beyond plotting the edge length against edge angle. Essentially, more angular edges create longer lengths and larger angles, and less angular edges create shorter lengths and smaller angles. The surficial characteristics and lithology of the boulders were also noted.
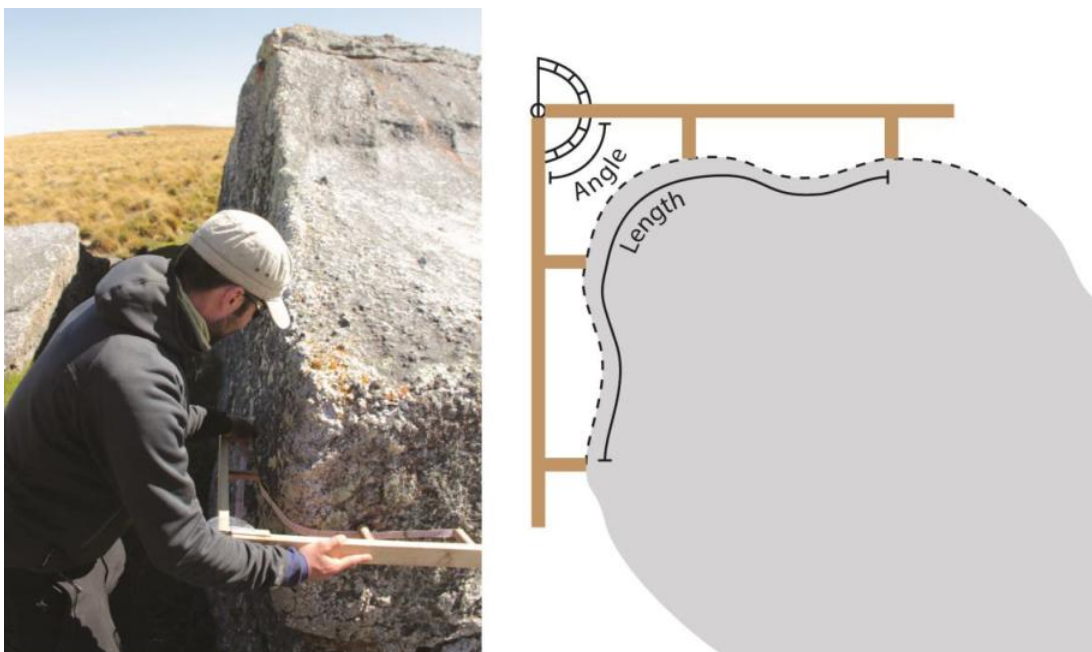
Figure 4.8. Photograph and illustration of the technique used to measure angularity of boulder edges. The tool is similar to Kirkbride (2005) and measures the length and angle between two hinged points. Relative differences between the combinations of these values for different boulders relate to changes in edge angularity.

4.3.3 Schmidt hammer

The Schmidt hammer has been used to measure rock-surface hardness as an indicator of the amount of time that rock has been exposed to subaerial processes (Matthews & Owen, 2010). Rebound values (*R*-values) produced by the impact of the hammer decline with increased rock-surface weathering, and can be used as a relative measure of exposure history (McCarroll, 1991; McCarroll & Nesje, 1993; Nesje *et al.*, 1994; Goudie, 2006; Shakesby *et al.*, 2011). We used an N-type Schmidt hammer to analyse 50 boulders from two of the boulder trains thought to be from different glacial cycles (BI 1 and RC 1). Fifty Schmidt hammer blows were recorded per boulder, with a total of 2500 blows per boulder train (5000 blows in total). On each boulder, 10 blows were recorded per face (approximately: north, east, south, west, and top) to explore whether aspect is a control on rock-surface weathering. The Schmidt hammer R-values were corrected for the angle at which the Schmidt hammer was held following Day & Goudie (1977), see Table 4.4. A correction was also made to account for instrumental drift based on an average trend, cross-checked against measurements on a calibration anvil.

There are a number of potential limitations in using the Schmidt hammer as a relative dating tool. Small rock sizes and changes in lithology can influence results, although the boulders here were far larger than the minimum size suggested by Sumner & Nel (2002) and they were monolithological, and so this was not a limitation. Measurements can also be affected by discontinuities and moisture (especially in weak rocks), cracks, edges, and the surface roughness of the measured face (Goudie, 2006). Measurements were consistently taken on planar surfaces, away from cracks and edges, and our roughness measurements suggested little difference between the boulder trains. However, it is possible that the range of our results was caused by variability in these factors. Evans *et al.* (1999) also suggested that re-worked material may play a role in producing scattered R-values, although we suggest that this is unlikely to have been an issue given that the large size, high angularity and lack of subglacial abrasion of the boulders.

Table 4.4. Angle corrections applied to Schmidt hammer R-values (Day & Goudie, 1977).

Rebound value	Upward impact		Downward impact	
R	+90°	+45°	-45°	-90°
10			+2.4	+3.2
20	-5.4	-3.5	+2.5	+3.4
30	-4.7	-3.1	+2.3	+3.1
40	-3.9	-2.6	+2.0	+2.7
50	-3.1	-2.1	+1.6	+2.2
60	-2.3	-1.6	+1.3	+1.7

4.3.4   Profile gauge

Rock surface roughness can be used to compare the effects of weathering where it is assumed that initial surface texture was roughly the same (McCarroll & Nesje, 1993; 1996). This can then be used as an indicator of the relative time that a rock surface has been exposed to weathering processes. A profile gauge is a quick and easy tool for measuring rock surface roughness (McCarroll & Nesje, 1996), and we used a 25-cm gauge consisting of 250 × 1 mm independent pins to sample planar rock surfaces. The profile gauge samples only a small part of any surface and cannot characterise the overall roughness of a boulder, but with numerous samples on numerous boulders, it can demonstrate relative differences in roughness between populations (McCarroll & Nesje, 1996). Converting the profiles into numerical values of roughness is the principal source of uncertainty. This has been discussed in detail in the literature (McCarroll & Nesje, 1996) and can be accounted for, to some degree, by comparing roughness wavelengths (8, 16, 24 and 32 mm in this case; Figure 4.9) and statistical techniques (Index A and RMS in this case). In this study, we assume that the glacial erosion and transport of all of the EBTs is essentially the same and that, given that the boulders are monolithological, differences in roughness result from the time exposed to weathering or variable weathering processes.

The gauge was pressed firmly against the surface and then traced onto graph paper in the field and later digitized (Figure 4.9). Pin positions were recorded every 8, 16, 24 and 32 mm to evaluate different roughness wavelengths. We measured roughness profiles for 50 boulders in three boulder trains (BI 1, BI 2, and RC 2). Five profiles were recorded per boulder, making a total of 250 profiles per boulder train (750 profiles in total). On each boulder, one profile was recorded per face

(approximately: north, east, south, west, and top) to show whether roughness varied with aspect.
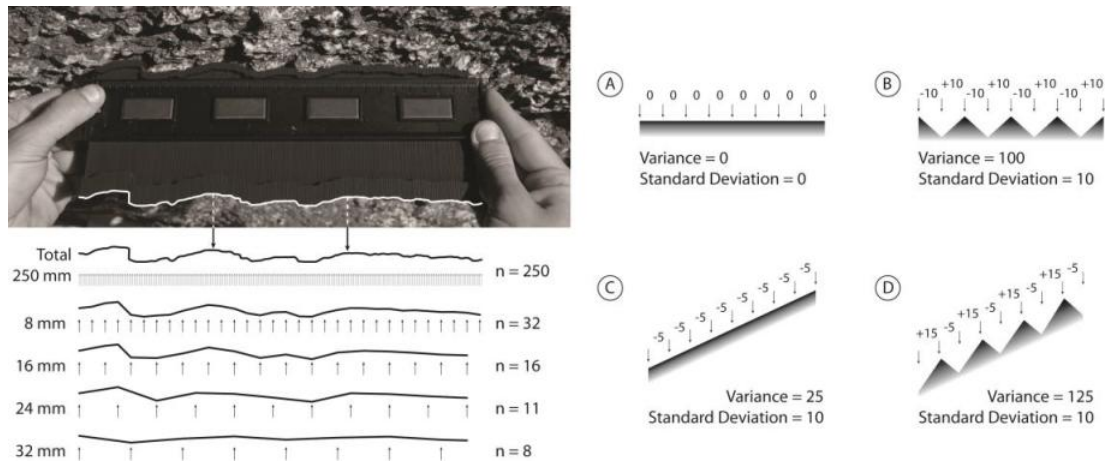
Figure 4.9. The profile gauge used to measure rock surface roughness. Increasing the distance between measured points along the profile (i.e., the wavelength) has a smoothing effect, but also captures roughness at different resolutions. In this study, >20 mm wavelengths were the most useful. (A-D) illustrate the effects of surface slope on the recorded roughness. Hence, standard deviation removes the issue of surface curvature (adapted from McCarroll & Nesje, 1996).

4.4 Results

4.4.1 Distribution

We mapped a total of 1248 boulders and distinguished four EBTs. From innermost (ice-proximal) to outermost (ice-distal), these are: BI 1, BI 2, SSb 1, and RC 1 (Figure 4.4). In addition, a large spread of boulders lies between Bahía Inútil and Bahía San Sebastián (intermediates in Figure 4.4B). These are dispersed rather than tightly clustered and so are not classed as an EBT for the purposes of our study. However, we highlight that these intermediate boulders bridge the gap between BI 1 / BI 2 and SSb 1 / RC 1. It was not possible to access the SSb 1 EBT or some of the intermediate boulders for field-checking or analysis, but both were sampled for cosmogenic nuclide exposure dating by Kaplan *et al.* (2007). A summary of the characteristics of the boulder trains is given in Table 4.5 and example photos are given in Figures 4.10, 4.11 and 4.12.

Table 4.5. The spatial characteristics and geomorphological context of the EBTs on Tierra del Fuego. Hypothesised ages are from Meglioli (1992).

EBT	No. boulders mapped	Approx. train length (km)	Approx. train width (km)	Approx. train height (m asl)	Spatial distribution	Geomorphological context	Hypothesised ages
BI 1	98	5.5	0.5	50 - 70	A highly linear train extending to the coast of Bahía Inútil.	On a moraine belt, parallel to meltwater channels and with one meltwater channel dissecting it.	MIS 2
BI 2	238	11.0	7.5	60 - 220	Elements of linearity, but spread over a wider area than BI 1. May consist of more than one EBT, but not possible to distinguish in the field.	Deposited across numerous moraines, with several meltwater channels cutting through.	MIS 2
Intermediates	267	26.0	8.0	30 - 80	Boulder density is much less than the other EBTs, so the boulders were not studied further.	Lies across several moraines.	Possibly relates to more than one glacial limit
SSb 1	476	15.0	4.0	0 - 80	Boulder density varies, delimited to the north and south by the extent of kettle and kame drift.	Sits on a broad band of kettle and kame drift and continues eastward into the Atlantic Ocean.	MIS 10
RC 1	162	20.0	4.0	0 - 40	Boulder density varies, delimited to the north and south by the extent of kettle and kame drift. There are two tight, linear clusters of boulders roughly 1.7 km long and 1.5 km long.	Sits on a broad band of kettle and kame drift and continues eastward into the Atlantic Ocean.	MIS 12

Figure 4.10. Example photographs of the BI 1 boulder train (A), surface texture (B) and boulders (C-H). A person and 1 m measuring staff is featured in A and C-H for scale.
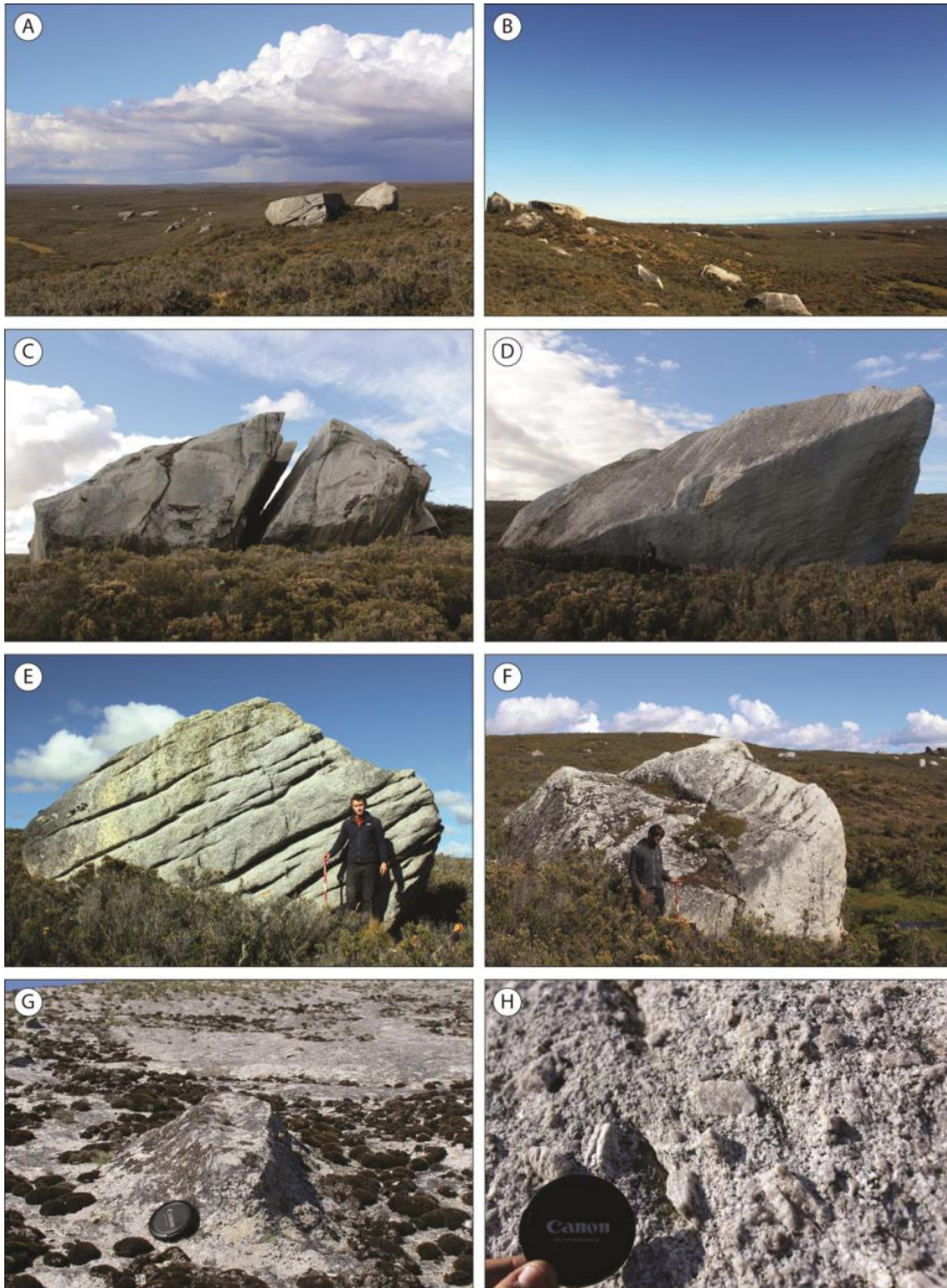
Figure 4.11. Example photographs of the BI 2 boulder train (A and B), boulders (C-F) and surface texture (G and H). A person and 1 m measuring staff is featured in C-F for scale.

Figure 4.12. Example photographs of the RC 1 boulder train (A and B) and boulders (C-H). A person is featured in C-H for scale.

4.4.2 Volume characteristics

The total volume of rock within the measured boulders in BI 1, BI 2, and RC 1 combined is > 22,000 m^3, within which the total volume of BI 1 is > 5,000 m^3, BI 2 is > 14,000 m^3, and RC 1 is > 2,000 m^3 (Figure 4.13). The largest boulders were in BI 2, with three boulders exceeding 1000 m^3. Of all boulders sampled, only one was found to be taller than it was wide, and we interpret this to indicate that almost all boulders are stable and 'at rest'. Several examples of 4-6 near-consecutive boulders were found to increase in volume down-ice (Figure 4.13). This is masked in the field by scattered smaller boulders, and the pattern is least distinct in BI 2 where boulders are more dispersed. However, we suggest that these trends are real because they cannot be explained by measurement uncertainty or by changing the point from which EBT distance is measured.

4.4.3 Angularity

Little difference in angularity was recorded between boulder trains, and all showed a dominance of angular or subangular boulders, supported by RA values of 64% for BI 1 / BI 2 and 54% for RC 1 (see Figure 4.14).

4.4.4 Rock surface hardness

The Schmidt hammer *R*-values were corrected for the angle at which the Schmidt hammer was held and for instrumental drift. The total mean *R*-values for the two boulder trains are 43.6 ±19.9 for BI 1 and 37.7 ±19.7 for RC 1 (Figure 4.15), and the means of different aspect faces also show consistently lower *R*-values for RC 1 than BI 1, in the range of 2.8-8.4. A Mann-Whitney U test reveals a statistical difference between the median values of the two EBTs at the 0.95 significance level ($p = < 0.05$), when comparing total values and for each of the aspect faces.
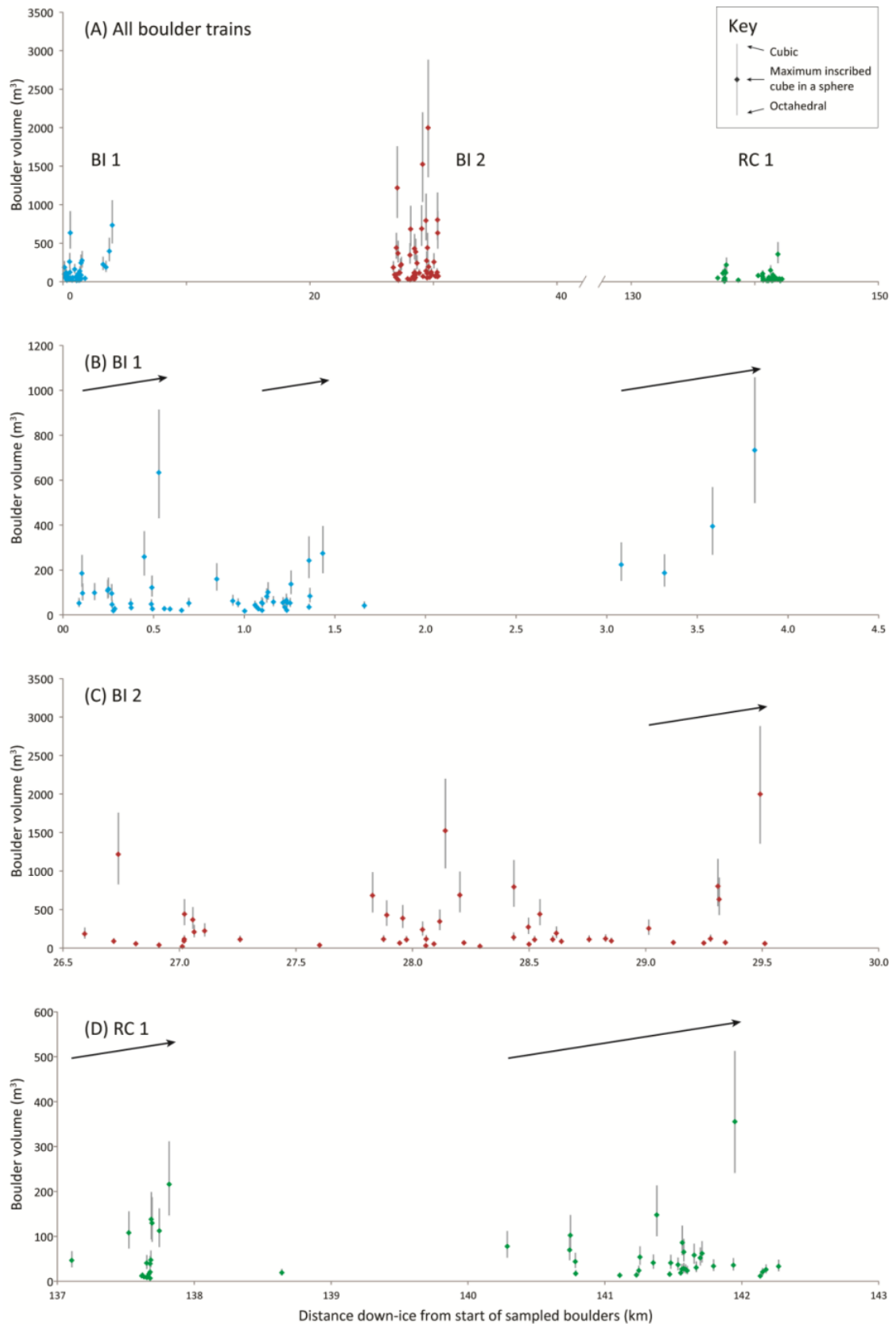
Figure 4.13. The results of boulder volume measurements. (A) Shows the results for all three boulder trains, which are shown individually beneath: (B) BI 1; (C) BI 2; (D) RC 1. Arrows highlight an apparent repeated pattern of increasing down-ice volume across several near-consecutive boulders in all three EBTs.
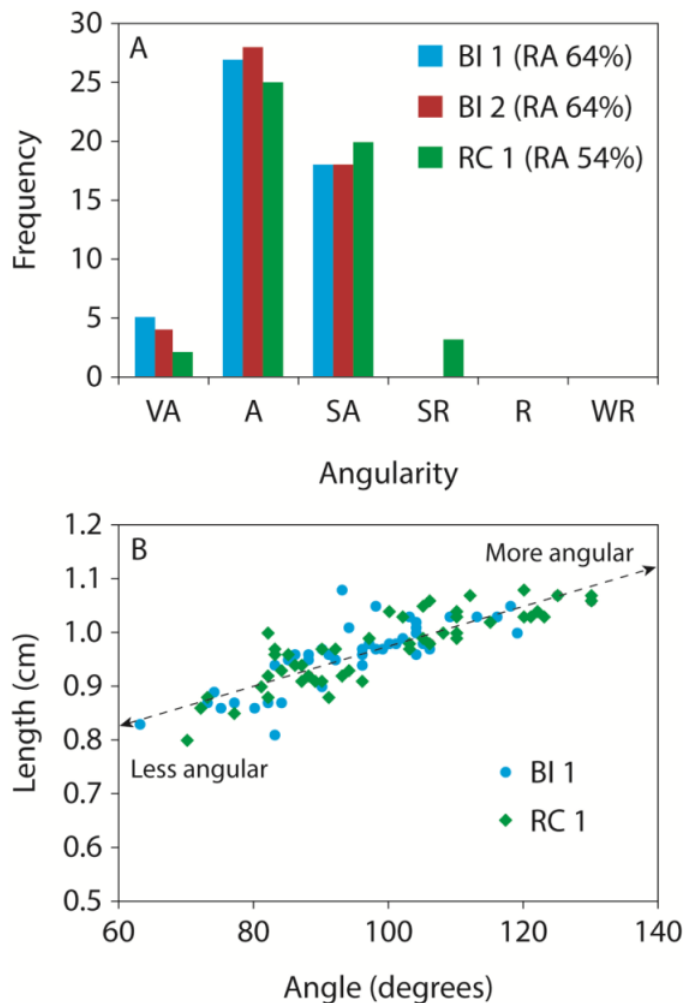
Figure 4.14. The results of angularity measurements. (A) Is a frequency histogram of observed boulder roundness, showing a dominance of angular boulders supported by high RA values (percentage of angular and very angular boulders). (B) Shows the similarity in boulder edge roundness between BI 1 and RC 1

4.4.5 Rock surface roughness

Following McCarroll & Nesje (1996), we present our roughness data in two ways. Index A uses the standard deviation of measurements and removes the influence of rock surface slope, whereas root mean square (RMS) represents roughness more accurately as the deviation from the mean, but will be affected by surface curvature (Figure 4.9). The profile gauge was used on all three boulder trains, and a strong correlation was found between Index A and RMS values (Figure 4.16), indicating that surface curvature did not affect the roughness results. Consequently, RMS values are used to assess differences in surface roughness (Figure 4.16). Reducing the wavelength reduces the mean roughness and spread of values, but McCarroll & Nesje (1996) suggested that lower wavelengths were unlikely to capture true

surface roughness. We found that the greatest rock crystal size was generally > 20 mm; hence we focus on the 32-mm wavelength data. The different number and spacing of data points along the profiles when the wavelength was varied did not affect the mean results, suggesting that the results indicate actual changes in roughness and are not caused by sampling strategy. The total mean values for the three boulder trains are 2.4 ±1.8 mm for BI 1, 2.3 ±1.6 mm for BI 2, and 2.8 ±2.3 mm for RC 1 at the 32-mm wavelength (Figure 4.16). Like the Schmidt hammer data, patterns exists within the roughness results, with RC 1 consistently showing greater roughness — mean values 0.19-0.64 mm greater than the lowest mean value from BI 1 or BI 2 — for the total and different aspect faces. A Mann-Whitney U test shows a statistical difference between the total median values of all three EBTs at the 0.95 significance level ($p = < 0.05$). Likewise, some, but not all, of the aspect faces also show a statistical difference when comparing all three of the EBTs, and this applies when comparing BI 1 and BI 2 as well as BI 1 / BI 2 and RC 1.

.
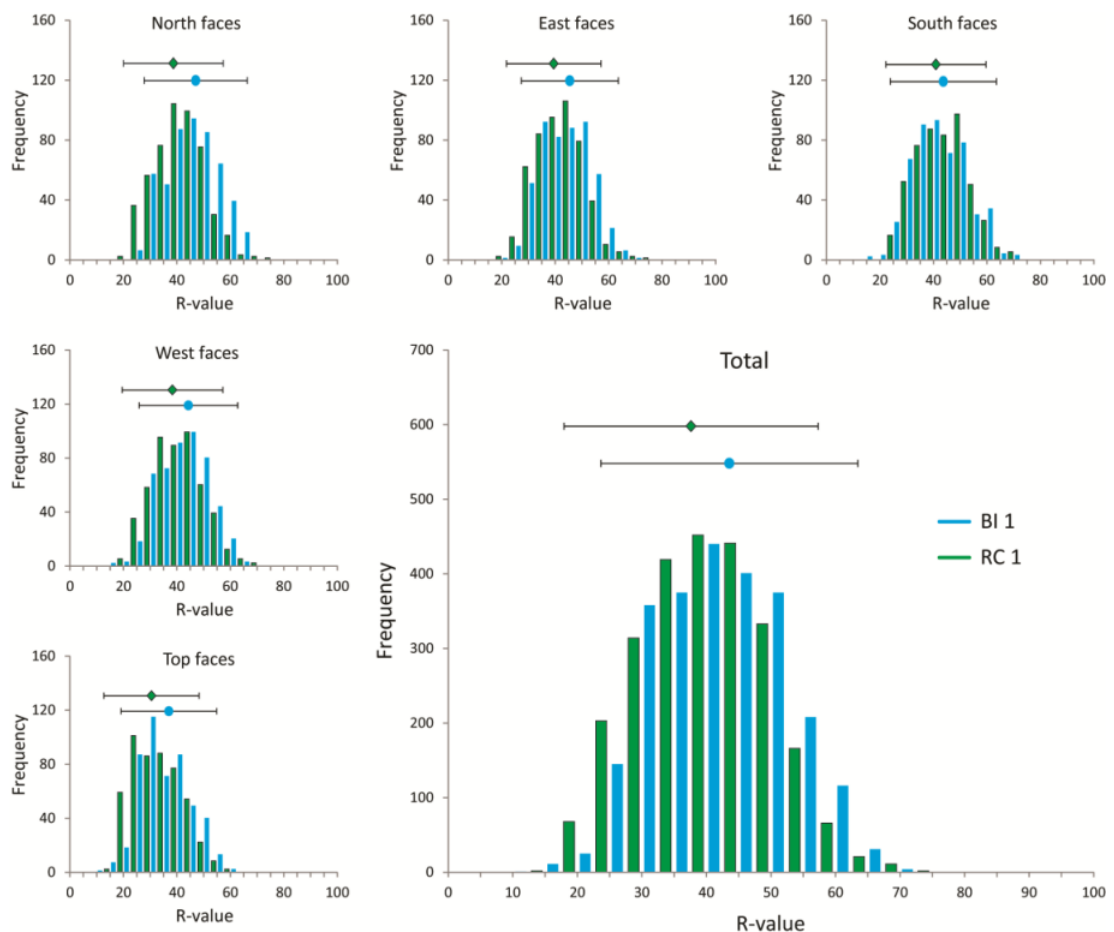
Figure 4.15. Results of Schmidt hammer rock hardness analysis on the BI 1 and RC 1 EBTs, as total data and split into directional faces. Mean data are shown with 2σ errors, in addition to frequency histograms that illustrate the overlap between the two boulder trains.
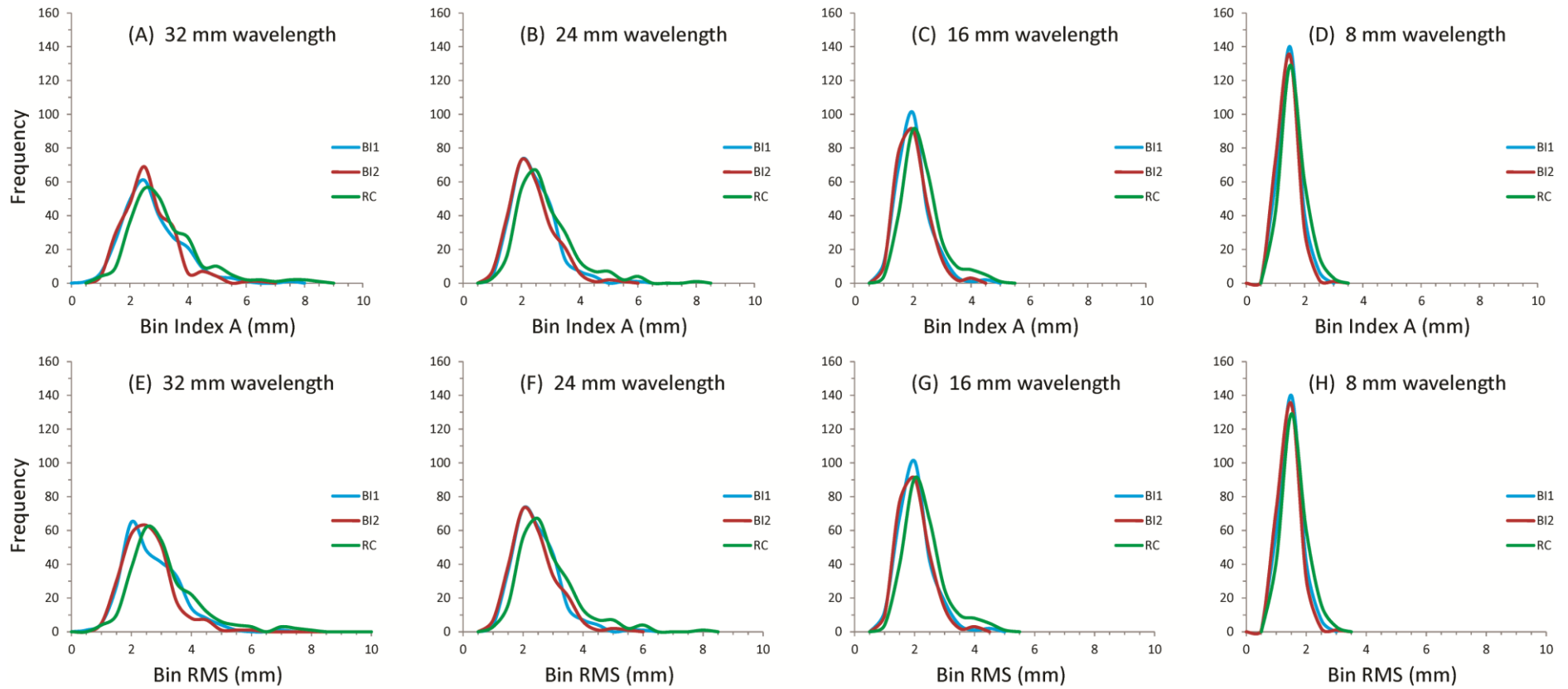
Figure 4.16. Results of profile gauge rock surface roughness analysis on the BI 1, BI 2, and RC 1 EBTs, shown as frequency distributions. (A – D) are Index A results and (E – H) are RMS results. Note the similarity between the results of the two methods. RMS data is used in this study, focussing on the 32-mm wavelength.

4.5 Discussion

4.5.1 Source

Kaplan *et al.* (2007) and Evenson *et al.* (2009) described the boulders from BI 1, BI 2, and RC 1 as hornblende granodiorites. The only source for this lithology is a small area of the Cordillera Darwin mountain range (Figure 4.3), where lower Tertiary intrusive units outcrop within the former glacial accumulation area (Natland *et al.*, 1974; Nelson, 1980; Evenson *et al.*, 2009). This source suggests that the BI–SSb ice lobe originated from the central Cordillera Darwin to the south. It also helps to position the ice divide between the BI–SSb and Fagnano ice lobes at peak glaciation; and the presence of supraglacial rock debris on Tierra del Fuego implies that granodiorite nunataks existed within the central Cordillera Darwin during peak glaciation. Thus, peak ice thickness could not have exceeded around 2500 m, which acts as a constraint on ice cap reconstructions.

The large boulders in Tierra del Fuego (up to 1000 m^3) are unlikely to have been transported subglacially given that erosion during the distance from their source (*ca.* 250 km) should have considerably reduced their size (Figure 4.2). Furthermore, our data show that the boulders are dominantly angular or subangular. Numerous angular boulders up to 21 m in diameter are unlikely to have been transported beneath the ice over such a long distance. We found no evidence of subglacial abrasion (e.g. polishing or striae), and the angularity of the boulders suggests that such signs have not been removed by weathering. A similar conclusion was reached by Evenson *et al.* (2009). As such, the most likely formation mechanism is supraglacial debris at the source location in the Cordillera Darwin.

Previous workers all noted the tight distribution, large size, angularity, and monolithology of the EBTs on Tierra del Fuego (Meglioli, 1992; Bentley *et al.*, 2005; McCulloch *et al.*, 2005b; Evenson *et al.*, 2009); and we suggest that these features match the characteristics expected of a supraglacial rock avalanche deposit (Shulmeister *et al.*, 2009). Studies routinely estimate total rock avalanche deposit volumes of > 1,000,000 m^3 (Shugar & Clague, 2011; Sosio *et al.*, 2012; Delaney & Evans, 2014) and even > 10,000,000 m^3 (Jibson *et al.*, 2006; McColl & Davies, 2011; Shugar & Clague, 2011; Sosio *et al.*, 2012), far in excess of our minimum estimates of > 22,000 m^3 (or > 150,000 m^3 assuming that the coarse fraction accounts for around 15% of the total volume; Delaney & Evans, 2014). This suggests that the size of the deposit is not unreasonable for a supraglacial rock avalanche. The clustering of the EBTs suggests that the erosion of the boulders

occurred in discrete events and implies that gradual erosion at the source is improbable. Debuttressing during glacial retreat could have resulted in episodic deposition of debris caused by joint failures. However, we note that the boulders cut across a range of glacial geomorphology — both small moraine ridges and kettle and kame topography (Figure 4.4) — and that the RC 1 EBT was deposited when the ice lobe was still fully extended. Additionally, whilst the EBTs might have been deposited during recession, they represent flowline features, not ice-marginal deposits.

The production of boulder trains as a result of supraglacial rock avalanches has not been explicitly examined in previous work. Shulmeister *et al.* (2009) noted that for large supraglacial rock avalanches, a greater proportion of thicker debris remains on the glacier surface rather than being incorporated into the subglacial system, and a characteristic 'carapace' of coarser debris generally caps deposits (Reznichenko *et al.*, 2011). Coarse distal rims are found in numerous deposits (Hewitt, 1999; Chevalier *et al.*, 2009; Hewitt, 2009; McColl & Davies, 2011; Shugar & Clague, 2011) and, theoretically, these could result in boulder trains, especially if divergent flowlines drew the boulders into a train prior to deposition (Evenson *et al.*, 2009). However, large boulders may also be found across the debris sheet, with the rim simply representing a greater density of large boulders caused by bulldozing (Shugar & Clague, 2011). It thus remains unclear exactly how a rock avalanche debris sheet is transformed into EBTs, but we now discuss a conceptual model for their transport and deposition.

4.5.2 Transport and deposition

The lateral position of the EBTs on Tierra del Fuego probably resulted from ice to the north (the Magellan lobe) deflecting the BI–SSb lobe to the east (Figure 4.3), with divergent flow lines focusing the boulders in a lateral position (Evenson *et al.*, 2009). Thus, we envisage that the boulders were transported supraglacially from the central Cordillera Darwin, east of Isla Dawson, before turning sharply east into Bahía Inútil to be deposited on the south side of the former ice lobe (Figure 4.3). Given that the Cordillera Darwin has experienced seismic activity in the past (Cunningham, 1993; Klepeis, 1994; Bentley & McCulloch, 2005), the four distinct boulder trains may have resulted from separate rock avalanche pulses (Larsen *et al.*, 2005; Jibson *et al.*, 2006). Ice crevassing, subaerial weathering, and meltwater may have acted to remove much of the finer material (Shulmeister *et al.*, 2009), and

ice flow and the divergence of flow lines then dragged the distal rim and boulder carapace into trains (Evenson *et al.*, 2009).

Our mapping shows that the EBTs are significantly more extensive than previously thought (Evenson *et al.*, 2009) and occur at several places along the southern limit of the former ice lobe. There are also numerous boulders that do not cluster as boulder trains (intermediates), but act as a continuum between BI 1 / BI 2 and SSb 1 / RC 1. Whilst the EBTs may represent distinct spatial and temporal events (as proposed by Kaplan *et al.*, 2007, and Evenson *et al.*, 2009), they could also represent rock avalanche pulses during the same period, possibly linked to seismic activity (Larsen *et al.*, 2005; Chevalier *et al.*, 2009). Studies in New Zealand have suggested that supraglacial rock avalanches may result in the deposition of non-climatic moraines (Anderson & Mackintosh, 2006; Tovar *et al.*, 2008; Shulmeister *et al.*, 2009; Reznichenko *et al.*, 2011). However, given the small area and isolated nature of the EBTs compared to the area covered by the BI–SSb ice lobe, a similar debris-induced, non-climatic model is improbable.

The patterns of increasing down-ice boulder volume observed within each of the EBTs (Figure 4.13) are unlikely to have been preserved in any scenario other than deposition onto — and transport on top of — the former ice. However, the formation of these patterns is unclear. Little evidence suggests that gravitational sorting of avalanche debris occurs (Marangunic & Bull, 1968; Shugar & Clague, 2011), but trains of debris several metres wide and parallel to the direction of debris flow have been described (Hewitt, 2009; Shugar & Clague, 2011; Delaney & Evans, 2014). These likely resulted from snow ploughing of a large boulder, with finer material following behind on exposed glacial ice (Delaney & Evans, 2014), and currently offer the best analogue for the patterns of boulder size trends seen in Tierra del Fuego.

4.5.3   *Rock surface weathering*

The Schmidt hammer data show a statistical difference between the RC 1 and BI 1 EBTs, indicating that the RC 1 boulders have been subjected to a greater degree of weathering than the BI 1 boulders. However, the differences are not as great as might be expected if intense, episodic erosion has taken place (Table 4.2). The *R*-values showed a total average difference of 5.9, whereas McCarroll & Nesje (1993) demonstrated differences of 25-40 between Little Ice Age and late glacial sites in western Norway; and Matthews & Owen (2010) highlighted differences of 21-35 between Little Ice Age and Preboreal sites in southern Norway. Rock weathering (and therefore *R*-values) could have reached saturation in Tierra del Fuego.

However, despite agreement that *R*-values will progress toward a dynamic equilibrium over time (White *et al.*, 1998; Engel, 2007; Sánchez *et al.,* 2009; Černá & Engel, 2011; Stahl *et al.*, 2013), numerous studies have effectively distinguished gLGM and pre-gLGM deposits using the technique on timescales of 10s to 100s ka (Ballantyne *et al.*, 1997; Rae *et al.*, 2004; Černá & Engel, 2011; Stahl *et al.*, 2013). Very high rates of weathering are required to reduce the ages of the RC 1 boulders (Table 4.2), yet no obvious jump in *R*-values occurs between these and the BI 1 / BI 2 boulder trains.

The roughness data show a statistical difference between the total values of RC 1 and BI 1 / BI 2, but also between the BI 1 and BI 2 total values. Because BI 1 and BI 2 are assumed to be roughly the same age (lying within the same ice marginal deposits; Figure 4.3), this implies that the difference between RC 1 and BI 1 / BI 2 is not necessarily related to a significant difference in age. Differences between BI 1 and BI 2 could be driven by the highly variable values measured for the top aspect faces of the boulders, but statistical similarities also exist between the BI 1 / BI 2 and RC 1 aspect faces, suggesting that any differences are unlikely to be the result of a large difference in age between these EBTs. Most importantly, and like the Schmidt hammer data, we do not find a jump in values between RC 1 and BI 1 / BI 2 that might be expected if intense, episodic erosion has taken place (Table 4.2). The average total difference in roughness between RC 1 and BI 2 is 0.5 mm at the 32-mm wavelength. Given that the large crystal size is > 20 mm and that the averages for all three boulder trains are between 2.3 and 2.8 mm, this difference is negligible. McCarroll & Nesje (1996) recorded much greater differences in roughness values when studying salt spray and chemical weathering of boulders. We cannot directly compare studies of different lithologies in different environments, but we would expect a clear difference in roughness values between the RC 1 and BI 1 / BI 2 boulder trains if intense erosion has occurred.

Kaplan *et al.* (2007) suggested that proximity to the coastline may have caused higher rates of salt-spray weathering of the RC 1 boulders. Similarly, the dominant effect of the westerly winds in the region could have caused increased aeolian abrasion. Figure 4.17 shows the results for averaged rock surface hardness and rock surface roughness from each boulder, with total boulder values and east/west faces shown. Correlations between these results and the distance from the start of the BI 1 and RC 1 boulder trains are negligible. Given the variability in the data, there is no indication that salt-spray weathering or aeolian abrasion has had a

variable effect on boulders within RC 1 or a markedly greater effect on RC 1 than BI1.

Weathering could have been operating on a scale greater than that recorded by our proxies. However, whilst examples of microgullies and potholes are abundant on the top surfaces of the RC 1 boulders (Kaplan *et al.*, 2007), similar features exist on the BI 1 and BI 2 boulders, and we found little difference in top surface weathering between the boulder trains (Figures 4.10, 4.11 and 4.12). The similarity in weathering results between the EBTs suggests that they have probably experienced similar local climatic conditions. This is important given that the intense weathering needed to reduce the ages of the RC 1 boulder train during, or since, the gLGM should have also reduced the ages of the BI 1 and BI 2 boulder trains. The cosmogenic exposure dates for the BI 1 and BI 2 boulder trains are believed to be good estimates of the time of deposition (around the gLGM), agreeing with radiocarbon dates in the area (Heusser, 2003; McCulloch *et al.*, 2005b; Kaplan *et al.*, 2008a; Hall *et al.*, 2013) and factors that reduced the RC 1 boulder dates by hundreds of thousands of years are highly unlikely to have also reduced the BI 1 and BI 2 dates.
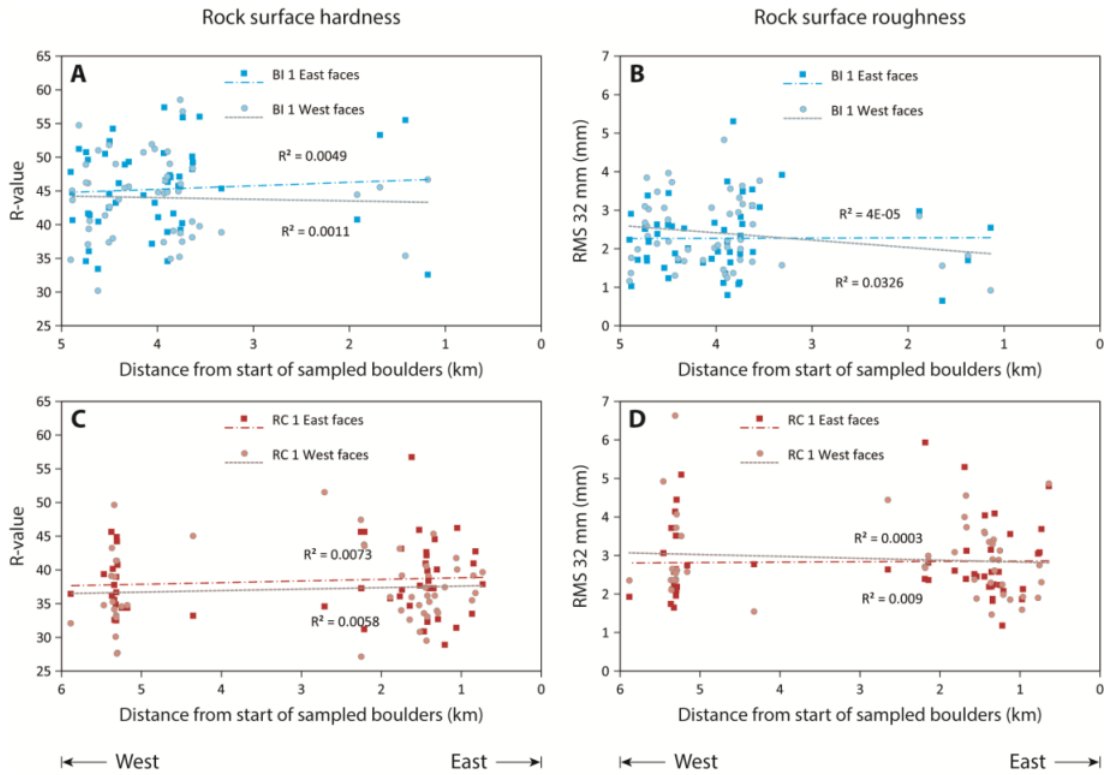
Figure 4.17. The rock surface hardness and roughness results from Figures 4.15 and 4.16 plotted to illustrate variations in aspect with distance along the boulder trains (data points relate to individual boulders and are only shown for BI 1 and RC 1). (A) Shows hardness results for the east and west faces of BI 1, and (B) shows roughness results for the east and west faces of BI 1. (C) Shows hardness results for the east and west faces of RC 1, and (D) shows roughness results for the east and west faces of RC 1. In all graphs, boulder values toward the right are located farther to the east and those toward the left are located farther to the west. No discernible trends are found in either of the boulder trains, as illustrated by very low R^2 values, suggesting that salt weathering has not affected RC 1 significantly more than BI 1, as hypothesised by Kaplan *et al.* (2007), despite closer proximity to the coast.

4.5.4 Alternative (post-)depositional model

The EBTs on Tierra del Fuego were thought to have been deposited during different glacial episodes (MIS 12, 10, and 2), but cosmogenic nuclide exposure dating from all of the EBTs yielded dates predominantly around 20 ka (Kaplan *et al.*, 2007; Evenson *et al.*, 2009). One hypothesis (the boulders are 'old') explains this anomaly by invoking intensive post-depositional exhumation and erosion of the RC 1 boulders (Kaplan *et al.*, 2007), but a second (the boulders are 'young') suggests that supraglacial debris may have an inheritance signature. Our study demonstrates that the distribution, volume, and monolithology of the boulder trains are indicative of supraglacial transport of rock avalanche material, and our rock surface weathering data do not support intensive post-depositional exhumation and erosion of the RC 1 boulders. Given this information, our data support the second, 'young' hypothesis, whereby the EBTs were transported and deposited at roughly the same time (i.e. within a few thousands of years, rather than separated by 100s of thousands of years). Under this scenario, one would anticipate mostly young ages from the boulders, but with some anomalously old dates resulting from an inheritance signal owing to pre-exposure of boulders in the cliff face, which were not then sufficiently eroded during supraglacial transport (Applegate *et al.*, 2010; Heyman *et al.*, 2011; Applegate *et al.*, 2012).

This scenario is similar to that envisaged for the Foothills boulder train in Alberta, where Jackson *et al.* (1997) suggested that an erratic boulder that yielded a date of *ca.* 53 ka (four times older than the next oldest date) was improbable and most likely caused by pre-exposure prior to glacial transport. This implies that, for a supraglacial EBT deposit, a fraction of boulders should be expected to yield anomalously old dates. Assuming that the majority of [10]Be cosmogenic exposure dates are roughly correct, three anomalously old dates are apparent from the Tierra del Fuego boulder trains (Kaplan *et al.*, 2007; Evenson *et al.*, 2009). For RC 1, one date (*ca.* 57 ka) out of 7; and for BI 2, one date (*ca.* 56 ka) out of 17 may have been pre-exposed. The similarity between these ages could indicate a consistent (pre-)exposure pattern, but more samples would be needed to support this idea. The outlier from SSb 1 is significantly older at *ca.* 222 ka, although this is only one of two samples from that boulder train.

Leaving aside the anomalously old dates, substantial variability remains in the cosmogenic nuclide exposure dates of the RC 1 EBT, a fact that Kaplan *et al.* (2007) highlighted. Variability in the dates could have been caused by variability in

the residence time on the ice during transport. Hubbard *et al.* (2005) modelled ice flow velocities of up to 2000 m a^{-1} for the northern Patagonian Ice Sheet. Assuming similar velocities and a transport distance of up to 250 km for the BI–SSb lobe, transport time may have been as little as 0.125 ka: insignificant given dating uncertainty. Slower velocities of 100 m a^{-1} or even 50 m a^{-1} would have resulted in residence times of 2.5 or 5 ka, respectively; but given that the clustering of the EBTs suggests that they were deposited as discrete events, this could only have resulted in age differences between, not within, boulder trains.

Rather, we suggest three mechanisms that could have produced the variability in RC 1. First, RC 1 has probably experienced greater erosion than BI 1 / BI 2 as it was deposited first, causing variable reduction in cosmogenic nuclide exposure dates. Secondly, we agree with Kaplan *et al.* (2007) that many boulders in the RC 1 train show signs of surface weathering, although we find similar signs in the BI 1 / BI 2 EBTs. Sampling of the RC 1 boulder train may have been more affected by weathered surfaces than BI 1 / BI 2 because fewer larger boulders are found in RC 1 and this could have resulted in sampling of boulders that were 'less ideal' than those in the other boulder trains.

Thirdly, Jackson *et al.* (1997) suggested that boulder orientation can affect the spread of dates in a boulder train. We have demonstrated that all boulders in Tierra del Fuego are likely 'at rest', but do not know how long they were sitting on melting ice before reaching this state. The RC 1 and SSb 1 boulder trains are located on large bands of kettle kame drift, a characteristic deposit of 'dead ice' terrain (Dyke & Evans, 2003; Schomacker, 2008), whereas BI 1 and BI 2 are located on small, sharp moraines interspersed by meltwater channels. Ground ice within the kettle and kame topography could have taken a long time to fully melt and settle, and occasional examples of boulders exposed at the coastline, within the kettle and kame deposits, may be a result of this slow process of settling (Figure 4.12H). Thus, the RC 1 boulder train may have taken *ca.* 10 ka to come to rest and implies that ground ice melting may have prevailed long after the recession of the ice lobe.

To summarise, the main implication behind this alternative history of the EBTs on Tierra del Fuego is that the established age model for the timing of glaciations in the region may need re-examining. Whilst this study provides a new approach to interpreting the cosmogenic nuclide exposure dates, further independent age controls for the glacial limits are needed to investigate the timing of glacial advances.

4.6 Conclusion

Erratic boulder trains make valuable targets for flow-line indicators and cosmogenic nuclide exposure dating, but few have been reported in detail and further studies are needed to understand their formation, transport, and deposition. Based on the limited number of EBTs that have been reported in the literature, we identify an apparent trend between boulder size, transport distance, and likely mode of transport. The EBTs containing boulders greater than *ca.* 5 m in diameter and/or demonstrating transport from the source lithology of greater than *ca.* 10 km are likely to have been transported supraglacially.

In Tierra del Fuego, the distribution and volume of three boulder trains suggest that they were formed by a rock avalanche and transported and deposited supraglacially. This highlights a former ice flow line from the Cordillera Darwin and helps to constrain the position of ice divides and the maximum ice surface elevation. Using a variety of techniques and measurements, we do not identify any major changes in rock surface weathering characteristics across EBTs that have been previously interpreted to be from different glacial cycles. Thus, we suggest that they are much closer in age (probably within a few thousand years), which is also consistent with previous cosmogenic nuclide exposure dates from the boulders. Occasional, anomalously old samples should be expected from supraglacial boulder trains caused by pre-exposure prior to and during glacial transport, and an understanding of the likely history of an EBT should be an integral part of using the features for dating.

Chapter 5.   Extensive MIS 3 glaciation in southernmost Patagonia revealed by cosmogenic nuclide dating of outwash sediments

Darvill, C.M., Bentley, M.J., Stokes, C.R., Hein, A.S. & Ródes, Á. (in prep.) 'Extensive MIS 3 glaciation in southernmost Patagonia revealed by cosmogenic nuclide dating of outwash sediments', *Earth and Planetary Science Letters*.

Abstract

The timing and extent of former glacial advances can demonstrate leads and lags during periods of climatic change and their forcing, but this requires robust glacial chronologies. In southernmost Patagonia, dating pre-gLGM ice limits has proven difficult due to post-deposition processes affecting the build-up of cosmogenic nuclides in moraine boulders. Here we provide ages for the Río Cullen and San Sebastián glacial limits of the former BI-SSb ice lobe on Tierra del Fuego (53-54°S), previously hypothesised to represent advances during MIS 12 and 10, respectively. Our approach uses cosmogenic ^{10}Be and ^{26}Al exposure dating, but targets glacial outwash associated with the limits and uses depth-profiles and surface cobble samples, thereby accounting for surface deflation and inheritance. The data reveal that the limits formed more recently than previously thought, giving ages of 45.6 ka (+139.9/-14.3) for the Río Cullen, and 30.1 ka (+45.6/-23.1) for the San Sebastián limits. These dates indicate extensive glaciation in southern Patagonia during MIS 3, prior to the well-constrained, but much less extensive MIS 2 gLGM limit. This suggests the pattern of ice advances in the region was different to northern Patagonia, with nested limits relating to the last glacial cycle, rather than progressively less extensive glaciations over hundreds of thousands of years. However, the dates are consistent with MIS 3 glaciation elsewhere in the southern mid-latitudes, and the combination of cooler summers and warmer winters, with increased precipitation, may have caused extensive glaciation prior to the gLGM.

5.1 Introduction

The terrestrial record of former Southern Hemisphere ice masses has been used to assess inter-hemispheric synchroneity of glacial advance and retreat (Sugden *et al.*, 2005; Kaplan *et al.*, 2010; Putnam *et al.*, 2013a) and how climatic forcing, such as changes in the Southern Westerly Winds (Figure 5.1), triggered ice growth or wastage through time (Kohfeld *et al.*, 2013). Patagonia is an ideal location for such records given that it spans a large latitudinal range and exhibits well-preserved glacial geomorphology reflecting former advances of the Patagonian Ice Sheet. However, coupling glacial reconstructions with robust chronologies is challenging.
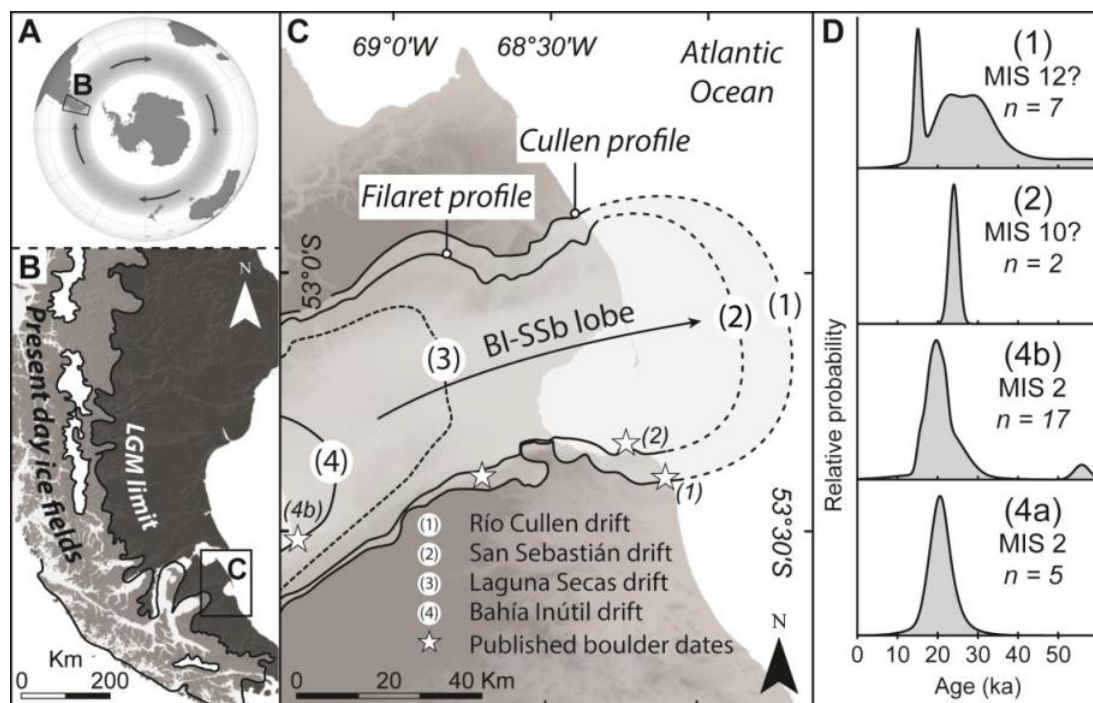
Figure 5.1. (A) Location of the study area, with shading indicating the approximate present extent of the Southern Westerly Wind system. (B) Map of Patagonia with gLGM ice extent from Singer *et al.* (2004a). (C) Drift limits of the former BI-SSb ice lobe across northern Tierra del Fuego from Meglioli (1992) and Chapter 3. Dashed lines indicate inferred extents. Stars show approximate locations of previously published [10]Be exposure dates from boulder trains (McCulloch *et al.*, 2005b; Kaplan *et al.*, 2007; Evenson *et al.*, 2009), and the Filaret and Cullen depth profiles from this study are labelled. The Bahía Inútil drift (4) correlates with the gLGM. (D) Previously published [10]Be dates, shown as cumulative probability density function plots (McCulloch *et al.*, 2005b; Kaplan *et al.*, 2007; Evenson *et al.*, 2009). Graphs are labelled according to drift limits in C, along with the published hypothesised MIS age (Coronato *et al.*, 2004) and the number of samples. One additional exposure date for limit 2 is 222 ± 7 ka.

The established model for the timing of glaciations in this region hypothesises that, following the 1.1 Ma GPG (Caldenius, 1932), the Patagonian Ice Sheet lobes oscillated in unison, creating a pattern of 'nested' glacial limits resulting from a series of progressively less-extensive glaciations throughout the Quaternary (Coronato *et al.*, 2004; Figure 5.1). Chronologies from northern Patagonia have demonstrated such a pattern (Singer *et al.*, 2004a; Kaplan *et al.*, 2005; Hein *et al.*, 2009; Hein *et al.*, 2011), but the timing of glacial advances in southernmost Patagonia is more open to conjecture. On Tierra del Fuego, moraines hypothesised to have been deposited during MIS 12 (*ca.* 450 ka) and MIS 10 (*ca.* 350 ka) have been dated using cosmogenic nuclide exposure dating of erratic boulders and yielded dates centred around *ca.* 21 ka, similar to the gLGM limit (Figure 5.1; Kaplan *et al.*, 2007; Evenson *et al.*, 2009). It has been suggested that this could be due to intense post-depositional exhumation and erosion of the boulders from MIS 12/10 limits (Kaplan *et al.*, 2007), but an alternative hypothesis, suggested here, is that the dates are closer to the true age of the glacial advance whereby, following the GPG, the ice lobe was most extensive during the last glacial cycle (MIS 4-2).

In this study, we test these two opposing hypotheses using a new method that can account for post-depositional exhumation processes. Specifically, Hein *et al.* (2009) demonstrated that cosmogenic nuclide depth-profiles through outwash associated with moraine limits can yield robust ages for glacial limits where post-depositional erosion and exhumation may compromise traditional moraine-boulder samples. We present ^{10}Be and ^{26}Al dates from two depth profiles through outwash associated with glacial limits of the BI-SSb ice lobe on Tierra del Fuego (53-54°S) and use these results to test the established age model for the timing of glacial advance.

5.2 Study area

The BI-SSb depression in central Tierra del Fuego was the former location of an eastward flowing ice-lobe sourced from the Cordillera Darwin range to the southwest (Evenson *et al.*, 2009; and Chapter 4). Two large bands of kettle and kame drift (Figures 5.2 and 5.3) correspond with two former ice limits (Figure 5.1). The inner limit is the San Sebastián drift (Meglioli, 1992) and is hypothesised to date from MIS 10 based on correlations to Uranium-series dated marine terraces (Bujalesky *et al.*, 2001; Coronato *et al.*, 2004). The outer limit forms the Río Cullen drift (Meglioli, 1992), and is hypothesised to date from MIS 12 (Coronato *et al.*, 2004) based on ages of <760 ka by palaeomagnetism of basal till (Walther et al., 2007). However, direct cosmogenic nuclide exposure dating of boulders on both drifts yielded

substantially younger ages, ranging from 15 to 222 ka with most <50 ka (Figure 5.1; Kaplan *et al.*, 2007; Evenson *et al.*, 2009).

5.3 Methods

5.3.1 *Sampling*

We identified locations where the San Sebastián and Río Cullen limits could be linked unequivocally to their associated outwash units. An overview of the glacial geomorphology of this part of Tierra del Fuego is shown in Figure 5.2, and an enlarged version of the sampling area is shown in Figure 5.3 (see also Appendix). The outwash is considered to relate unambiguously to the glacial limits in question and, in both cases, it was possible to walk directly from the sample locations on the outwash surfaces onto the kettle kame drift deposits of the glacial limits.

The outwash surfaces retained original surface morphology and appeared to be relatively undisturbed. The path of meltwater issuing from the inner San Sebastián glacial limit could be clearly traced through the outer Río Cullen glacial limit, and formed an incised channel in the Río Cullen outwash surface that did not affect the Cullen profile (Figure 5.4). Furthermore, meltwater younger than the San Sebastián glacial limit was topographically confined to the central BI-SSb depression (Figure 5.4), where it flowed directly east toward the Atlantic. Two depth profiles were sampled at these locations, relating to the San Sebastián glacial limit (Filaret profile) and the Río Cullen glacial limit (Cullen profile; Figure 5.1). The surfaces of these units possessed a well preserved morphology (e.g. braided meltwater channels), graded directly to the moraines of the drift limit (Figures 5.6 and 5.9), and showed no evidence of post-depositional reworking. Consequently, they are ideal locations for dating using outwash depth-profiles (Hein *et al.*, 2009; Hein *et al.*, 2011).
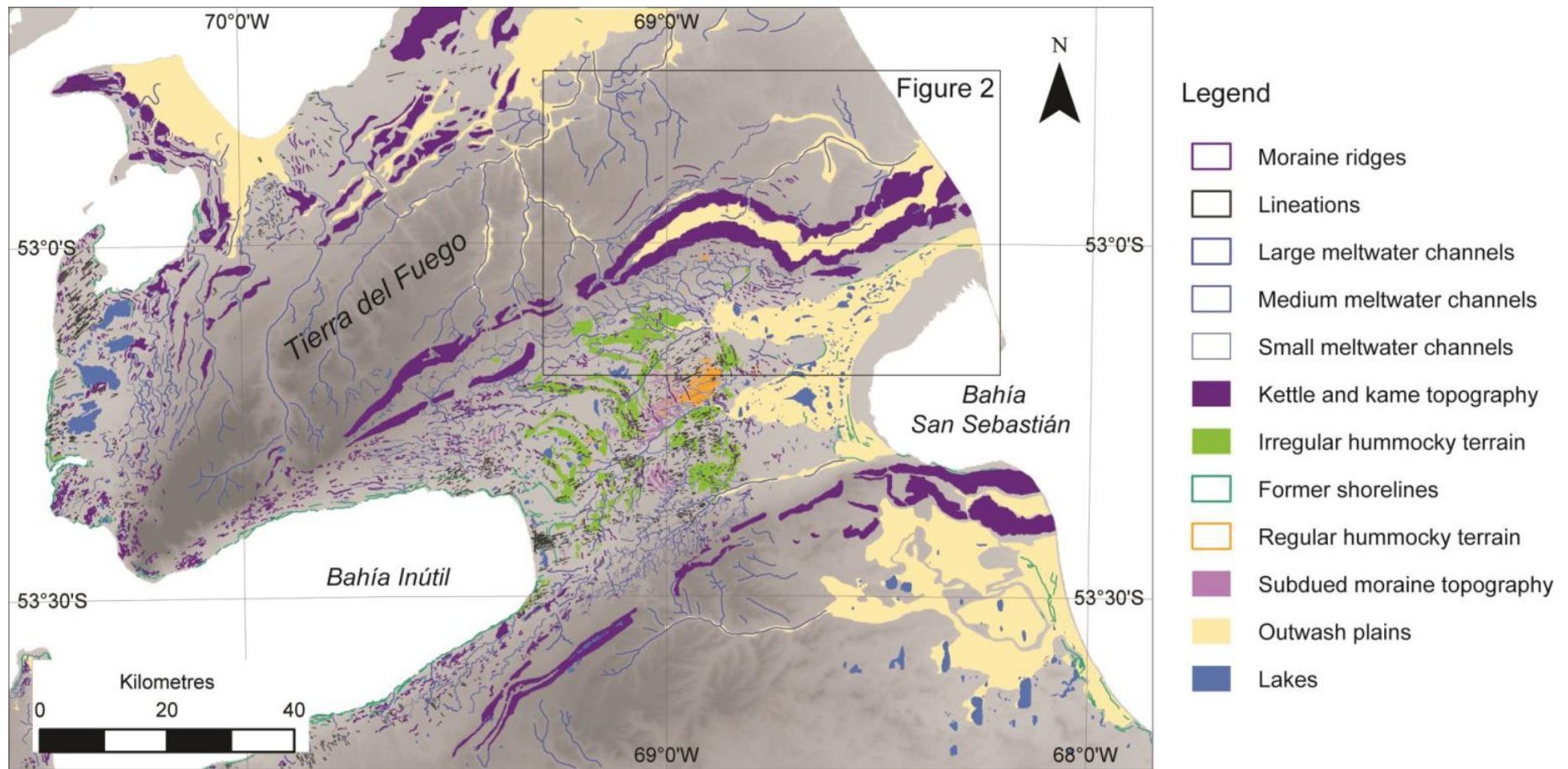
Figure 5.2. The glacial geomorphology of the former BI-SSb ice lobe in Tierra del Fuego, adapted from Chapter 3.
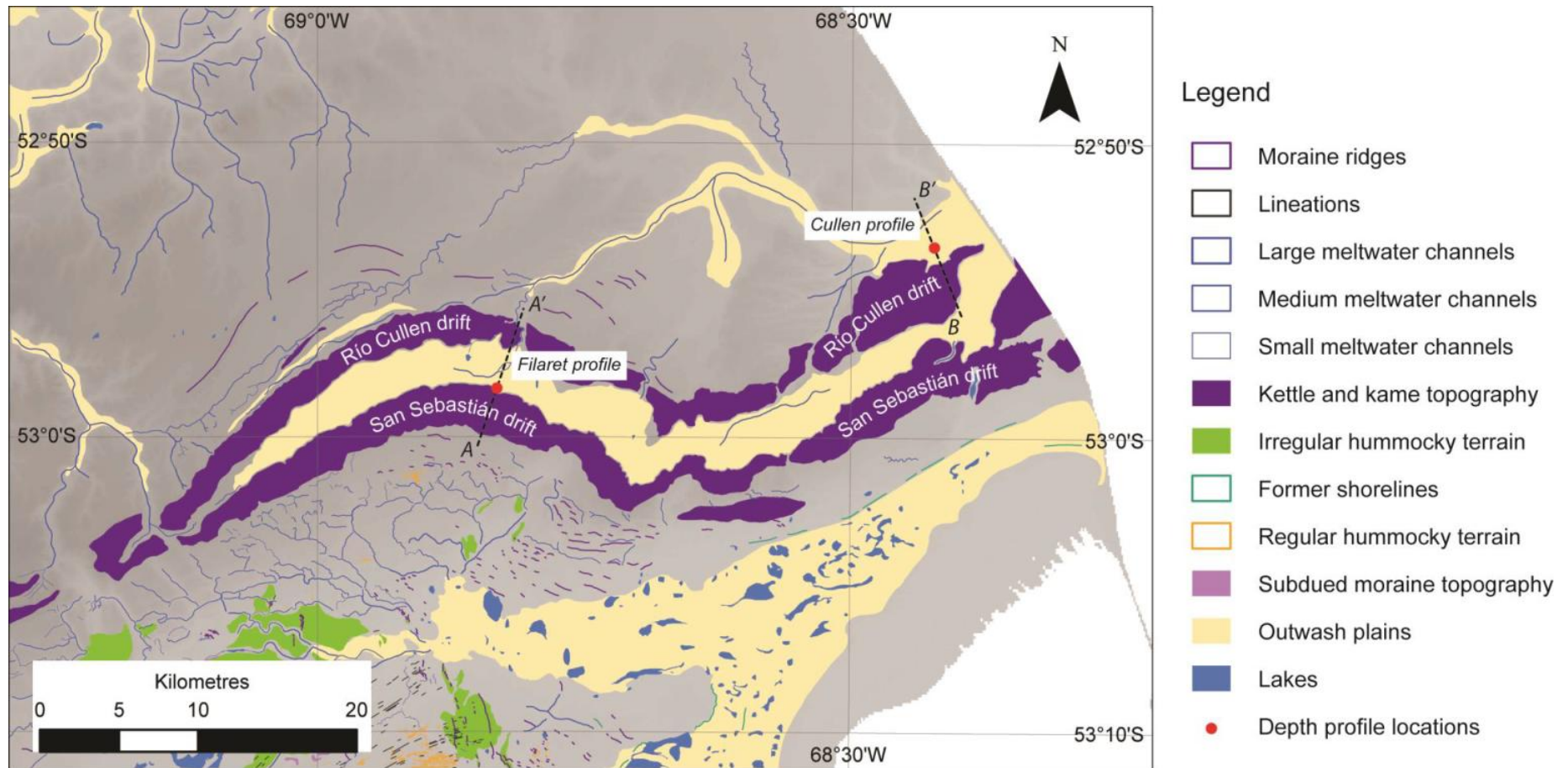
Figure 5.3. Zoomed version of Figure 5.2 to show the sampling area and the locations of the depth profiles, adapted from Chapter 3.
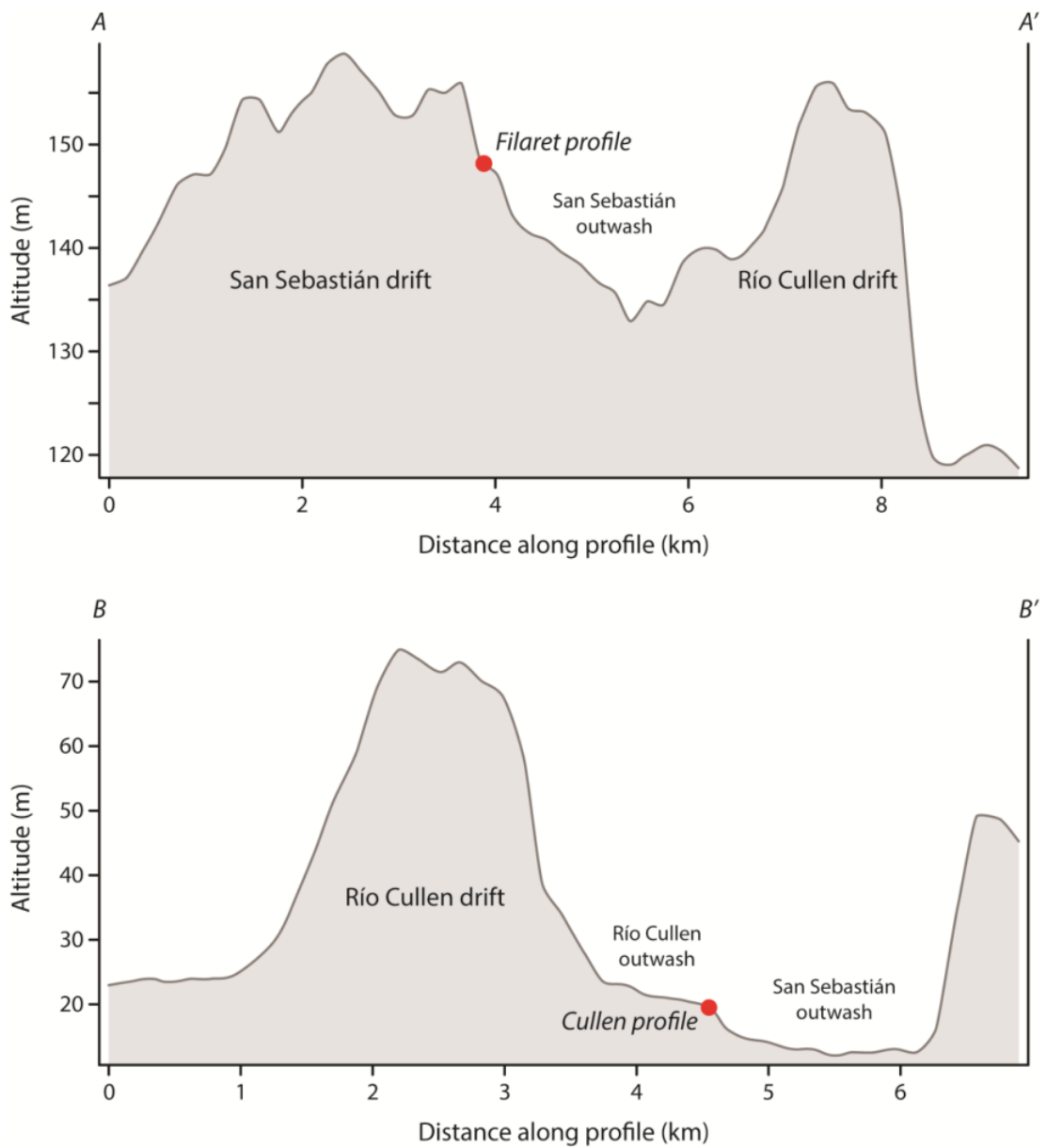
Figure 5.4. Transects *A-A'* and *B-B'* from Figure 5.3 showing the elevation change across the glacial drift limits and the sampled outwash.

The depth profiles were sampled from exposures within small, contemporary road-side quarries. These were cleared and logged, exhibiting sediments ranging from silts to cobbles of various, mixed lithologies (Figures 5.6 and 5.9). Our field observations suggested that each outwash terrace accumulated continuously as a discrete deposit associated with the meltwater issuing from the nearby glacial limit. Both were covered in low grass and were capped by brown, silty, poorly-developed soils up to ~ 25 cm deep. Each contained a single outwash unit of silts, sands, gravels and cobbles at various grades, but with no obvious signs that their source had changed over time. There were no frost wedges within the sediments and no clear signs of cryoturbation or pedogenic carbonate formation. Depths through the outwash were measured with a tape measure from the surface and were demarcated for sampling using a spirit level and spray-paint. We followed Hein *et al.* (2009) in collecting depth and surface samples to allow modelling of cosmogenic ^{10}Be and ^{26}Al accumulation to give a most probable unit age, whilst constraining inheritance and post-depositional surface erosion.

Small (*ca.* 6 cm) quartz cobbles embedded within the outwash surface in the vicinity of the exposures were sampled, crushed whole, and analysed individually as independent estimates of exposure time – shown before and after sampling in Figures 5.7 and 5.10. We also collected ~1 kg samples of mixed lithology pebbles (>0.5 cm and <4 cm) at 25 cm depth intervals (depth error ≤4 cm), including a sample at the base of the section to help calculate inheritance in the profile. Each depth sample was amalgamated and analysed for ^{10}Be and ^{26}Al concentrations. One sample (FP025cs) consisted half of sand matrix due to insufficient clasts at that depth. In both profiles the lowermost sample consisted of two separate depth samples combined (i.e. an unprocessed weight of ~ 2 kg) due to insufficient quartz; hence the apparent thickness of these samples is greater.

All physical and chemical preparation and ^{10}Be/^{9}Be and ^{26}Al/^{27}Al AMS measurements were carried out at the Scottish Universities Environmental Research Centre (SUERC) as part of the NERC Cosmogenic Isotope Analysis Facility (CIAF), as per Wilson *et al.* (2008).
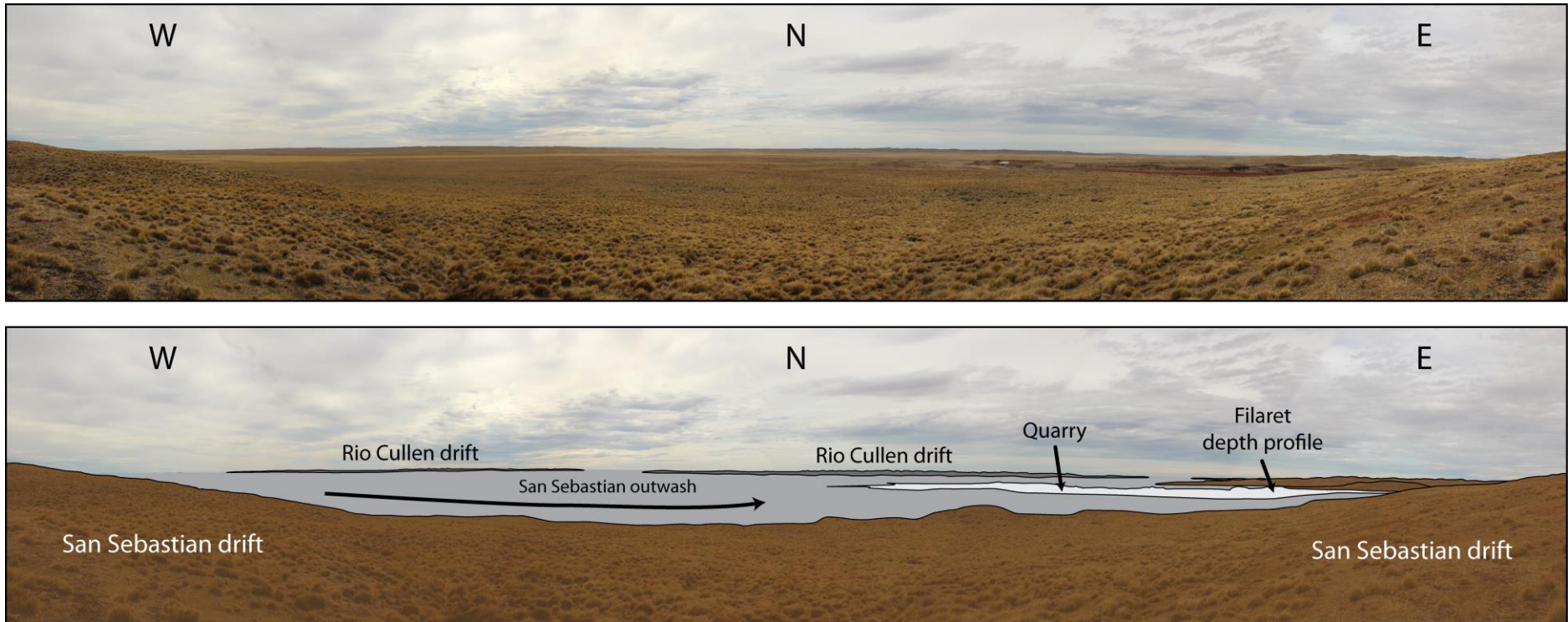
Figure 5.5. Panorama of the Filaret profile location (top) with annotations (bottom). (W)est, (N)orth and (E)ast directions are shown.
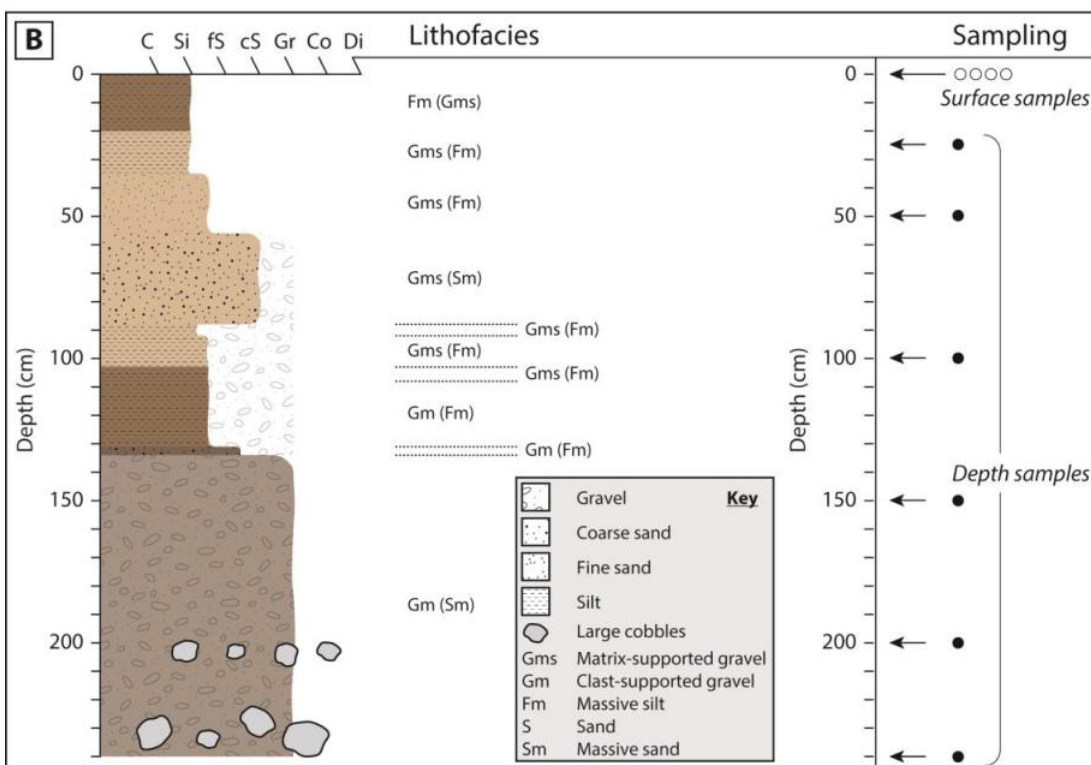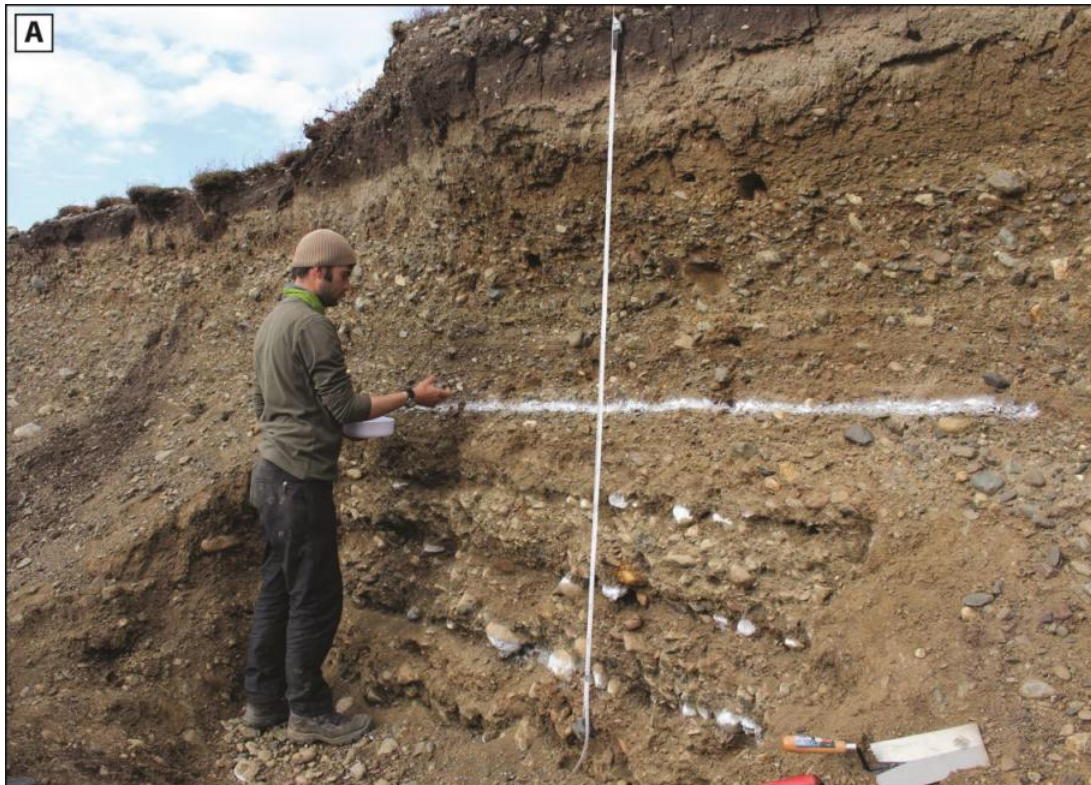
Figure 5.6. (A) Photograph of the Filaret depth profile during sampling. The top of the profile was taken from the local soil level, given there was also some spoil from the quarry. (B) sediment log and description for the Filaret profile, highlighting the depths of samples analysed in this study.

Figure 5.7. Pictures of the surface cobble samples from the Filaret profile before (left) and after sampling (right). Each caption shows the sample name, and those on the right also show the calculated ^{10}Be / ^{26}Al ages from Table 5.2.
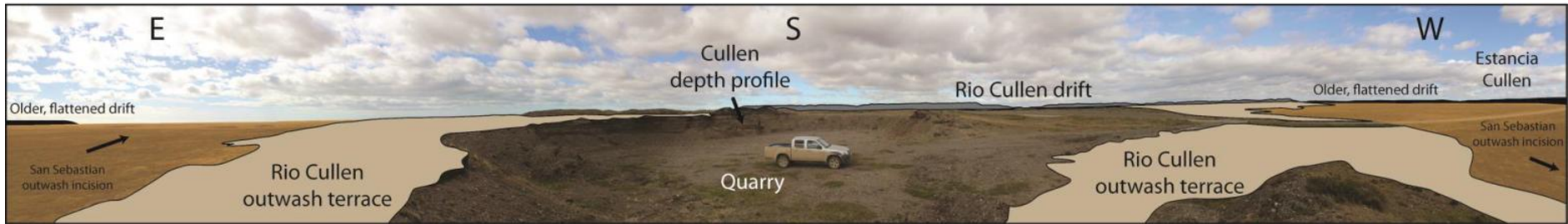
Figure 5.8. Panorama of the Cullen profile location (top) with annotations (bottom). (E)ast, (S)outh and (W)est directions are shown.
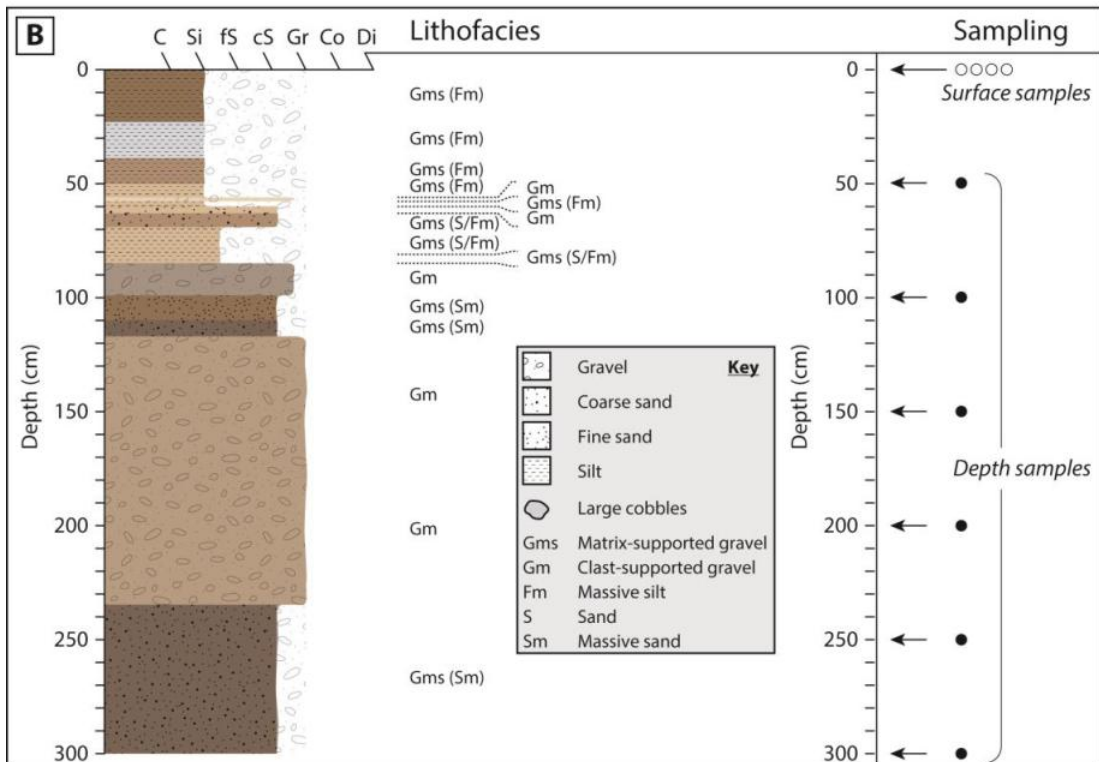
Figure 5.9. (A) Photograph of the Cullen depth profile during sampling. The top of the profile was taken from the local soil level, given there was also some spoil from the quarry. (B) sediment log and description for the Cullen profile, highlighting the depths of samples analysed in this study.
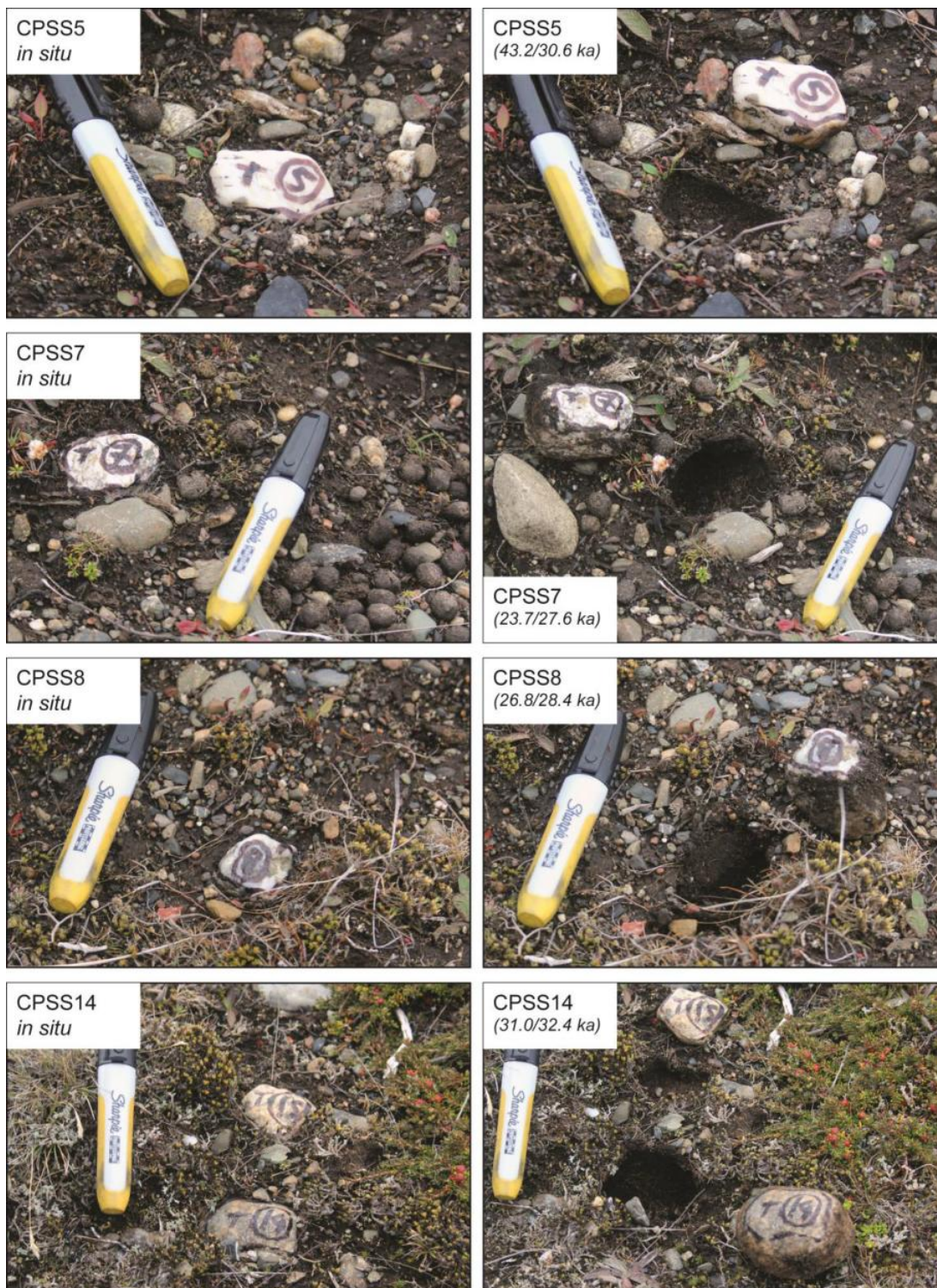
Figure 5.10. Pictures of the surface cobble samples from the Cullen profile before (left) and after sampling (right). Each caption shows the sample name, and those on the right also show the calculated ^{10}Be / ^{26}Al ages from Table 5.2.

5.3.2 Chemical analysis

Surface cobbles were treated individually, whereas depth samples were treated as amalgams. All samples were crushed whole, milled and sieved, and the >125 μm <500 μm fraction was then magnetically separated using a Frantz machine prior to chemical analysis. They were treated with a 2:1 mixture of H_2SiF_6 and HCl on a shaker table to dissolve non quartz minerals. The quartz was then purified by repeat etching in HF on a shaker table to remove >30 % of the starting mass; with the ion concentration gauged using assays measured by ICP-OES.

All samples were dissolved in 40% HF dry-downs on a hotplate. 0.2 mg of ^{9}Be carrier was added to each sample and ^{26}Al carrier was added to most samples so that 2 mg of Al per sample was reached. The solutions were passed through anion exchange columns to remove Fe and other contaminants, and then precipitated to remove Ti prior to being passed through cation exchange columns to separate Be and Al. The separate Be and Al fractions were precipitated and converted to BeO and Al_2O_3, before being prepared for AMS analysis.

NIST-SRM4325 and PRIME-Z93-0005 primary standards were used for AMS measurements, with nominal ratios of 2.97×10^{-11} ^{10}Be/^{9}Be and 4.11×10^{-11} ^{26}Al/^{27}Al, respectively. The reported uncertainties of the nuclide concentrations include 2.5% for the AMS and chemical preparation. Blank corrections ranged between 3 and 15% of the sample ^{10}Be/^{9}Be ratios and between 0 and 0.9% of the sample ^{26}Al/^{27}Al ratios. The uncertainty of the blank measurements is included in the stated uncertainties.

Table 5.1. Sample descriptions and nuclide concentrations.

Be ID	Al ID	Type *	Sample ID	Latitude (DD)	Longitude (DD)	Altitude (m asl)	Elv. flag	Thickness (cm) †	Density (g cm^{-2}) §	Shielding correction	Erosion (cm yr^{-1})	^{10}Be (atoms g^{-1})	1σ (atoms g^{-1})	Be AMS std	^{26}Al (atoms g^{-1})	1σ (atoms g^{-1})	Al AMS std
Filaret profile																	
b6888	a1765	a	FP025CS	-52.9743	-68.8310	148	std	4	-	0.999999	0	123056	5543	NIST_27900	923474	34485	Z92-0222
b6889	a1766	a	FP050	-52.9743	-68.8310	148	std	4	-	0.999999	0	108030	4819	NIST_27900	756901	35858	Z92-0222
b6890	a1767	a	FP100	-52.9743	-68.8310	148	std	4	-	0.999999	0	72733	3034	NIST_27900	461039	17810	Z92-0222
b6891	a1768	a	FP125	-52.9743	-68.8310	148	std	4	-	0.999999	0	61958	2861	NIST_27900	382692	15694	Z92-0222
b6892	a1769	a	FP150	-52.9743	-68.8310	148	std	4	-	0.999999	0	38461	1812	NIST_27900	306046	11766	Z92-0222
b6894	a1771	a	FP200230	-52.9743	-68.8310	148	std	34	-	0.999999	0	50200	3342	NIST_27900	347187	22568	Z92-0222
b6895	a1772	s	FPSS1	-52.9743	-68.8310	148	std	6	2.7	0.999999	0	127390	3653	NIST_27900	856986	29261	Z92-0222
b6896	a1773	s	FPSS12	-52.9743	-68.8310	148	std	6	2.7	0.999999	0	118438	4222	NIST_27900	792773	35652	Z92-0222
b6897	a1774	s	FPSS13	-52.9743	-68.8310	148	std	6	2.7	0.999999	0	131073	5696	NIST_27900	819874	26226	Z92-0222
b6898	a1775	s	FPSS16	-52.9743	-68.8310	148	std	6	2.7	0.999999	0	118430	4081	NIST_27900	860572	36911	Z92-0222
Cullen profile																	
b6903	a1778	a	CP025	-52.8899	-68.4244	17	std	4	-	0.999999	0	111182	5361	NIST_27900	840414	31669	Z92-0222
b6904	a1819	a	CP050	-52.8899	-68.4244	17	std	4	-	0.999999	0	101669	6596	NIST_27900	738532	32418	Z92-0222
b6905	a1779	a	CP075	-52.8899	-68.4244	17	std	4	-	0.999999	0	154494	5576	NIST_27900	1095953	37862	Z92-0222
b6906	a1780	a	CP100	-52.8899	-68.4244	17	std	4	-	0.999999	0	85944	3075	NIST_27900	579643	21486	Z92-0222
b6908	a1820	a	CP150	-52.8899	-68.4244	17	std	4	-	0.999999	0	58815	2940	NIST_27900	359452	15955	Z92-0222
b6909	a1821	a	CP250275	-52.8899	-68.4244	17	std	29	-	0.999999	0	72573	3981	NIST_27900	550438	23670	Z92-0222
b6910	a1781	s	CPSS5	-52.8899	-68.4244	17	std	6	2.7	0.999999	0	180591	4619	NIST_27900	868057	29274	Z92-0222
b6911	a1782	s	CPSS7	-52.8899	-68.4244	17	std	6	2.7	0.999999	0	99630	2922	NIST_27900	784025	27306	Z92-0222
b6912	a1784	s	CPSS8	-52.8899	-68.4244	17	std	6	2.7	0.999999	0	112414	3101	NIST_27900	806137	29141	Z92-0222
b7197	a1785	s	CPSS14	-52.8899	-68.4244	17	std	6	2.7	0.999999	0	130107	3377	NIST_27900	918950	33591	Z92-0222

* a – amalgamated depth profile sample; s – individual surface cobble sample.
† depth sample thickness set at a standard 4cm error, with amalgamated samples including the depth between samples; surface cobble samples set at a standard 6cm error.
§ surface sample density is estimated at 2.7 g cm^{-3}; depth samples density is constrained during modelling.

Table 5.2. Calculated ages for surface samples using CRONUS-Earth calculator (Balco *et al.*, 2008). Grey shading indicates the production rate and scaling scheme used.

Sample ID	P_{NZ} St age (a)	±	De age (a)	±	Du age (a)	±	Li age (a)	±	Lm age (a)	±	P_{PTGN} Lm age (a)	±	P_{GLOBAL} Lm age (a)	±	P_{NZ} Lm age (a)	±
Filaret profile																
Be																
FPSS1	26050	944	26824	964	27102	974	26387	940	26633	961	26260	1163	22871	2048	**26633**	**961**
FPSS12	24208	1017	24933	1041	25197	1052	24544	1019	24750	1036	24404	1199	21256	1956	**24750**	**1036**
FPSS13	26808	1312	27603	1345	27885	1358	27145	1316	27407	1338	27024	1491	23536	2245	**27407**	**1338**
FPSS16	24206	992	24931	1016	25195	1026	24542	993	24749	1011	24403	1178	21255	1946	**24749**	**1011**
Al																
FPSS1	25892	1062	26660	1086	26936	1098	26229	1062	26469	1082	26088	1264	22741	2091	**26469**	**1082**
FPSS12	23929	1210	24643	1241	24905	1254	24265	1216	24463	1234	24111	1368	21021	2029	**24463**	**1234**
FPSS13	24757	969	25494	992	25762	1002	25093	969	25309	987	24945	1169	21747	1982	**25309**	**987**
FPSS16	26001	1267	26773	1299	27049	1312	26339	1271	26582	1292	26199	1444	22838	2184	**26582**	**1292**
Cullen profile																
Be																
CPSS5	42169	1431	43052	1447	43388	1458	42272	1407	43215	1459	42609	1811	37095	3298	**43215**	**1459**
CPSS7	23154	850	23669	862	23936	872	23358	844	23704	867	23373	1044	20364	1827	**23704**	**867**
CPSS8	26145	925	26717	937	27007	947	26332	915	26769	942	26396	1150	22995	2051	**26769**	**942**
CPSS14	30291	1034	30944	1046	31257	1057	30457	1020	31022	1053	30588	1303	26643	2365	**31022**	**1053**
Al																
CPSS5	29862	1216	30505	1235	30815	1247	30031	1207	30580	1241	30140	1454	26275	2416	**30580**	**1241**
CPSS7	26933	1121	27519	1138	27812	1150	27117	1114	27575	1144	27179	1331	23699	2187	**27575**	**1144**
CPSS8	27703	1185	28304	1204	28601	1216	27883	1178	28365	1210	27957	1397	24376	2262	**28365**	**1210**
CPSS14	31640	1367	32318	1389	32638	1402	31800	1358	32404	1396	31937	1608	27839	2593	**32404**	**1396**

Production rates: P_{NZ} – New Zealand production rate of Putnam *et al.* (2010b); P_{PTGN} – Patagonian production rate of Kaplan *et al.* (2011); P_{GLOBAL} – global production rate of Balco *et al.* (2008) and Nishiizumi *et al.* (2007). **Scaling schemes:** St – Lal (1991) and Stone (2000); De – Desilets *et al.* (2006); Du – Dunai (2001); Li – Lifton *et al.* (2005); Lm – time-dependent version of Lal (1991) and Stone (2000).

5.3.3 Age determination

5.3.3.1 Scaling scheme and production rate

For consistency, the time-dependent scaling scheme of Lal (1991) and Stone (2000) was used in surface sample age calibrations and recalibrations of published data. Likewise, the production rate of Putnam *et al.* (2010b) from New Zealand was used throughout to calibrate ^{10}Be and ^{26}Al measurements, given that it is now in common use in Patagonia and the Southern Hemisphere and that it overlaps at 1σ with an independent production rate from Lago Argentino in Patagonia (Kaplan *et al.*, 2011; see Table 5.2). We assessed the implications of choosing this production rate and scaling scheme combination using our surface sample ages calculated using the New Zealand production rate and Lal (1991) and Stone (2000) time-dependent scaling scheme. The global production rate gave ages <17% older or younger than our ages (irrespective of scaling scheme), but the Patagonian production rate gave ages <6% older or younger than our ages (irrespective of scaling scheme) or <5% older or younger when the same scaling schemes were compared. Using the New Zealand production rate, altering the scaling scheme resulted in <3% older or younger ages. Therefore, aside from not using the global production rate, our choice of production rate and scaling scheme does not alter our conclusions.

Table 5.3. Details of comparison moraine boulder ^{10}Be chronologies from Patagonia for the last 100 ka. Where appropriate, updated data from Kaplan *et al.* (2011) have been used.

Ice lobe	Total no. ^{10}Be dates	References
Lago Buenos Aires	77	Douglass *et al.* (2005); Kaplan *et al.* (2004); Kaplan *et al.* (2005); Douglass *et al.* (2006)
Lago Pueyrredón	12	Hein *et al.* (2009); Hein *et al.* (2011)
San Martín valley	10	Glasser *et al.* (2011)
Última Esperanza (Bella Vista / Río Gallegos lobe)	8	Sagredo *et al.* (2011); Kaplan *et al.* (2007); Evenson *et al.* (2009)
Magellan	17	McCulloch *et al.* (2005b); Kaplan *et al.* (2007); Kaplan *et al.* (2008a)
Bahía Inútil – San Sebastián	41	McCulloch *et al.* (2005b); Kaplan *et al.* (2007); Kaplan *et al.* (2008a); Evenson *et al.* (2009)

5.3.3.2 Surface samples

Apparent [10]Be and [26]Al exposure ages and internal uncertainties from surface sample measurements were calculated using the CRONUS-earth online calculator version 2.2 (available at http://hess.ess.washington.edu/math/; Wrapper script: 2.2; Main calculator: 2.1; Objective function: 2; Constants: 2.2.1; Muons: 1.1; see Balco *et al.*, 2008). We assumed a density of 2.7 g cm^{-3} (equivalent to the density of pure quartz) and used a standard, excess thickness of 6 cm for all samples to correct for self-shielding. Topographic shielding was measured in the field using an abney level but this correction was minimal (scaling factor >0.999999). Present day snow and vegetation cover is thin, and is unlikely to have increased during glacial times, so no correction was applied for shielding by snow cover or vegetation. Likewise, no erosion correction was applied given that the quartz cobbles showed no significant signs of surface erosion. As a result of these assumptions, the ages should be considered minimum estimates.

5.3.3.3 Depth profiles

The depth profiles were modelled using Hidy *et al.* (2010; version 1.2), which applies Monte Carlo simulations to find the most probable values for surface exposure age, erosion rate and nuclide inheritance. For both depth profiles, there were samples that deviated from the theoretical nuclide decay curve: FP150 for the Filaret profile and CP75 and CP150 for the Cullen profile. We tested whether these were outliers by running the model with wide parameters, initially including all samples (the model would not run) and then excluding all the samples one at a time. The model would only run with the outliers mentioned above removed from the profiles and they were not included in further modelling. This resulted in normally decreasing nuclide concentrations with depth, though the modelling was constrained by fewer samples.

The [26]Al/[10]Be ratio for CP150 plotted well below the steady state erosion island (Figure 5.11), normally indicative of a period of burial that results in a lower [26]Al/[10]Be ratio. However, it is unclear why the FP150 and CP75 samples yielded anomalous results, given that the [26]Al/[10]Be ratios are not low. Furthermore, there is no evidence for changing sedimentary processes at any of these three depths. Alternatively, anomalous results could have been caused by issues with the physical or chemical preparation of these samples, though no issues were recorded at the time and it is not possible to state the exact cause. With only four samples in the Cullen profile, the model yielded weaker constraint in the final age estimates.

There are two potential issues with using the Monte Carlo approach of Hidy *et al.* (2010) for our profile samples. First, it may artificially create a maximum age for a profile if the upper age-erosion rate area is narrow (Rodés *et al.*, 2014). Secondly, without constraint on either erosion rate or age, our profiles may only yield minimum ages (see Hidy *et al.*, 2010). We addressed the first issue by comparing initial results (from model runs with wide parameters) with an alternative model by Rodés *et al.* (2014). Both the Hidy *et al.* (2010) and the Rodés *et al.* (2014) models gave similar results, despite modelling the ages in different ways, suggesting that our data yielded minimum and maximum ages. We then continued modelling using the Hidy *et al.* (2010) model because it allows the user to constrain geological input parameters. We tackled the second issue by running sensitivity tests and also applying *a priori* knowledge to constrain the model parameters. We discuss the nature of these constraints in more detail in Section 5.4.2.

5.3.3.4 *Previous exposure dating studies*

We compare our chronology with other moraine boulder ^{10}Be exposure ages from studies in Patagonia. For consistency, we re-calculated all ages using the New Zealand production rate of Putnam *et al.* (2010b) and the time-dependent scaling scheme of Lal (1991) and Stone (2000). Ages were re-calculated using the CRONUS-earth online calculator version 2.2 (available at http://hess.ess.washington.edu/math/); Wrapper script: 2.2; Main calculator: 2.1; Objective function: 2; Constants: 2.2.1; Muons: 1.1; see Balco et al., 2008). We used all information provided in the original studies and assumed a density of 2.7 g cm^{-3} where no density information was provided. Although almost certainly unrealistic, we applied no erosion correction so that the studies could be directly compared in a simple way.

We present the data in the form of probability density plots, including all published ^{10}Be ages, with each moraine set normalised to one. This has the advantage of illustrating the cumulative ages from numerous samples and their errors and not biasing comparisons based on the assumptions of different authors regarding age reliability and geomorphic processes. However, this is a simplified presentation that is strongly influenced by the number of samples taken at different locations and does not take into account the likelihood that any samples may be anomalous, or that they have been affected by (variable) erosion. Therefore, we refer the reader to the respective studies for detailed discussions of all published dates. For reference, the details of the studies presented in Figure 5.3 are shown in Table 5.3. Data from

the Chilean Lake District are the synthesized, recalibrated radiocarbon dates of Denton *et al.* (1999).

5.4 Results

5.4.1 *Surface sample results*

The four Río Cullen surface sample ^{10}Be exposure ages range from 23.7 to 43.2 ka. The oldest sample (CPSS5) yielded a ^{26}Al/^{10}Be ratio below the steady state erosion island, indicating a complex exposure-burial history (Figure 5.11). Removing this outlier reduces the range to 23.7 to 31.0 ka (n = 3). The four San Sebastián surface sample ^{10}Be exposure ages are tightly clustered, ranging from 24.7 to 27.4 ka (n = 4), with all samples showing ^{26}Al/^{10}Be ratios consistent with a simple exposure history (Figure 5.11).
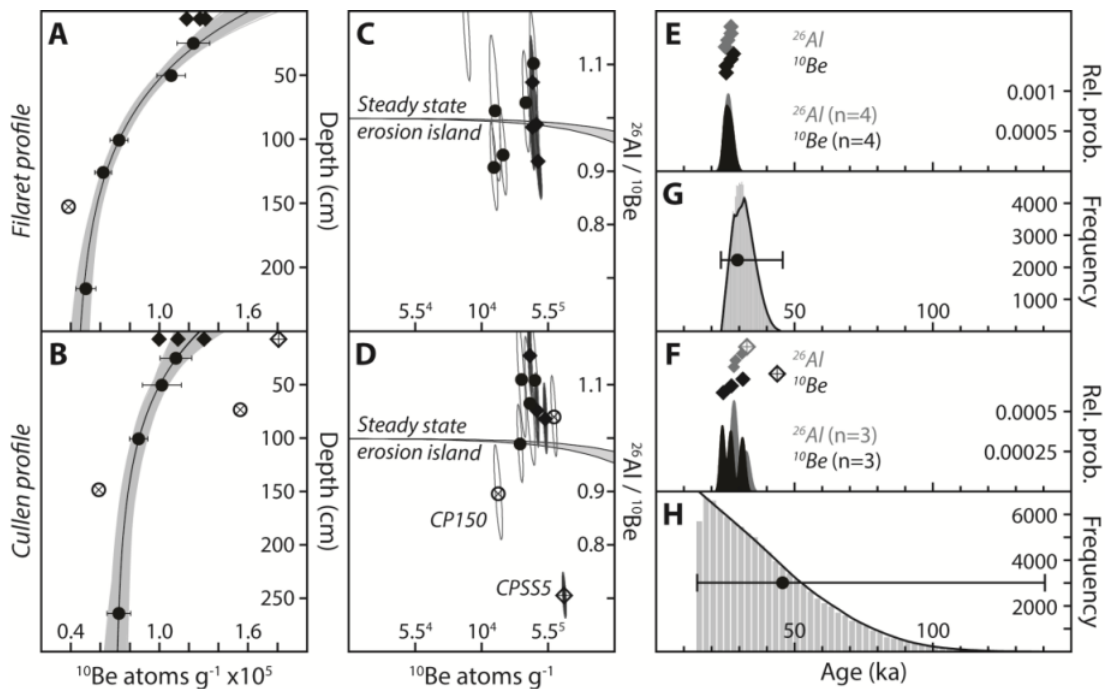
Figure 5.11. Cosmogenic nuclide results for the depth and surface samples from the Filaret profile (A,C,E,G) and Cullen profile (B,D,F,H). Circles are depth samples; diamonds are surface cobble samples; and crosses show excluded anomalies. A and B show results from 100,000 model runs (grey lines) and the optimum χ^2 profile (black line) through ^{10}Be depth samples, with ^{10}Be surface samples shown for reference. C and D show all samples as normalized ^{26}Al/^{10}Be ratios plotted against ^{10}Be concentration. The predicted range for a stable and steadily eroding surface is also shown (shaded area; Lal, 1991); samples plotting beneath this area may have undergone post-depositional shielding. E and F show the ^{26}Al (grey) and ^{10}Be (black) surface cobble results in age order and associated cumulative probability density function plots. G and H show the age results for 100,000 ^{10}Be depth profile model runs plotted as frequency histograms with the χ^2 optimum age (circle) and ≤95% maximum and minimum ages (whiskers).

5.4.2 Depth profile modelling

There is a paradox involved in modeling cosmogenic nuclide depth profiles. Often, parameters are unknown, but models require some constraint to produce an age. In theory, very wide, even unrealistic, parameters will yield the most reliable estimates of age, erosion rate and inheritance. However, the wider the constraints, the slower the model will run (if at all) and the wider the resulting error ranges. Consequently, a balance must be found between applying constraints to aid modeling and not inadvertently constraining the age, erosion rate and inheritance without good reason. In this section, we outline the conservative constraints that we applied to the Hidy *et al.* (2010) model. We present χ^2 sensitivity tests to check that the model output was not inadvertently affected and discuss where there is good reason to apply constraint based on *a priori* knowledge. Model parameters are given in Table 5.4 and a summary of the [10]Be depth profile results is given in Table 5.5.

5.4.2.1 Sensitivity tests

χ^2 sensitivity tests were conducted whereby broad model parameters were used (Table 5.4) and a single controlling parameter was then varied with each model run (Figures 5.12 and 5.13). Importantly, the controlling parameters only reduced the χ^2 maximum age, and did not significantly affect the χ^2 optimum or minimum age estimates. The sensitivity tests demonstrated that there were three model parameters which controlled the χ^2 maximum ages: *maximum total erosion*, *maximum age*, and *inheritance*. Of these, the *maximum total erosion* is the key determinant given that *maximum age* can be constrained to *ca.* 1100 ka by independent dating of the GPG across Patagonia (Meglioli, 1992; Singer *et al.*, 2004a) and *inheritance* can be constrained using the deepest samples. The *maximum total erosion* parameter differs from the *erosion rate* parameter in that the former is a threshold depth of erosion which the model is not permitted to exceed, regardless of the *erosion rate* or age of the sedimentary unit.

5.4.2.2 Density

Density through the profiles was unknown, and could not be measured in the field. However, it is an important age determinant in profile modelling, especially as most models behave according to the time-averaged density, rather than the present density (Rodés *et al.*, 2011). We ran sensitivity tests with very wide constraints (between 1 and 3 g cm^{-3}) and then used the change in maximum age outputs to constrain values slightly, although these were still extremely conservative given the nature of the sediments (between 1 and 2.7 g cm^{-3}).

5.4.2.3 Inheritance

Inheritance was essentially unknown. We ran sensitivity tests to assess the effect of inheritance constraint on maximum age outputs and then selected wide constraints. Given that we had deep samples in both profiles, we could also back-check the modelled inheritance in all model runs with the deep-sample nuclide concentrations. In all cases, our maximum inheritance constraints were well in excess of the measured deep nuclide concentrations.

5.4.2.4 Age limits

Initial modelling in conjunction with the Rodés *et al.* (2014) model gave maximum ages far older (5000 ka for the Filaret profile and 4000 ka for the Cullen profile) than the known age of the GPG at 1100 ka (Meglioli, 1992; Singer *et al.*, 2004a). We used these extreme upper limits for sensitivity tests and then 1100 ka as a more reasonable, but still highly conservative, maximum age limit for all other modelling. We applied no lower age limit during sensitivity tests, but then used an age of 14.348 ka for all other modelling. This is from a well dated Reclus tephra layer, known to have been deposited after the deposition of the gLGM glacial limit close to Bahía Inútil (McCulloch *et al.*, 2005b; Wastegård *et al.*, 2013). Again, this is highly conservative, and is only used to prevent a stratigraphic age reversal for the Cullen profile due to it containing fewer depth samples.

5.4.2.5 Erosion rate

The erosion rate was unknown, but sensitivity tests suggested it played no significant role in age determination (the *maximum erosion threshold* was always more important, see following sections), so we selected broad constraints throughout the model runs.

5.4.2.6 Maximum erosion threshold

Sensitivity tests showed that the maximum erosion threshold strongly affected age outputs, but is an unknown. It was, therefore, the key determinant in constraining maximum modelled age.

Table 5.4. Model parameters.

Filaret profile ^{10}Be

Parameter	Sensitivity tests		Unconstrained		4 m erosion		0.5 m erosion	
	Min.	Max.	Min.	Max.	Min.	Max.	Min.	Max.
Density (g cm^{-3})	1	3	1	2.7	1	2.7	1	2.7
Age (ka)	0	5000	14.348	1100	14.348	1100	14.348	1100
Erosion rate (cm ka^{-1})	0	5	0	5	0	5	0	5
Total erosion (cm)	0	10000	0	10000	0	400	0	50
Inheritance (atoms g^{-1})	0	200000	0	180000	0	180000	0	180000

Cullen profile ^{10}Be

Parameter	Sensitivity tests		Unconstrained		4 m erosion		0.5 m erosion	
	Min.	Max.	Min.	Max.	Min.	Max.	Min.	Max.
Density (g cm^{-3})	1	3	1	2.8	1	2.8	1	2.8
Age (ka)	0	4000	14.348	1100	14.348	1100	14.348	1100
Erosion rate (cm ka^{-1})	0	20	0	20	0	20	0	20
Total erosion (cm)	0	10000	0	10000	0	400	0	50
Inheritance (atoms g^{-1})	0	400000	0	300000	0	300000	0	300000

Other parameters

Location (deg):	Filaret profile: -52.9743, -68.8310;	Cullen profile: -52.8899, -68.4244	
Altitude (m.a.s.l.):	Filaret profile: 148 m;	Cullen profile: 17 m	
Strike/dip (deg)	0	Depth of muon fit	5 m
Shielding	0.999999	Error in total production rate	0%
Cover	1	Sigma confidence level	2
^{10}Be half-life	1.387 (5% error)	# profiles	100,000
Scaling scheme	Stone (2000) after Lal (1991)	No parallelisation	
Reference production rate	3.74	Neutrons	160 ± 5
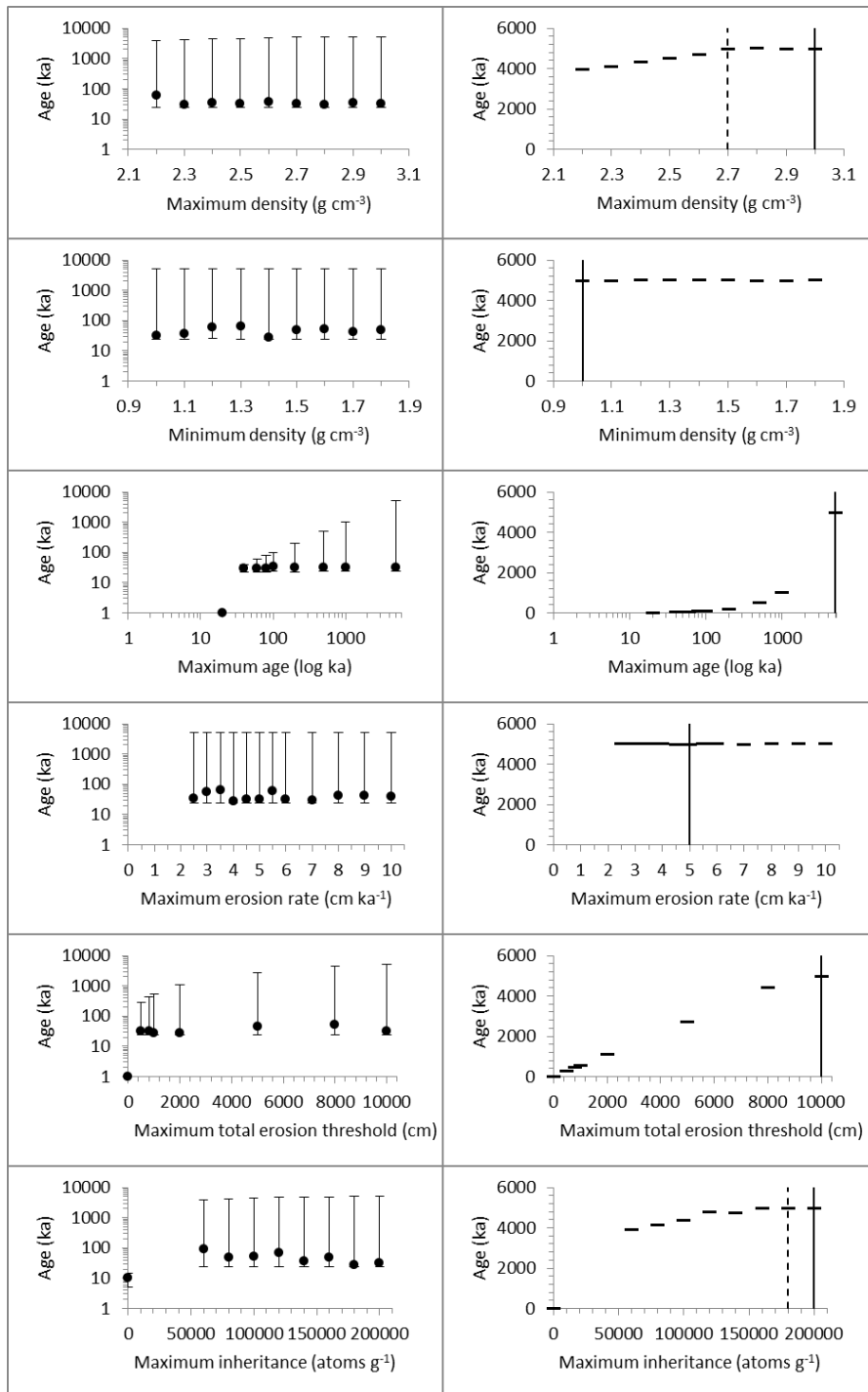
Figure 5.12. Sensitivity tests for the [10]Be Filaret profile. Plots in the left-hand column show the results of model runs when a single parameter was varied each time, with optimum χ^2 ages (circles) and ≤95% maximum and minimum ages (whiskers). Plots in the right-hand column show the same results but with only the ≤95% maximum ages. A solid vertical line shows the initial values used in modelling and a dashed vertical line shows where this was changed after sensitivity tests. The clear outcome of the sensitivity testing is that maximum ages are sensitive to the choice of some parameters, but that optimum ages are relatively insensitive.
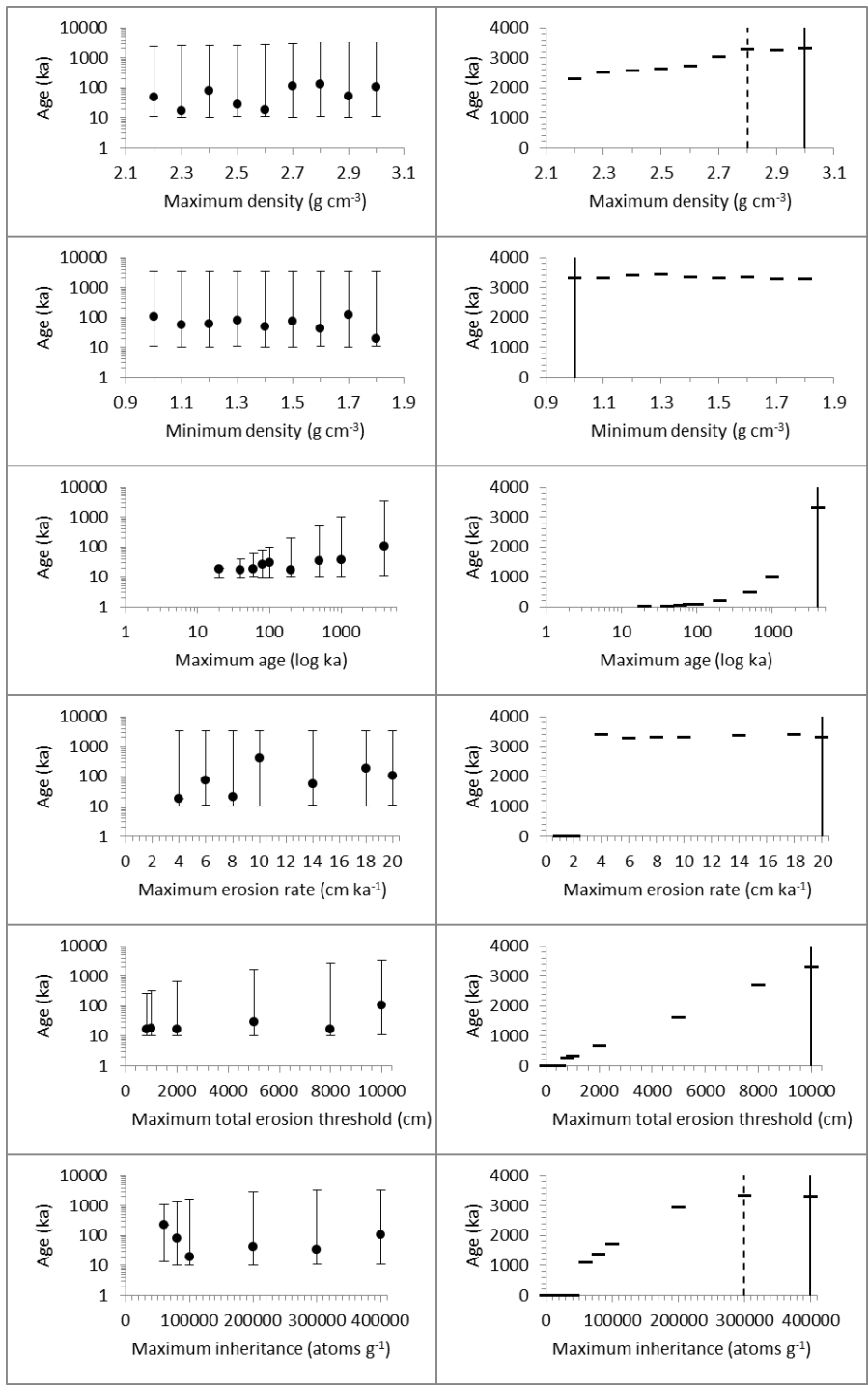
Figure 5.13. Sensitivity tests for the ^{10}Be Cullen profile. Plots in the left-hand column show the results of model runs when a single parameter was varied each time, with optimum χ^2 ages (circles) and ≤95% maximum and minimum ages (whiskers). Plots in the right-hand column show the same results but with only the ≤95% maximum ages. A solid vertical line shows the initial values used in modelling and a dashed vertical line shows where this was changed after sensitivity tests. The clear outcome of the sensitivity testing is that maximum ages are sensitive to the choice of some parameters, but that optimum ages are relatively insensitive.

5.4.2.7 Approach to modelling

To provide the most reliable estimates of age, erosion rate and inheritance from the depth profile modelling, we ran three models for each profile. First, we ran the model 'unconstrained' using very wide parameter ranges from the χ^2 sensitivity tests. All of these parameters were essentially unrealistically wide (e.g. up to 10 m of erosion and 2.7 g cm^{-3} density), but this was useful to gauge if constraining the maximum erosion threshold altered the age results. Next, we constrained the maximum erosion threshold to 4 m, to test whether there had been significant surface deflation similar to the moraine exhumation of Kaplan *et al.* (2007), and then 0.5 m, which is more likely given field observations of preserved geomorphology and the tight clustering of surface cobble ages.

Total erosion of the profile is a key parameter, and modelling shows that a minimum of ~4 m of moraine exhumation is required to have artificially reduced the ages of corresponding moraine boulders (Kaplan *et al.*, 2007). However, a maximum of 0.5 m of outwash surface deflation is more likely given:

1) The surface cobble samples are susceptible to deflation, but do not show scattered ages as would be expected if surface lowering had occurred (Hein *et al.*, 2011);

2) The preservation of braided meltwater channels is not consistent with several metres of surface deflation. Consequently, we constrained the *maximum total erosion* parameter (i.e. outwash surface deflation) within these two hypothetical scenarios, and applied conservative constraints to all other modelling parameters according to sensitivity tests. A consequence of this conservative approach is wider age uncertainties, and only optimum χ^2 values are given with ≥95% confidence (see Hidy et al., 2010).

5.4.3 Depth profile modelling results

The modelled Río Cullen profile yielded a ^{10}Be age of 45.6 ka ($^{+139.9}/_{-14.3}$) when constrained to a maximum of 4 m of surface deflation (Figures 5.14 and 5.15). Allowing 0.5 m of deflation created a stratigraphic age reversal younger than the gLGM, which is unrealistic compared to regional radiocarbon ages (McCulloch *et al.*, 2005b), and suggests that some (>0.5 m) surface deflation has affected the age estimate. However, even with an unrealistic 100 m of deflation, the optimum age remained below 50 ka. The model yielded an erosion rate of 48.7 mm ka^{-1} (equating to 2.2 m of apparent erosion after 45.6 ka) and a low inheritance signature of 6.73 ×

10^4 atoms g^{-1}. The San Sebastián profile yielded a ^{10}Be age 30.1 ka ($^{+45.6}$/$_{-23.1}$) when constrained to 0.5 m of deflation (Figures 5.16 and 5.17) and, again, even allowing for 100 m of deflation, the optimum age remained below 50 ka. The model yielded an erosion rate of 0.59 mm ka^{-1} (equivalent to 0.2 m of apparent erosion after 30.1 ka) and a low inheritance signature of 3.94 × 10^4 atoms g^{-1}.

Table 5.5. ^{10}Be depth sample modelling summary. The optimum values used are highlighted. Bayesian values cannot be used because χ^2 optimisation failed to reach a unique value.

Filaret ^{10}Be profile

	Unconstrained (100 m)			4 m			0.5 m		
	Age (ka)	Inheritance ($\times 10^4$ atoms g^{-1})	Erosion rate (cm ka^{-1})	Age (ka)	Inheritance ($\times 10^4$ atoms g^{-1})	Erosion rate (cm ka^{-1})	Age (ka)	Inheritance ($\times 10^4$ atoms g^{-1})	Erosion rate (cm ka^{-1})
Mean	582.5	2.18	2.93	80.1	3.4	2.31	31.6	3.82	0.76
Median	597.8	2.18	2.93	75.7	3.42	2.42	31.2	3.87	0.79
Mode	822.9	2.35	2.76	31.5	3.47	2.38	29.9	3.89	1.15
Optimum χ^2	35.5	3.84	1.25	34.6	3.92	1.11	**30.1**	**3.94**	**0.59**
Maximum χ^2	1100	4.81	4.14	206.8	4.86	4.04	**45.6**	**4.91**	**1.63**
Minimum χ^2	23.3	0	0	23.1	1.77	0	**23.1**	**2.43**	**0**
Bayesian most probable	37.9	2.35	2.77	37.9	3.52	2.45	26.1	3.91	1.14
Bayesian 2σ upper	1078.8	4.2	4.71	158.7	4.51	4.28	37.8	4.8	1.55
Bayesian 2σ lower	36.1	0.03	1.82	17.6	1.12	0.29	14.8	1.42	-

Cullen ^{10}Be profile

	Unconstrained (100 m)			4 m			0.5 m		
	Age (ka)	Inheritance ($\times 10^4$ atoms g^{-1})	Erosion rate (cm ka^{-1})	Age (ka)	Inheritance ($\times 10^4$ atoms g^{-1})	Erosion rate (cm ka^{-1})	Age (ka)	Inheritance ($\times 10^4$ atoms g^{-1})	Erosion rate (cm ka^{-1})
Mean	575.7	7.53	7.46	40.1	6.63	5.11	17.9	6.71	1.54
Median	590.5	7.29	7.18	35.7	6.66	4.95	17.5	6.75	1.59
Mode	559.6	6.49	6.29	17.3	6.71	4.5	14.9	6.71	1.73
Optimum χ^2	25.6	6.84	3.81	**45.6**	**6.73**	**4.87**	15.8	6.92	0.85
Maximum χ^2	1100	12.93	15.25	**139.9**	**7.81**	**13.28**	29.6	7.84	3.46
Minimum χ^2	14.3	3.84	0.03	**14.3**	**4.75**	**0**	14.3	4.9	0
Bayesian most probable	14.3	6.85	5.65	14.3	6.85	4.35	14.3	6.85	2.39
Bayesian 2σ upper	1074.6	10.74	13.24	87.9	7.47	10.4	24.7	7.47	3.25
Bayesian 2σ lower	25.7	4.88	3.63	NaN	5.28	0.45	-	5.36	-
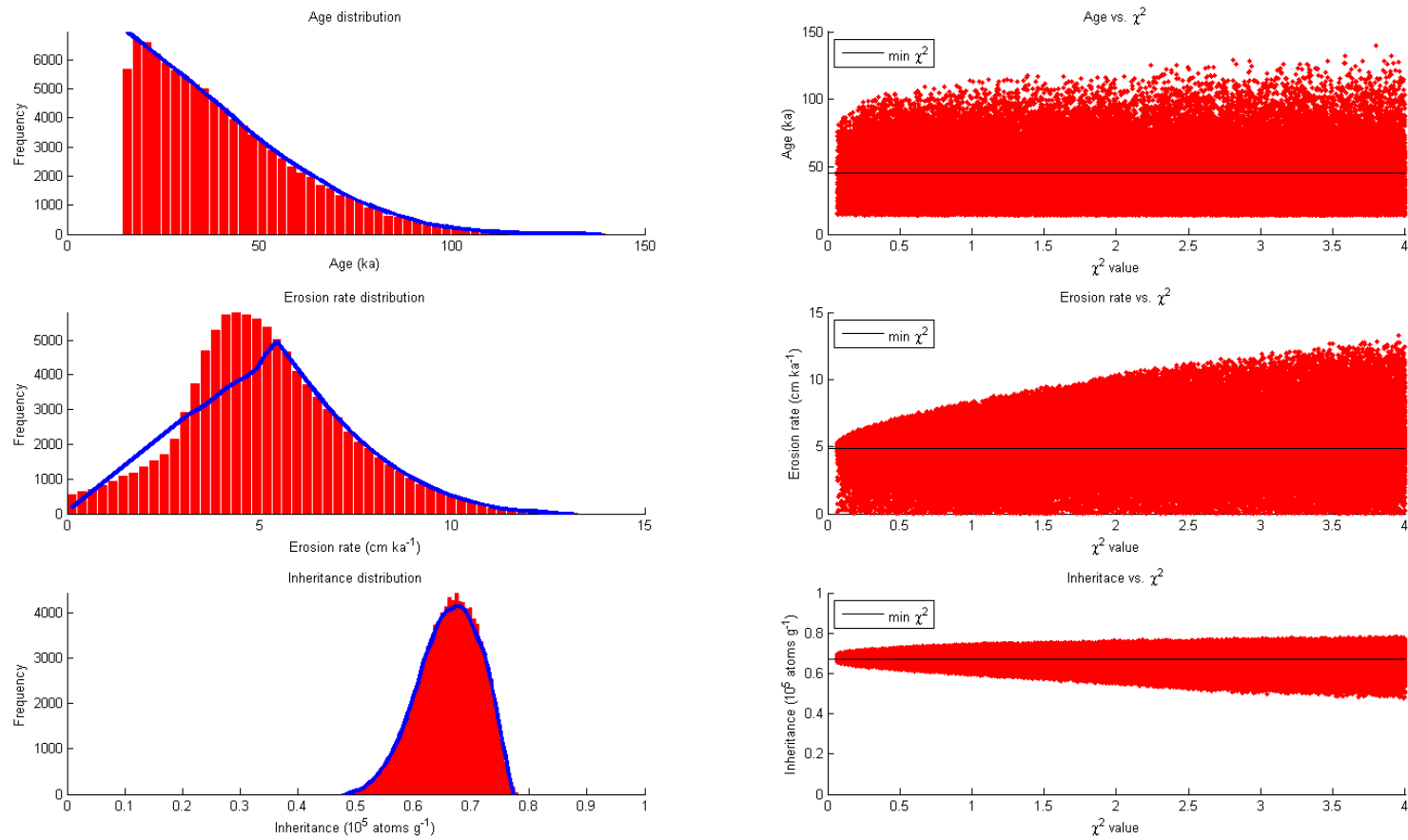
Figure 5.14. Cullen [10]Be profile age, erosion rate and inheritance output for the 4 m maximum erosion model run. Red bars/points show the results of 100,000 model runs, blue line shows the frequency distribution and black line shows the optimum χ^2 value.
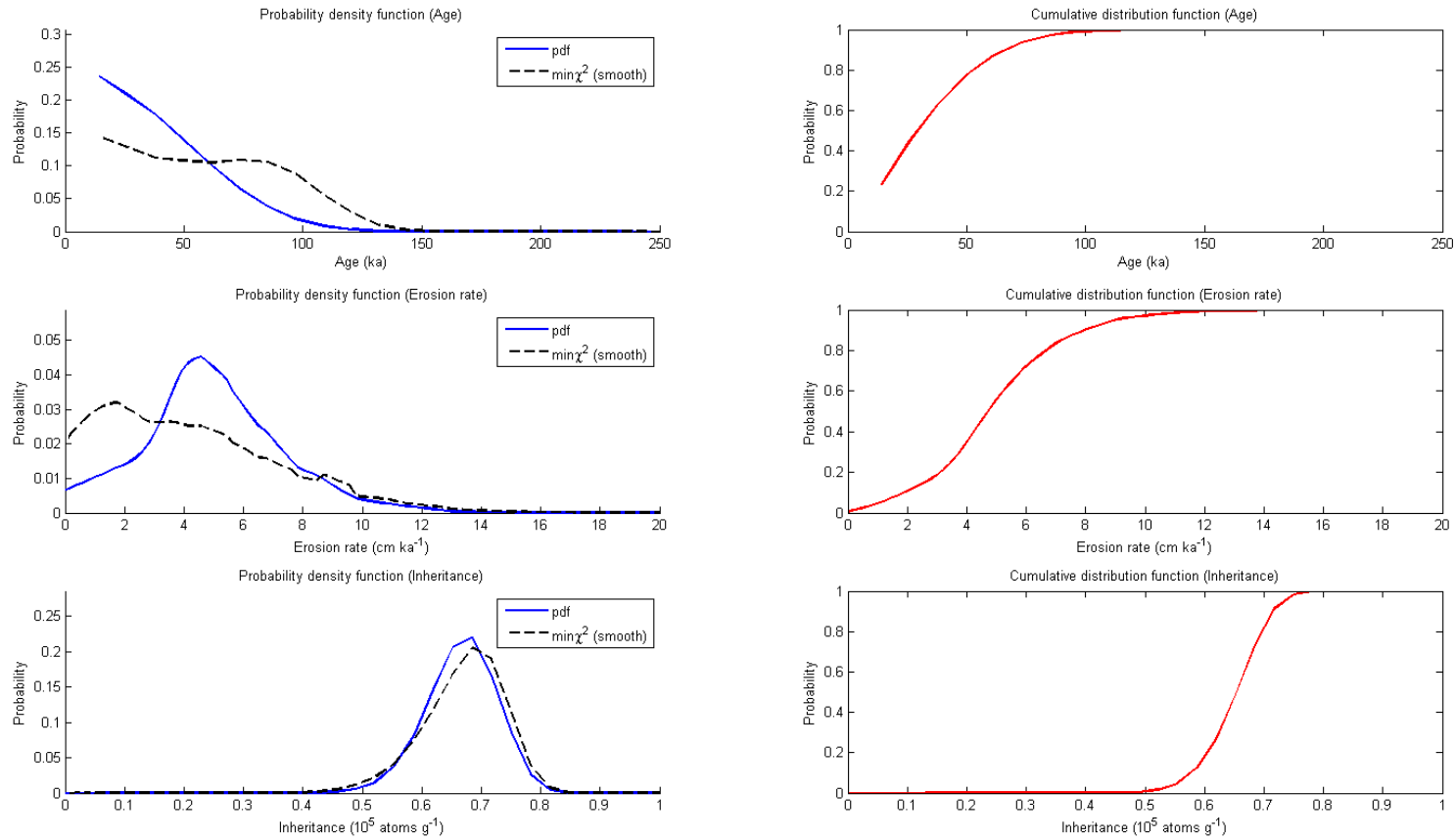
Figure 5.15. Cullen [10]Be profile age, erosion rate and inheritance output for the 4 m maximum erosion model run. Black line shows the smoothed χ^2, blue line shows the probability density function and red line shows the cumulative distribution function.
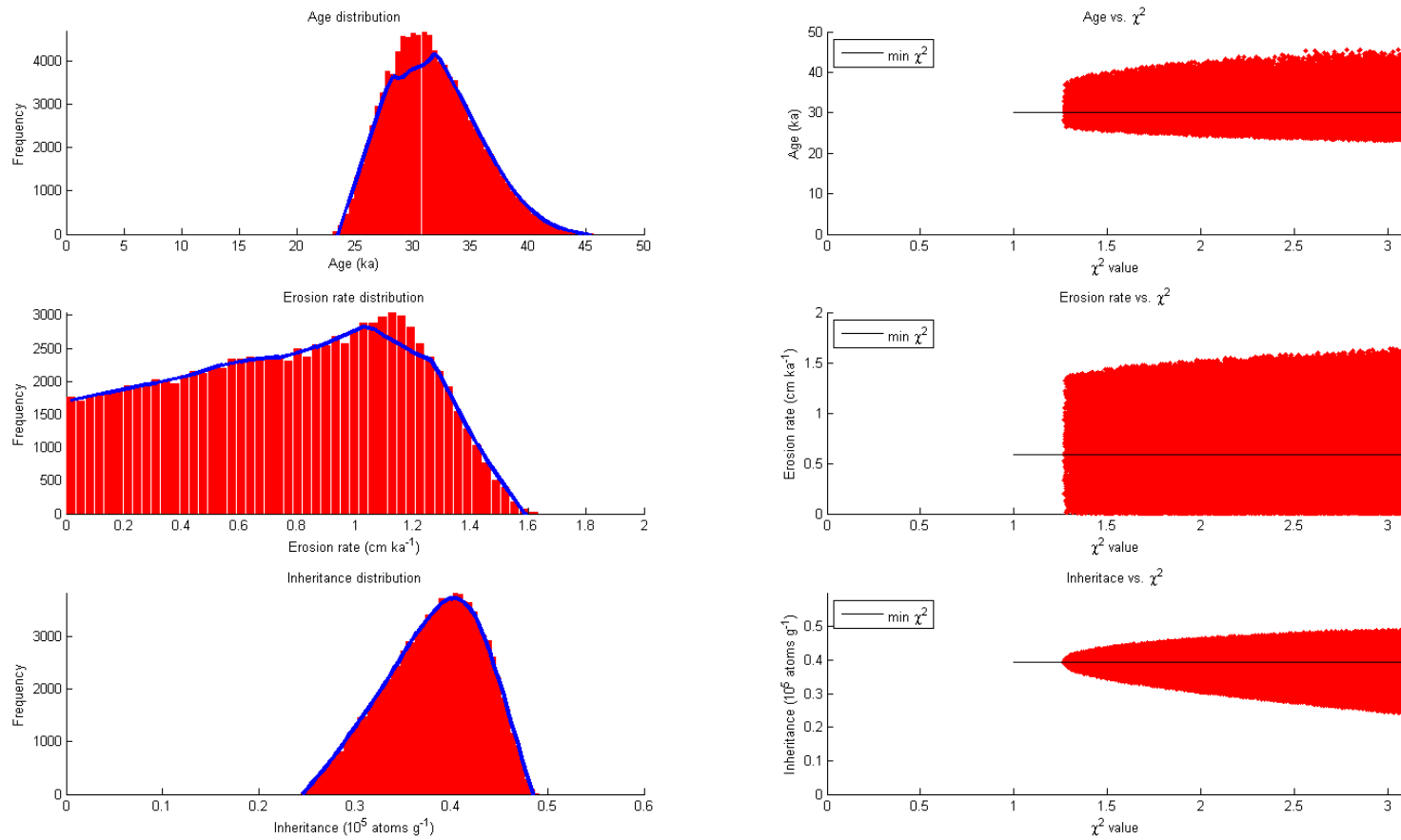
Figure 5.16. Filaret [10]Be profile age, erosion rate and inheritance output for the 0.5 m maximum erosion model run. Red bars/points show the results of 100,000 model runs, blue line shows the frequency distribution and black line shows the optimum χ^2 value.
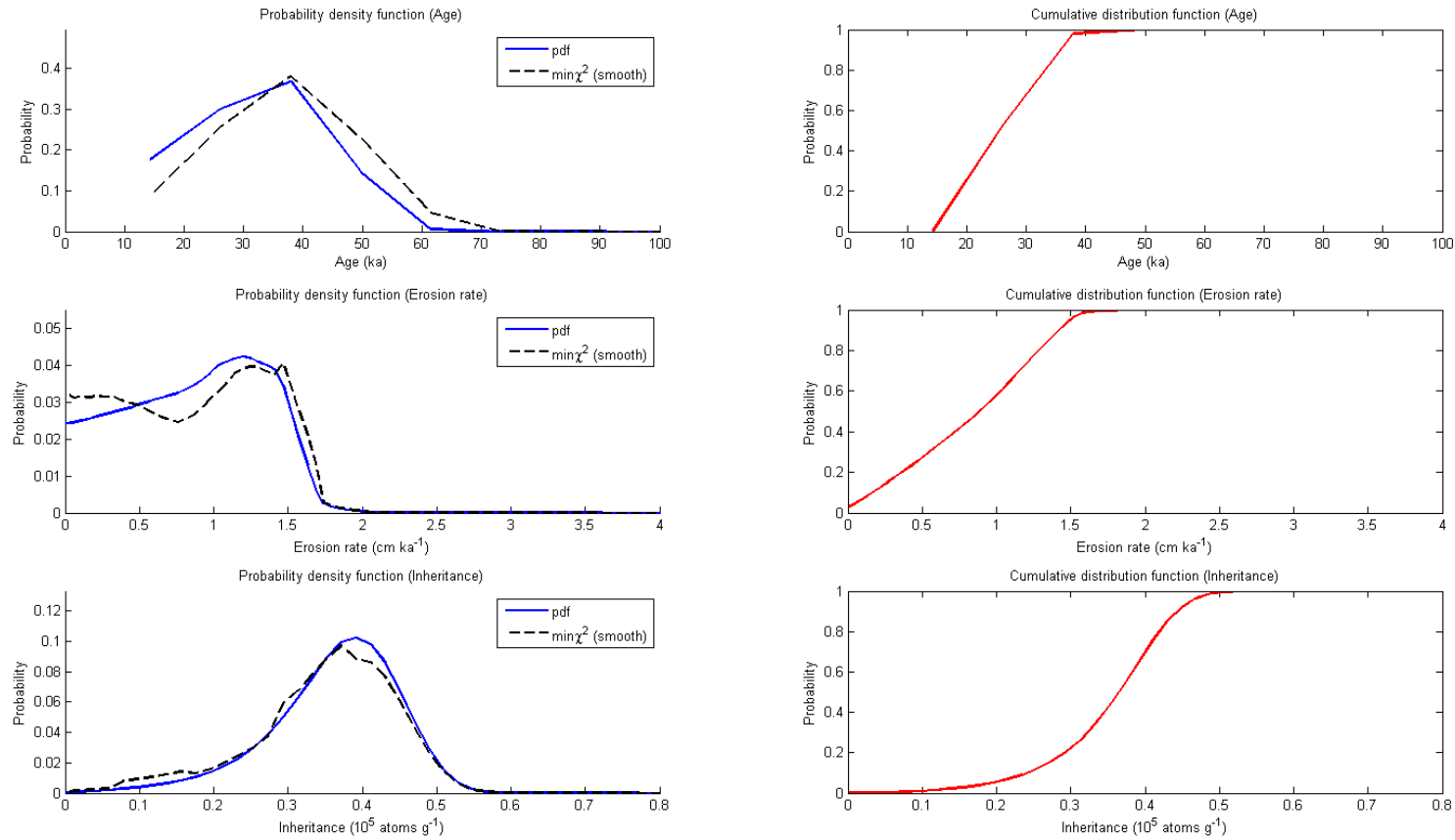
Figure 5.17. Filaret ^{10}Be profile age, erosion rate and inheritance output for the 0.5 m maximum erosion model run. Black line shows the smoothed χ^2, blue line shows the probability density function and red line shows the cumulative distribution function.

5.5 Discussion

5.5.1 New ages for BI-SSb glacial limits

The depth profile and surface sample ages for the outwash associated with the Río Cullen and San Sebastián glacial limits suggest that these surfaces are substantially younger than previously thought. For the depth profiles, the optimum ages are 45.6 ka ($^{+139.9}$/$_{-14.3}$) for the Río Cullen limit and 30.1 ka ($^{+45.6}$/$_{-23.1}$) for the San Sebastián limit (Figure 5.11). The surface samples yield apparent mean ages of 27.2 ± 3.7 ka for the Río Cullen limit and 25.9 ± 1.3 for the San Sebastián limit, which suggests that there has not been substantial deflation of the outwash surfaces that would otherwise result in a scatter of ages. Moreover, the depth profiles and the surface samples are consistent with published dates from moraine boulders (Figure 5.1), which were previously hypothesised to be poor estimates of moraine age due to erosion (Kaplan *et al.*, 2007). Rather, we show that the Río Cullen and San Sebastián limits were deposited during the last glacial cycle (MIS 4-2), with optimum ages during MIS 3. These new constraints radically alter the glacial chronology of the BI-SSb lobe and demonstrate that it was more extensive during the last glacial cycle, but prior to the gLGM.

5.5.2 Geomorphic considerations

As noted, high moraine exhumation rates have been invoked to suggest that exposure ages from moraine boulders on these glacial limits underestimated their age (Kaplan *et al.*, 2007). Our data suggests surface deflation rates of 48.7 mm ka^{-1} and 0.59 mm ka^{-1} for the Río Cullen and San Sebastián outwash, respectively. The former is relatively high because the age and erosion rates are not well constrained, which is due to fewer samples and our conservative modelling constraints. In contrast, the San Sebastián outwash age and deflation rate estimates are well-constrained. The differences between ages from the depth profiles and those from surface samples are not due to deflation because the nuclide concentrations are lower than those modelled for the surface, and may instead be due to movement of clasts towards the surface from frost-heaving (Hein *et al.*, 2009). Crucially, all modelled erosion rates are substantially lower than those required for the limits to be hundreds of thousands of years old (Kaplan *et al.*, 2007), and the close agreement of the depth and surface ages suggests that deflation has not substantially lowered our ages.

A) Surface deflation   B) Little/no surface change   C) Inflation of clasts
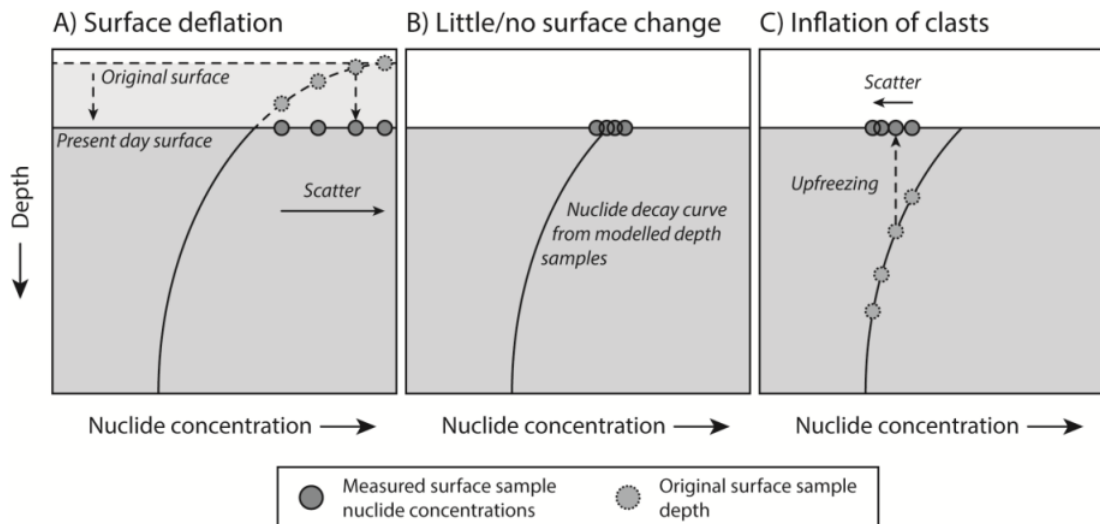
Figure 5.18. An illustration of how geomorphic effects would be expected to alter the relationship between measured surface sample nuclide concentrations and the modeled nuclide decay curve from depth samples. The three diagrams show cosmogenic nuclide concentrations increasing towards the right and depth increasing towards the bottom. The nuclide decay curves, sample concentrations and depths are purely hypothetical. (A) Deflation of the outwash surface will result in surface cobbles that were within the original surface being uncovered at the present day surface. Such samples will show a scatter of nuclide concentrations greater than that modelled for the unit from the depth samples. (B) Little or no surface processes will result in accordance between surface samples and the modelled nuclide concentration for the unit, with the former showing little or no scatter. (C) Inflation of the surface samples due to processes such as upfreezing will raise cobbles to the surface, such that the surface samples will show a scatter of nuclide concentrations lower than that modelled for the unit from the depth samples.

Kaplan *et al.* (2007) suggested that episodic exhumation and erosion of moraine boulders may have occurred during the gLGM, artificially reducing their ages. Our modelling does not support erosion rates consistent with the loss of metres of surface sediment that might be expected if this was the case (i.e. deflation of the outwash surface). However, our erosion rates are assumed to be steady over time, and do not consider rapid, episodic erosion. Nonetheless, there are three reasons why we believe that high rates of episodic exhumation and erosion has not occurred:

1) Mass stripping of the outwash surfaces should have caused deflation of surface cobbles. However, the surface cobble sample ages are relatively tightly clustered, suggesting that surface deflation is unlikely (Figure 5.18). Our sensitivity tests showed that a maximum χ^2 age of 350 ka (MIS 10) for the Filaret profile required ~ 6.4 m of erosion and a maximum χ^2 age of 450 ka for the Cullen profile required ~ 17 m of erosion. This is unlikely given the tight clustering of surface cobble ages.

2) The exceptionally high erosion rates associated with exhumation and erosion of the moraine boulders would likely have destroyed the glacial geomorphology, including the kettle kame topography and braided meltwater channels. The good preservation of geomorphology and boulders suggests that this was not the case.

3) Intense erosion to artificially reduce the ages of the moraine boulders associated with the San Sebastián and Río Cullen glacial limits should also have affected boulders associated with the Bahía Inútil glacial limit. However, the Bahía Inútil limit is independently dated to the regional gLGM and the Bahía Inútil boulders also yield cosmogenic ages consistent with other dating techniques, suggesting that intense erosion has not occurred.

5.5.3 Comparison with other southern mid-latitude studies

Our BI-SSb chronology is unusual because none of the preserved glacial limits of the BI-SSb lobe pre-date the last glacial cycle and two major limits were deposited ~100 km down-ice from the gLGM limit during MIS 3. Other pre-gLGM glacial advances have been recorded at a similar time during the last glacial cycle in Patagonia, but none are as extensive (Figure 5.19). Glasser *et al.* (2011) reported ages of *ca.* 34-38 ka, 61 ka and ≥99 ka for limits of the San Martín valley lobe (49°S) and Sagredo *et al.* (2011) found ages of *ca.* 37-39 ka and 61 ka for the Última Esperanza lobe (52°S) in southern Patagonia. In northern Patagonia, Hein *et al.* (2010) found ages of 27-32 ka for the Lago Pueyrredón valley lobe (47.5°S) and Denton *et al.* (1999) suggested that glacial advances occurred by ≥34 ka in the Chilean Lake District (41-43°S). Elsewhere in the southern mid-latitudes, Rother *et al.* (2014) found an age of *ca.* 28 ka for moraines of the Rangitata glacier (43°S), and Putnam *et al.* (2013b) reported an age of *ca.* 33 ka for pre-gLGM moraines of the Ohau glacier (44°S) in the Southern Alps of New Zealand. These correlate with other pre-gLGM ages in New Zealand, Australia and Tasmania (e.g. Barrows *et al.*, 2002; Suggate & Almond, 2005) and support the assertion that, globally, not all ice sheets reached their maximum extents at the gLGM during the last glacial cycle (Hughes *et al.*, 2013). Notably, however, these published advances for MIS 3 glaciation across the southern mid-latitudes were only slightly more extensive than their respective gLGM limits. Our study supports the occurrence of MIS 3 glaciation, but also suggests that this was much more extensive in southernmost Patagonia than elsewhere.
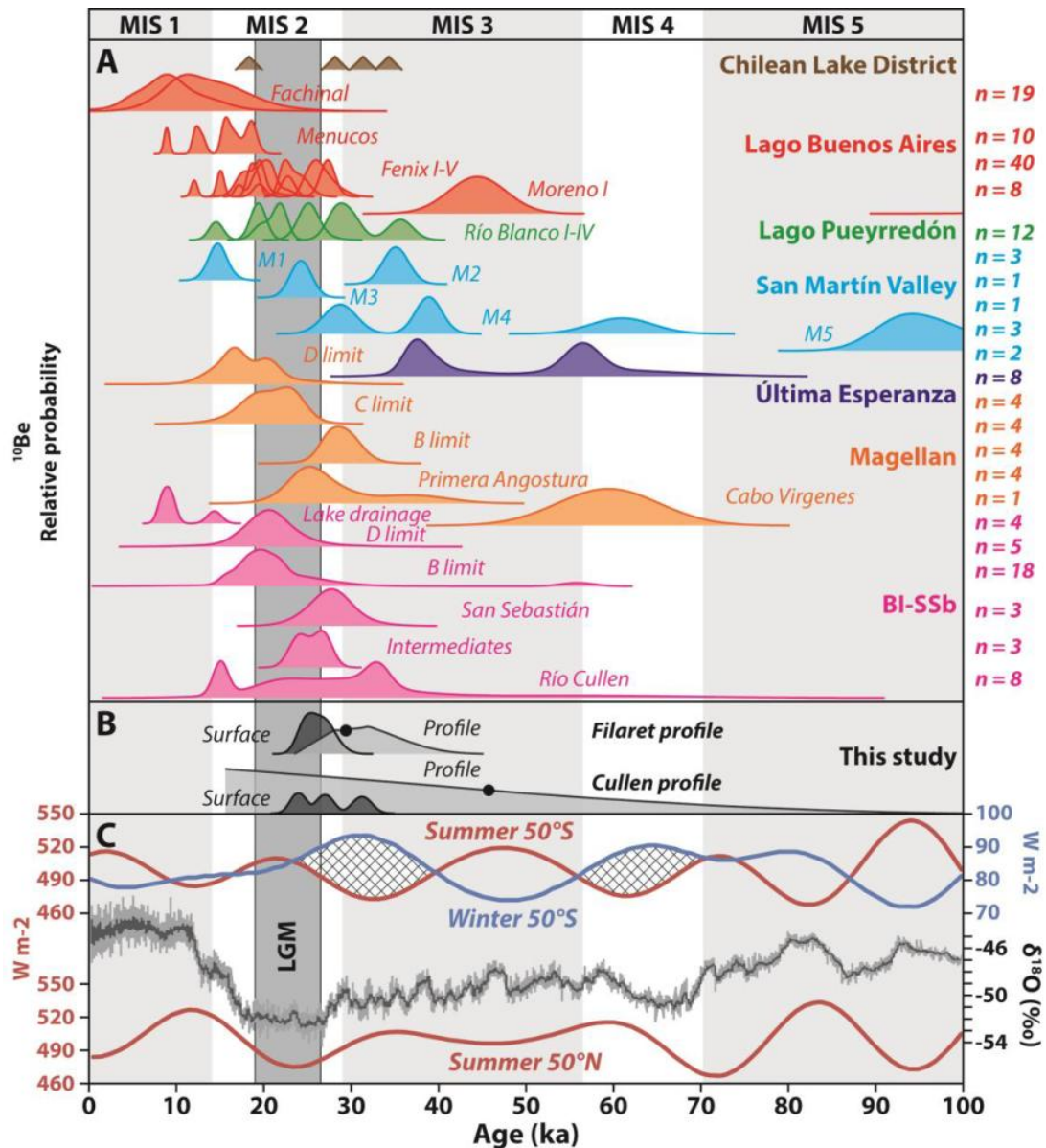
Figure 5.19. (A) Published dating of selected former ice lobe advances over the last 100 ka in Patagonia from north to south, with MIS limits (light grey bars) from Lisiecki & Raymo (2005) and the gLGM (dark grey bar) from Clark *et al.* (2009). For each location except the radiocarbon dates from the Chilean Lake District, all moraine boulder [10]Be data are shown as cumulative probability density function plots, with each curve corresponding to a moraine belt and normalized to 1 (n = no. of samples). All dates have been recalculated consistently, but note that: the number of samples varies between sites; no erosion or geomorphic processes have been considered; and some data have been truncated at 100 ka. (B) Surface cobble (dark shading) and depth profile (light shading) results for the BI-SSb lobe from this study (as in Figure 5.11). (C) Insolation data for summer and winter at 50°S and summer at 50°N (Berger & Loutre, 1991) and the $\delta^{18}O$ record, with 10-pt moving average, from Dronning Maud Land (EPICA, 2006). Hatching in the southern insolation curves highlights times of low summer insolation and high seasonality during MIS 4-2.

Without further chronological controls on southern ice lobes, it is not possible to discount internal dynamic processes (e.g. surging) of the BI-SSb lobe as the cause of the MIS 3 glacial advances. However, if the lobe is representative of southernmost Patagonia, then an external forcing likely triggered glacial advance. The consistent occurrence of an MIS 3 advance across the southern mid-latitudes, centred on 34-30 ka, coincides with minimum summer insolation at *ca.* 32.5 ka in the Southern Hemisphere; in the Northern Hemisphere, the summer insolation minimum coincided with the gLGM (Figure 5.19). Southern winter insolation also peaked at *ca.* 32.5 ka, and the combination of cooler summers and warmer winters may have promoted ice expansion prior to the coldest global temperatures during the gLGM. Thus, the extensive advance of the BI-SSb lobe during MIS 3 could have been caused by increased ice accumulation due to decreased temperatures and/or increased precipitation. However, $\delta^{18}O$ ice core records indicate that global temperatures reached a minimum after this time, and so the forcing is more likely to have been increased precipitation; indeed, Kerr & Sugden (1994) demonstrated latitudinal sensitivity of Patagonian glaciers to precipitation south of 50°S. It is therefore possible that a southward shift in the Southern Westerly Winds delivered greater precipitation to the BI-SSb lobe during MIS 3. That said, the uncertainty in the age of the Río Cullen limit does not preclude the possibility that it was deposited during the previous summer insolation minimum/winter insolation maximum at *ca.* 61.5 ka.

5.6 Conclusions

Cosmogenic nuclide dating of depth profiles through outwash sediments demonstrate that two limits of the BI-SSb lobe on Tierra del Fuego previously ascribed to MIS 12 and 10 relate to the last glacial cycle, between MIS 4 and 2. The San Sebastián limit was deposited at *ca.* 30.1 ka, suggesting that there was an MIS 3 glacial advance when the BI-SSb lobe was significantly more expansive than at the global gLGM. The Río Cullen limit is not as well constrained, but was likely deposited at *ca.* 45.6 ka and not before 139.9 ka. The results indicate extensive glaciation in southernmost Patagonia during MIS 3, which we interpret to reflect increased precipitation at this time, compared to the gLGM.

Chapter 6.   The glacial history of five ice lobes in the southernmost Patagonian Ice Sheet

Darvill, C.M., Stokes, C.R. & Bentley, M.J. (in prep.) 'The glacial history of five ice lobes in the southernmost Patagonian Ice Sheet', *Journal of Quaternary Science*.

Abstract

This paper presents a reconstruction of the glacial history of five ice lobes in southernmost South America: the Río Gallegos, Skyring, Otway, Magellan and BI-SSb ice lobes. We use previous geomorphological mapping of glacial landforms from satellite imagery and field observations to reconstruct former glacial limits, demarcate flowsets from glacial lineations, reconstruct former proglacial lakes and evaluate possible landsystems represented in the region. We reconstruct between 10 and 18 glacial limits for each ice lobe, a total of 26 different flowsets, and six major proglacial lakes across the region. We identify eight time steps that are supplemented with our interpretations of the nature of ice advances and previously published chronological information.

A landsystem approach is used to help indicate the likely nature of advances based on landform assemblages. We suggest that there is evidence that the ice lobes operated under an active temperate glacial landsystem, with warm-based ice displaying active re-advances during overall retreat of the ice margin. This differs from previous hypotheses of cold-based ice margins in the region and suggests that the ice lobes responded to regional climate variability in a dynamic way. We reconstruct the potentially catastrophic drainage of the palaeo-Laguna Blanca proglacial lake associated with the Skyring lobe, as well as late-stage rapid retreat, or even collapse, of some of the ice lobes associated with proglacial lake development and calving at the ice margin. There is also tentative evidence for rapid ice flow and possible surge-like activity at times.

Given recent dating suggesting that all of the limits of the BI-SSb ice lobe were deposited during the last glacial cycle, we use our glacial history to examine previously published chronological data for the ice lobes. There are few age constraints for the Río Gallegos, Skyring and Otway lobes. However, our glacial limits, combined with recalculated cosmogenic nuclide dates, suggest that several of the ice lobes advanced prior to the gLGM to deposit limits around 30 ka. More extensive limits may have been deposited during the last glacial cycle or during earlier glacial stages.

6.1 Introduction

The well-preserved glacial geomorphology relating to the former Patagonian Ice Sheet provides an excellent record of the fluctuations of glaciers over the course of the Quaternary period (Clapperton, 1993; Glasser & Jansson, 2008; Glasser *et al.*, 2008). This record can be used to reconstruct ice-sheet dynamics (Glasser & Jansson, 2005; Lovell *et al.*, 2012) and may be supplemented with chronological constraints to yield useful information about how the ice sheet changed over time as a result of climatic forcing (e.g. McCulloch *et al.*, 2005b; Douglass *et al.*, 2006; Kaplan *et al.*, 2008b; Hein *et al.*, 2010; Hein *et al.*, 2011). For example, the southernmost part of the ice sheet is heavily influenced by the atmospheric Southern Westerly Winds and oceanic Antarctic Circumpolar Current, both tied to the position of the Sub-Tropical and Sub-Antarctic Fronts that influence oceanic temperature gradients (Lamy *et al.*, 2007; Kaplan *et al.*, 2008a; Kilian & Lamy, 2012; Kohfeld *et al.*, 2013; Sime *et al.*, 2013). Consequently, reconstruction of the southernmost ice lobes can help to establish the likely changes in these climatic systems over time. However, this process requires a combination of detailed geomorphological mapping and robust chronological techniques.

Previous studies of the southernmost ice lobes of the Patagonian Ice Sheet have focussed on dating glacial limits, with a particular emphasis on the gLGM and late glacial limits, but there has been a lack of detailed mapping over a wide extent and there remains distinct uncertainty about the timing and nature of pre-gLGM glacial advances. Chapter 3 produced a high resolution map of the glacial geomorphology relating to five former ice lobes in this region as a basis for glacial reconstruction and chronological investigation. Furthermore, Chapter 5 demonstrated that the pre-gLGM limits of the BI-SSb lobe, previously assigned to MIS 12 and 10 (Coronato *et al.*, 2004), were in fact deposited during the last glacial cycle. This suggests that significant MIS 3 (and possibly MIS 4) glacier advances are represented in this area, and that much of the geomorphology may have been deposited more recently than previously thought. This paper builds on this work by presenting a detailed reconstruction and relative glacial history for the region and uses this to reinterpret the timing of glacial advances for the southernmost ice lobes.
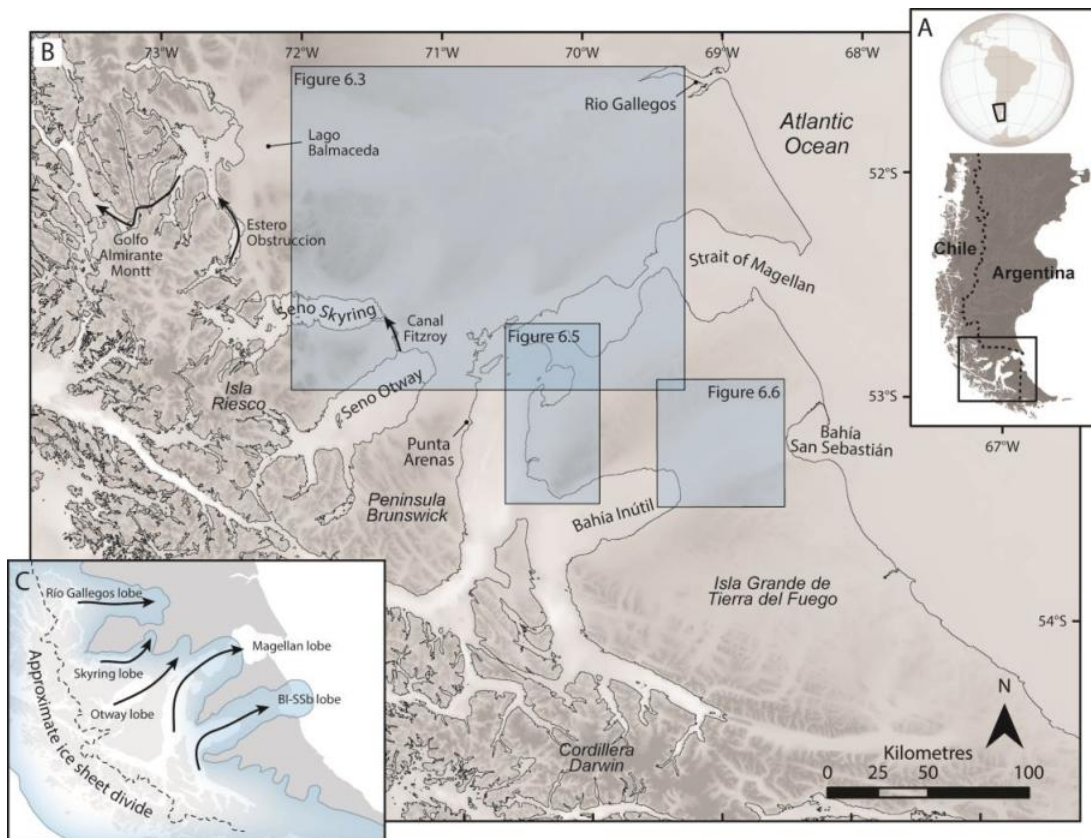
Figure 6.1. (A) Location of the study area in southern South America. (B) Overview map of the study area, with key locations mentioned in the text and the locations of other overview figures. (C) Stylised representation of the southernmost portion of the former Patagonian Ice Sheet, with flow paths shown for the five former ice lobes discussed in this paper.

6.2 Study area

Our study area lies between 51-55°S and 68-73°W, and encompasses the area occupied by five former piedmont ice lobes extending from the Patagonian Ice Sheet (Figure 6.1). From north to south, these are: the Río Gallegos, Skyring, Otway, Magellan and BI-SSb lobes. The topography of the area changes dramatically from southwest to northeast, with the southern Andes (dominantly Cordillera Darwin) marking the western and southern boundaries and casting a strong rain shadow over the low, flat pampas and coastal areas to the north and east (Coronato *et al.*, 2008). The locations of the former ice lobes are marked by prominent straits and sounds, which may have been cut during one or more major glacial events during the Quaternary (Rabassa, 2008). The configuration of the former ice lobes within over-deepened valleys promoted the development of pro-glacial lakes during recession, which are recorded by numerous raised shorelines in the region (Chapter 3). The reconstruction of these lakes can be useful both in terms of establishing ice

132

dynamics (when former lobes calved into proglacial lakes; Porter *et al.*, 1992) and creating a relative history using lake drainage events (Kilian *et al.*, 2013).

The glacial geomorphology was first described in detail by Caldenius (1932), and Meglioli (1992) subsequently used weathering indices to establish a hypothetical age model for the region, whereby nested moraine limits were deposited during successive glacial episodes from MIS 12 to 2 (Coronato *et al.*, 2004). Since then, little attention has been given to examining the nature of ice dynamics from the geomorphological record, apart from localised work on the gLGM or late glacial limits (e.g. Porter *et al.*, 1992; Benn & Clapperton, 2000a; b; Bentley *et al.*, 2005; Lovell *et al.*, 2012). Techniques such as radiocarbon, amino-acid racemisation, optically stimulated luminescence and cosmogenic nuclide exposure dating have been used to constrain the age of some moraine limits deposited during the gLGM and late glacial (Rutter *et al.*, 1989; Porter, 1990; Meglioli, 1992; Clapperton *et al.*, 1995; McCulloch *et al.*, 2005b; Sagredo *et al.*, 2011; Blomdin *et al.*, 2012; Hall *et al.*, 2013). Age constraints prior to the gLGM are ambiguous (Kaplan *et al.*, 2007; Evenson *et al.*, 2009) or non-existent in this region, although argon dates suggest that the outermost limits of the Río Gallegos, Skyring, Otway and Magellan lobes could date to 1070-450 ka (Meglioli, 1992). Beyond this, the Río Gallegos lobe has only a few scattered cosmogenic exposure ages (Kaplan *et al.*, 2007; Evenson *et al.*, 2009; Sagredo *et al.*, 2011) and the Skyring and Otway lobes have no pre-late glacial age controls at all (Kilian *et al.*, 2007; Kilian *et al.*, 2013). Given that Chapter 5 demonstrated that the conceptual age model presented by Meglioli (1992) may need revising, there is a need for a detailed reconstruction of the nature and timing of glacial activity relating to the southernmost ice lobes, particularly prior to the gLGM.

6.3   Methods

6.3.1   *Geomorphological mapping*

Geomorphological mapping was conducted by Darvill *et al.* (2014; see Chapter 3 and Appendix) using remote sensing analysis and field-checking. Landsat and ASTER scenes, aerial photographs and Google Earth imagery and SRTM digital elevation data were used in combination to digitise glacial landforms (Figure 6.2). Much of the area was also cross-checked in the field, with an emphasis on verifying mapped landforms and checking cross-cutting features, though the Río Gallegos lobe was mainly studied using remote sensing. Further details can be found in Chapter 3.
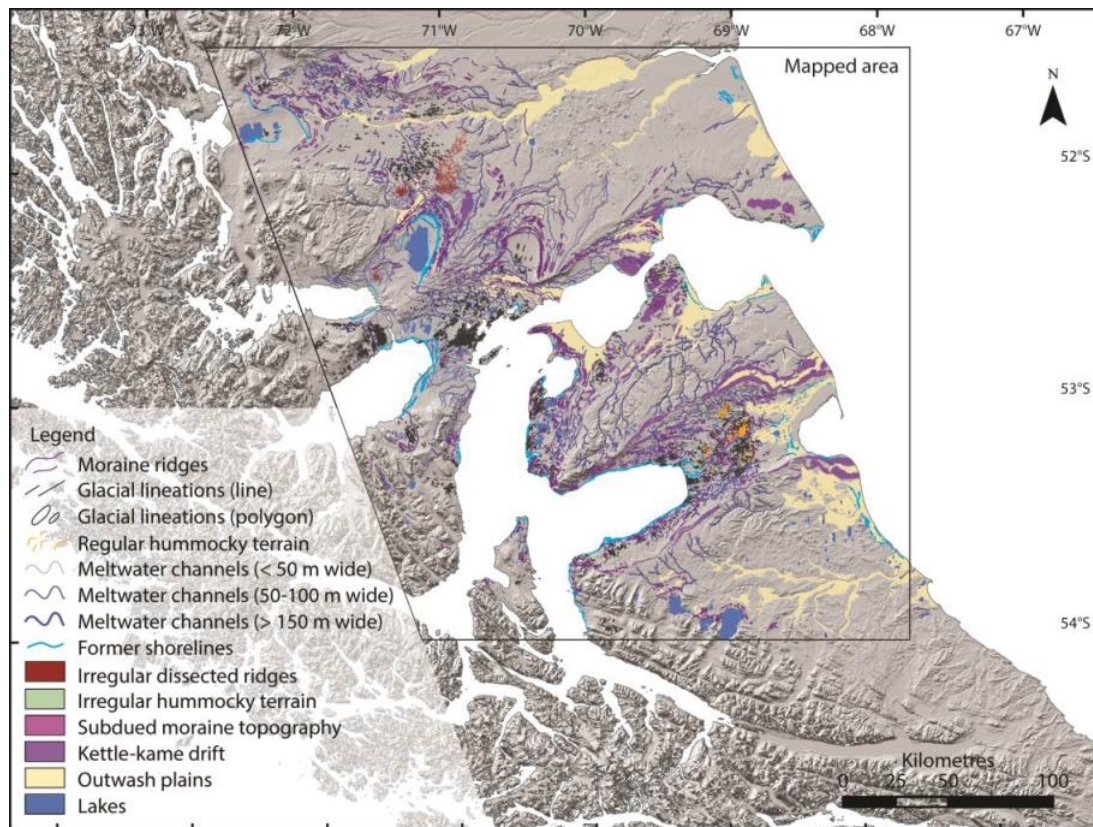
Figure 6.2. Overview of the glacial geomorphology mapped in the study area. The mapped area from Darvill *et al.* (2014) is shown within a larger DEM for context, and a full and detailed version of the geomorphological map can be found in the Appendix.

6.3.2 *Glacial flowsets, limits and landsystems*

Glacial landforms can yield information on the extent of former ice advances and, using glacial inversion methods, can also be used to reconstruct the former dynamics of an ice sheet (Kleman *et al.*, 2006). For example, ice flow indicators such as glacial lineation flowsets can demonstrate changes in flow direction. Furthermore, a landsystem approach can tie suites of glacial geomorphological features to particular styles of glaciation (Evans, 2003), many of which have modern analogues and are helpful in ascertaining former glacial and climatic conditions. Glacial lineations were grouped into flowsets according to their proximity and similar orientations, as well as relationships to ice marginal features such as moraines and meltwater channels (Clark, 1999). By mapping a range of glacial landforms, we were able to reconstruct glacial limits and assess landsystems based on landform suites.

6.3.3 *Proglacial lake reconstruction*

The reconstruction of former proglacial lakes can yield information on the relative position of ice lobes (Lovell *et al.*, 2012) and their dynamics (Porter *et al.*, 1992).

Following Stokes & Clark (2004) and Lovell *et al.* (2012), we modelled proglacial lake formation using a Digital Elevation Model (DEM) constructed from *ca.* 90 m resolution SRTM data for areas of land and a *ca.* 900 m ETOPO data for areas of sea that may have been previously exposed. This DEM was filled in 10 m increments to examine where lakes developed and over-spilled in relation to former shorelines. The DEM data is sufficient for the purpose of this exercise, but the coarser resolution of the ETOPO data means that over-spill channels beneath present sea-level may have been missed, and a lack of bathymetric data for present-day lakes means that their exact depths are unknown. Additionally, the DEM provides present-day land elevation and not that during glaciation, when the mass of the Patagonian Ice Sheet would have depressed the mountain range. This should be corrected for Glacio-Isostatic Adjustment (GIA), but the resolution of the ICE-5G model output (Peltier, 2004), which is the best global estimate of the solid earth at the gLGM, is too coarse to be of use for this purpose. Moreover, it does not reflect the timing of maximum ice thickness for this region based on Chapter 5. Consequently, we reconstructed palaeolakes based on a contemporary DEM, but with the caution that they are likely minimum estimates of lake depth.
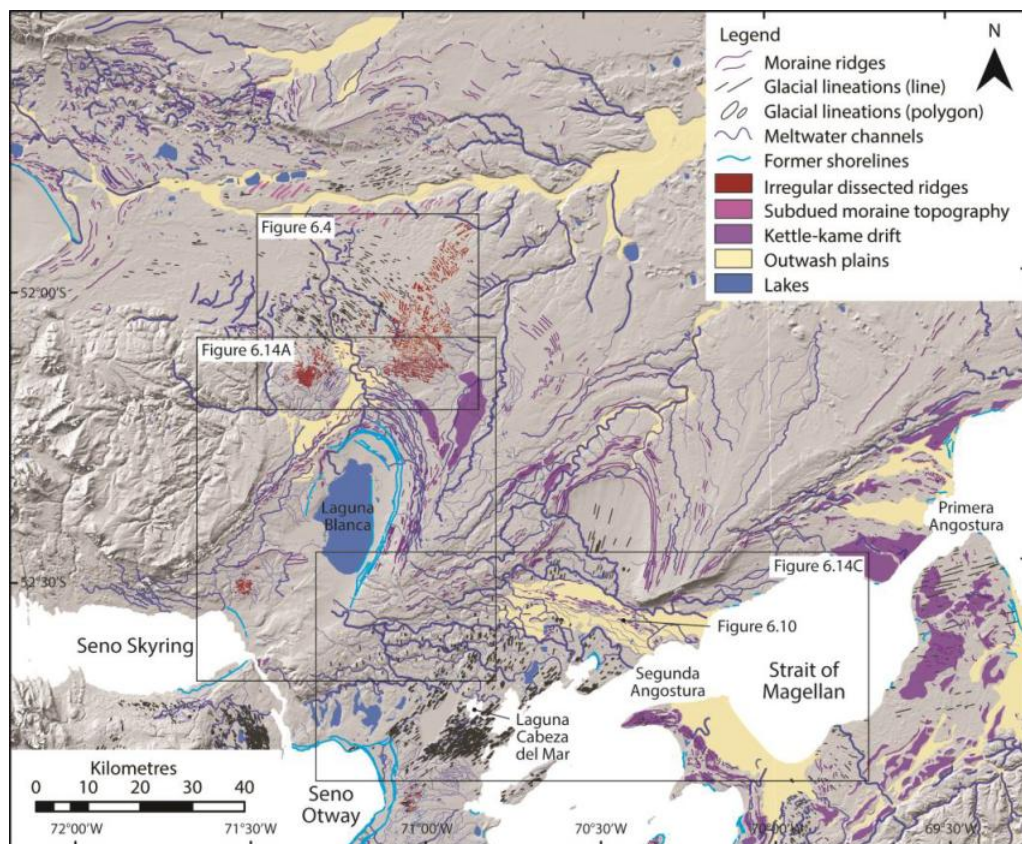
Figure 6.3. An overview of the glacial geomorphology associated with the Río Gallegos, Skyring, Otway and Magellan lobes (location shown in Figure 6.1) including key place names mentioned in the text.

6.4 Results

This section briefly describes the nature of the principal glacial landforms mapped in the study area. Further details can be found in Chapter 3, and a full glacial geomorphological map can be found in the Appendix.

6.4.1 Moraine ridges

The clearest moraine ridges in the study area are those of the Skyring and Otway lobes, where numerous, relatively sharp-crested, arcuate ridges are nested around the main depressions (Figure 6.3 and Figure 6.14), marking the point at which the lobes were flowing onto higher relief areas (Barr & Lovell, 2014). These continuous or semi-continuous ridges, typically 5-10 m high, are delineated by meltwater channels and outwash trending northeastward. Similar moraines are found on the northern side of the Magellan lobe, particularly across Primera Angostura, and within *ca.* 10 km of Bahía Inútil in the BI-SSb lobe. The arcuate moraines nested in the Río Gallegos lobe depression also show this morphology in remote sensing imagery.

Smaller, less distinctive ridges are often draped over other glacial features within the central Magellan and BI-SSb lobes. For example, on Punta Gente, ridges are draped over drumlinised terrain north of Porvenir (Bentley *et al.*, 2005; Figure 6.5). Similarly, in the centre of the BI-SSb depression, ridges can be seen draped over both lineations and subdued moraine topography (Figure 6.6). In both cases, the ridges are less than 10 m high and are roughly parallel to former ice limits.

6.4.2 Hummocky terrain

Hummocky terrain is abundant in the BI-SSb lobe, but is also found in the Magellan lobe. It consists of semi-rounded hills and hollows on a markedly smaller scale than the kettle and kame topography, and forms arcuate bands running parallel to moraine ridges. Although the hummocks are dominantly irregular and chaotic (named 'irregular hummocky terrain'), there is also a large swath north of Laguna Larga in the central BI-SSb depression that form regularly-oriented mini-ridges ('regular hummocky terrain' Figure 6.7).
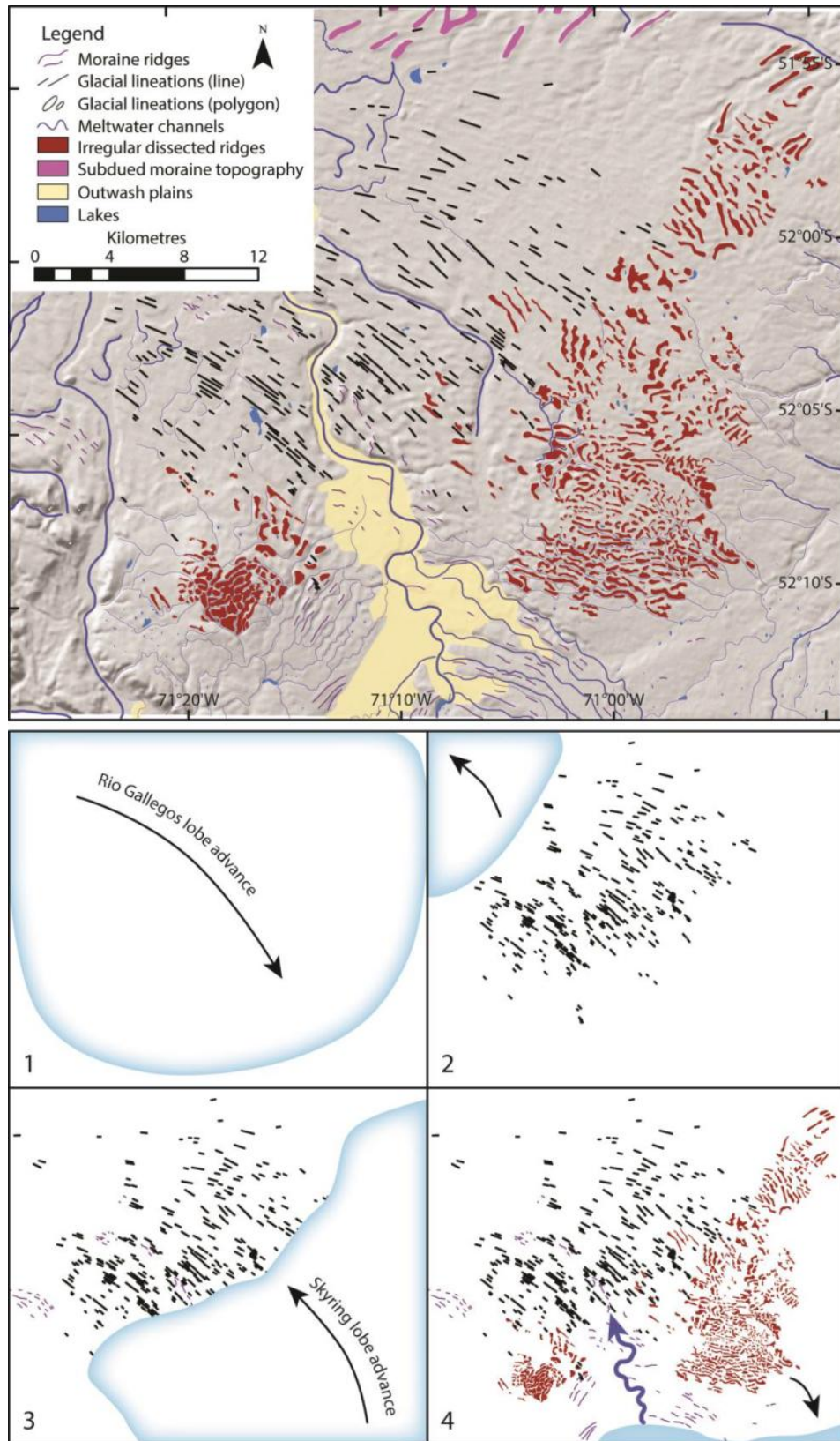
Figure 6.4. The IDR and drumlin field at the intersection of the Río Gallegos and Skyring lobes (location shown in Figure 6.3). Boxes 1-4 Illustrate the likely formation of this geomorphology, starting with the advance of the Río Gallegos lobe (1) to deposit lineations (2) and probably terminal moraines. Following retreat of the Río Gallegos lobe, the Skyring lobe advanced over the lineations and moraines (3) creating a large area of irregular dissected ridges (4).
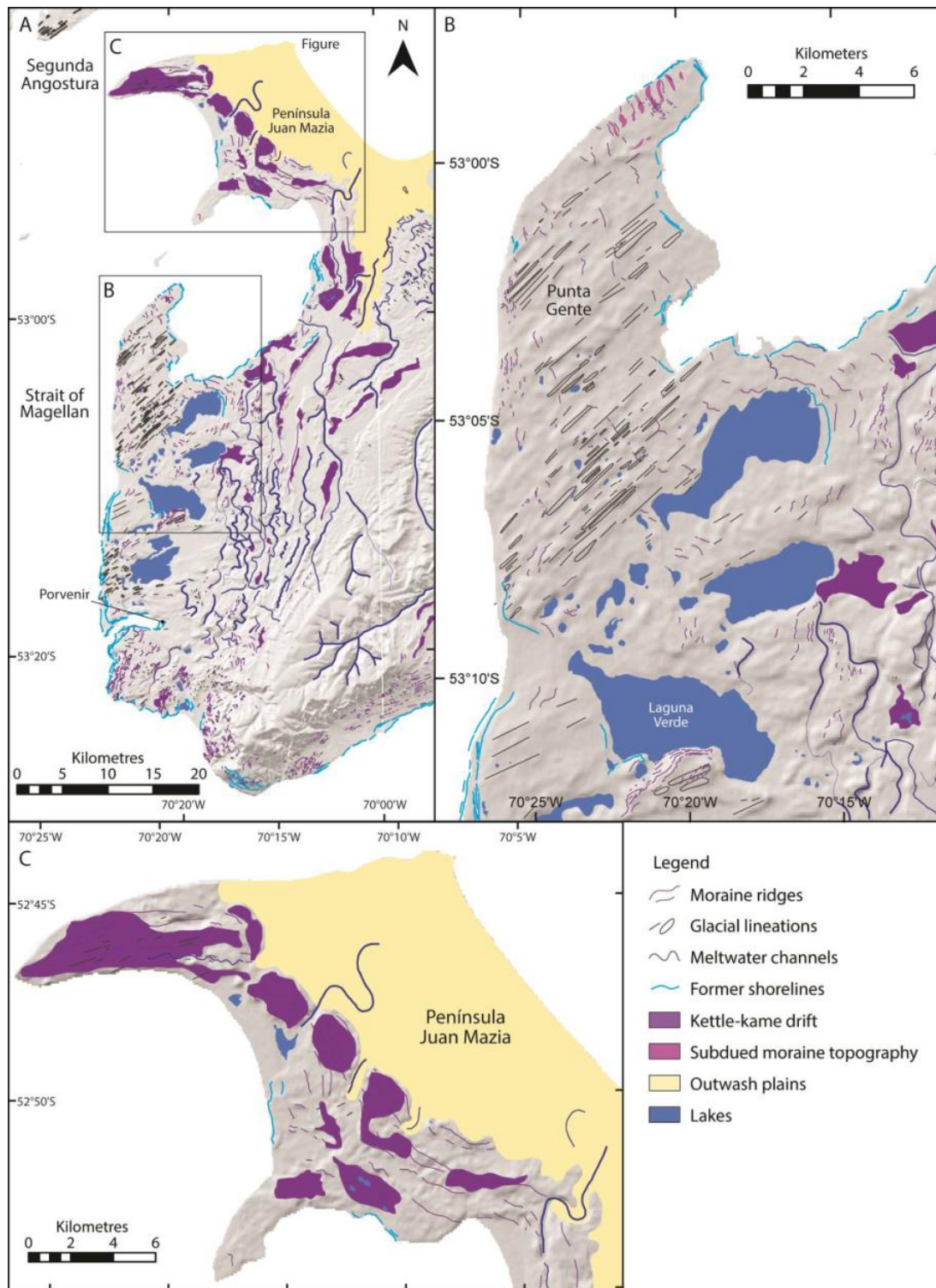
Figure 6.5. (A) Overview of the glacial geomorphology associated with the Magellan lobe (location shown in Figure 6.1). (B) Enlargement of Punta Gente to show a large field of rounded drumlins, in places draped by small moraine ridges. The location of Laguna Verde is shown, which is surrounded by rhythmically laminated palaeolacustrine sediments. (C) Enlargement of Península Juan Mazia, which may represent the terminus of a surge-like advance.

138

6.4.3 Kettle-kame topography

Bands of kettle and kame topography mark the Primera Angostura and Segunda Angostura limits of the Magellan lobe, but are seen most clearly as a double band on both the north and south of the BI-SSb depression (Figure 6.2 and Figure 6.6). The topography consists of chaotic hills surrounding rounded hollows, with a relief of 10 m or more and delimited by broad outwash plains. Chapter 4 mapped a series of erratic boulder trains along the southern edge of the BI-SSb lobe, two of which drape the kettle and kame topography.

6.4.4 Glacial lineations

Lineations occur in association with all five ice lobes, but vary in morphology in different parts of the study area, from low-relief flutings to prominent oval-shaped drumlins. For example, clusters of subdued flutings occur around Bahía Inútil (Figure 6.6), whilst large swaths of classic drumlins are found in the Río Gallegos, Skyring, Otway and Magellan lobes. Of particular note are the fields consisting of hundreds of elongate drumlins that occur in the outermost part of the Río Gallegos lobe (Ercolano *et al.*, 2004; Figure 6.4), around Laguna Cabeza del Mar in the Otway lobe (Clapperton, 1989; Benn & Clapperton, 2000b; Figure 6.3) and on the eastern side of the Magellan Strait (Bentley *et al.*, 2005; Lovell *et al.*, 2012; Figure 6.5).

6.4.5 Subdued moraine topography

Subdued moraine topography consists of low, arcuate changes in relief, often over-printed by other moraine ridges or bands of hummocky terrain (Figure 6.7). The features are difficult to observe clearly on the ground are best picked-out in SRTM imagery as positive relief over a kilometre or more, or as changes in vegetation in Landsat imagery. Subdued moraine topography is dominantly found in the centre of the BI-SSb lobe and is fragmented in a regular pattern north of Laguna Larga.

6.4.6 Irregular dissected ridges (IDR)

These relatively disorganised ridges are found in association with the Skyring and Río Gallegos lobes, in places intersected by meltwater channels and most prominently to the southeast of the large swath of drumlins oriented southeastward in the Río Gallegos lobe (Figure 6.4). The formation of the features is unclear (Lovell *et al.*, 2011), although the largest group appears to be situated at the intersection between the Río Gallegos and Skyring geomorphology.
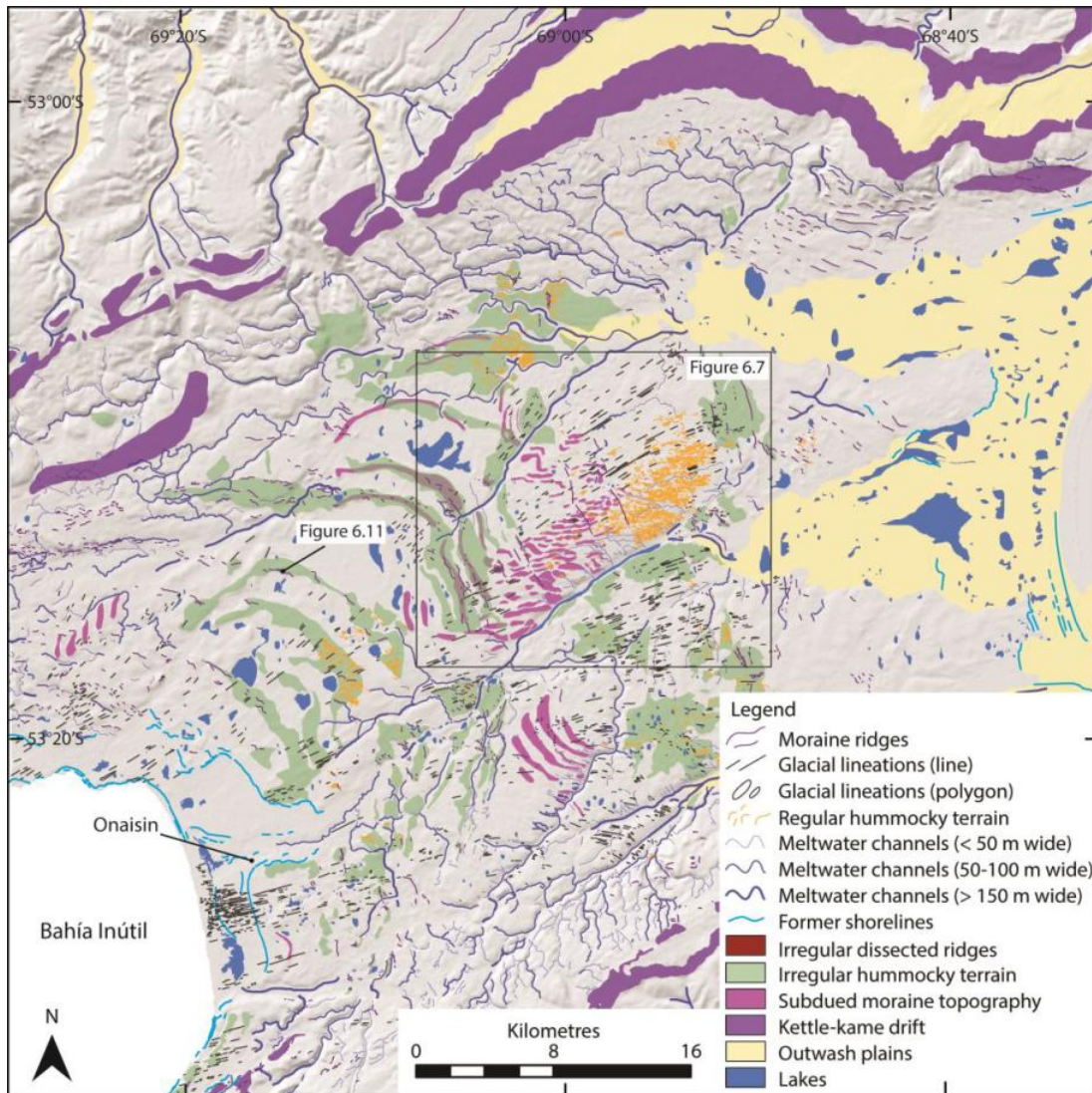
Figure 6.6. Overview of the glacial geomorphology associated with BI-SSb lobe (location shown in Figure 6.1). Note the spillway marked by former shorelines associated with a proglacial lake that drained at Onaisin through Laguna Larga (see Figure 6.7).

6.4.7 Meltwater channels

The glacial geomorphology of the study area is dominated by meltwater signatures, including hundreds of sinuous meltwater channels. In places, such as the outer moraines of the Skyring, Otway and Magellan lobes, the channels flow between clearly marked moraine limits, but elsewhere, such as the BI-SSb depression and inner parts of the Río Gallegos, Skyring, Otway and Magellan lobes, meltwater channels are clearer than associated moraines (see Appendix). The channels vary in size, from less than 50 m wide to more than 150 m wide, and are indistinguishable from channels of outwash in places where ice overtopped topographic constraints (e.g. northeast of the Skyring and Otway lobes or north of the BI-SSb lobe).

6.4.8 Outwash plains

Outwash plains are associated with moraines, kettle and kame topography and hummocky terrain in all of the ice lobes. Where they are unconstrained by topography, wide, open sandur plains grade eastward. A prominent exception is the outwash originating from Laguna Blanca in the Skyring lobe, which trends southeastward into the Strait of Magellan and has eroded a former moraine belt associated with the Otway lobe.

6.4.9 Former shorelines

Numerous fragmentary shorelines are found within *ca.* 10 m of contemporary coastal areas. In addition, continuous shorelines are found above 10 m and, further inland, around Lago Balmaceda in the Río Gallegos lobe; Seno Skyring; Seno Otway; Laguna Blanca in the Skyring lobe (Figure 6.3 and Figure 6.14); south of Primera Angostura in the Strait of Magellan; and Bahía Inútil. Whilst the Skyring, Otway, Magellan and Bahía Inútil shorelines are within *ca.* 60 m of present day sea-level, those around Lago Balmaceda (Figure 6.3) and Laguna Blanca are substantially higher.
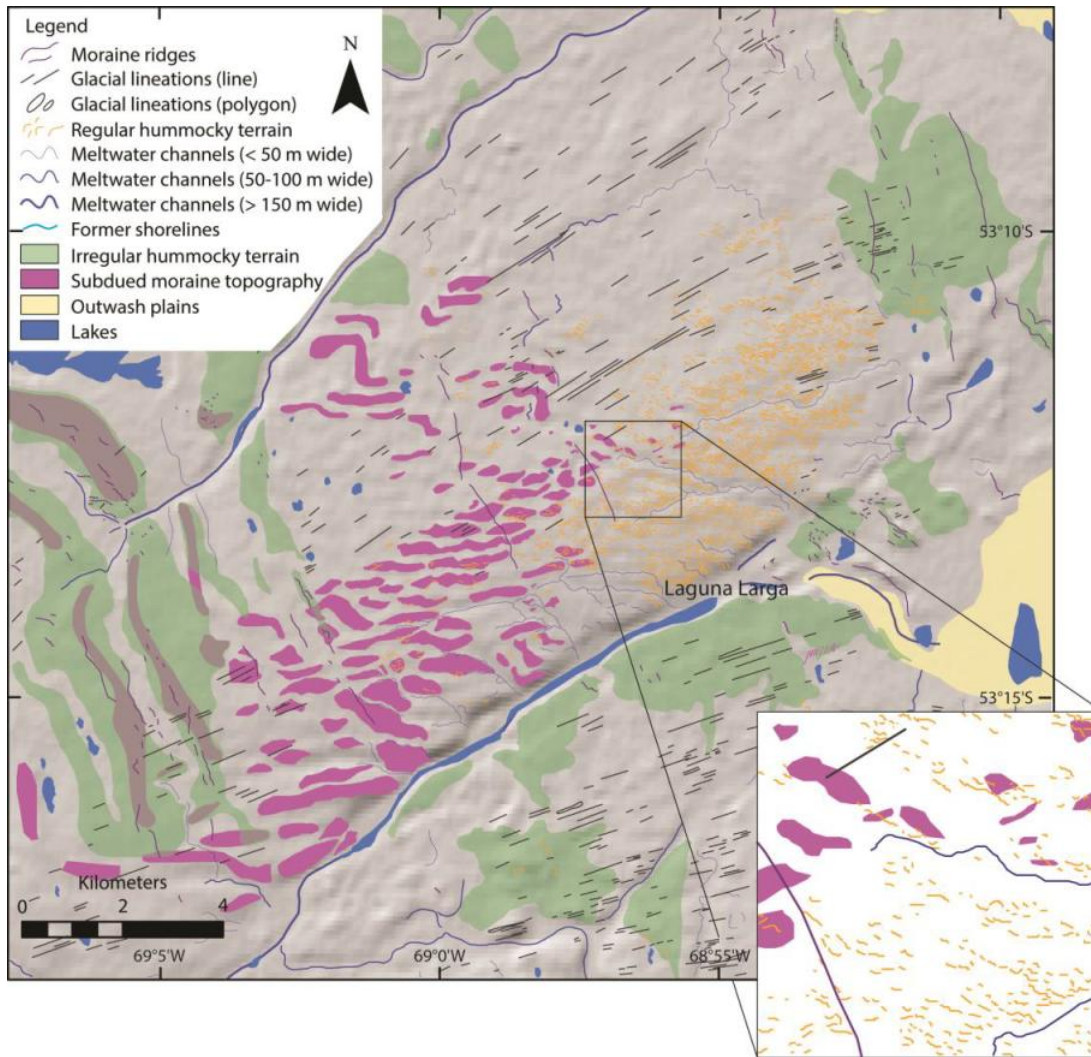
Figure 6.7. Enlarged portion of the central BI-SSb lobe geomorphology to show the cross-cutting relationships between subdued moraine topography and moraine ridges, glacial lineations and hummocky terrain. The zoomed box shows the ordered nature of the regular hummocky terrain mini-ridges and the cross-cutting relationships more clearly. The location of the figure is shown in Figure 6.6.

6.5   Interpretation

6.5.1   *Glacial limits and flowsets*

Our reconstruction used four sets of ice-marginal landforms to demarcate former glacial limits: morainic landforms (including hummocky terrain and kettle and kame topography), glacial lineation flowsets (see below), meltwater channels and proglacial shorelines (Figure 6.8). These were synthesised separately to illustrate former ice margins (Figure 6.9). The different lines of evidence yielded a consistent pattern and the data were combined to create a map of prominent glacial limits for each ice lobe (Figure 6.9). Many of these limits corroborate previous work defining

glacial limits in the region (Meglioli, 1992; Clapperton *et al.*, 1995; Coronato *et al.*, 2004; Bentley *et al.*, 2005; Lovell *et al.*, 2012), although the wider scope of our mapping has revealed a more detailed pattern than has been previously reported. For completeness, we also included less extensive limits from Kilian *et al.* (2007) for the Skyring lobe, although these are not based on our own geomorphological observations. The accumulation areas for each ice lobe are hypothesised based on contemporary catchment systems. This is almost certainly unrealistic given that the former ice sheet need not have been confined to modern drainage divides and the division between different ice lobes would likely have changed over time according to ice dynamics and changes in precipitation. However, as there is no geomorphological evidence that can be used to define the former accumulation areas, contemporary catchments are a good approximation for the purposes of this study.

We identified 26 flowsets in the study area (Figure 6.8). These flowsets were defined in a similar manner to Clark (1999) and Lovell *et al.* (2012) based on the parallel concordance, close proximity and similar morphometry of glacial lineations. For the Skyring and Otway lobes, our flowsets are similar to those proposed by Lovell *et al.* (2012). One key exception is FS 8 and 9 (Fs-4 of Lovell *et al.* (2012)), which we divide into two, either side of a clear band of moraines, based on differing morphology: the large swath of drumlins around Laguna Cabeza del Mar are noticeably longer, wider, and higher than the long flutings further to the northeast. This division is important because FS-9 corresponds with moraines dissecting the Otway depression. Many of the flowsets within the inner parts of the Río Gallegos, Skyring, Magellan and BI-SSb lobes have been discussed in previous studies (Benn & Clapperton, 2000b; Ercolano *et al.*, 2004; Bentley *et al.*, 2005; Lovell *et al.*, 2012), but the outer flowsets of the Río Gallegos and BI-SSb lobes have not been reported previously.
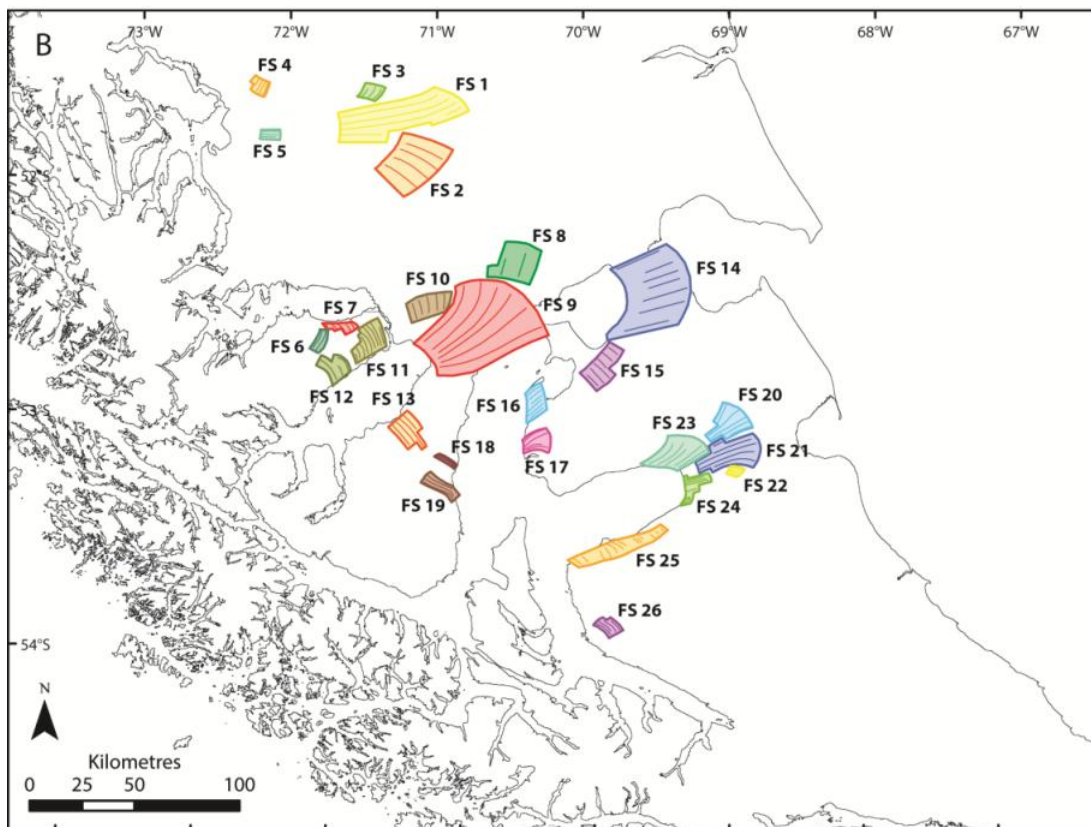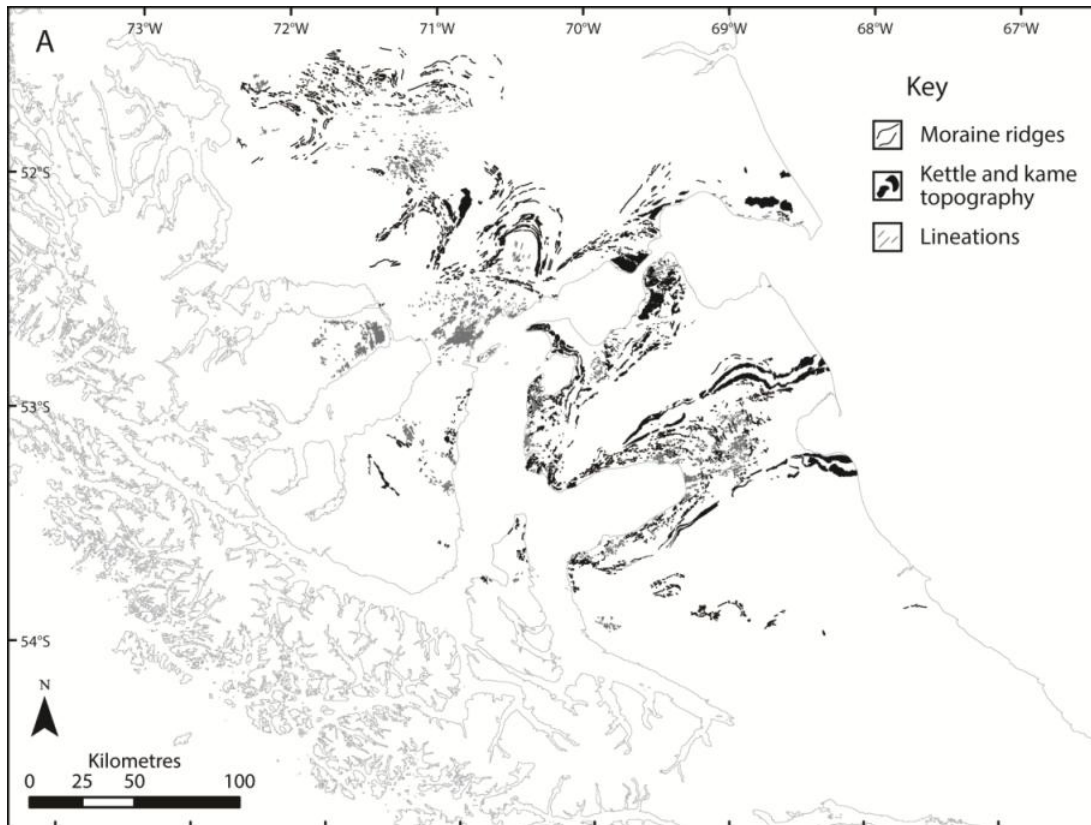
Figure 6.8. (A) A simplified version of the glacial geomorphology to show the dominant ice flow and ice marginal features. (B) The twenty six flowsets identified from the mapped glacial lineations.

144
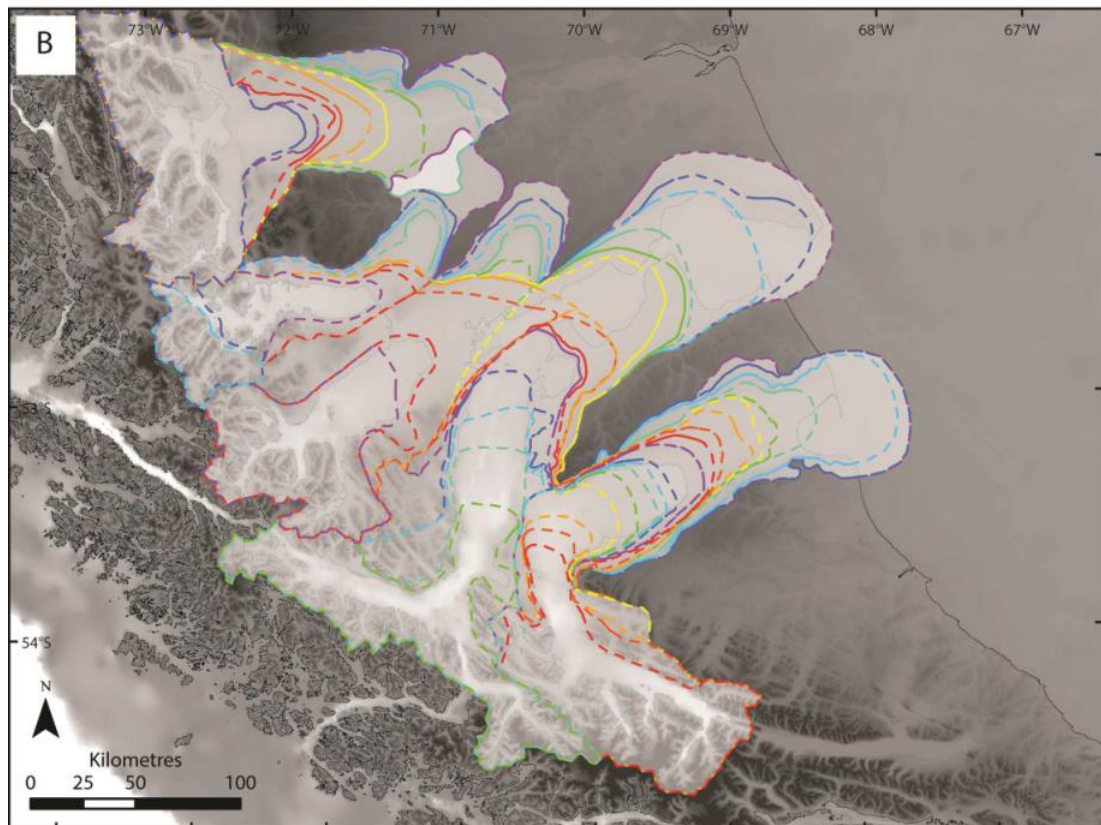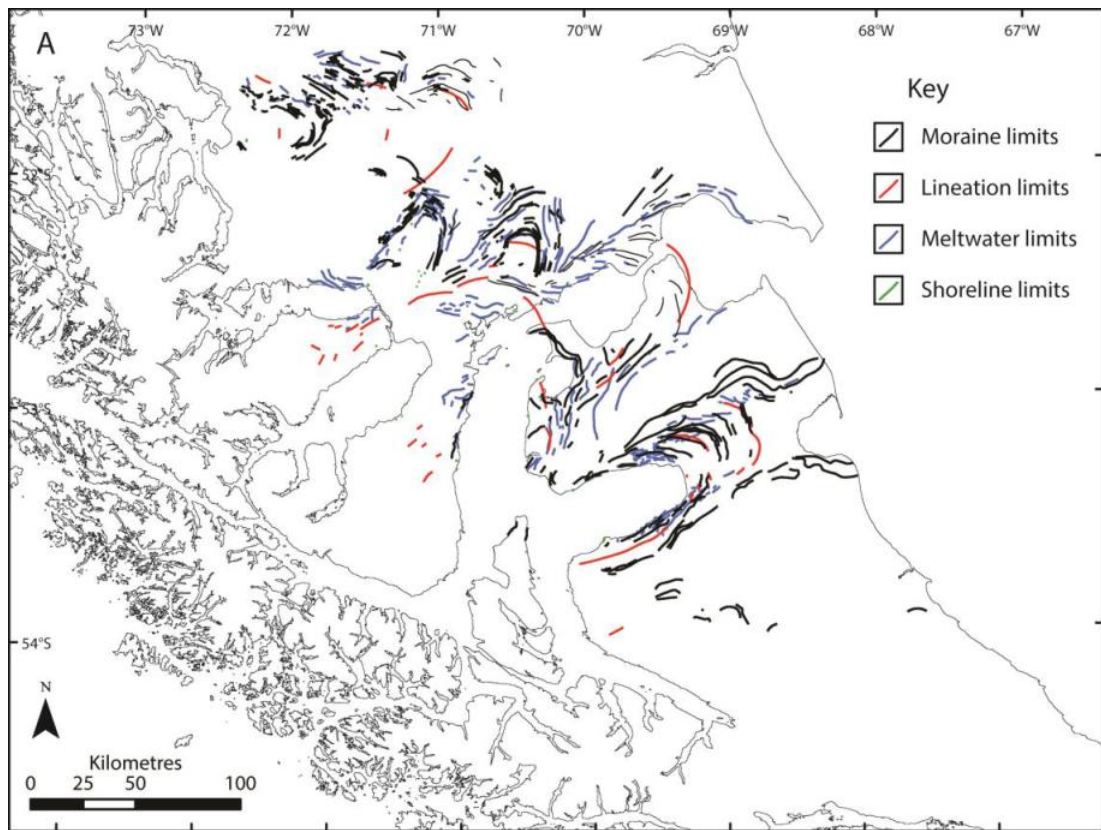
Figure 6.9. (A) The dominant limits associated with four different sets of ice-marginal features. These were then synthesized into glacial limits, shown in (B).

6.5.2   Glacial landform assemblages

The different geomorphological features that have been mapped in the study area can be grouped into five broad landform assemblages according to their interpreted role in the glaciological system.

6.5.2.1   Ice-marginal morainic landforms

Ice-marginal morainic features mapped in the study area include moraine ridges, hummocky terrain and kettle and kame topography. The clearest are moraine ridges, which likely include terminal and recessional moraines, though it is difficult to distinguish their form based on morphology alone. Two exceptions are where we have supplementary sedimentological evidence to support the landform data. A section through one of the moraine ridges in the Otway lobe shows faulted sands and gravels (Figure 6.10). Similarly, sediments through a moraine in the BI-SSb lobe contain silts and sands that have been strongly faulted and folded (Figure 6.11). The deformation of moraine sediments in this way is indicative of proglacial tectonisation (Hart & Boulton, 1991; Hambrey & Huddart, 1995; Boulton *et al.*, 1999), and we interpret the deformation to represent thrusting and folding during active re-advances of the ice lobes (Price 1970, 1973; Sharp, 1984a, b; Evans & Twigg, 2002). The BI-SSb moraine contains deformed lacustrine sediments, indicating that the timing and extent of retreat and re-advance must have been sufficient to allow a proglacial lake to accumulate. Our interpretation supports similar sedimentary evidence of thrust moraine complexes around the Strait of Magellan (Clapperton *et al.*, 1995; Benn & Clapperton, 2000a, b). Although the focus of this study was on landform mapping and interpretation, it is clear that there is scope for future sedimentological work.

Hummocky terrain is dominantly found in association with the BI-SSb lobe and exhibits morphology similar to hummocky moraine, though we opt for the generic term because we cannot be certain about how the features formed. This landform is indicative of supraglacial debris deposition (Boulton, 1972; Kjær & Krüger, 2001, Johnson & Clayton, 2003, Schomacker, 2008), and we suggest that it is consistent with a model whereby at least the BI-SSb lobe had supraglacial debris available to deposit (Chapter 4). The transport pathway of the debris resulting in hummocky moraine is controversial (Evans, 2009), with some authors advocating debris-covered ice stagnation during recession (e.g. Johnson & Clayton, 2003 and associated references) and others suggesting supraglacial debris flows (Lukas, 2005; 2007) or englacial thrusting (e.g. Graham *et al.*, 2007 and associated

references). However, we infer that the disorganised nature of the landform may be indicative of periods of ice stagnation and down-wasting during overall recession of the ice lobes, leaving behind buried ice that resulted in the hummocky terrain (Clayton, 1964; Boulton, 1972; Kjær & Krüger, 2001; Schomacker, 2008).
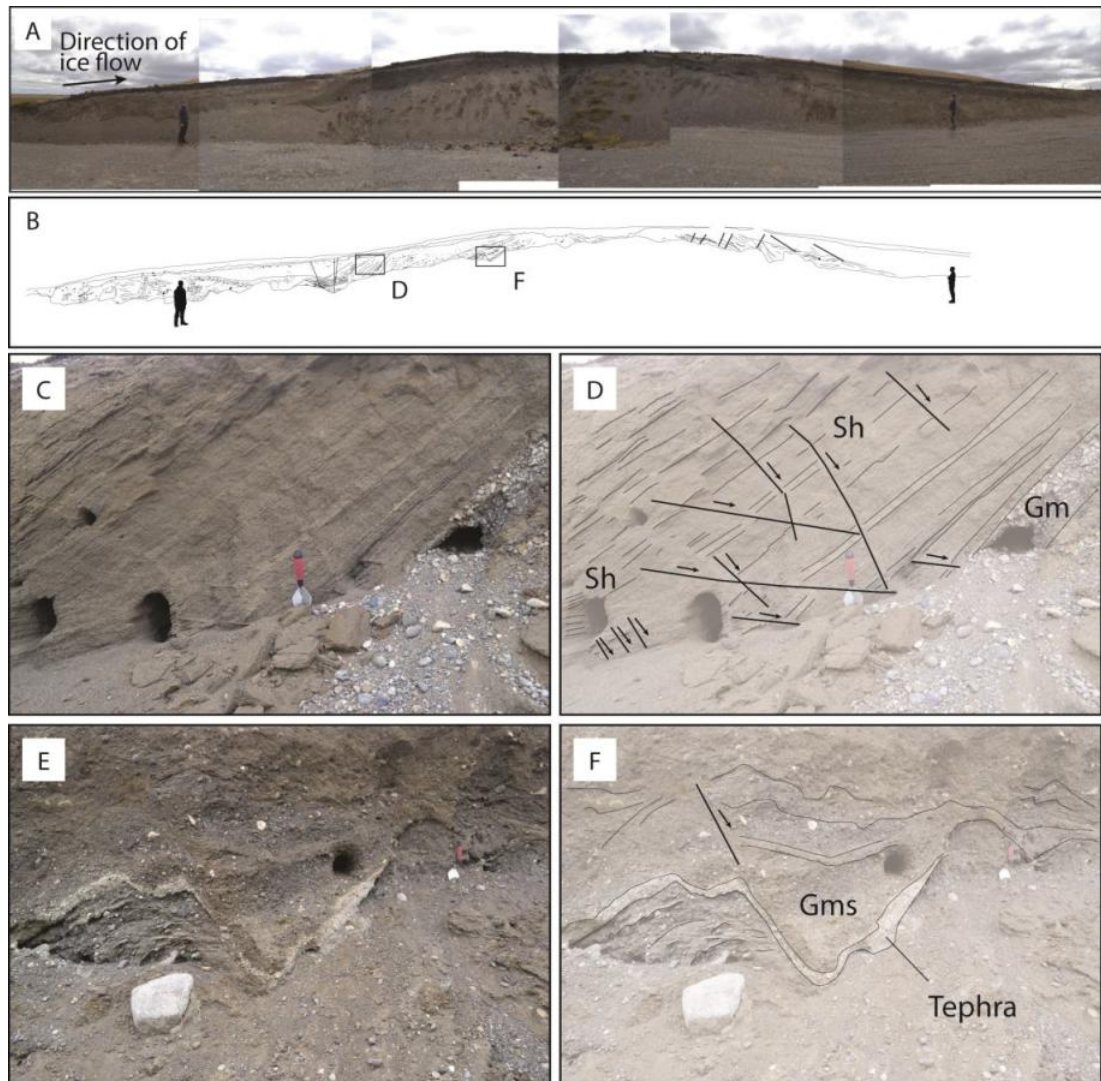
Figure 6.10. (A) Photographs and (B) sketch of a section through the glaciotectonised moraine associated with re-advance of the Otway lobe (location shown in Figure 6.3). (C-F) show photographs and accompanying sketches of normal thrust faults within the moraine sediments, particularly highlighted in (E) by a white tephra layer. The sediments are characteristic of outwash material that was likely deposited during retreat of the ice prior to re-advance and proglacial thrusting.
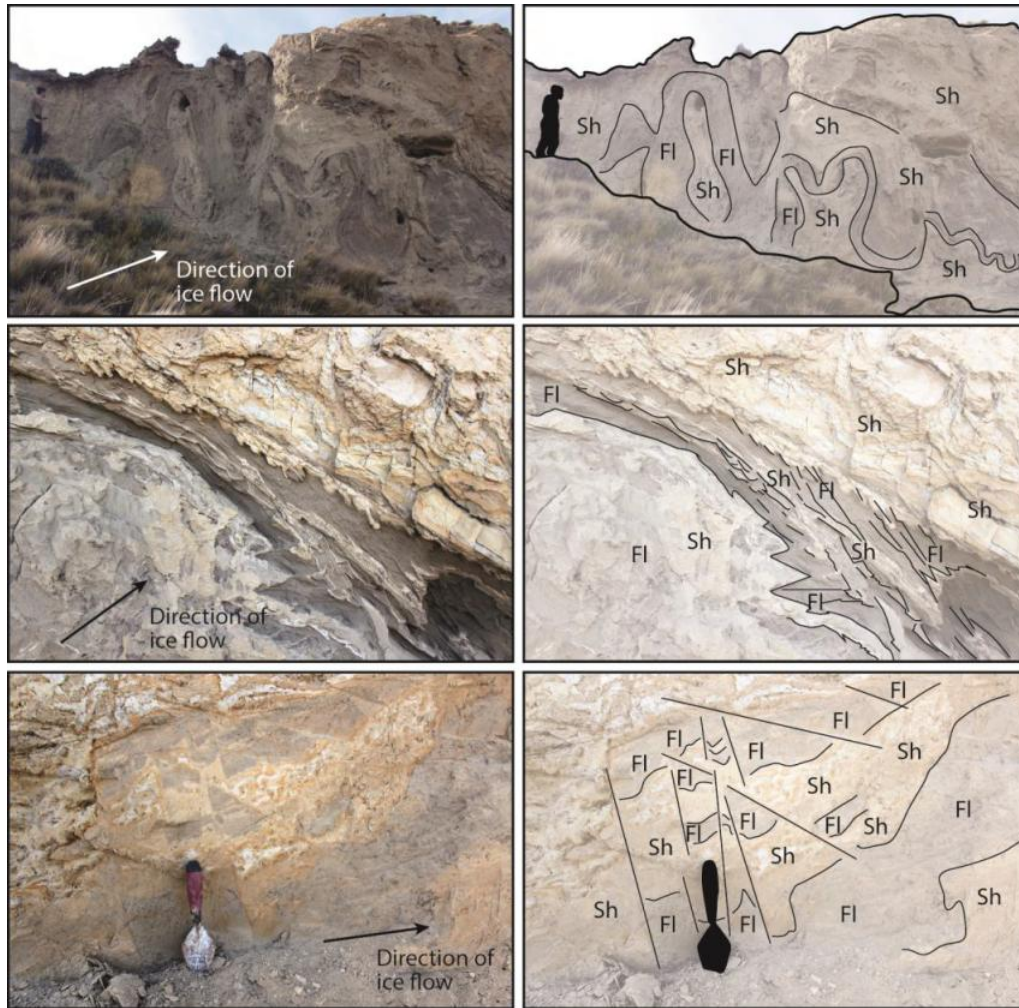
Figure 6.11. Photographs and accompanying sketches of proglacially tectonised lacustrine silts and sands within an end moraine of the BI-SSb lobe (location shown in Figure 6.6). There is a high degree of folding and faulting. The large section of lacustrine sediments suggests that the ice lobe retreated sufficiently for a sizeable proglacial lake to develop prior to re-advance.

Kettle and kame topography is particularly clear in the wide bands to the north and south of the BI-SSb lobe. A section through the inner (San Sebastián) band shows two diamict units separated by outwash sands and gravels. This suggests that the ice lobe advanced to form the outer (Río Cullen) band first before retreating into the BI-SSb depression and re-advancing (Figure 6.12). We infer that, like the hummocky terrain, the kettle and kame topography was produced by supraglacial deposition of material at the ice margins during ice stagnation (Clayton, 1964; Benn & Evans, 1998; Schomacker, 2008). However, unlike hummocky terrain, the ice was likely stagnant at these locations for longer, allowing for greater quantities of supraglacial debris to be deposited.
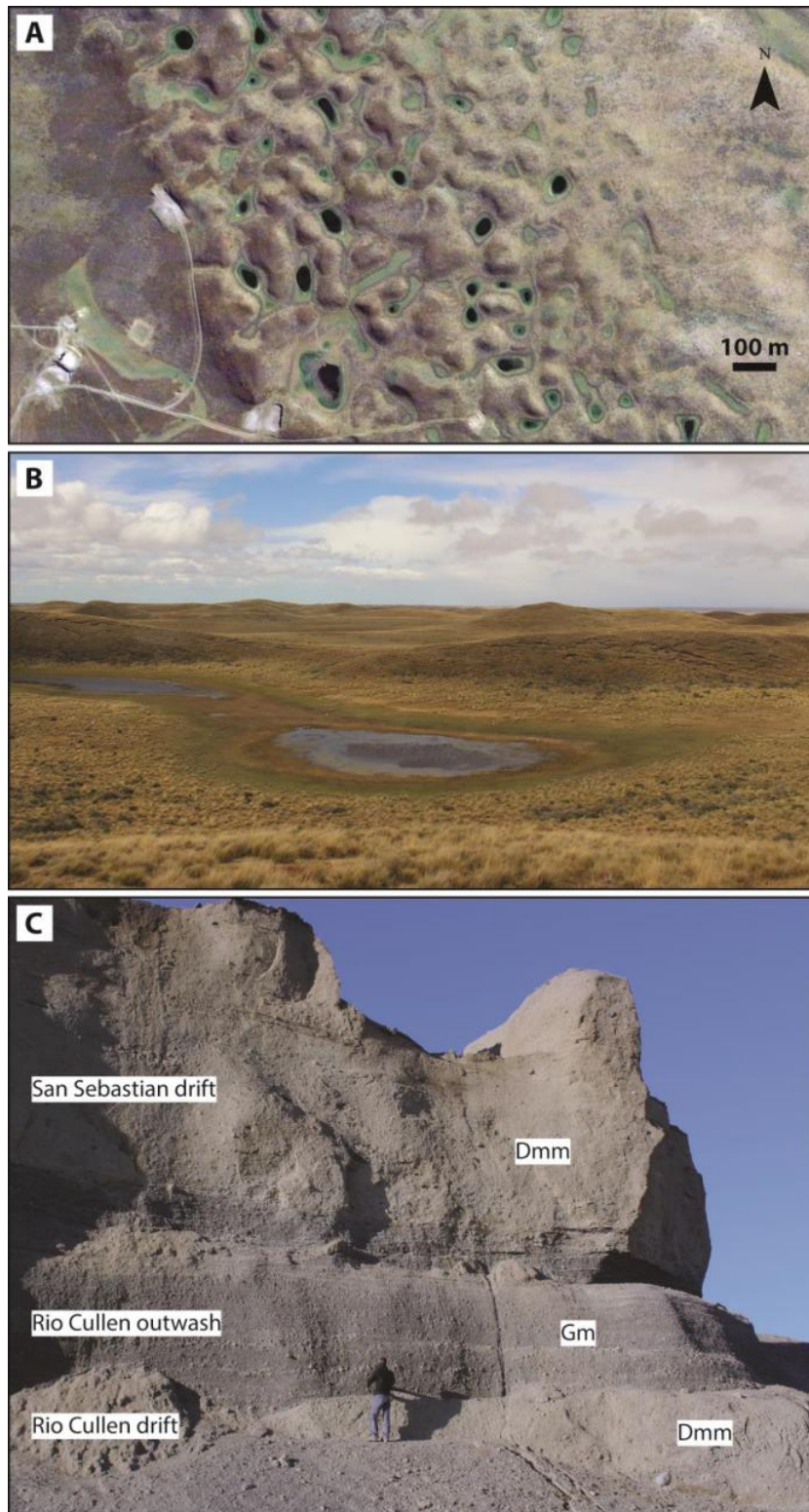
Figure 6.12. (A) Google Earth™ Image of the kettle and kame topography on the south side of the BI-SSb lobe. (B) Photograph of the kettle and kame topography on the north side of the BI-SSb lobe. (C) A section through the inner kettle and kame topography on the north side of the BI-SSb lobe. The top diamict unit relates to this glacial limit (the San Sebastián drift) but overlies an earlier diamict and associated outwash (the Rio Cullen drift), indicating that the ice lobe re-advanced.

149

6.5.2.2 Subglacial landforms

Subglacial features found in the study area include glacial lineations, subdued moraine topography and IDR. Glacial lineations are common across all of the ice lobes in the form of flutings and drumlins, indicating the active advance of ice. Given that all of the ice lobes were likely advancing over former glaciofluvial deposits, the lineations were probably formed by subglacial deformation during advances of wet-based ice (Benn & Clapperton, 2000b), consistent with the presence of deformed sediments in at least the Magellan lobe (Clapperton, 1989; Benn & Clapperton, 2000b). However, the precise formation processes that result in glacial lineations are contentious (Stokes *et al.*, 2011). Generally, the lineations occur in conjunction with ice marginal features, but a few dense swaths of drumlins occur away from any apparent ice margin and show elements of convergence and divergence, most clearly in the area around Laguna Cabeza del Mar in the Otway lobe (Benn & Clapperton, 2000b; Lovell *et al.*, 2012; Figure 6.3). In these locations, we suggest that the lineations are indicative of areas of rapidly flowing ice (Stokes & Clark, 1999; Stokes & Clark, 2002; Evans *et al.*, 2008; Lovell *et al.*, 2012).

Subdued moraine topography is considered morainic because of its arcuate form and consistency with other ice marginal features. Raedecke (1978) suggested that the topography represented linear *en echelon* deposits linked to crevassing in the BI-SSb lobe, but the subtle nature of the topography makes it difficult to ascribe a formation process. However, the topography is clearly draped by younger features such as moraine ridges, glacial lineations and hummocky topography (Figure 6.7). Consequently, we infer that the subdued topography resulted from ice-marginal moraines that were subsequently overridden and moulded subglacially, similar to landforms observed in Iceland that were formed during earlier glacial advances (Krüger, 1987; Evans & Twigg, 2002). Subdued moraine topography is only found in small sections of the BI-SSb, Magellan and Río Gallegos lobes, which may indicate differences in the re-advance patterns of these ice lobes compared to the Skyring and Otway lobes, but could also be linked to differential moraine preservation during subglacial moulding.

IDR mainly occurs at the intersection between geomorphology of the Río Gallegos and Skyring lobes and takes the form of relatively disorganised, hilly ridges, sometimes interweaved by meltwater channels. It has previously been unclear what formed these features (Lovell *et al.*, 2011; Chapter 3), but the presence of a large swath of drumlins (FS 2; see Section 6.5.1) oriented southeastward may help

explain how the IDR formed (Figure 6.4). We suggest that the Río Gallegos lobe advanced first into this area, depositing a drumlin field and moraine ridges. Subsequently, the Río Gallegos lobe retreated and the Skyring lobe advanced over the drumlins and moraines, causing subglacial deformation that resulted in an irregular pattern of hills and meltwater channels (Figure 6.4). The stratigraphic order is dictated by the fact that meltwater from the Skyring lobe drained into the Río Gallegos depression.

6.5.2.3 *Glaciofluvial landforms*

Glaciofluvial landforms are abundant within the study area and include meltwater channels and outwash plains. Hundreds of meltwater channels are associated with all of the ice lobes, often running parallel to former ice margins and sometimes exploiting former channels. Some of these meltwater channels are so large that they form corridors of outwash. For example, the meltwater issuing from the northern and southern lateral margins of the BI-SSb lobe was directed down large, pre-existing valleys, creating an outwash-fill. Broader outwash plains are also common and can be traced back to corresponding moraines and meltwater channels. The extensive nature of the glaciofluvial features implies that all of the ice lobes produced large quantities of meltwater both during stillstands (in association with kettle and kame topography and moraines) and during retreat. However, the absence of outwash associated with some glacial limits may mean that some outwash plains have been subsequently destroyed.

Whilst meltwater channels and outwash plains are abundant within the study area, features such as ice contact fans, pitted outwash plains and eskers are not. One possible esker, mapped by Clapperton (1989), Lovell *et al.* (2011) and Darvill *et al.* (2014) remains highly ambiguous. It is likely that surface erosion and the vegetation of the landscape has removed some of these landforms. However, the general absence of eskers associated with the ice lobes, despite the apparent availability of sediment and meltwater, remains a mystery (Lovell *et al.*, 2012; Darvill *et al.*, 2014).

6.5.2.4 *Geometrical ridge landforms*

The swath of regular hummocky terrain located within the centre of the BI-SSb lobe resembles the geometrical ridge networks described by Bennett *et al.* (1996). These landforms are ridge-like but discontinuous; cross-cut one another in places; and are generally oriented perpendicular to former ice flow (Figures 6.7 and 6.13). They have not been reported prior to Darvill *et al.* (2014), but their similarity to geometrical ridge networks implies that they may be linked to crevasse-squeeze ridges (Bennet

et al. 1996), contrary to the suggestion that such features are not present in the region (Benn & Clapperton, 2000a). Studies of contemporary crevasse-squeeze ridges shows that they are formed by surging glacial systems (Sharp, 1985a, b; Bennett *et al.*, 1996; Evans & Rea, 1999, 2003; Evans *et al.*, 2007), where glacier movement and crevasse-filling occurs close to the ice margin during the overall melt-out of ice (Spedding & Evans, 2002). Whilst there are similarities between the morphology of the regular hummocky terrain and crevasse-squeeze ridges (Figure 6.13), the genetic connection is only tentative because we have no sedimentological analysis to support our inferences. Furthermore, preservation of the terrain is unexpected given the abundance of supraglacial debris (Benn & Evans, 1998) and there is little additional evidence for surging activity in the study area (Lovell *et al.*, 2012).
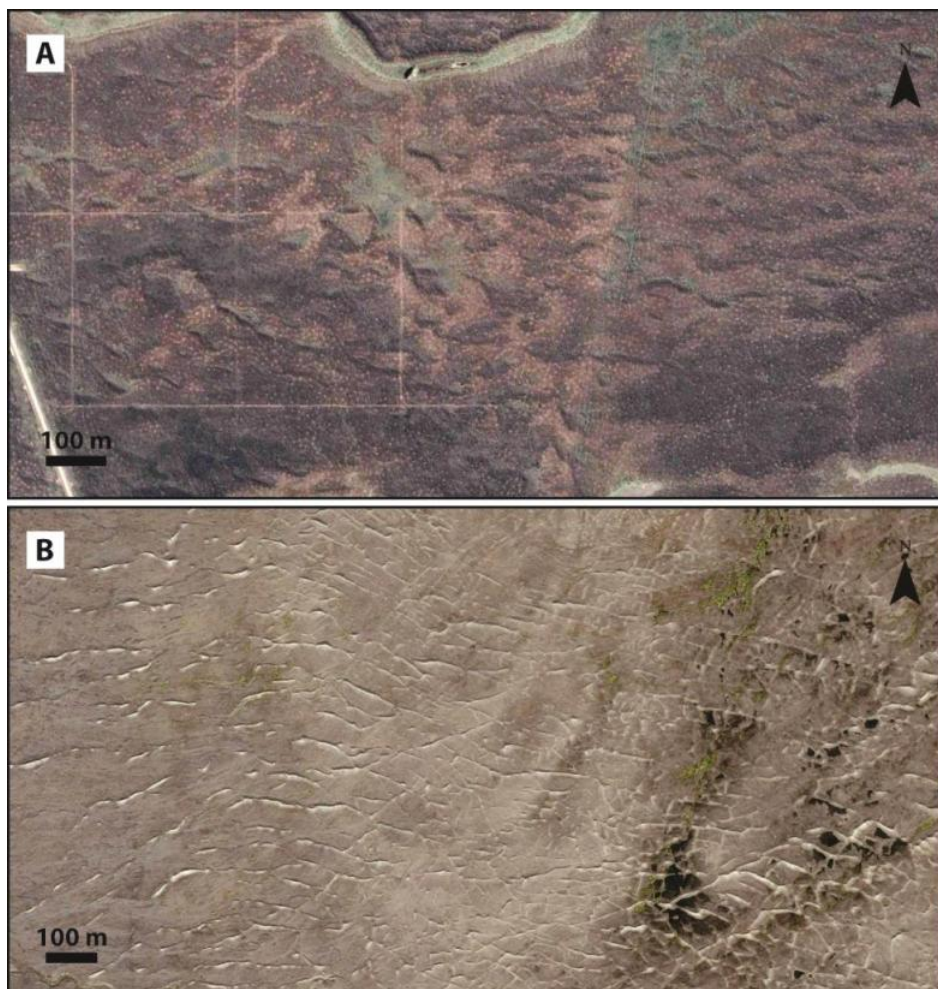
Figure 6.13. (A) The regular hummocky terrain from the centre of the BI-SSb lobe shown in a Google Earth™ image and (B) crevasse-squeeze ridges in front of the surging Brúarjökull glacier in Iceland shown in a Microsoft Bing Maps™ image.

6.5.2.5 Palaeolacustrine landforms

There are abundant raised shorelines in the area that may be linked to former lakes. Of note are semi-continuous, well-preserved shorelines around the present day Seno Skyring, Seno Otway, the Strait of Magellan and Bahía Inútil. Similar shorelines also occur above Laguna Blanca in the Skyring lobe and Lago Balmaceda in the Río Gallegos lobe (Figure 6.1). Our glacial reconstruction, combined with DEM modelling, and the occurrence of palaeolacustrine sedimentary evidence in places, leads us to infer that these shorelines relate to several large palaeolakes, supporting previous work on palaeolacustrine reconstruction in the area (Porter *et al.*, 1992; Clapperton *et al.*, 1995; McCulloch *et al.*, 2005a; Sagredo *et al.*, 2011; Stern *et al.*, 2011; Lovell *et al.*, 2012; Kilian *et al.*, 2007; Kilian *et al.*, 2013). The ice-marginal truncation of these shorelines suggests that they formed in front of the ice lobes, likely during recession into their respective topographic basins.

The clearest palaeolacustrine landforms are within the Skyring lobe, where meltwater accumulated above the present day Laguna Blanca. Shorelines and DEM modelling indicate a maximum lake depth of *ca.* 190 m.a.s.l., which drained northward into the basin previously occupied by the Río Gallegos lobe. Our reconstruction is supported by the presence of rhythmically laminated silt and clay sediments containing dropstones northeast of Laguna Blanca (Figure 6.14). Unlike Lovell *et al.* (2012), our reconstruction of the lake also shows water accumulating on the northern lateral side of the ice lobe. Our ice limit for the Otway lobe also differs from Lovell *et al.* (2012), such that a similar proglacial lake did not form in front of the Otway lobe because meltwater could drain southeastward in front of the Magellan lobe. Once the Skyring lobe retreated beyond the topographic bluff separating it from the Otway lobe, the palaeo-Laguna Blanca proglacial lake drained in a south-eastward direction, in front of the Otway and Magellan lobes and into the Strait of Magellan. Large meltwater channels and an associated outwash plain record this potentially catastrophic drainage of the lake (Figure 6.14).

Another lake formed in front of the BI-SSb lobe to a maximum depth of *ca.* 20 m.a.s.l. and drained eastward at Onaisín (Figure 6.6) toward the Atlantic through a channel now marked by Laguna Larga (Figure 6.7). A similar lake formed in front of the Magellan lobe, draining eastward towards the Atlantic, though the height and route of the drainage are less clear as the channel is below present day sea-level (Clapperton *et al.*, 1995; McCulloch *et al.*, 2005a). The northern extent of the lake has been previously unclear, but our reconstruction suggests that it extended onto

the low plain in front of the Otway lobe. McCulloch *et al.* (2005a) reported sediments associated with both of these lakes. Small lakes also formed on the eastern flank of the Magellan lobe at *ca.* 10-20 m.a.s.l., north of Porvenir. One of these deposited a large section of rhythmically laminated silt and clay sediments at Laguna Verde, complete with dropstones (Figure 6.15).

A proglacial lake formed in front of the Otway lobe once ice had retreated into the present-day Seno Otway (Figure 6.3), and there is evidence for a channel draining north-eastward into the contemporary Strait of Magellan (Mercer, 1976; McCulloch *et al.*, 2005a). However, once the lake level had lowered to *ca.* 20 m.a.s.l., drainage would have been to the northeast through Canal Fitzroy (Figure 6.1) into a similar lake at *ca.* 10-20 m.a.s.l. within present-day Seno Skyring. The Skyring proglacial lake drained northward through Estero Obstruccion into a large lake in front of the Río Gallegos lobe, the extent of which is unclear (Sagredo *et al.*, 2011; Stern *et al.*, 2011). There is a drainage channel eastward from the Río Gallegos lobe towards the Atlantic, which suggests that the maximum lake level was at *ca.* 150 m.a.s.l., but final drainage of the Rio Gallegos proglacial lake would have been westward through Golfo Almirante Montt (Figure 6.1) once ice had receded into the mountains.
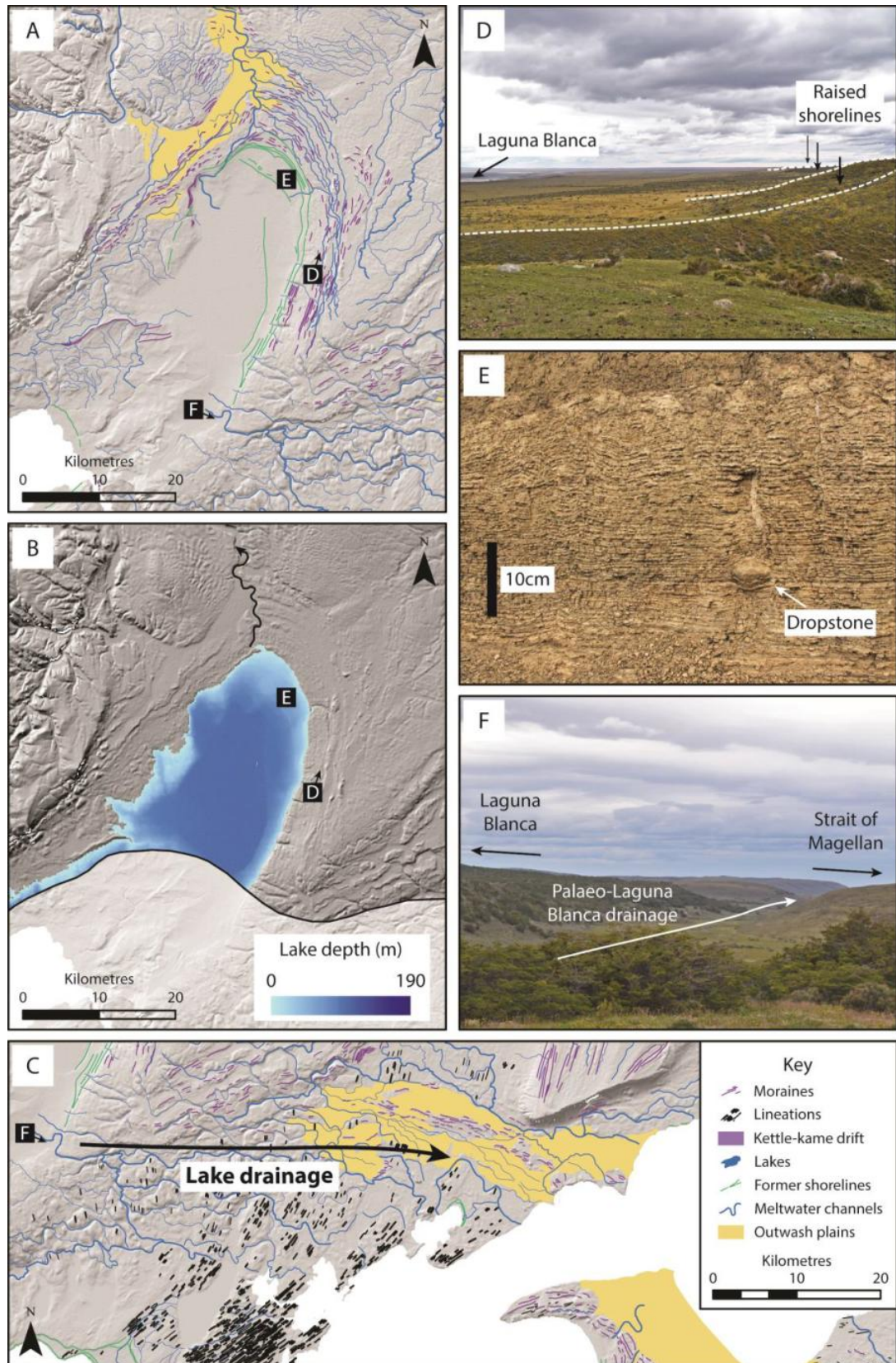
Figure 6.14. The evidence for palaeo-Laguna Blanca and its drainage. (A) shows the glacial geomorphology and (B) shows the reconstructed ice limit and proglacial lake just prior to drainage, when discharge flowed northwards (location shown in Figure 6.3). (C) illustrates the geomorphological evidence for lake drainage eastward into the Strait of Magellan (location shown in Figure 6.3). (D-F) show raised shorelines, laminated sediments and a drainage channel associated with the former lake (locations shown in A).

155
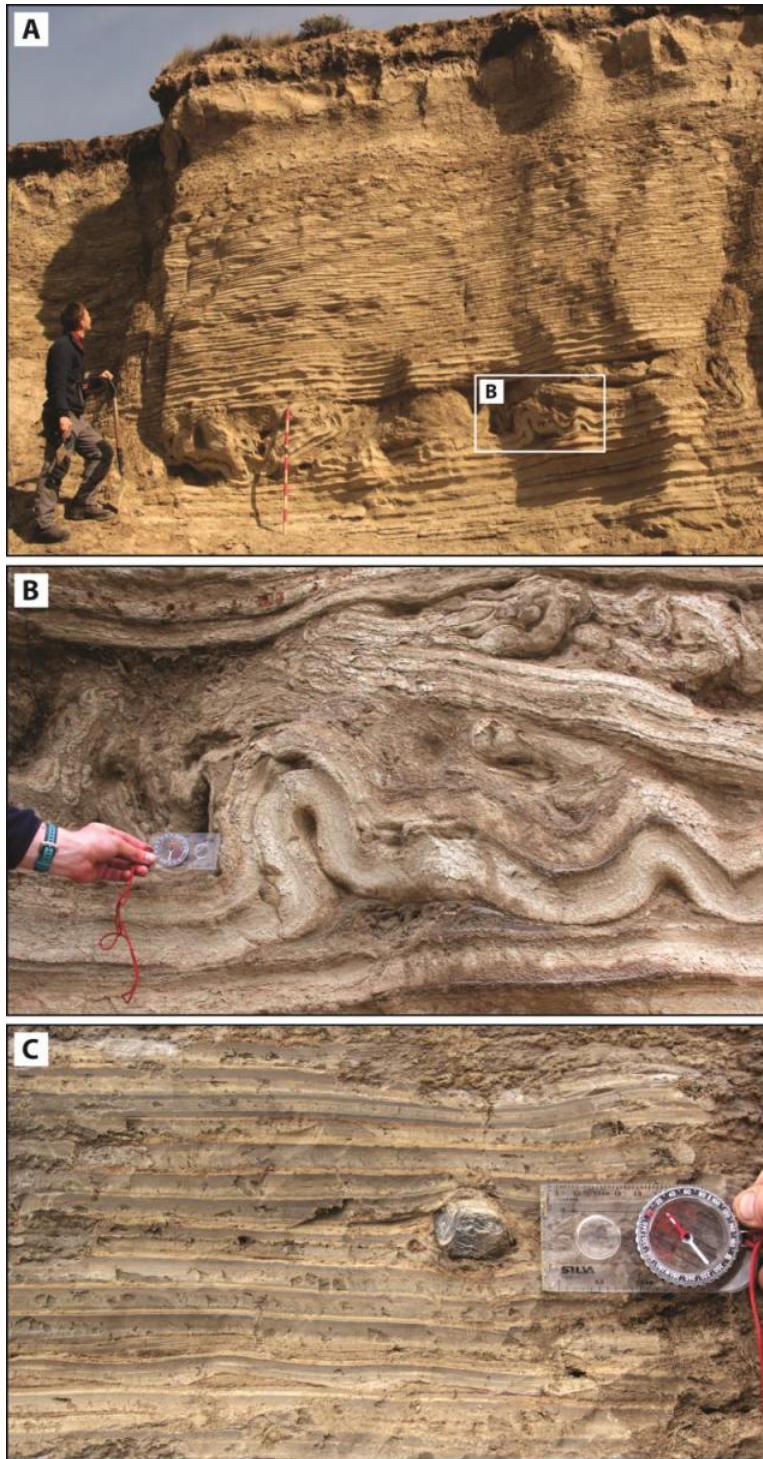
Figure 6.15. (A) Rhythmically laminated sediments at Laguna Verde (see Figure 6.5 for the location of the lake). (B) Enlarged part of the section to show how several of the laminated layers have been heavily deformed. The cause of this deformation has not been determined. (C) In places, dropstones demonstrate that the sediments were deposited within a former proglacial lake.

6.6 Discussion

6.6.1 *Active temperate glacial landsystem*

The glacial geomorphology in the study area can be broadly divided into three principal landform assemblages: morainic, subglacial and glaciofluvial (Figure 6.16). Taken together these groups are consistent with an active temperate glacial landsystem in operation during the advance and retreat of the ice lobes (Evans & Twigg, 2002; Evans, 2003). Temperate glaciers are generally warm-based and are characterised by their ability to actively advance during periods of overall recession (Evans, 2003). Modern examples of this landsystem include Breiðamerkurjökull, Fjallsjökull, Heinabergsjökull and Skalafellsjökull in Iceland (Evans & Twigg, 2002; Evans & Orton, 2014).

The wet-based active recession of this landsystem produces three characteristic landform-sediment associations (Evans & Twigg, 2002; Evans, 2003; Table 6.1). Firstly, dump, push and squeeze moraines composed of proglacial sediments mark the ice limit, sometimes displaying annual signatures or evidence for stillstands that create stacked features (Price, 1970; Krüger, 1987; Evans *et al.*, 1999; Evans & Twigg, 2002). Low amplitude ridges formed from overridden push moraines may also be found, draped by glacial lineations and moraines (Evans & Twigg, 2002). Secondly, subglacially streamlined flutings and drumlins occur between these moraines (Krüger, 1987; Evans *et al.*, 1999; Evans & Twigg, 2002). Thirdly, extensive glaciofluvial landforms occur where meltwater flows away from the warm-based ice front. These features include ice-contact and spillway-fed outwash fans; ice marginal outwash tracts; kame terraces; pitted outwash and eskers (Evans & Twigg, 2002).

The similarity between the landform assemblages in our study area (Figure 6.16) and those associated with active temperate glaciers supports the assertion that the ice lobes dominantly operated under an active temperate glacial landsystem (Table 6.1). This is especially clear in the geomorphology of the central BI-SSb lobe (Figure 6.6 and Figure 6.16). The other ice lobes show the characteristics associated with active temperate glaciers, but the geomorphology is either not as well preserved (as in the Río Gallegos and Magellan lobes) or the moraines are tightly nested due to topographic constraints (as in the Skyring and Otway lobes) so that the assemblages are not as clear. In addition, whilst outwash is associated with all of the ice lobes, subtleties such as fans and pitted outwash was not recorded, likely due to degradation hindering their identification.

An unusual aspect of the geomorphology in our study area is the evidence for supraglacial debris that formed the hummocky terrain and kettle and kame topography, particularly in the BI-SSb lobe. Evans & Twigg (2002) suggested that flutings and drumlins were prominent in this landsystem in part due to the lack of supraglacial sediment associated with active temperate glaciers in Iceland, so the presence of supraglacial landforms is surprising. However, the ice lobes are significantly larger than the Icelandic glaciers and so may have been able to transport greater quantities of debris. Additionally, Evans & Twigg (2002) did note that hummocks could be produced during the melting of debris-rich ice margins where marginal freeze-on of debris had occurred. Another complexity is the absence of eskers in the study area (Lovell et al., 2011; Darvill *et al.*, 2014). Like the outwash features, this may be related to preservation, but the general lack of eskers in Patagonia (e.g. Glasser *et al.*, 2008) suggests that there may be other reasons that are not yet resolved. Regardless, we suggest that, overall, the ice lobes are best represented by an active temperate landsystem.

Table 6.1. The landforms expected in an active temperate glacial landsystem (adapted from Evans & Twigg, 2002; Evans, 2003) and where these landforms are present in our study.

Landform group	Landforms	Río Gallegos	Skyring	Otway	Magellan	BI-SSb
Morainic landforms	Low-amplitude moraines (marginal dump, push and squeeze)	✓	✓	✓	✓	✓
	Low amplitude, hummocky terrain				✓	✓
Subglacial landforms	Flutings and drumlins	✓	✓	✓	✓	✓
	Overridden push moraines	✓				✓
Glaciofluvial landforms	Outwash (fans, ice margin-parallel tracts, topographically channelized, pitted)	✓	✓	✓	✓	✓
	Eskers			?		
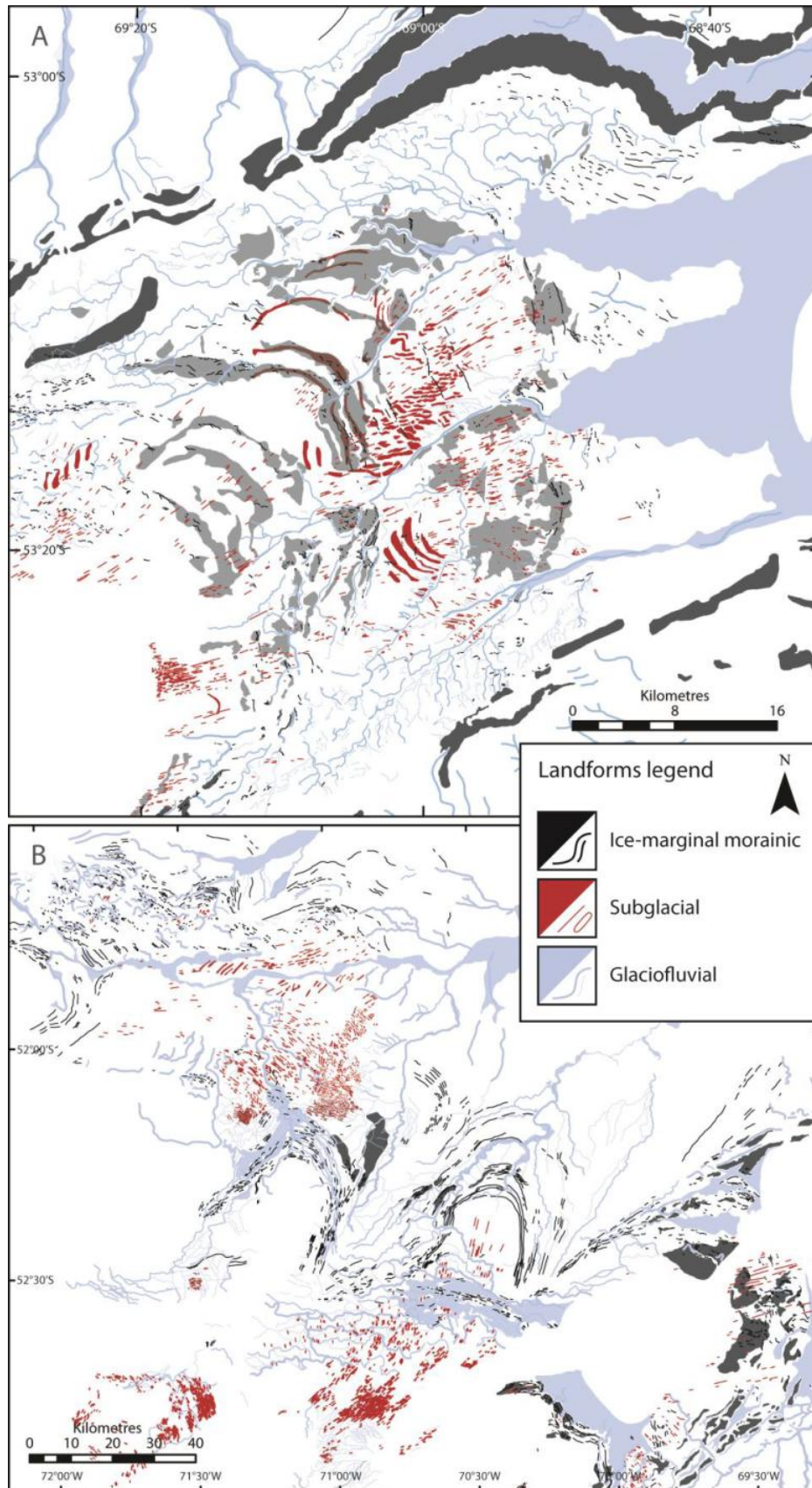
Figure 6.16. The glacial geomorphology of the central BI-SSb lobe (A) and the Río Gallegos, Skyring, Otway and Magellan lobes (B), grouped according to the three landform assemblages indicative of an active temperate glacial landsystem (see Figure 6.6 and Figure 6.3 for original versions).

159

6.6.2 Other landform signatures

Although the ice lobes dominantly conformed to an active temperate landsystem, the glacial geomorphology also supports the presence of subglacial landforms, such as swaths of elongated drumlins and possible crevasse-squeeze ridges, which may be indicative of rapid ice flow. Furthermore, palaeolacustrine landforms indicate the presence of former proglacial lakes that may have induced ice-front calving. Both of these landsystems would have influenced ice lobe dynamics.

6.6.2.1 Rapid ice flow

A large swath of elongated, closely-spaced drumlins in the inner part of the Otway lobe (FS 9) has previously been hypothesised to relate to palaeo-ice streaming (Benn & Clapperton, 2000b; Lovell *et al.*, 2012). Glacial lineations are found across the study area, but this drumlin field around Laguna Cabeza del Mar (Figure 6.3) displays some of the geomorphological characteristics expected from a terrestrial palaeo-ice stream, such as convergent flowlines, attenuated bedforms and abrupt lateral margins (Stokes & Clark, 1999; Clark & Stokes, 2003; Lovell *et al.*, 2012).

Additionally, Lovell *et al.* (2012) discussed the possibility for surge-like behaviour in the Otway lobe, though like Benn & Clapperton (2000a, b), they found no definitive evidence for cyclical surges from the landform evidence. However, some of the landforms associated with surging activity are exhibited in the study area (Evans & Rea, 2003; Schomacker *et al.*, 2014). These include thrust moraines, flutings, drumlins, hummocky terrain and possible crevasse-squeeze ridges. The latter are particularly intriguing given that Benn & Clapperton (2000a, b) ruled out surge-like behaviour due to the lack of crevasse-squeeze ridges and 'concertina' eskers. However, there are no sediment-landform assemblages that display definitive evidence of palaeo-surging activity, and given the fragmentary nature of the geomorphology, it is not possible to say that any of the ice lobes surged.

6.6.2.2 Proglacial lake development

Raised shorelines indicate that a total of six different lakes existed at various times in front of all five former ice lobes. The sediments deposited within the proglacial lakes have been used as a source of chronological constraint (McCulloch *et al.*, 2005a; McCulloch *et al.*, 2005b), and could yield further palaeoenvironmental records in the future.

6.6.3 Landsystem implications

There are a number of significant implications associated with the assignation of an active temperate glacial landsystem in this study. Principally, Benn & Clapperton (2000a, b) suggested that the Magellan lobe operated under subpolar conditions, with a cold-based margin, during the gLGM. By contrast Bentley *et al.* (2005) advocated warm-based conditions extending to the ice margin based on differing moraine gradient evidence. The presence of proglacially tectonised moraines and glaciofluvial features such as meltwater channels and outwash plains are consistent with cold-based ice or a polythermal basal regime (Benn & Clapperton, 2000b; Ó Cofaigh *et* al., 2003; Dyke & Evans, 2003; Evans, 2009). However, there is also evidence for glacial lineations extending to the ice margins and overridden moraine topography, both of which indicate extensive warm-based ice (Evans & Twigg, 2002; Evans, 2003), and so our landsystem approach does not fit with a model of cold-based ice margins. Rather, we suggest that the warm-based conditions that have been reconstructed for the interior parts of the ice lobes (Benn & Clapperton, 2000a, b; Lovell et al., 2012) extended to the margins.

Additionally, Benn & Clapperton (2000b) noted that the landforms that they inferred to represent cold-based ice (thrust moraines, glacigenic debris flows, hummocky and controlled moraines and lateral meltwater channels) could only have occurred in a narrow strip around the ice margin due to the presence of drumlins in the interior. However, Evans & Twigg (2002) described a narrow frozen zone that can develop at the margin of some active temperate glaciers, which may help to explain the presence of these features. The hypothesis that the ice lobes operated under sub-polar conditions invoked permafrost conditions at the gLGM (Benn & Clapperton, 2000a, b). However, the presence of active temperate ice could still have operated alongside discontinuous permafrost and there is independent evidence of permafrost features such as ice-wedge casts in the region (e.g. Bockheim et al., 2009).

Evans (2003) suggested that the landform-sediment signature of an active temperate landsystem was indicative of glaciers controlled by regional climatic variability. Therefore, our reconstruction of active advance and retreat of the ice lobes suggests that the glacial dynamics were primarily controlled by climatic variability. Consequently, topographic controls (Kaplan et al, 2009; Anderson et al; Barr & Lovell, 2014) or internal dynamics (Benn & Clapperton; Lovell et al, 2012)

would have been of secondary importance, though these would also have varied between lobes.

In addition to the overriding active temperate glacial landsystem, our reconstruction of fast-flowing ice would have affected ice dynamics in parts of the ice lobes. Similar fast-flowing systems in northern Patagonia during the gLGM are hypothesised to have resulted in greater ice discharge rates (Glasser & Jansson, 2005), and rapid ice flow across much of the eastern portion of the Patagonian Ice Sheet may help to explain mismatches between model outputs and landform reconstructions (Hulton *et al.*, 2002; Glasser & Jansson, 2005). The presence of landforms possibly linked to surge-like advances implies that, at times, the ice lobes may have briefly advanced in response to non-climatic forcing. The evidence for palaeo-surges is very limited, but the possibility that they occurred in this area warrants further research, particularly given the paucity of examples of surging systems in the palaeo-record and the fact that some contemporary active temperate glaciers, such as Breiðamerkurjökull, have also displayed surging activity (Evans & Twigg, 2002).

Former proglacial lakes would also have affected glacial dynamics by promoting increased rates of ice retreat (Porter *et al.*, 1992; Teller, 2003; Lovell *et al.*, 2012; Carrivick & Tweed, 2013). The presence of a proglacial lake at the margin of a glacier can trigger positive feedbacks such as increased englacial water pressure and temperature; increased subglacial pressure; and increased ice surface gradients, which can result in calving, ice-margin flotation and the flushing of sediment from beneath the ice (Carrivick & Tweed, 2013). This results in greater ice mass loss and glacial draw-down and was suggested by Lovell *et al.* (2012) as a possible mechanism to explain the rapid ice-flow in the Otway lobe. Porter *et al.* (1992) also suggested that calving of the Magellan and BI-SSb lobes could have resulted in a rapid loss of ice that may explain rapid retreat, or even collapse, of the ice lobes back into Cordillera Darwin during the lateglacial period (Hall *et al.*, 2013).

6.6.4 *Glacial reconstruction*

The glacial limits that we have defined can be used to reconstruct a relative glacial history for the region, enhanced by information about ice dynamics from our landsystems approach. Correlating between the glacial limits of adjacent ice lobes can be problematic because they are generally reconstructed from fragmentary records, and joining-up limits can over-emphasise correlation without robust chronological controls. However, in places, our approach informs the relative timing of ice advance and retreat between lobes based on cross-cutting landform

assemblages. Of particular note is the interplay between the outermost limits of the Skyring and Río Gallegos lobes (Section 6.5.2.2); the large flowset of lineations (FS 9) which crosses both the Magellan and Otway lobes (Section 6.6.2.1); and the drainage of the Skyring proglacial lake in front of the Otway and Magellan lobes (Section 6.5.2.5). The relative isolation of the BI-SSb lobe means that it is difficult to correlate between this and the other lobes. Based on our glacial limits, the nature of glacial dynamics from our landsystem approach and the logical (though conservative) configuration of the different ice lobes based on cross-cutting landform assemblages, we propose eight relative time steps for the region, against which chronological constraints have been applied where possible (Figures 6.17, 6.18, 6.19 and 6.20). We now discuss these time steps in detail.

6.6.4.1 Time step 1

The Río Gallegos lobe flowed rapidly to its greatest extent, creating flowsets FS 1, FS 2 and FS 3 (Figure 6.17). The extent of the other ice lobes is unclear, but the Skyring lobe cannot have been fully extended because the geomorphology of the Río Gallegos and Skyring lobes overlaps and Skyring drainage later flowed into the former Río Gallegos depression (Figure 6.4). [10]Be ages of 56.0 ka and 138 ka relating to the outer limits of the Río Gallegos lobe are substantially younger than the Bella Vista flow (Kaplan *et al.*, 2007), which has been [40]Ar/[39]Ar dated to 1.17 Ma by Singer *et al.* (2004a) and underlies till deposits thought to relate to the maximum glacial advance. This could be due to post-depositional processes affecting the sampled moraine boulders (Kaplan *et al.*, 2007), but we also caution that it is difficult to tie distal drift sediments to limits defined by glacial geomorphology (Meglioli (1992) also dated flows to 8.0 and 8.5 Ma within this ice lobe); the Bella Vista flow only provides a maximum age for the limit; and it is not inconceivable that the ice lobe extended towards this maximum extent on several occasions. Consequently, we cannot rule out the possibility that this time step occurred more recently than previously thought.
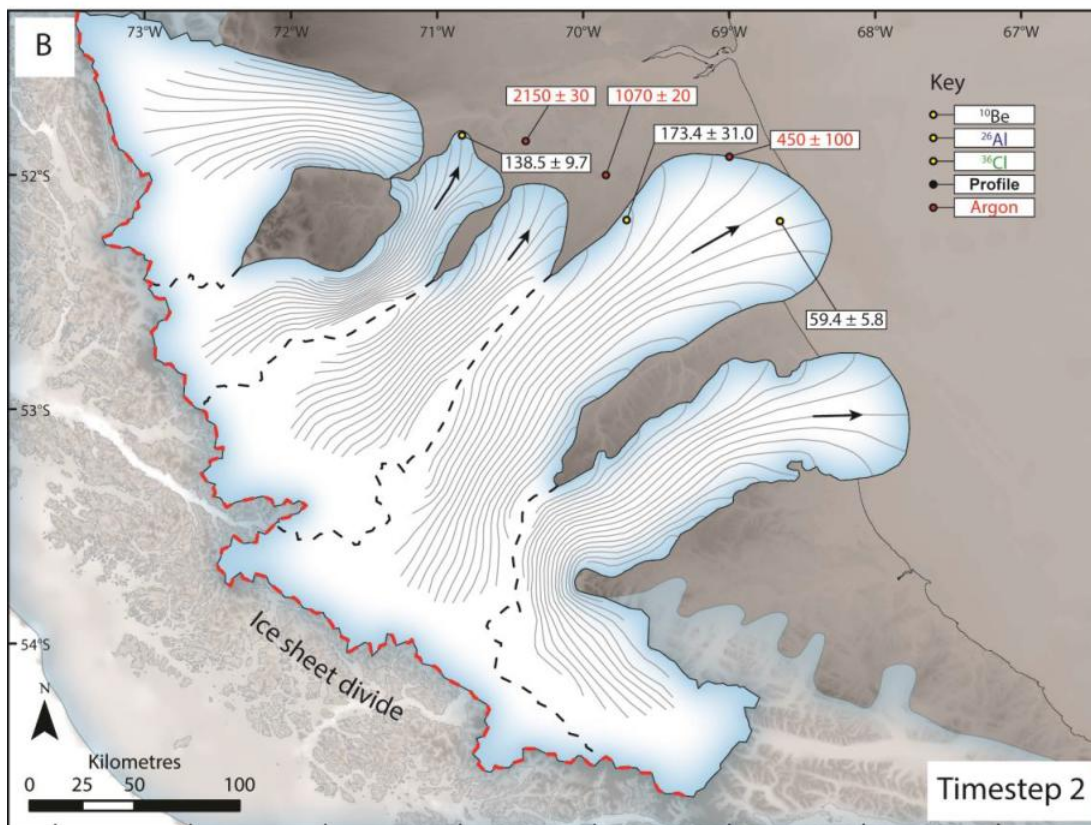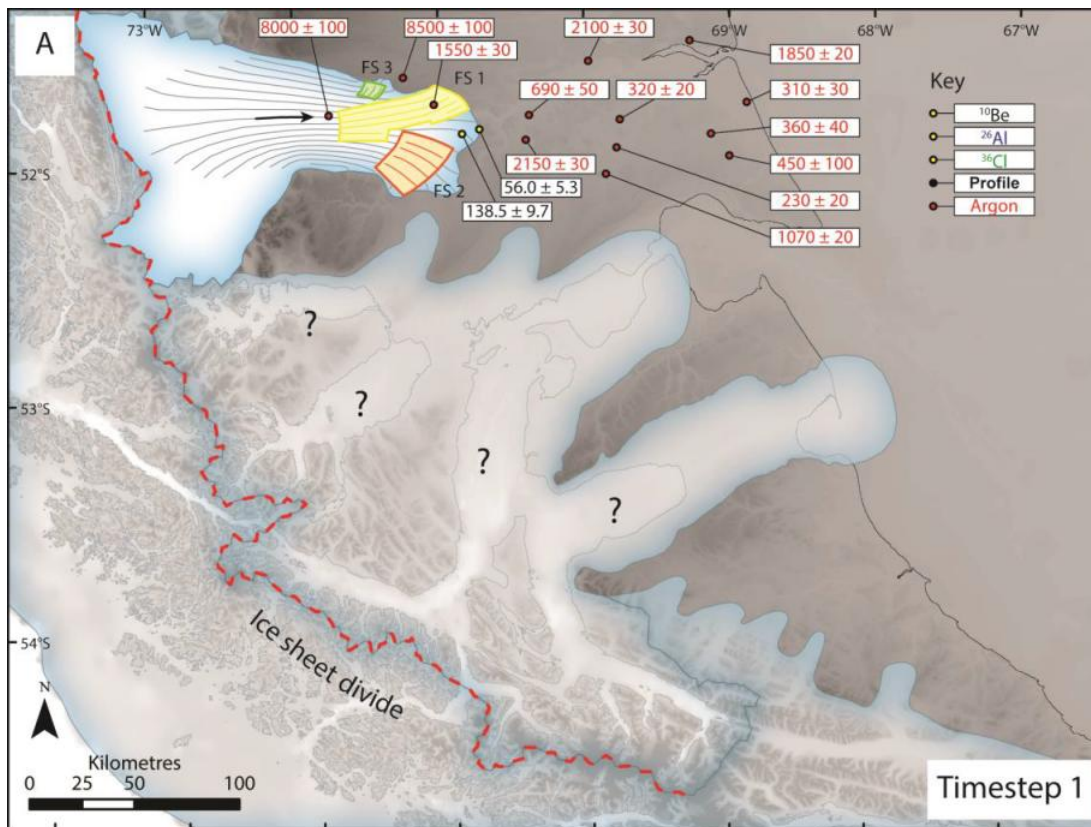
Figure 6.17. (A) Time step 1 and (B) time step 2. Dates are shown in ka (see text for details) and flowsets are shown where appropriate. Black arrows indicate ice advance and the hypothetical ice sheet divide is shown by the red dashed line.

164
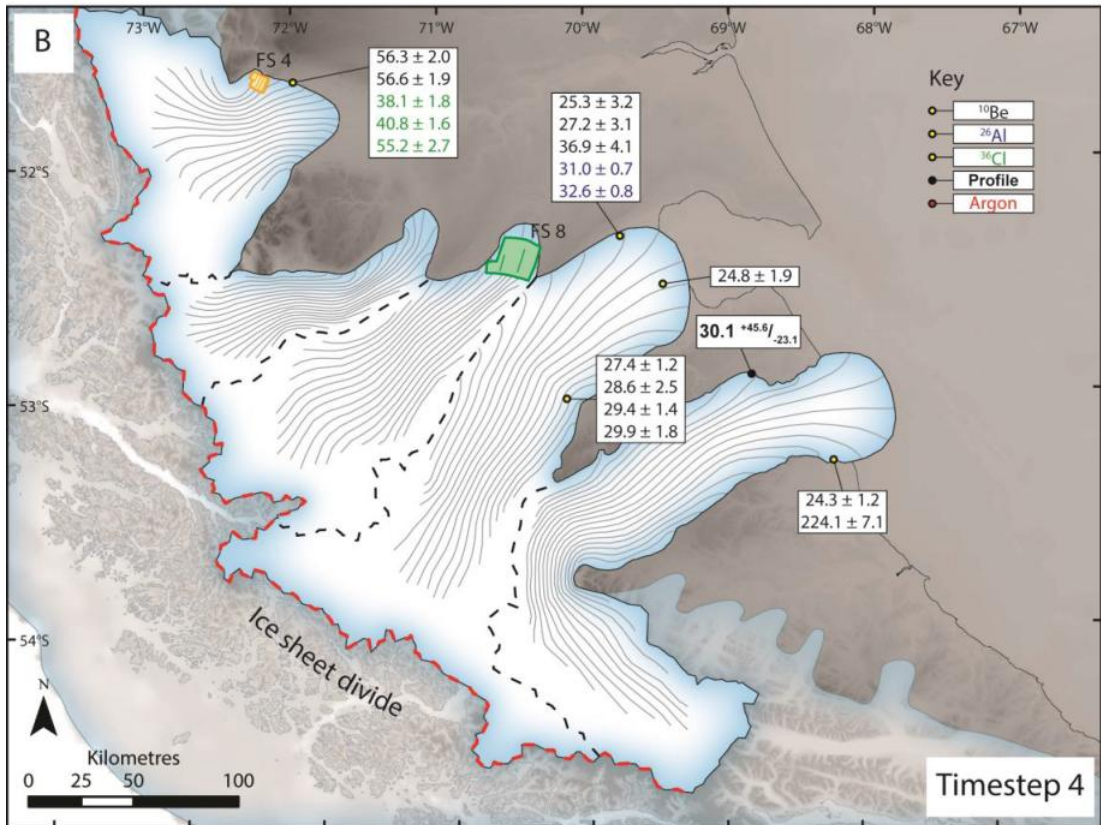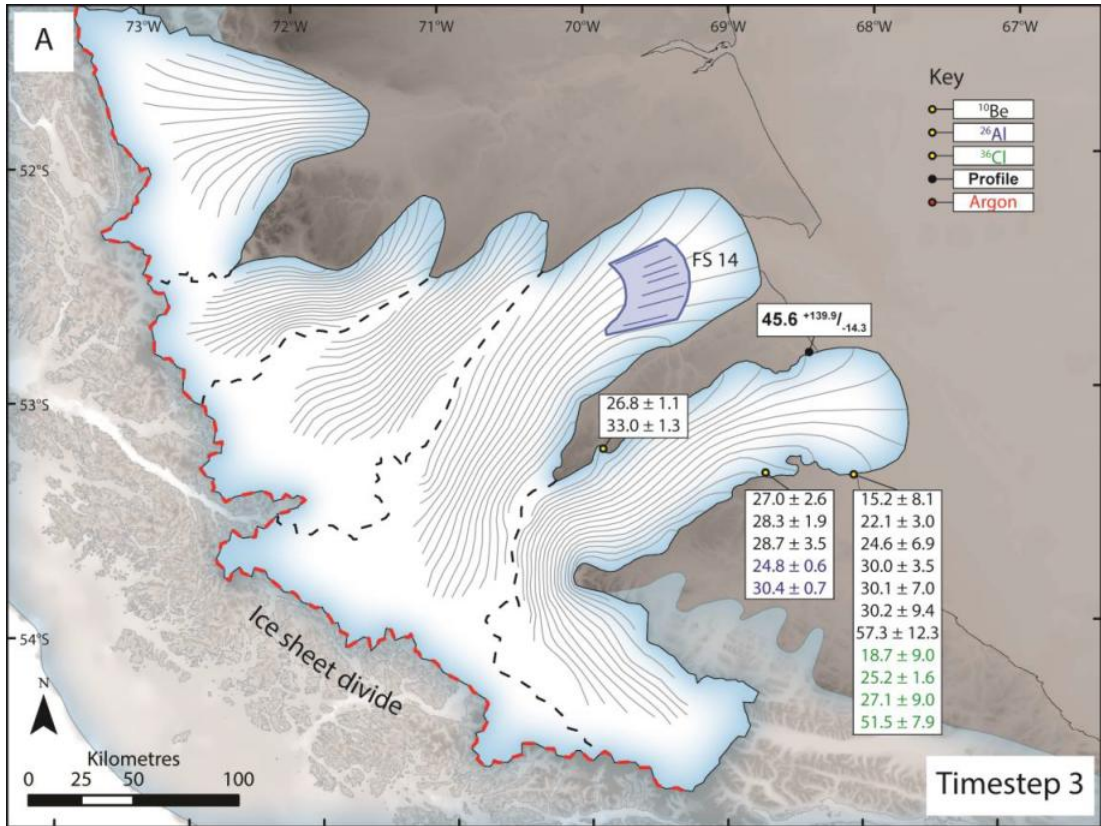
Figure 6.18. (A) Time step 3 and (B) time step 4. Dates are shown in ka (see text for details) and flowsets are shown where appropriate. The hypothetical ice sheet divide is shown by the red dashed line.

165

6.6.4.2 Time step 2

The Skyring, Otway, Magellan and BI-SSb ice lobes advanced to their maximum extents, whereas the Río Gallegos lobe retreated (Figure 6.17). The Skyring lobe advanced into the Río Gallegos depression, overriding former moraines and glacial lineations to leave irregular dissected ridges (Figure 6.4; Lovell *et al.*, 2011; Chapter 3). The exact extent and timing of the advances is unclear, and correlation cannot be made between the ice lobes. The [10]Be ages of 56.0 ka and 138 ka (Kaplan *et al.*, 2007) in time step 1 could reasonably relate to time step 2 if they were actually deposited by the Skyring lobe. Two further ages of 59.4 ka and 173 ka from the Magellan lobe are similarly young compared to local [40]Ar/[39]Ar ages (Meglioli, 1992; Singer *et al.*, 2004a; Kaplan *et al.*, 2007). However, tying dated tills to glacial limits may not be straightforward. It is conceivable that the ice lobes advanced more than once to similar limits at radically different times, possibly due to topographic constraints (Kirkbride & Winkler, 2012; Barr & Lovell, 2014) or erosional feedbacks (Kaplan *et al.*, 2009; Anderson *et al.*, 2012). For example, The BI-SSb lobe was also close to this limit in at least time steps 3 and 4. The four cosmogenic dates available for time steps 1 and 2 may indicate two separate advances at around 173-138 ka and 59-56 ka, but the dates are not apparently in stratigraphic order, disagree with the conceptual age model for the region (Meglioli, 1992), and do not take into account erosion and/or exhumation processes (Kaplan *et al.*, 2007).

6.6.4.3 Time step 3

The Río Gallegos lobe continued to recede and the Skyring and Otway lobes retreated to close to the limits of their topographic basins. The Magellan lobe may have re-advanced slightly, forming FS 14 (Figure 6.18), though this flowset may have formed in time step 1 or 2. There are no chronological constraints for the Río Gallegos, Skyring, Otway or Magellan lobes and correlation between the lobes cannot be made, but the BI-SSb ice limit has been [10]Be dated (Kaplan *et al.*, 2007; Kaplan *et al.*, 2008a). Twelve ages range from 15.2 ka to 57.3 ka, though eight of these are within 26.8 ka and 33.0 ka. In addition, two [26]Al dates of 24.8 ka and 30.4 ka and four [36]Cl dates of 18.7 ka, 25.2 ka, 27.1 ka and 51.5 ka have been recorded (Kaplan *et al.*, 2007; Evenson *et al.*, 2009).

Post-depositional erosion and exhumation may have affected these boulder ages (Kaplan *et al.*, 2007), so Chapter 5 used a [10]Be/[26]Al depth profile through outwash associated with the same limit to obtain an independent estimate of age. The errors on the depth-profile are large, but it indicates that the limit was deposited during the

last glacial cycle, possibly around 45.6 ka. Thus, numerous dating campaigns have yielded ages younger than previously thought, and a best estimate of age may be somewhere between 26.8 ka and 57.3 ka. The large spread of ages may result from post-depositional processes, possibly linked to gradual melt-out of the dead ice in kettle and kame topography (Schomacker, 2008; Chapter 4), or boulder erosion (Kaplan *et al.*, 2007). The latter could explain the offset between the dominant cluster of boulder ages between 27.0 ka and 36.2 ka, and the depth profile at 45.6 ka, in which case, the depth profile may be a better estimate of the time of deposition (see Chapter 5).

6.6.4.4 Time step 4

The Skyring and Otway lobes retreated to skirt the edges of their respective basins, with the Otway lobe possibly re-advancing to form FS 8 (Figure 6.18). The Magellan lobe retreated to Primera Angostura and the Río Gallegos lobe continued to retreat, possibly re-advancing slightly to deposit FS 4. The BI-SSb lobe re-advanced close to the limit of time step 3, depositing a second band of kettle and kame topography, which has yielded [10]Be dates of 24.3 ka and 224.1 ka (Kaplan *et al.*, 2007). These dates are ambiguous, but a depth-profile through associated outwash yielded a more robust age of *ca.* 30.1 ka (Chapter 5). Like time step 3, there is scatter in the boulder ages, perhaps due to post-depositional processes. For the Magellan lobe, four [10]Be ages between 24.8 ka and 36.9 ka and two [26]Al ages of 31.0 ka and 32.6 ka (Kaplan *et al.*, 2007) imply that the limit may have been deposited at a similar time to that of the BI-SSb lobe. In addition, we suggest that four dates on Peninsula Juan Mazia, previously ascribed to a later advance, may have been deposited at this time, given the similarity between these [10]Be ages of 27.4 ka to 29.9 ka and those on Primera Angostura (McCulloch *et al.*, 2005b; Kaplan *et al.*, 2008a). For the Río Gallegos lobe, two [10]Be ages of 62.4 ka and 62.7 ka, and three [36]Cl ages of 38.1 ka to 55.2 ka (repeat samples; Evenson *et al.*, 2009), imply that the limit may be older, but these dates are all from a single boulder, and the lateral configuration of this ice lobe is challenging to map. There are no ages for the Skyring or Otway lobes.
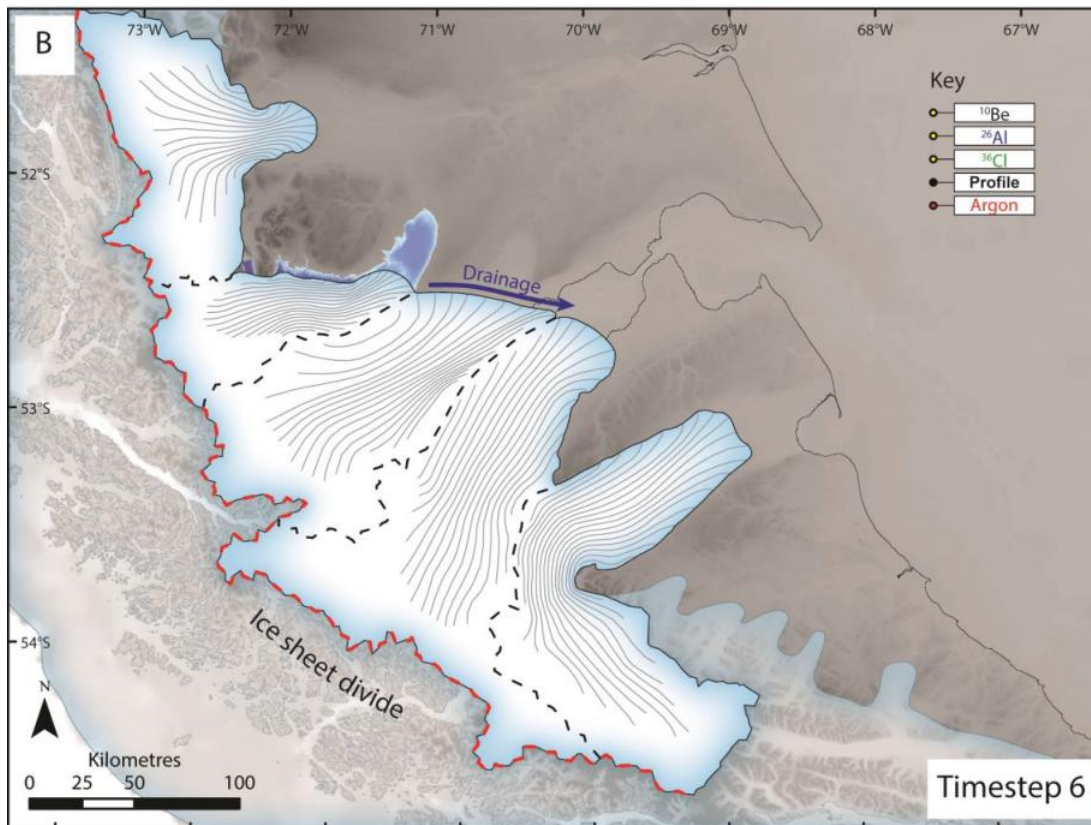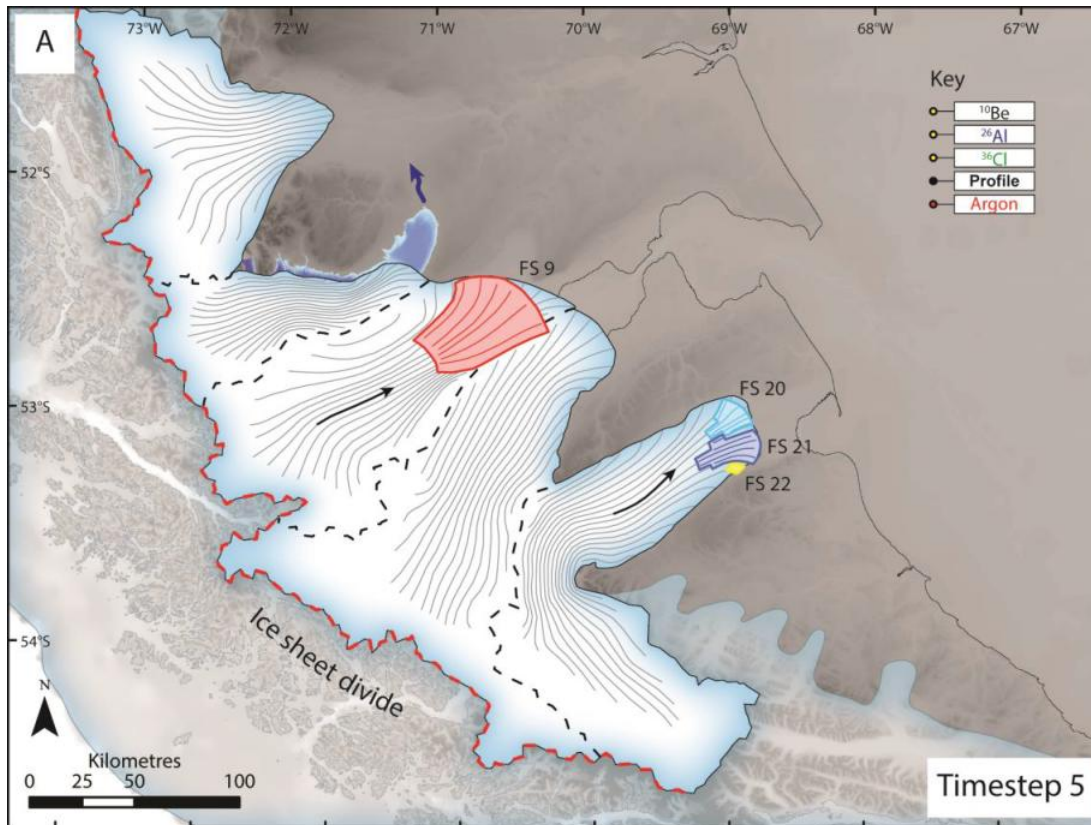
Figure 6.19. (A) Time step 5 and (B) time step 6. Dates are shown in ka (see text for details) and flowsets are shown where appropriate. Proglacial lakes are shown along with their drainage routes (blue arrows) and black arrows indicate advance. The hypothetical ice sheet divide is shown by the red dashed line.

168
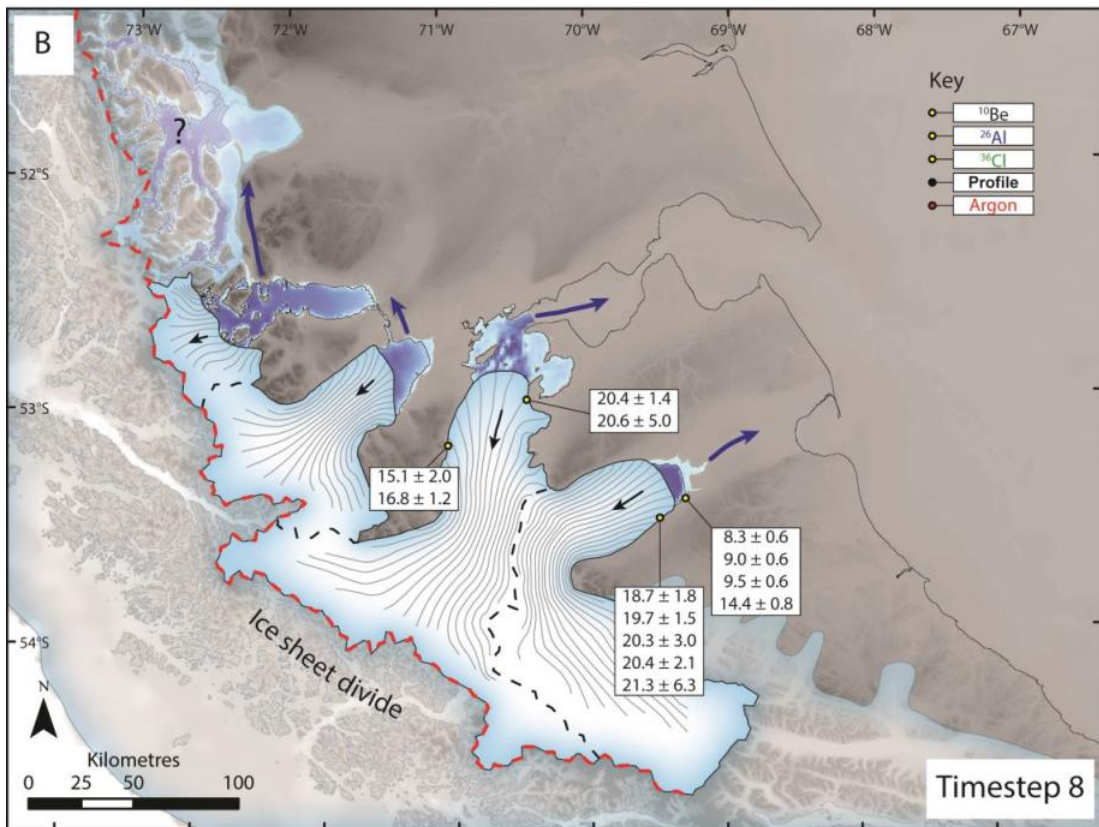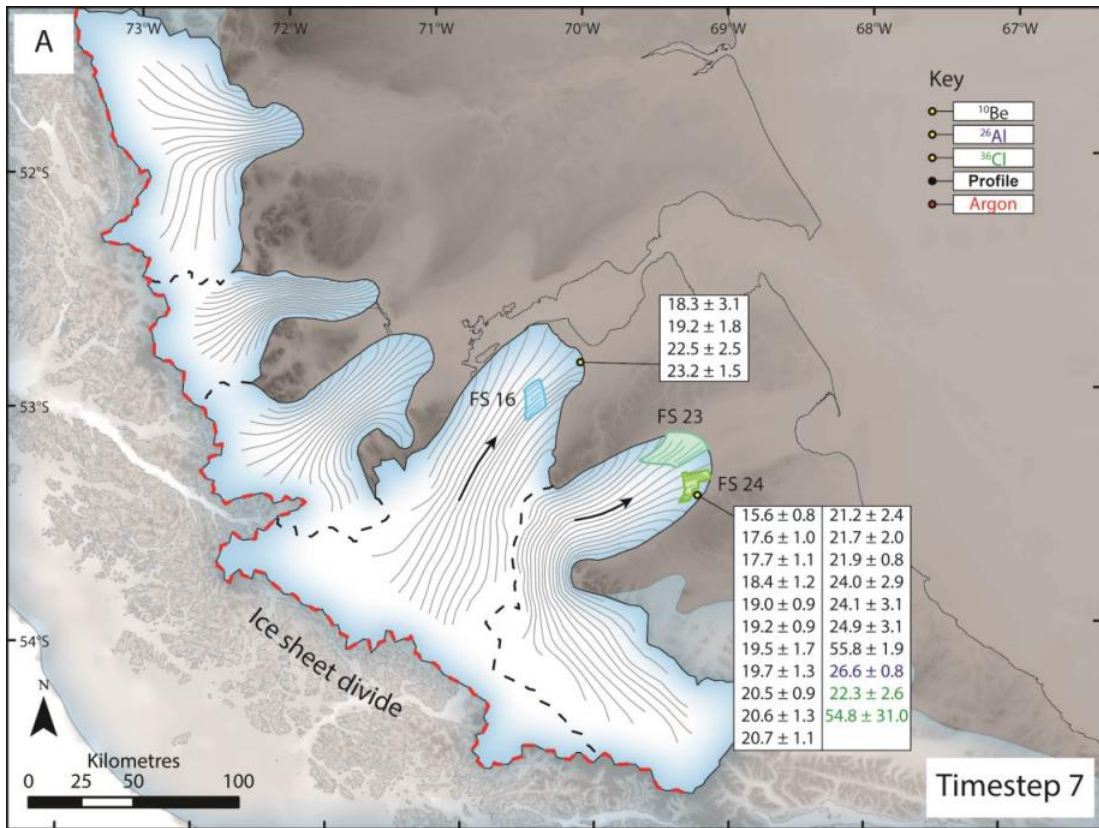
Figure 6.20. (A) Time step 7 and (B) time step 8. Dates are shown in ka (see text for details) and flowsets are shown where appropriate. Proglacial lakes are shown along with their drainage routes (blue arrows) and black arrows indicate ice advance or retreat. The hypothetical ice sheet divide is shown by the red dashed line.

169

6.6.4.5 Time step 5

The Río Gallegos, Magellan and Skyring lobes retreated, with the latter triggering the development of a proglacial lake – palaeo-Laguna Blanca – which may have further facilitated ice loss from a calving front (Figure 6.19). This lake drained northwards into the Río Gallegos depression, indicating recession of the Río Gallegos lobe. The Otway lobe re-advanced significantly, forming FS 9 around Laguna Cabeza del Mar and shifting the ice divide between the Otway and Magellan lobes south-eastward into the present-day Strait of Magellan. The BI-SSb lobe also re-advanced to a limit close to Bahía San Sebastián, depositing a large terminal moraine that is still preserved east of Laguna Larga and forming FS 20, 21 and 22. The re-advances of these two ice lobes may have been in response to rapid ice flow, or possible surge-like activity. Thus, between time steps 4 and 5, all ice lobes receded and the Otway and BI-SSb lobes re-advanced. There are no chronological constraints for any of the ice lobes in this time step, but the thrust moraines deposited by the Otway lobe also indicate the position of the Skyring and Magellan lobes.

6.6.4.6 Time step 6

All ice lobes retreated during this time step (Figure 6.19). The Skyring, Otway and Magellan lobes did not retreat far because the potentially catastrophic drainage of palaeo-Laguna Blanca passed from in front of the Skyring lobe east to south-easterly in front of the Otway and Magellan lobes. It is unclear how far the Río Gallegos and BI-SSb lobes retreated during this time step, but the presence of deformed lacustrine sediments in re-advance moraines of the BI-SSb lobe in time step 7 suggests that this ice lobe must have retreated sufficiently for a pro-glacial lake to develop. Again, there are no chronological constraints for any of the ice lobes in this time step, but we note that for the Skyring, Otway and Magellan lobes, time steps 5 and 6 are broadly constrained by dates in the Magellan lobe for time steps 4 and 7, and that the limits can be correlated reasonably robustly across the three ice lobes. Dating the drainage of palaeo-Laguna Blanca would improve this chronology and test our interpretation of the dates for time steps 4 and 7.

6.6.4.7 Time step 7

This time step has previously been defined as the gLGM limit (Figure 6.20). There are no supporting ages for the Río Gallegos, Skyring and Otway lobes, although they were likely situated within the present-day fjords, with the termini of the Skyring and Otway lobes splitting after time step 6. The Magellan and BI-SSb lobes had

retreated upstream – though it is not clear how far – and re-advanced during this time step, possibly displaying surge-like behaviour and forming FS 16 and FS 23 and 24. The Magellan lobe has been [10]Be dated four times on Peninsula Juan Mazia to between 18.3 ka and 23.2 ka. The BI-SSb lobe has also been dated, with 18 [10]Be dates yielding ages of between 15.6 ka and 55.8 ka, though with sixteen of these dates between 17.6 ka and 24.9 ka, one [26]Al date of 26.6 ka, and two [36]Cl dates of 22.3 ka and 54.8 ka (McCulloch *et al.*, 2005b; Kaplan *et al.*, 2007; Kaplan *et al.*, 2008a; Evenson *et al.*, 2009). The reason for the scatter in ages is unclear, though the [10]Be date of 55.8 ka may be due to inheritance, given most of the dates are from a large erratic boulder train on the south-eastern side of Bahía Inútil (see Chapter 4). Nonetheless, the dates for the Magellan and BI-SSb lobes generally support the assertion that this time step relates to the gLGM.

6.6.4.8   Time step 8

All of the ice lobes were in full post-gLGM retreat during this time-step, likely developing proglacial lakes in front of their receding margins that could have increased the rate of ice retreat due to frontal calving (Figure 6.20; Porter *et al.*, 1992; Kilian *et al.*, 2007). The Magellan and BI-SSb proglacial lakes drained eastward toward the Atlantic, although their extent is uncertain. Drainage of the Otway proglacial lake initially occurred east to north-eastward into the Magellan lake (McCulloch *et al.*, 2005a), but as lake levels dropped during ice retreat, drainage switched to north-westward into the Skyring proglacial lake (McCulloch *et al.*, 2005a; Kilian *et al.*, 2013), cutting the Fitzroy channel and depositing large deposits of climbing ripple structures. In turn, the Skyring proglacial lake drained into the Río Gallegos proglacial lake that, by this time, may have drained westward into the Pacific ocean through ice-free fjords dissecting the Andes (McCulloch *et al.*, 2005a; Kilian *et al.*, 2013). That said, it is possible that Río Gallegos ice was still extensive, such that drainage occurred later and was southward, reaching the Pacific through Seno Otway (Stern *et al.*, 2011). Uncertainty in the configuration of the Río Gallegos lobe makes it difficult to assess drainage routes.

The Skyring and Otway lobes were located well within their respective fjords, with cores suggesting ice-free conditions in Seno Skyring and Seno Otway dated to at least 14.8 ka and 14.7 ka, respectively, using radiocarbon dating and tephrostratigraphy (Kilian *et al.*, 2013). Kilian *et al.* (2007) suggested that this was part of a rapid retreat of the Skyring lobe, likely linked in part to proglacial calving. The Magellan lobe has been [10]Be dated to 20.4 ka and 20.6 ka on Península Juan

Mazia and also 15.1 ka and 16.8 ka on the western lateral side of the lobe (Kaplan *et al.*, 2008a), perhaps indicating relatively rapid retreat of the ice lobe during and after this time step, and supporting ice recession by *ca.* 22 ka, as indicated by luminescence ages on the western side of the Strait of Magellan (Blomdin *et al.*, 2012). The BI-SSb lobe has yielded five similar [10]Be dates between 18.7 ka and 21.3 ka (McCulloch *et al.*, 2005b; Kaplan *et al.*, 2008a), and four [10]Be dates from a boulder below the proglacial lake shoreline suggest that drainage may have occurred between 14.4 ka and 8.3 ka (Evenson *et al.*, 2009). Numerous radiocarbon dates suggest that retreat of the Magellan and BI-SSb ice lobes was well under way by at least 14-15 ka (Clapperton *et al.*, 1995; McCulloch & Bentley, 1998; McCulloch *et al.*, 2005b), although the presence of the Reclús tephra within lake sediments suggests full retreat and lake drainage cannot have been before *ca.* 14.3 ka. The rapid retreat, and possible collapse, of the BI-SSb lobe during and after this time step is supported by radiocarbon dates in the accumulation area of the lobe in central Cordillera Darwin by Hall *et al.* (2013) that suggest that the constituent outlet glaciers that formed the ice lobe in this time step may have retreated into small interior fjords as early as 16.8 ka. These dates suggest early deglaciation and no significant re-advance during the Antarctic Cold Reversal, though the hypothesis remains a matter of debate (McCulloch *et al.*, 2005b; Moreno *et al.*, 2009b; Hall *et al.*, 2013).

6.7 Conclusions

This study presents a reconstruction of the relative history of five ice lobes in southernmost South America. We reconstruct eight time steps, which highlight the dynamic nature of the former ice and use a landsystem approach to show that the ice lobes dominantly displayed behaviour similar to active temperate glaciers. This involved warm-based ice actively re-advancing during overall retreat of the ice margin and refutes the hypothesis that the ice lobes displayed sub-polar characteristics with cold-based margins. The implication is that the active temperate ice lobes would have been primarily controlled by regional climate variability, and topographic or internal processes would have had only a secondary role in ice dynamics.

There is also some evidence to suggest rapid ice flow at times, and even possible surge-like activity, particularly in the Otway and Magellan lobes, though this requires further investigation. Additionally, our field observations have confirmed the presence of the palaeo-Laguna Blanca proglacial lake, which developed in front of the Skyring lobe, and drained, potentially catastrophically, prior to the gLGM. The development of other proglacial lakes in front of all of the ice lobes would have also promoted calving of the ice margins and rapid retreat, or even eventual collapse, of the ice lobes after the gLGM.

A critical issue is whether ice limits relate to successive glaciations through the Quaternary or were all deposited more recently, such as during the last glacial cycle. For the BI-SSb lobe, all limits seem to relate to the last glacial cycle (Chapter 5), and we use this as a catalyst to reassess previous dating evidence in the region. For the Río Gallegos, Skyring and Otway lobes, age constraints are scarce and contradictory, but our recalculation of cosmogenic nuclide dates for older limits of the Magellan lobe suggests that at least one limit of greater extent than the gLGM limit was deposited around 30 ka. This suggests that the BI-SSb and Magellan lobes advanced in a similar manner and at similar times. There is, therefore, a chance that all glacial limits could be substantially younger than previously thought. Similarities in the timing of ice advances from the available chronological information implies that, broadly speaking, underlying, external climatic forcing is likely responsible for glacial advances and supports our assertion that the ice lobes responded to climate variability. However, additional chronological controls are needed to test this further, especially for the Río Gallegos, Skyring and Otway lobes.

Chapter 7.   Evaluating the timing and cause of glacial advances in the southern mid-latitudes during the last glacial cycle based on compiled exposure ages from Patagonia and New Zealand

Darvill, C.M., Bentley, M.J., & Stokes, C.R. (in prep.) 'Evaluating the timing and cause of glacial advances in the southern mid-latitudes during the last glacial cycle based on compiled exposure ages from Patagonia and New Zealand', *Quaternary Science Reviews*.

Abstract

Advances of glaciers in the southern mid-latitudes during the last glacial cycle (*ca.* 110-10 ka) were controlled by changes in temperature and precipitation linked to several important climatic systems. As such, the timing of advances can yield important insights into the mechanisms of Southern Hemisphere climate change. This is particularly important given that several recent studies have demonstrated significant glacial advances prior to the gLGM in Patagonia and New Zealand, the cause of which is uncertain. The large increase in recent chronological studies in these regions offers the opportunity to robustly compare regional trends in glacial activity. Here, we compile two [10]Be exposure dating chronologies from published glacial records in Patagonia and New Zealand to highlight the broad pattern of mid-latitude glacial advances. We assess whether pre-gLGM advances are a common feature, and examine whether glacial advances were synchronous between the two regions. Results suggest that the similarity between the chronologies from Patagonia and New Zealand indicate that they were driven by common factors during the last glacial cycle from at least 45 ka, with advances at 41-43 ka, 32-38 ka, 26-27 ka, 18-19 ka and 13-14 ka. Hence, glaciers were generally advancing by the latter half of MIS 3. Subsequent advances, or stillstands, occurred both before and after the gLGM, and during the Antarctic Cold Reversal, rather than the Younger Dryas. Glacial advances in Patagonia and New Zealand were probably driven by underlying orbital parameters, involving a combination of summer intensity, seasonality and the duration of winter, but the precise timing is likely to have been intrinsically linked to migration of the coupled ocean-atmosphere system. For these reasons, late MIS 3 was conducive for glacial advances in these regions. Summer insolation reached a minimum, seasonality was reduced, winter duration was increasing, and sea ice had expanded significantly, inducing stratification of the ocean and triggering northward migration of oceanic fronts and the Southern Westerly Winds.

7.1 Introduction

Patagonia in southern South America and South Island, New Zealand, have hosted the two largest non-Antarctic ice sheets in the Southern Hemisphere during Quaternary glaciations (Figure 7.1). The former Patagonian Ice Sheet extended from the Andean range to cover significant parts of Chile and Argentina between ~36 and ~56°S (Coronato & Rabassa, 2011), and the New Zealand Ice Sheet occupied much of the southern Alps between ~40 and ~46°S (Barrell, 2011). Together, the glaciers extending from these two ice sheets covered a broad latitudinal range in the southern mid-latitudes and were influenced by key global climatic systems. These include the oceanic Sub Tropical, Sub Antarctic and Polar Fronts, the Antarctic Circumpolar Current and Agulhaus Current leakage, and the position and/or strength of the Southern Westerly Wind system. As a result, glaciers in Patagonia and New Zealand have been used to reconstruct past climatic change.

Recent work (Glasser *et al.*, 2011; Putnam *et al.*, 2013b; Kelley *et al.*, 2014; Rother *et al.*, 2014; Chapter 5) has identified that some of these glaciers advanced to greater extents prior to limits deposited during the global Last Glacial Maximum (gLGM; *ca.* 26.5-19 ka; Clark *et al.*, 2009). This is not necessarily surprising. Hughes *et al.* (2013) suggested that many ice sheets around the world did not achieve maximum extent at the same time during the last glacial cycle (*ca.* 110-10 ka). However, it does indicate that our understanding of southern mid-latitude glacial advances is incomplete, with implications for our understanding of southern climate systems more generally. Specifically, the new glacial chronologies raise two important issues. First, it is unclear whether pre-gLGM ice advances were representative of the Patagonian and New Zealand Ice Sheets more broadly and, if so, whether the advances were synchronous across the southern mid-latitudes. Secondly, the forcing factors behind southern mid-latitude glaciation during the last glacial cycle are ambiguous, as is the relationship to climatic drivers in the Northern Hemisphere.

Tackling these problems requires a synthesis of the evidence for the timing of glacial advances in Patagonia and New Zealand. Given the high volume of new chronological data that has been published in recent years, this paper compiles glacial chronologies for both regions during the last glacial cycle to examine if similar trends are evident from the published literature and whether these are replicated over a large geographic area. We then compare the timing of glacial advances with terrestrial, marine and ice core proxy records and test hypotheses regarding how

176

southern climatic systems operated over time. Whilst other ice caps and glaciers existed in Chile, Australia, Tasmania, North Island (New Zealand) and elsewhere in the sub-Antarctic during the last glacial cycle, we limit our focus to Patagonia and South Island in this review. This is because they hosted the largest ice sheets and produced similarly detailed and well-preserved glacial records that have been studied in the greatest detail. We also focus predominantly on ^{10}Be cosmogenic nuclide dating because it offers direct age estimates for glacial moraine records and has been used extensively in both regions.

7.2   Methods

7.2.1 ^{10}Be dating compilation

Our compilation consists of ^{10}Be cosmogenic nuclide exposure data from studies across Patagonia and New Zealand (Table 7.1). We collated all ^{10}Be dates presented by authors for moraine boulders and outwash cobbles, but excluded bedrock and moraine cobble samples due to potential issues with re-setting and because they do not necessarily represent glacial advances in the same way. We also excluded the depth profiles of Hein *et al.* (2009) and Chapter 5 because these broadly duplicate outwash cobble dates. For consistency, we recalculated all dates, applying the Putnam *et al.* (2010b) New Zealand ^{10}Be production rate for dates in New Zealand and Patagonia, as well as the Kaplan *et al.* (2011) Patagonian ^{10}Be production rate for dates in Patagonia. We also calculated ages using five scaling schemes and a range of erosion rates (1 mm ka^{-1} intervals between 0 and 10 mm ka^{-1}) to evaluate the effects of these parameters on age distributions. All other parameters, including standards, were taken from the original literature or subsequent updates (e.g. Kaplan *et al.*, 2011), and we used a standard density of 2.7 g cm^{-3} where none was given in the original studies. To aid the identification of cumulative peaks in exposure time we employ cumulative Probability Density Functions (PDFs; Barrows *et al.*, 2002) and we exclude any dates that, within errors, fall outside the last glacial cycle between 110 and 10 ka.
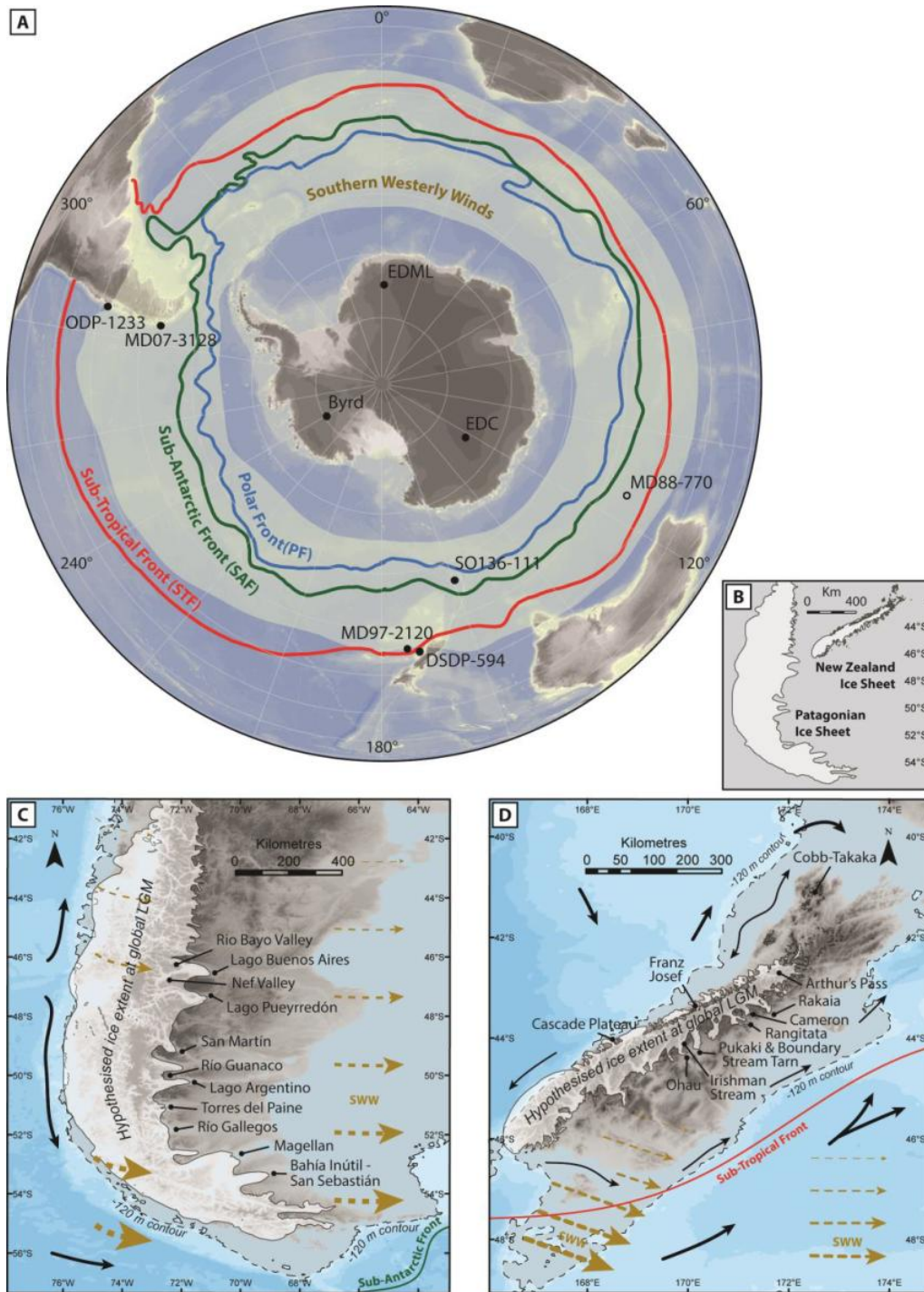
Figure 7.1. (A) Map of the Southern Hemisphere showing the positions of the Sub-Tropical Front (red), Sub-Antarctic Front (green) and Polar Front (blue), as well as the core region of the Southern Westerly Winds (yellow-brown) and the locations of ice and marine core records referred to in the text. Note the latitudinal difference of the oceanic frontal systems around Patagonia compared to New Zealand. (B) Comparison of the hypothesized size and latitudinal extent of the former Patagonian and New Zealand ice sheets at the global Last Glacial Maximum (gLGM) from (Ehlers *et al.*, 2011). The size and latitude of the ice sheets is faithful, but they are not shown against actual longitude. (C and D) Details of the Patagonian and New Zealand ice sheets, shown at their hypothesized gLGM extents with the -250 m bathymetric contour included to give an impression of the likely drop in sea-level at that time. Glacial valleys or systems used in this study are labelled as well as major oceanic circulations (black arrows), Southern Westerly Wind direction (brown dashed arrows), the Sub-Antarctic Front (green line) and and Sub-Tropical Front (red line).

Table 7.1. Details of the original works compiled in this study, ordered by glacial system and showing the latitude, longitude and total number of dates without (no brackets) and with (in brackets) author-identified outliers removed.

Glacier system	Lat. (°S)	Long. (°W/E)	Total no. dates		References
Patagonia					
Lago Bueno Aires	-46/-47	-71/-73	101	(82)	(Kaplan *et al.*, 2004; Douglass *et al.*, 2005; Kaplan *et al.*, 2005; Douglass *et al.*, 2006; Glasser *et al.*, 2012)
Rio Bayo valley	-47	-73	3	(3)	(Glasser *et al.*, 2006)
Nef valley	-47	-73	6	(5)	(Glasser *et al.*, 2012)
Pueyrredon	-47/-48	-71/-73	42	(36)	(Hein *et al.*, 2009; Hein *et al.*, 2010; Hein *et al.*, 2011; Glasser *et al.*, 2012)
San Martin valley	-49	-72/-73	10	(10)	(Glasser *et al.*, 2011)
Rio Guanaco	-50	-73	21	(21)	(Murray *et al.*, 2012)
Lago Argentino	-50	-73	30	(28)	(Ackert *et al.*, 2008; Kaplan *et al.*, 2011)
Torres del Paine	-51	-73/-74	57	(46)	(Fogwill, 2003; Fogwill & Kubik, 2005; Moreno *et al.*, 2009b; García *et al.*, 2012)
Rio Gallegos	-51/-52	-71/-72	8	(6)	(Kaplan *et al.*, 2007; Evenson *et al.*, 2009; Sagredo *et al.*, 2011)
Magellan	-52/-53	-69/-71	18	(10)	(McCulloch *et al.*, 2005b; Kaplan *et al.*, 2007; Kaplan *et al.*, 2008a)
Skyring/Otway/Magellan	-53	-71	3	(1)	Unpublished data
BI-SSb	-53/-54	-68/-70	49	(33)	(McCulloch *et al.*, 2005b; Kaplan *et al.*, 2007; Kaplan *et al.*, 2008a; Evenson *et al.*, 2009; Chapter 5)
Total			*348*	*(276)*	
Total within last glacial cycle			*290*	*(235)*	
New Zealand					
Cobb-Takaka	-41	173	1	(1)	(Thackray *et al.*, 2009)
Cobb Valley	-41	173	12	(6)	(Shulmeister *et al.*, 2005)
Taramakau	-43	171/172	36	(34)	(Barrows *et al.*, 2013)
Arthur's Pass	-43	172	5	(4)	(Ivy-Ochs *et al.*, 1999)
Rakaia Valley	-43/-44	171/172	56	(47)	(Shulmeister *et al.*, 2010; Putnam *et al.*, 2013a)
Cameron glacier	-43	171	45	(39)	(Putnam *et al.*, 2012)
Franz Josef	-43/-44	170	8	(8)	(Barrows *et al.*, 2007b)
Rangitata Valley	-43/-44	171	56	(51)	(Rother *et al.*, 2014)
Pukaki	-44	170/171	83	(78)	(Schaefer *et al.*, 2006; Putnam *et al.*, 2010a; Kelley *et al.*, 2014)
Ohau	-44	170	116	(102)	(Kaplan *et al.*, 2013; Putnam *et al.*, 2013b)
Irishman Stream	-44	170	35	(31)	(Kaplan *et al.*, 2010)
Cascade Plateau	-44	168	20	(15)	(Sutherland *et al.*, 2007)
Boundary Stream Tarn	-44	170	10	(10)	(Putnam *et al.*, 2010b)
Total			*506*	*(426)*	
Total within last glacial cycle			*414*	*(372)*	

7.2.2 Radiocarbon dating

To cross-check with the ^{10}Be chronology, we also compiled radiocarbon dates from the literature relating to glacial advances in Patagonia or New Zealand. The dates were separated into minimum or maximum ages according to the original studies or based on our own inferences if this was not stated explicitly. All dates were recalculated using OxCal version 4.2 (Bronk Ramsey, 2009) using the Reimer *et al.* (2013) calibration curve. To avoid bias between authors, we plot all data as PDFs and, where appropriate, highlight the authors' interpretation of ages. Minimum ages are more relevant for this discussion because they indicate that a particular glacier advanced prior to that time. One notable exception is the chronology of Denton *et al.* (1999), who analysed 472 radiocarbon dates from moraine limits in the Chilean Lake District and then selected key dates to accurately bracket the moraine ages.

7.3 Results

7.3.1 ^{10}Be chronology

Glacial advances have yielded cosmogenic nuclide exposure ages throughout the last glacial cycle, and show a similar pattern in Patagonia and New Zealand (Figure 7.2). However, overlapping dates from different glaciers in both Patagonia and New Zealand begin at *ca.* 45 ka. Dates prior to 45 ka are scattered or are not reproduced across different glacial systems. There are also significant gaps in the record, with few or no dates between 57 and 110 ka (MIS 4 and 5). A key part of this study is to assess a large compilation dataset to see if there are regional trends that have previously been missed in individual studies. Therefore, it is important to ensure that author-identified outliers were not removed erroneously. We calculated all of the ages twice, once with all data included ($n_{Patagonia}$ = 290; $n_{New\ Zealand}$ = 414) and the second time with all author-identified outliers removed ($n_{Patagonia}$ = 235; $n_{New\ Zealand}$ = 372; Figure 7.3; Table 7.1). We only removed outliers that were clearly identified in the original studies – if there was ambiguity, we retained the data. Removing author-identified outliers made negligible difference to the timing of the compiled PDF peaks, and so the reduced compilation was used for all other analysis in this paper.
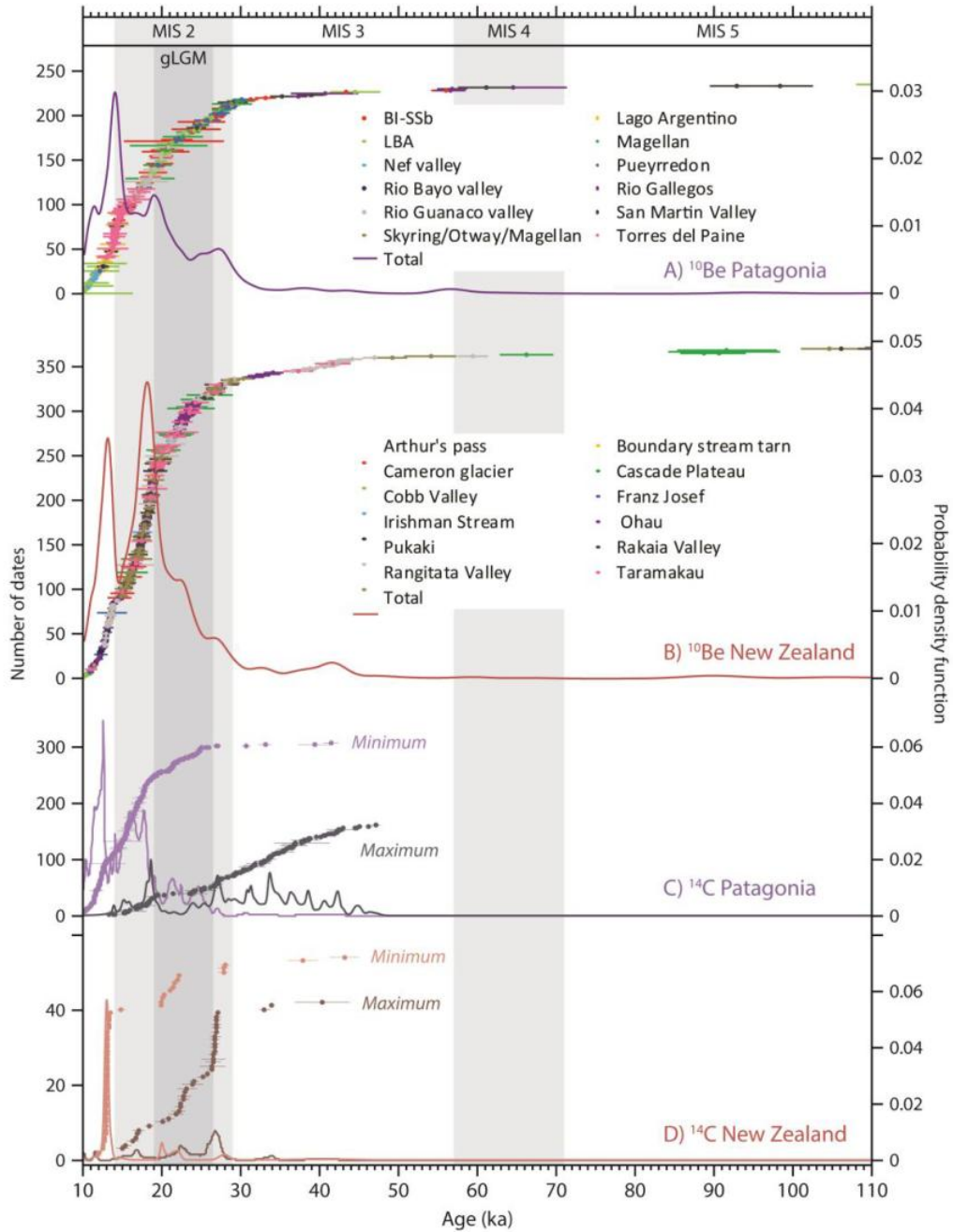
Figure 7.2. The compilation of [10]Be and radiocarbon dates from Patagonia and New Zealand used in this study, shown against the Marine Isotope Stages from Lisiecki & Raymo (2005) and the gLGM from Clark *et al.* (2009). (A and B) show all [10]Be dates within 110-10 ka after author-identified outliers have been removed as mean ages with standard errors that have been recalculated using the Putnam *et al.* (2010) production rate, with no erosion rate applied. The dates are colour-coded according to the glacial system from which they are derived, and associated references can be found in Table 7.1. Also shown are cumulative relative probability density function curves, calculated from all of the dates within each region. (C and D) show all of the minimum and maximum radiocarbon dates that have been compiled, separated into minimum (light purple and light red) and maximum (dark purple and dark red) limiting ages and shown as recalculated mean ages with standard errors. Probability density function curves are shown for all of the minimum and maximum dates in each region. Note that unless stated, the [10]Be dates, probability density curves, Marine Isotope Stages, and global Last Glacial Maximum boundaries used here are replicated in all other figures in this paper.

181

7.3.2 Radiocarbon dating

The radiocarbon dates reproduce the [10]Be model (Figure 7.2). Minimum ages extend back to 40.3 ka in New Zealand and 41.4 ka in Patagonia and maximum ages cap these timings at 43.1 ka in New Zealand and 47.1 ka in Patagonia. We caution that these ages are at the upper age limit of the radiocarbon dating technique, and that organic material may be less well preserved in heavily glaciated systems further back in time. Hence, the radiocarbon dating may be limited by factors other than the timing of glaciation, but the parallels with the cosmogenic nuclide chronologies are striking.

7.3.3 Relating [10]Be peaks to glacial advances

Peaks in the PDF plots for all dates in Patagonia and New Zealand help to illustrate times when more glaciers are more likely to have advanced. This technique is useful for identifying patterns in a large number of dates but should be used with caution, as it does not convey the spatial distribution (e.g. down-ice extent) of dates and can be influenced by uncertainty in factors such as erosion rate and inheritance during age calculation, factors which are explored in the following sections. Different glaciers within the compilation likely advanced at different times, and the PDF technique removes this subtle variability. However, in a discussion about the possible forcing factors responsible for regional glacial advances, we are interested in the commonality between the timing of glacial advances and in using a robust chronological dataset, so this broad-brush technique is useful. It is worth noting that the fact that our compilation produces PDF peaks suggests that there is regional commonality in the timing of glacial advances during the last glacial cycle.

The timing of PDF peaks in Patagonia and New Zealand is shown in Table 7.2. Additional, low amplitude peaks at 89.8 ka, 59.1 ka and 56.4 ka are intriguing, but because the replication of dates between glaciers is much weaker prior to 43 ka, we focus on peaks after this time. There appears to be a consistent offset between Patagonia and New Zealand in the timing of the three most recent PDF peaks. Before exploring whether there is a geographical or climatological reason for this, it is first necessary to examine whether inherent factors in the age calculation process can account for the offset. Specifically, we assess sensitivity to the production rate or scaling scheme used; the erosion rate applied; or possible inheritance issues. This exercise is also useful for assessing how the overall spread of ages changes when these parameters are varied.
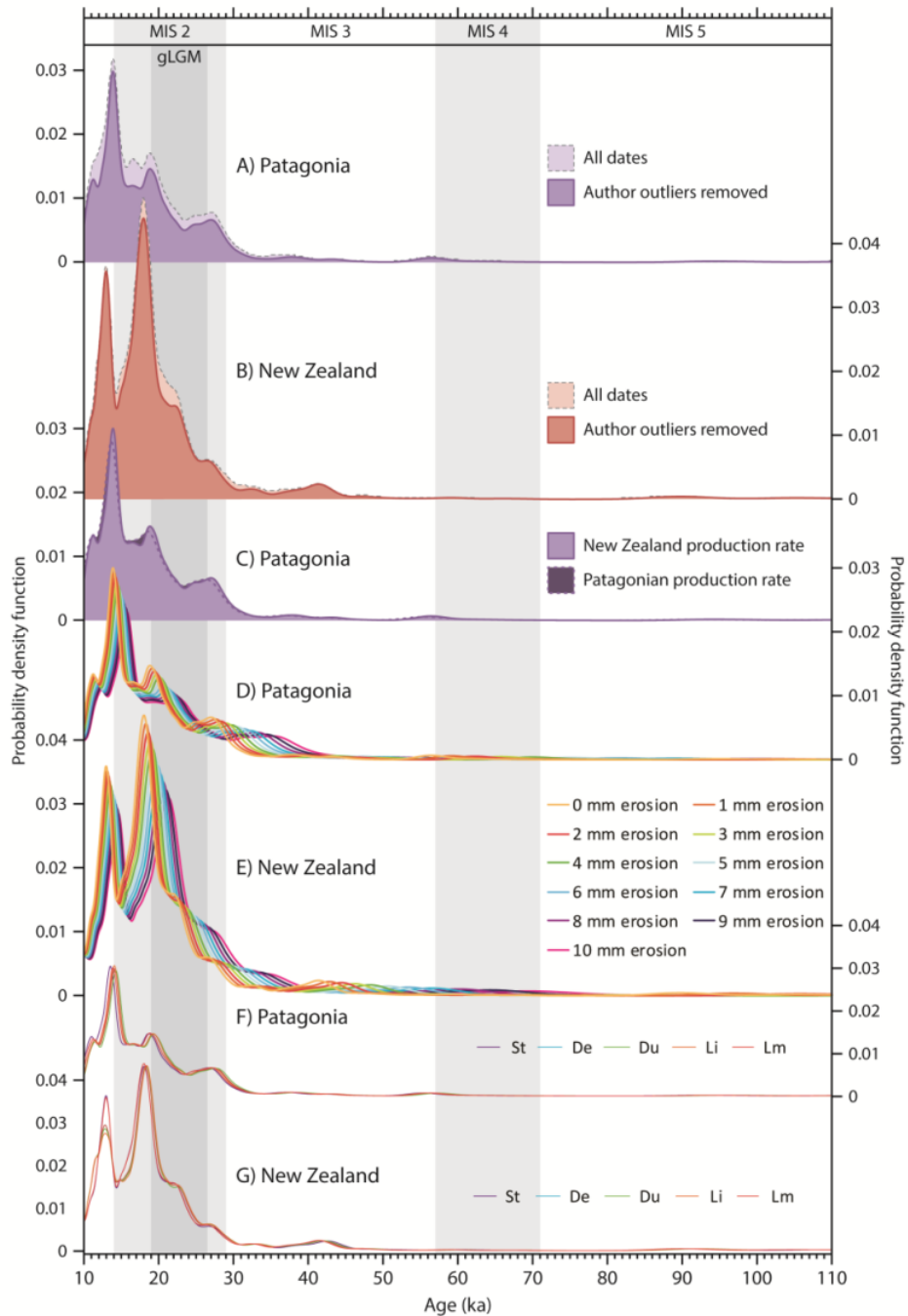
Figure 7.3. Examining the effects of calculation parameters on the overall spread of ages in our compilation. (A and B) show the probability density functions from Figure 7.2 in dark purple (A, Patagonia) and dark red (B, New Zealand), where all author-identified outliers have been removed, as well as the functions when author-identified outliers are included. There is little resulting difference in the timing of peaks. (C) shows the effect of calculating all dates from Patagonia with the New Zealand production rate of Putnam *et al.* (2010) and the Patagonian production rate of Kaplan *et al.* (2011). (D and E) show the effect on the resulting probability density functions of incrementally increasing the erosion rate by 1 mm ka^{-1} during the calculation of all ages in Patagonia and New Zealand and (F and G) show the effect of altering the scaling scheme used. The scaling schemes are: the time-dependent Lal (1991) and Stone (2000; St); Desilets *et al.* (2006; De); Dunai (2001; Du); Lifton *et al.* (2005; Li); and time-independent Lal (1991) and Stone (2000; Lm). In (C, D, E, F and G), all author-identified outliers have been removed, the New Zealand production rate is used and, where relevant, no erosion rate is applied.

7.3.3.1   Production rate and scaling scheme

An offset in the timing of PDF peaks in Patagonia and New Zealand could be an artefact of recalculating all ages using the New Zealand production rate, even though this overlaps with the Patagonian production rate at 1σ. Figure 7.3 and Table 7.2 show all dates recalculated using the Putnam *et al.* (2010b) Macaulay River, New Zealand ^{10}Be production rate of 3.74 ± 0.08 atoms g^{-1} a^{-1}, and also the Patagonian dates recalculated using the Kaplan *et al.* (2011) Lago Argentino, Patagonia ^{10}Be production rate of 3.81 ± 0.13 atoms g^{-1} a^{-1}. The production rate alone can only explain the offset in PDF peaks at 26-27 ka, although these peaks are very similar in age, regardless of the production rate used. When recalculated using the Patagonian production rate, the 43.1 ka peak can no longer be resolved and the 27.0 ka and 18.8 ka peaks become much broader.

We also calculated ages using different scaling schemes (Figure 7.3; using just the New Zealand production rate). It is illogical to use different scaling schemes for the Patagonian and New Zealand datasets, so the important part of this experiment is to see whether the choice of scaling scheme can account for a discrepancy in the timing of PDF peaks. While the choice of scaling scheme can alter the timing (by as much as 1.6 ka for the 37.8 ka peak in Patagonia) it does not explain the difference between Patagonia and New Zealand.

7.3.3.2   Surface erosion rate

Differential surface erosion rates in Patagonia or New Zealand could have affected the timing of PDF peaks because increased erosion offsets the build-up of ^{10}Be nuclides, artificially yielding older ages. To test the effects of the selected erosion rate, we recalculated all ages using increasing rates between 0 mm ka^{-1} and 10 mm ka^{-1} (Figure 7.3 and Table 7.2). When using the New Zealand production rate, Patagonia peaks occurred before New Zealand. However, the difference in the erosion rate required for the peaks in New Zealand to match Patagonia varied non-uniformly, from 6 mm ka^{-1} to 1 mm ka^{-1}. When using the Patagonian production rate, Patagonia peaks occurred before New Zealand, except for the *ca.* 26-27 ka peak, where the New Zealand peak was slightly earlier (though the 100 year difference is negligible given that 100 year bins were used in plotting probability density functions). At very high erosion rates (> 8 mm ka^{-1}), some of the older peaks flattened-out because there were insufficient high-precision dates. Overall, high (though not necessarily unreasonable) erosion rates are required for the 13-14 ka and 32-38 ka peaks to have been synchronous in Patagonia and New Zealand.

Lower erosion rates are required for the 18-19 ka and 26-27 ka peaks to have been synchronous. Altering the erosion rate and production rate for the 41-43 ka (and even older peaks) results in a spread of ages that do not resolve a peak in Patagonia.

7.3.3.3 Inheritance

Consistent inheritance in boulder populations in Patagonia could have resulted in an offset in PDF peaks compared to New Zealand. To test this, we constructed PDF plots for individual moraine sets. The shape of the PDF was heavily influenced by the number of boulder samples if the plot was constructed from less than four samples, so we excluded all moraine sets containing three dates or fewer and removed any moraine sets that were not completely resolved between 0-110 ka. We then used a skewness test to examine if moraine sets showed greater inheritance tails in either region – a simplified approach to the modelling of Applegate *et al.* (2010). Author-identified outliers had already been removed, so any inheritance-skew was in addition to the outliers that had already been removed (Figure 7.4). Patagonia contained moraine sets that were more skewed (max = 5.86) than New Zealand (max = 4.98), but the average for Patagonia (3.75) was less than for New Zealand (3.90). Hence, whilst individual moraine sets may show statistical signs of inheritance, there is no consistent signature that would lead to the observed offset in PDF peaks between Patagonia and New Zealand.

Figure 7.4. Binned results from an analysis of skewness of probability density functions from individual moraine sets in Patagonia and New Zealand as a crude proxy for differential inheritance signatures. The data suggest that inheritance cannot fully explain the consistent offset between Patagonia and New Zealand.

Table 7.2. The timing of peaks in glacial advances identified from relative cumulative probability density functions for New Zealand (NZ) and Patagonia (P) using the New Zealand production rate of Putnam *et al.* (2010b), and using the Patagonian production rate (Ppr) of Kaplan *et al.* (2011) for Patagonia. The bold values are those quoted in our study, but other values are given to show the effect of increasing erosion rate on the calculated dates. 'NZ erosion' refers to the erosion rate required (to the nearest 1 mm ka⁻¹) to create a peak in New Zealand at the same time as peaks in Patagonia with no erosion using both the New Zealand and Patagonian production rates (e.g. a 6 mm ka⁻¹ erosion rate is required to result in a peak in New Zealand at 13.9 ka, the same time as a peak in Patagonia with no erosion and using the New Zealand production rate). 'Ppr erosion' refers to the same estimation but for the erosion rate required to create in a peak in Patagonia using the Patagonian production rate at the same time as a peak in New Zealand with no erosion rate ans using the New Zealand production rate.

| Erosion (mm ka⁻¹) | Peaks | | | | | | | | | | | | | | |
| | *ca.* 13-14 ka | | | *ca.* 18-19 ka | | | *ca.* 26-27 ka | | | *ca.* 32-38 ka | | | *ca.* 41-43 ka | | |
	NZ	P	Ppr	NZ	P	Ppr	NZ	P	Ppr	NZ	P	Ppr	NZ	P	Ppr
0	**13.0**	**13.9**	13.7	**18.0**	**18.8**	18.5	**26.4**	**27.0**	26.3	**32.4**	**37.8**	37.2	**41.4**	**43.1**	-
1	13.1	14.0	13.8	18.3	19.1	18.8	27.0	27.6	26.8	33.2	39.0	38.3	42.8	44.7	-
2	13.3	14.2	14.0	18.6	19.4	19.1	27.6	28.2	27.4	34.2	40.2	39.6	44.4	46.4	-
3	13.4	14.4	14.1	18.9	19.7	19.4	28.1	28.9	28.1	35.2	41.6	40.9	46.2	48.4	-
4	13.6	14.5	14.3	19.2	20.1	19.7	28.8	29.6	28.7	36.3	43.1	42.4	48.2	50.6	-
5	13.7	14.7	14.5	19.5	20.3	20.0	29.5	30.4	29.4	37.5	44.8	44.0	50.6	53.0	-
6	13.9	14.9	14.7	19.8	20.7	20.3	30.3	31.2	30.1	38.8	46.6	45.8	53.4	55.8	-
7	14.0	15.1	14.9	20.1	21.0	20.7	31.1	32.1	30.9	40.2	48.7	47.8	56.5	59.0	-
8	14.2	15.3	15.0	20.5	21.4	21.1	31.9	33.1	31.7	41.8	51.0	50.0	60.2	62.7	-
9	14.4	15.5	15.2	20.9	21.8	21.4	43.5	34.1	32.6	-	53.7	52.6	64.3	67.0	-
10	14.6	15.7	15.5	21.3	22.3	21.8	45.5	35.2	33.4	-	56.7	55.4	69.4	-	-
NZ erosion		6	5		2 - 3	1 - 2		1			5 - 6	4 - 5		1 - 2	
Ppr erosion							0 - 1								

7.3.4 Summary of peaks in timing

Production rate, scaling scheme, erosion rate and inheritance all have an effect on the calculation of ages from [10]Be dates. However, none of these factors can provide a satisfactory explanation for the offset between Patagonia and New Zealand. This is because the offset does not decrease or increase uniformly back in time. Changing the scaling scheme does not reduce the offset, and using the Patagonian production rate neither reduces the offset sufficiently, nor accounts for a variable offset over time. Increasing the erosion rate in New Zealand can reduce the offset, but does not explain why the difference increases back in time, and it is unlikely that inheritance is responsible for the difference. A combination of these factors may explain the offset observed in the timing of PDF peaks in Patagonia and New Zealand, but this starts to invoke cyclical arguments, some of which are themselves climate-related (e.g. variable erosion rates over time). A simpler explanation is that the offset is real and PDF peaks in Patagonia occurred earlier than in New Zealand, which we now discuss.

7.4   Discussion

7.4.1   The timing of glacial advances

We interpret the peaks in the PDF distributions at *ca.* 41-43 ka, 32-38 ka, 26-27 ka, 18-19 ka and 13-14 ka to reflect the deposition of moraine boulders and cobbles during glacial advances, or at the very least stillstands. The resolution of these advances is determined in part by sampling strategies that have targeted glacial limits, and the corresponding dating errors – hence the gLGM and late glacial peaks are the best resolved in both regions. This does not mean that the pre-gLGM advances were necessarily less distinct (and our method says little about the extent of advances other than that they were preserved).

Our [10]Be compilation from Patagonia and New Zealand reveals a broad similarity in the timing of glacial advances in both regions, especially during MIS 3 and MIS 2. This suggests that the same forcing factors may have controlled the timing of glacial advances in both regions over the last glacial cycle. Prior to around 45 ka, scattered dates have been recorded during MIS 5 and MIS 4 in both regions, but the timing of these advances is uncertain as they are heavily influenced by the erosion rate used and are not replicated over several glaciers. It is also unclear whether an absence of dates at times before 45 ka relates to a lack of sampling (i.e. no one has analysed boulders on down-ice moraines) or a genuine lack of advances (or advances

extensive enough to not have been subsequently destroyed). What is clear from the compilation is that the replication of dates over different glaciers in both Patagonia and New Zealand strongly suggests that glaciers had advanced by at least 45 ka, or mid-MIS 3, well before the gLGM. Although this study focuses on chronology, it is worth highlighting that several studies found the limits relating to these advances to be as extensive, if not significantly more so, than those deposited during the gLGM (Glasser *et al.*, 2011; Putnam *et al.*, 2013b; Kelley *et al.*, 2014; Rother *et al.*, 2014; Chapter 5).

Generally speaking, there is good agreement between the broad spread of minimum radiocarbon dates and the ^{10}Be chronology, in that the radiocarbon dates extend back to roughly 40-45 ka. The Chilean Lake District chronology of Denton *et al.* (1999) highlighted limits deposited at *ca.* 34.1 ka, 31.1 ka, 27.9 ka and 18.0 ka, which support ^{10}Be peaks at *ca.* 27 ka and 18 ka and pre-30 ka advances during the last glacial cycle. The replication of ^{10}Be dates over multiple glaciers in Patagonia and New Zealand, supported by radiocarbon dates, gives us confidence in discussing peaks in the timing of deposition as regional glacial advances. We now compare these events with other proxies for glacial and climatic change in order to assess possible forcing mechanisms within the terrestrial-ocean-atmosphere system during the last glacial cycle.

7.4.2   Comparison with other records

7.4.2.1   Ice-rafted debris and dust records

The presence of Ice-Rafted Debris (IRD) in sites proximal to former marine-terminating glaciers indicates when those glaciers advanced and produced icebergs through calving (Carter *et al.*, 2002; Caniupán *et al.*, 2011). Similarly, dust records in Antarctica have been linked to dust production in the southern mid-latitudes, and particularly Patagonia, whereby fine sediment is produced during glacial advances and then exposed to subaerial erosion on large proglacial outwash plains during retreat (Sugden *et al.*, 2009; Kaiser & Lamy, 2010; McGee *et al.*, 2010). Consequently, we would anticipate peaks in IRD during advances of marine-terminating glaciers, such as the west coast of Patagonia and the northwest coast of New Zealand, and peaks in dust during and after advances, particularly in Patagonia. An IRD record from core MD07-3128 off the west coast of southern Patagonia shows a large IRD peak (>5%) centred on 27 ka that matches a Patagonian glacial advance at that time (Caniupán *et al.*, 2011; Figures 7.6 and 7.7). Dust records from the East Dronning Maud Land (EDML) and EPICA Dome C

(EDC) ice cores show a significant increase in dust during MIS 4 and 2, and much lower levels during MIS 5 and 3 (Fischer *et al.*, 2007; Figures 7.6 and 7.7). However, there are peaks during MIS 3 at *ca.* 56, 49, 44 and 42 ka (in the EDML ice core) that are separated by reductions in dust flux that align with glacial advances in Patagonia and New Zealand.

In short, then, there are peaks in IRD and Antarctic dust that support glacial advances in Patagonia during the last glacial cycle. However, not all advances align with IRD and dust peaks and New Zealand is not well represented by similar records.

7.4.2.2   Other terrestrial records

It is worth comparing our glacial record with other terrestrial records of palaeoenvironmental change to see how they compare as records of climatic change. Records in Patagonia spanning the gLGM and late glacial period support the timing of cooler periods and glacial expansion in our compilation (Kilian & Lamy, 2012). There are a limited number of terrestrial palaeoenvironmental studies in Patagonia that pre-date the gLGM, but a key exception is the Potrok Aike record that spans the last *ca.* 51 ka (Zolitschka *et al.*, 2013). Lake level changes may indicate a slight increase in temperature around 40 ka, although the lake reached a maximum level indicative of glacial conditions between 34 ka and 17 ka (Hahn *et al.*, 2013; Kliem *et al.*, 2013a). Median Destructive Field of Isothermal Remnant Magnetisation (MDF_{IRM}), a proxy for wind intensity, does not show a great difference between MIS 3 and MIS 2 and, although magnetic susceptibility shows a significant increase during the gLGM, this increase begins after *ca.* 32 ka (Lisé-Pronovost *et al.*, 2015).

Unlike Patagonia, New Zealand contains several long records of palaeoenvironmental change. A compilation of 21 speleothem records by Williams *et al.* (2015) can be used to show relative changes in temperature and moisture availability over much of the last 130 ka. The compilation suggests cooler periods at 67-63 ka, 51-45 ka and from 33 ka into the gLGM, marked by reduced growth at these times. Particularly wet conditions are recorded at 71-61 ka and around 24.7 ka, despite cool temperatures (Williams *et al.*, 2015). The stratigraphy of the Te Anau cave system in the southwest of South Island also suggests glacial advances at *ca.* 40 ka and 48 ka (Williams, 1996), although the Aurora Cave speleothem indicates continuous growth between 55.3 ka and 42.8 ka, suggesting local ice-free conditions at this time (Williams, 1996; Williams *et al.*, 2015). Likewise, the

Hollywood Cave speleothem from the northeast of South Island shows continual growth from 73 ka to the Holocene, indicating relatively mild conditions despite glacial activity further south (Whittaker *et al.*, 2011).

Long pollen records also exist in New Zealand. Forest pollen declined significantly around 82 ka until after 20 ka (Ryan *et al.*, 2012; Vandergoes *et al.*, 2013), although an expansion of conifer woodland in North Island around the start of MIS 3 has been interpreted as indicating wetter conditions at this time (Shane & Sandiford, 2003). Barrell *et al.* (2013) suggested that full glacial conditions may have begun around 28.8 ka based on a large increase in herb pollen around this time (Vandergoes *et al.*, 2005). Climatic amelioration occurred around 18 ka, based on pollen assemblages and speleothem records (Williams *et al.*, 2015).

Overall, there are similarities between terrestrial palaeoenvironmental records and our glacial compilation. Cooler periods are exhibited in Patagonia and/or New Zealand around 67-63 ka, 47-38 ka and 33-18 ka, with a clear early deterioration into the gLGM. Two significant discrepancies are a glacial advance in our compilation at 32-38 ka that is not obviously recorded in other terrestrial records and the absence of significant evidence for glacial advances during MIS 4, even though palaeoenvironmental reconstructions clearly show this to have been a period of colder and possibly wetter climate, ideally suited for ice sheet expansion.
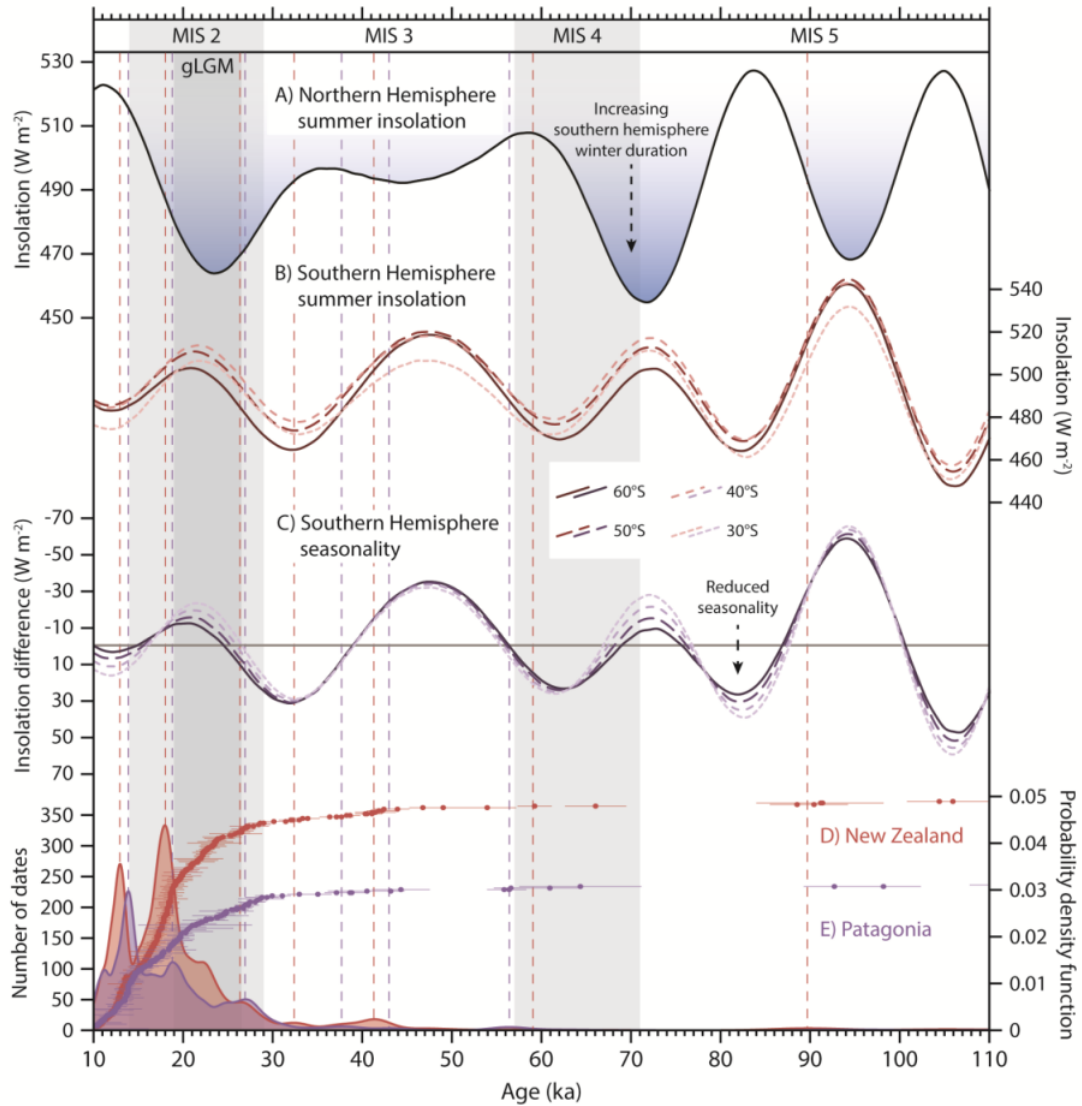
Figure 7.5. Orbital insolation parameters relevant to this study, from Berger & Loutre (1991). (A) Northern Hemisphere summer (June) insolation intensity at 60°N. This also shows Southern Hemisphere winter duration, given that decreasing northern summer insolation covaries with increasing southern winter length (Huybers & Denton, 2008). (B) Southern Hemisphere summer (December) insolation intensity at 60°S, 50°S, 40°S and 30°S to show any latitudinal variability. (C) Southern Hemisphere seasonality at 60°S, 50°S, 40°S and 30°S, shown here as summer insolation subtracted from winter insolation at a given time, such that decreasing seasonality indicates cooler summers and warmer winters. Values are shown subtracted from the mean seasonality at each latitude for 110-10 ka, so increased seasonality is negative and decreased seasonality is positive (note the axis is reversed). There is a distinct latitudinal variability in changing seasonality between *ca.* 30 ka and 18 ka. (D and E) our [10]Be compilation from Patagonia and New Zealand.

7.4.3 Possible forcing factors

7.4.3.1 Insolation changes

The expansion of large ice sheets in the Northern Hemisphere broadly followed decreases in summer insolation intensity, promoting the build-up of ice as recorded in the similarity between summer insolation and the global $\delta^{18}O$ stack of Liesicki & Raymo (2003; Figure 7.5). There are two conundrums associated with this model in the Southern Hemisphere. The first is that, broadly speaking, the descent into and rise out of glacial and interglacial periods in the Southern Hemisphere happened in phase with the Northern Hemisphere, despite covariance of summer insolation (Berger & Loutre, 1991). Secondly, the occurrence of significant glacial advances prior to the gLGM, as observed in our compiled chronology, is at odds with a model whereby the conditions suited to maximum ice growth occurred during the gLGM (Barrows et al., 2007; Wolff et al., 2009). These issues might be explained by delayed climatic responses due to atmospheric or oceanic teleconnections. However, such teleconnections appear to lead to a bipolar seesaw system during deglaciation (Denton *et al.*, 2010), and so it is unclear why covariance is observed during the rest of the last glacial cycle.

Instead, Huybers & Denton (2008) used radiative equilibrium estimates to show that, for the Southern Hemisphere, the duration of seasons may exert a greater control on climate than insolation intensity. Thus, increasing southern winter duration in synchrony with decreasing northern summer insolation could explain why broad glacial-interglacial changes in both hemispheres occurred at the same time (Putnam *et al.*, 2013b). Winter duration may also explain why glacial advances in the southern mid-latitudes occurred prior to the gLGM, given that there was a trend toward longer winters during MIS 3 and into MIS 2 (Huybers & Denton, 2008). Reduced seasonality might also have promoted ice sheet growth (taken here as times of cooler summers and warmer winters; Chapter 5), and any offset could explain the differences observed between the timing of advances in Patagonia compared to New Zealand (Figure 7.5). Greater seasonality occurs at lower latitudes earlier than at higher latitudes, perhaps indicating that the earlier rise in summer insolation (or drop in winter insolation) at lower latitudes resulted in delayed glacial advances in New Zealand compared to Patagonia.

193
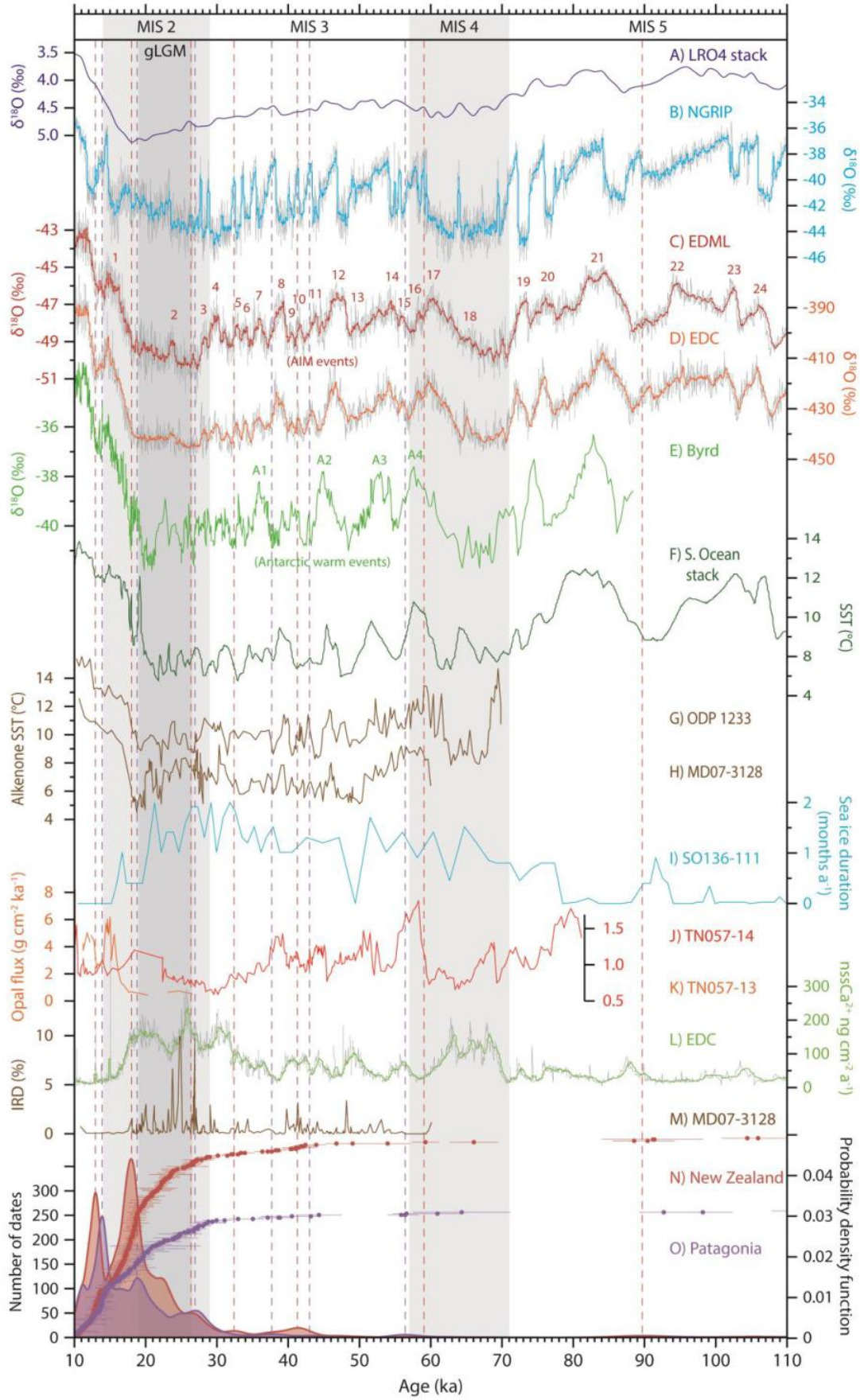
Figure 7.6. A comparison of the timing of glacial advances in the southern mid-latitudes during 110-10 ka (red and purple dashed vertical lines) from our compiled ^{10}Be chronology (N and O) with a range of other palaeoclimatic proxies. (A) The LR04 benthic foraminiferal stack from Lisiecki & Raymo (2005), which shows a combined signature of global temperature and ice volume. (B) The NorthGRIP (NGRIP) ice core δ^{18}O record from Greenland as a proxy for North Atlantic temperature changes (Rasmussen *et al.*, 2006). (C) The East Dronning Maud Land (EDML) ice core δ^{18}O record (EPICA, 2006), (D) the EPICA Dome C (EDC) ice core δD record (EPICA, 2006) and (E) the Byrd ice core δ^{18}O record (Blunier & Brook, 2001) as proxies for Antarctic temperature changes from different parts of the ice sheet. The NGRIP, EDML and EDC records are shown on the AICC2012 common timescale (Veres *et al.*, 2013), whereas the Byrd ice core is plotted on its own timescale. (F) The Southern Ocean Sea Surface Temperature (SST) Stack of Barrows *et al.* (2007) as a proxy for broad SST change around New Zealand. (G and H) The alkenone-derived SST reconstructions of Kaiser *et al.* (2005) for ODP-1233 off the western coast of northern Patagonia and Caniupan *et al.* (2011) for MD07-3128 off the western coast of southern Patagonia, both plotted on the same scale. (I) A diatom-based reconstruction of sea ice extent from south of the Sub-Antarctic Front by Crosta *et al.* (2004), measured as the number of months per year that sea ice covered site SO136-111. (J and K) Records of opal flux from two cores in the South Atlantic, south of the Polar Front, as a proxy for wind-driven upwelling (Anderson *et al.*, 2009). Note that the scales are different. (L) Ca^{2+} flux as recorded in the EDC ice core as a proxy for dust deposition over Antarctica, thought to be sourced predominantly from Patagonia. (M) A record of Ice-Rafted Debris (IRD) from core MD07-3128 (Caniupan *et al.*, 2011).

Following page

Figure 7.7. As per Figure 7.6, but scaled to cover just 50-10 ka.
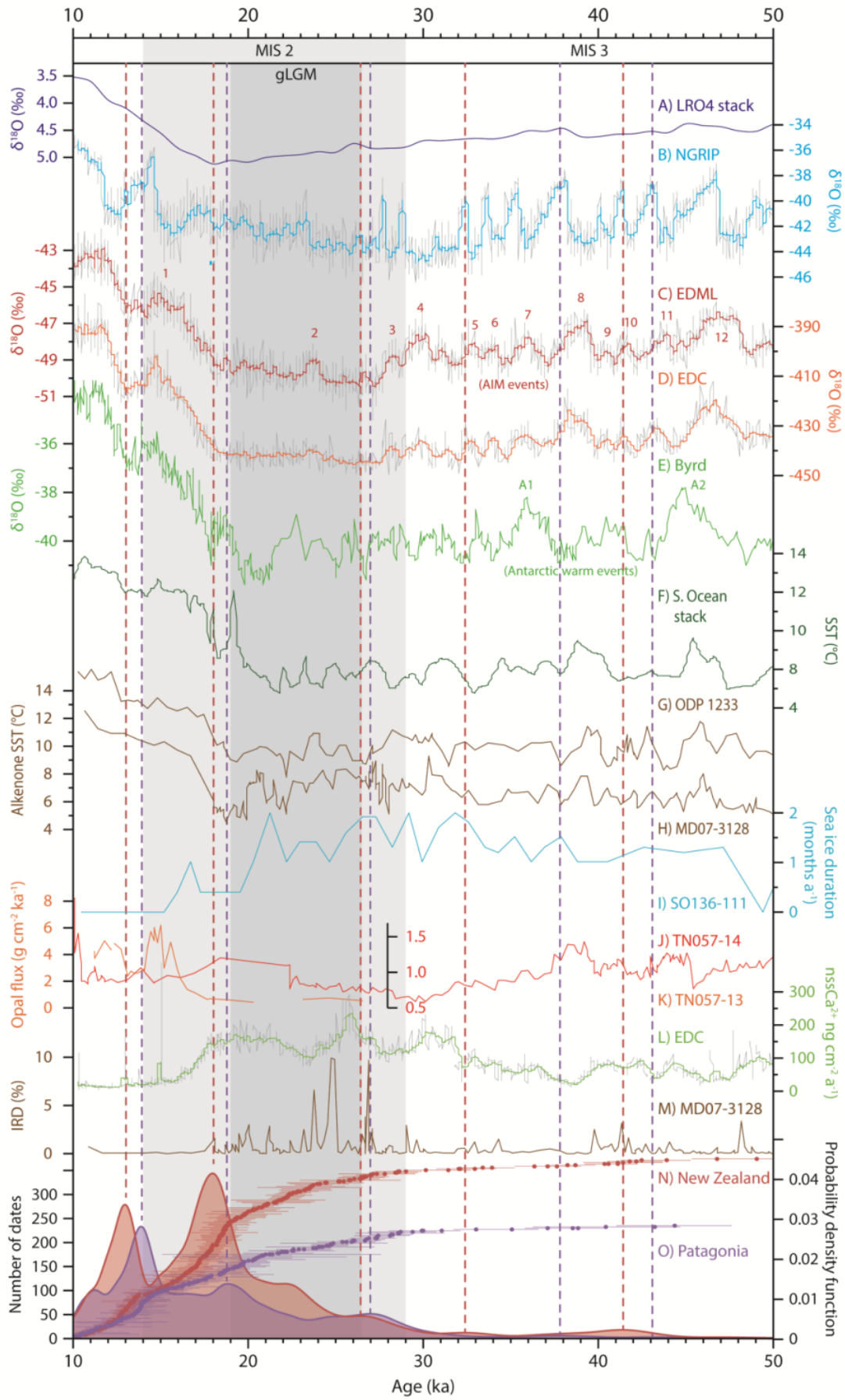
7.4.3.2   Ice core temperature changes

Ice core temperature records from Antarctica and Greenland can help to illustrate interhemispheric climate (a)synchrony during the last glacial cycle (EPICA, 2006; Barker *et al.*, 2009; Wolff *et al.*, 2009; Wolff *et al.*, 2010b; Stenni *et al.*, 2011). Similarities between Antarctic ice core records and the Patagonia and New Zealand glacial advances would support the idea that temperature changes drove glacial advances, and operated across the southern mid-high latitudes.

Broadly speaking, the EDML (EPICA, 2006), EDC (EPICA, 2004; 2006) and Byrd (Blunier & Brook, 2001) ice cores from Antarctica, and North GRIP (NGRIP; Rasmussen *et al.*, 2006) ice core from Greenland, demonstrate a pattern of cooling through the last glacial cycle, with peak warmth during MIS 5 followed by a deterioration during MIS 4, warmer but decreasing temperatures during MIS 3, and peak cooling during MIS 2 (the gLGM), before warming into the Holocene (Figures 7.6 and 7.7). In the Antarctic cores, warming events during MIS 4 and MIS 3 (A1-4) were proposed by Blunier & Brook (2001) and have been correlated to similar events in the southern mid-latitudes (Lamy *et al.*, 2004; Barrows *et al.*, 2007a). Additional Antarctic Isotope Maxima (AIM) events, identified in the EDML core (EPICA, 2006), occur between A1-4 and appear to coincide with Dansgaard-Oeschger (D-O) events in NGRIP, implying that hemispheric climate changes occurred broadly in phase during much of the last glacial cycle (EPICA, 2006; Wolff *et al.*, 2009). This system broke down during the last glacial termination, where warming in the Antarctic ice cores was not followed by an abrupt warming in Greenland, resulting in continued warming in the south (Lamy *et al.*, 2007; Wolff *et al.*, 2009).

Taken together, the ice core records show broadly consistent global climatic changes throughout the last glacial cycle but also highlight short fluctuations which may represent short-lived temperature changes propagated across the southern hemisphere that could have induced glacier advances.

7.4.3.3   Sea surface temperature changes

Marine core records can be used to reconstruct more localised sea surface temperatures (SST) over time using microfaunal assemblages (e.g. foraminifera or diatoms) or geochemical alterations (e.g. Mg/Ca ratios from foraminifera or UK'37). This can help to show how oceanic fronts (which control surface temperature gradients) migrated over time. On the hemispheric level, similarities between SST and ice core temperature records would imply that temperature changes operated

across the Southern Hemisphere. Regionally, similarity between SST reconstructions implies that they were bounded by the same frontal systems, whereas significant difference suggests they were separated by an oceanic front, causing a significant difference in temperature. Mid-latitude glaciers are likely to have responded to cooler local SST changes.

Alkenone SST records from the south-eastern Pacific, close to the western margin of the northern Patagonian Ice Sheet, have been reconstructed from core ODP-1233 (Lamy *et al.*, 2004; Kaiser *et al.*, 2005; Lamy *et al.*, 2007), and can be compared with the Barrows *et al.* (2007a) Southern Ocean SST stack, which is a good representation of SST changes off New Zealand (Figures 7.6 and 7.7). The stack is an average of an Mg/Ca SST record from core MD97-2120 from south of New Zealand (Pahnke *et al.*, 2003) and a faunal-based SST record from core MD88-770 from the Indian Ocean (Labeyrie *et al.*, 1996). These SST records show patterns of temperature change similar to the Antarctic ice cores across the last glacial cycle (Barrows *et al.*, 2007a; Putnam *et al.*, 2013b). However, numerous SST reconstructions suggest that the decline towards peak glacial temperatures had started by at least 30 ka in the south-eastern Pacific (Lamy *et al.*, 2004; Kaiser *et al.*, 2005; Lamy *et al.*, 2007; Caniupán *et al.*, 2011), west of New Zealand and south of Australia (Pelejero *et al.*, 2006; Barrows *et al.*, 2007a; Calvo *et al.*, 2007), the Indian Ocean (Labeyrie *et al.*, 1996), and the southeast Atlantic (Barker *et al.*, 2009).

The millennial-scale events recorded in mid-latitude SST records occur rapidly, so likely reflect changes in the position of oceanic fronts (Barrows *et al.*, 2007a). The migration of the Sub-Tropical Front (STF) and Sub-Antarctic Front (SAF) over time would have altered SSTs around Patagonia and New Zealand by altering heat-transfer flows such as the Agulhas current off southern Africa (Barrows *et al.*, 2007a) and the position and/or intensity of the Antarctic Circumpolar Current (ACC) and Southern Westerly Wind system, whilst influencing latitudinal SST gradients (Shulmeister *et al.*, 2004; Kaiser *et al.*, 2005). Lamy *et al.* (2007) and Denton *et al.* (2010) described a coupled atmosphere-ocean system in which latitudinal shifts in the STF and Southern Westerly Winds occur in response to changes in the Inter-Tropical Convergence Zone (ITCZ), driven by Northern Hemisphere sea ice extent, and changes in the sea ice extent around Antarctica. Several records suggest northward migration of oceanic fronts during globally cooler periods that resulted in reduced SSTs around Patagonia and New Zealand. In the southwest and central Pacific, the STF may have migrated 1-2° (Sikes *et al.*, 2009) or more, whilst in the southeast Pacific the STF and SAF may have shifted substantially more, by as

much as 5-6° during MIS 2 (Gersonde *et al.*, 2005; Kaiser *et al.*, 2005; Caniupán *et al.*, 2011). In both regions, this could have resulted in reasonably rapid changes in SST, triggering terrestrial cooling and glacial advances.

In summary, SST records show broadly similar patterns of temperature change to the Antarctic ice core records, indicating hemispheric propagation of climate change over the last glacial cycle. However, SSTs had deteriorated by *ca*. 30 ka, earlier than Antarctic temperatures, which may have been due to northward migration of the oceanic fronts.

7.4.3.4 Sea ice

The build-up of sea ice may respond to northward migration of the Southern Westerly Winds and Antarctic Circumpolar Current, but also likely triggers these processes by altering overturning circulation and hence SST gradients. Unpicking the cause and effects within this system is challenging, but comparing sea ice records with the timing of glacial advances can at least help in evaluating whether there is a relationship between sea ice changes and the terrestrial realm. We might anticipate sea ice to generally reflect cooler conditions, and therefore increase at the same time that glaciers in Patagonia and New Zealand advanced.

A reconstruction from south of the Polar Front by Crosta *et al.* (2004) suggests that sea ice duration increased markedly after *ca.* 78 ka until *ca.* 15 ka, with peak duration between *ca.* 32 and 21 ka, in a pattern consistent with decreasing temperatures in Antarctica. This pattern was developed further using diatom reconstructions from a core transect in the southwest Atlantic, east of the Drake Passage (Gersonde *et al.*, 2003; Allen *et al.*, 2011). Maximum summer sea ice extent around Antarctica occurred between *ca.* 30 ka and 22 ka, prior to the gLGM, but it had retreated to south of 61°S by *ca.* 22 ka, although winter sea ice did not retreat until *ca.* 19 ka, causing a large expanse of seasonally open waters within the Scotia Sea from 22 ka onwards (Allen *et al.*, 2011).

Antarctic sea ice has been invoked in several explanations for global climate change during the last glacial cycle (Allen *et al.*, 2011). It is likely that increased sea ice would have increased deep water formation and expansion (Seidov & Maslin, 2001; Ferrari *et al.*, 2014) and promoted stratification of the Southern Ocean due to freshening of the surface waters (Putnam *et al.*, 2013b). Sea ice extent is also likely to have been reduced by a southward shift of the Southern Westerly Winds and oceanic fronts, helping to destabilise any stratification of the Southern Ocean.

There is, then, a potentially important link between Antarctic sea ice and global glacial-interglacial climate change (Denton *et al.*, 2010), and an intrinsic link between sea ice and Southern Ocean stratification (Putnam *et al.*, 2013b).

7.4.3.5 Upwelling

Upwelling of CO_2 in the Southern Ocean can be reconstructed using records of opal flux. For example, Anderson *et al.* (2009) used records from cores TN057-13PC and -14PC to show that productivity south of the Polar Front was linked to upwelling of deep water masses during the last glacial cycle, driven by increased wind stress on the surface ocean. Upwelling broadly increased and decreased during episodes of warming and cooling, respectively, including the Antarctic A events. Thus, upwelling reached a minimum as sea ice extent peaked, likely due to stratification of the Southern Ocean (Putnam *et al.*, 2013b), and we would anticipate increased upwelling during cooler periods.

The Southern Ocean may have entered a fully stratified state by *ca.* 70 ka (Anderson *et al.*, 2009), consistent with the build-up of Antarctic sea ice at this time (Crosta et al., 2004), and possibly linked to increased winter duration (Putnam et al., 2013). Greater sea ice extent would not only have promoted stratification but would have pushed the oceanic fronts in the Southern Ocean further north, creating stronger SST gradients and triggering northward migration of the Southern Westerly Winds, further increasing sea ice expansion and reducing upwelling. This model, advocated by Denton *et al.* (2010) and Putnam *et al.* (2013b), amongst others, provides a theoretical link between sea ice formation, STF, SAF and Southern Westerly Wind migration, and SST changes around Patagonia and New Zealand.

Thus, records of upwelling in the Southern Ocean suggest that it broadly followed global warming and cooling during the last glacial cycle linked to stratification of the water column. However, the ocean may have been partially or fully stratified by *ca.* 70 ka, which would have forced oceanic frontal systems northwards.

7.4.4 Summary of last glacial cycle time periods

7.4.4.1 Late MIS 5 (ca. 110-71 ka)

There is little evidence for glacial advances during MIS 5, apart from occasional dates from individual glaciers, such as around 90 ka (Sutherland *et al.*, 2007; Glasser *et al.*, 2011), supported by low dust concentrations in the EDML ice core at this time and low sea ice extent (Fischer *et al.*, 2007). Antarctic temperatures were warmer, though with millennial-scale variability including a cooler period between *ca.*

92 ka and 87 ka (EPICA, 2006). Temperature changes were similar to Greenland, but it is unclear precisely whether the hemispheres were in-phase or out-of-phase. Localised records suggest that warmer SSTs followed Antarctic temperature changes (Barrows *et al.*, 2007a), including the millennial-scale variability and the marked cooler period between 92 ka and 87 ka. Hemispheric temperature changes followed Northern Hemisphere summer insolation (Berger & Loutre, 1991), and winter duration in the Southern Hemisphere increased between 105 ka and 95 ka (Huybers & Denton, 2008), with no major latitudinal offset in seasonality. Whilst a cooler period between 92 ka and 87 ka could have triggered glacial advances in Patagonia and New Zealand, overall MIS 5 was not likely to have promoted ice sheet expansion in either region.

7.4.4.2 MIS 4 (ca. 71-57 ka)

There is limited evidence for glacial advances during MIS 4, although scattered dates suggest that some glaciers expanded during this time, supported by increases in dust production and sea ice extent (Wolff *et al.*, 2006; Fischer *et al.*, 2007) and a reduction in upwelling (Anderson *et al.*, 2009). Antarctic temperatures showed a marked cooling with a cold period equivalent to the gLGM in temperature in both Antarctic and Greenland ice cores until around 63 ka (EPICA, 2006; Rasmussen *et al.*, 2006). There was a similar drop in localised SST records around New Zealand (Barrows *et al.*, 2007a), likely due to northward migration of the STF (Sikes *et al.*, 2009). An even greater SST reduction occurred off the west coast of northern Patagonia, where temperatures reached their lowest levels during the last glacial cycle due to a 5-6° northward shift of the STF (Kaiser *et al.*, 2005). Northern Hemisphere summer insolation was increasing, but Southern Hemisphere summer insolation was decreasing (Berger & Loutre, 1991), and there was a period of longer duration winters just prior to MIS 4 (Huybers & Denton, 2008) followed by a period of decreased seasonality. Therefore, the evidence suggests that MIS 4 was a major cool period in the southern mid-latitudes, and should have instigated significant glacial advances. The absence of dates in our compilation either suggests that any glacial activity was not as extensive as later advances or MIS 4 moraines have not yet been sampled.

7.4.4.3 Early MIS 3 (ca. 57-45 ka)

There are only scattered dates from New Zealand during early MIS 3, and dust and IRD records show little activity beyond occasional small peaks (Fischer *et al.*, 2007; Caniupán *et al.*, 2011). The limited evidence does align in places, notably between

ca. 50 ka and 46 ka (Antarctic warming events A3 and A2), and may suggest that ice advances occurred but were of limited extent or have not been sampled. Overall, Antarctic temperatures warmed following MIS 4 (EPICA, 2006), though not as much as MIS 5 or MIS 1, and the rest of early MIS 3 showed a strong millennial-scale pattern of warming and cooling into and out of the A4-1 events (Blunier & Brook, 2001), broadly covarying with D-O events in Greenland (Rasmussen *et al.*, 2006; Wolff *et al.*, 2010b). These events are propagated into local SST changes, causing significant variability of up to 3°C that could have been caused by fluctuating shifts in the oceanic fronts (Barrows *et al.*, 2007a; Caniupán *et al.*, 2011). The absence of prolonged cooling or build-up of sea-ice (Crosta *et al.*, 2004; Wolff *et al.*, 2006) suggests that these were only transient events and probably prevented any significant glacial advances, supported by decreasing, but variable, upwelling in the Southern Ocean (Anderson *et al.*, 2009). Northern Hemisphere summer insolation peaked and then started to decrease during this time, and Southern Hemisphere summer insolation peaked alongside increasing seasonality (Berger & Loutre, 1991). The implication is that while millennial-scale events may have caused some glacial activity that is not well recorded in our compilation (e.g. between 50 ka and 46 ka), overall climatic conditions were not well suited for glacial advances during MIS 3.

7.4.4.4 Late MIS 3 (ca. 45-29 ka)

There is good evidence for glacial advances during late MIS 3, at 43.1 ka and 37.8 ka in Patagonia, and 41.4 ka and 32.4 ka in New Zealand. This is marked by small peaks in IRD and dust flux (Fischer *et al.*, 2007; Caniupán *et al.*, 2011), though the latter increases towards the end of the period. Antarctic ice cores show a subtle cooling trend that is heavily overprinted by millennial-scale variability, including the A1 event, the cool periods of which broadly align with glacial advances (Blunier & Brook, 2001; EPICA, 2006; Wolff *et al.*, 2009; Wolff *et al.*, 2010b; Kelley *et al.*, 2014). Local SST records suggest that average temperatures had reached values similar to MIS 2 by this time, although Antarctic millennial-scale variability continued to be propagated across the mid-latitudes, likely related to continued fluctuations in the STF (Lamy *et al.*, 2004; Kaiser *et al.*, 2005; Barrows *et al.*, 2007a). Significantly, there was a marked increase in Antarctic sea ice at this time (Crosta *et al.*, 2004; Allen *et al.*, 2011), correlating with a reduction in upwelling in the Southern Ocean (Anderson *et al.*, 2009), which reached a minimum in the last glacial cycle at 30 ka. Northern Hemisphere insolation was slowly decreasing towards MIS 2 and, whilst Southern Hemisphere winter duration increased over the whole of MIS 3, there was

a switch to more rapidly increasing winter duration from *ca.* 36 ka (Huybers & Denton, 2008), which occurred whilst Southern Hemisphere insolation and seasonality both decreased between *ca.* 45 ka to 30 ka. In short, climatic conditions in the southern mid-latitudes were well suited for glacial advances during late MIS 3. Longer duration winters, decreasing summer insolation and decreasing seasonality promoted ice growth and were enhanced by fluctuations in the oceanic fronts, periodically delivering cooler temperatures to Patagonia and New Zealand. This was likely in tandem with increases in sea ice extent which reduced upwelling by stratifying the Southern Ocean and forcing the SAF, STF and Southern Westerly Winds further north to deliver cooler and wetter conditions to more of the glaciers (Putnam *et al.*, 2013b).

7.4.4.5   MIS 2 (ca. 29-14 ka) and the gLGM period (26.5-19 ka)

There were clear glacial advances either side of the gLGM at 27.0 ka and 18.8 ka in Patagonia and 26.4 ka and 18.0 ka in New Zealand. These correlate with major peaks in IRD and dust flux during early MIS 2 (Fischer *et al.*, 2007). However, whilst dust levels remained relatively high, IRD reduced markedly through the gLGM, perhaps due to a retreat of marine-terminating glaciers (Caniupán *et al.*, 2011). The advances occurred at the very start and end of a period of intense cooling in Antarctica, similar to that in Greenland, and at the same time that significant millennial-scale variability ended in Antarctica (EPICA, 2006; Rasmussen *et al.*, 2006). This suggests that glaciers responded rapidly to a drop in Southern Hemisphere temperatures at around 27.5 ka, perhaps because they had already advanced during late MIS 3, and then did not advance in unison again until the very end of the cool period. Local SST records suggest a continuation of the cooler temperatures from late MIS 3 (Lamy *et al.*, 2004; Kaiser *et al.*, 2005; Barrows *et al.*, 2007a), with no marked change except for off the west coast of southern Patagonia where proximal ice melt likely caused enhanced cooling of surface waters (Caniupán *et al.*, 2011). The advances at 18.8 ka and 18.0 ka align with a severe reversal in warming in SST around New Zealand (Barrows *et al.*, 2007a), suggesting that the STF may have fluctuated rapidly: first southward, then northward, then southward again. This may have altered both the local temperature and precipitation regimes, triggering a glacial advance despite no obvious drop in hemispheric temperature. Other frontal reconstructions have suggested that the STF and SAF migrated northwards by 1-2° around New Zealand (Sikes *et al.*, 2009) and 5-6° around Patagonia (Kaiser *et al.*, 2005), although this likely happened during late MIS 3. Sea ice extent remained relatively high from late MIS 3, but reduced markedly

after *ca.* 20 ka, with an associated increase in upwelling (Crosta *et al.*, 2004; Anderson *et al.*, 2009; Allen *et al.*, 2011). This was a period of reduced summer insolation in the Northern Hemisphere (Berger & Loutre, 1991), and the large northern ice sheets responded by reaching maximum extents. In the Southern Hemisphere, summer insolation increased and peaked at around 21 ka, and seasonality increased, with a latitudinal offset from *ca.* 30 ka.

Overall, conditions during much of MIS 2 were not as well suited for glacial advances as late MIS 3: summer insolation and seasonality increased; winter duration decreased; local SSTs did not decrease further; and IRD, dust flux and Antarctic sea-ice reduced significantly. Stratification may have deteriorated with southerly migration of the STF, SAF and Southern Westerly Winds. Glacial advances were likely still recorded only because global temperatures reached a minimum around the gLGM, indicated by a prolonged cooling in Antarctica without substantial millennial-scale variability. Advances towards the end of MIS 2 may have been triggered by northward fluctuations of the STF, providing cooler temperatures and increased precipitation at a time when most other factors suggest deglaciation had already started in the southern mid-latitudes.

7.4.4.6 The late-glacial period (ca. 19-10 ka)

Our compilation suggests that glaciers advanced during the Antarctic Cold Reversal at 13.9 ka in Patagonia and 13.0 in New Zealand. The absence of evidence for advances in the IRD or dust records suggests that the advance was either weak or, more probably, a prolonged stillstand. Antarctic temperatures decreased at this time, in antiphase with a warm period in Greenland and thus prior to the Younger Dryas (EPICA, 2006; Rasmussen *et al.*, 2006). This temperature drop only registers as a plateau in warming in the local SST records (Caniupán *et al.*, 2011), supporting a minimal advance of glaciers at this time. Northern Hemisphere insolation was increasing and Southern Hemisphere insolation was decreasing (Berger & Loutre, 1991), but the sub-orbital timescale of the late glacial events suggests that they were not related to changes in insolation intensity. Sea ice does not seem to have expanded significantly, but there is an apparent drop in upwelling (Anderson *et al.*, 2009), which could indicate northern migration of the Southern Westerly Winds and oceanic fronts, triggering a slowdown in the recession of glaciers in Patagonia and New Zealand. This may have also caused the offset in timing between Patagonia and New Zealand, given that higher latitude glaciers would have benefitted first from a northward migration of precipitation. The effect on SSTs in northern Patagonia and

New Zealand (Lamy *et al.*, 2004; Barrows *et al.*, 2007a) compared to southern Patagonia (Caniupán *et al.*, 2011) supports the assertion that the stillstand was driven by movement of the coupled oceanic-atmospheric frontal system, rather than by hemisphere-wide cooling.

7.5   Conclusions

The first compilation of previously published [10]Be exposure dating for Patagonia and New Zealand suggests that glaciers advanced at various times throughout the last glacial cycle, supported by similar evidence from radiocarbon dating. There is commonality in the timing of glacial advances between numerous glaciers in both Patagonia and New Zealand, and we infer this to represent periods of broad, regional glacial advances. However, this does not mean that all glaciers advanced synchronously and does not provide information on the extent of the glacial advances. That said, the chronologies from Patagonia and New Zealand show remarkable similarities, suggesting that similar forcing factors may have been influencing both ice sheets during the last glacial cycle. In particular, both regions show a trend for glacial advances, replicated in different glaciers, from at least 45 ka, with advances at *ca.* 41-43 ka, 32-38 ka, 26-27 ka, 18-19 ka and 13-14 ka.

In general, our compilation reveals a number of significant characteristics in the timing of glacial advances in the southern mid-latitudes. Glaciers were advancing well before the gLGM, and indeed by the latter half of MIS 3, with two advances prior to 30 ka. Further advances were concentrated just before and after (but not during) the gLGM, and late glacial advances or stillstands in Patagonia and New Zealand occurred during the Antarctic Cold Reversal, rather than the Younger Dryas. Future work should target glacial limits beyond those dated to the gLGM. In particular, an absence of dated limits from MIS 4 is puzzling given that numerous proxy records suggest that this period resulted in significant climate deterioration in the southern mid-latitudes.

There is no clear correlation between a single climatic forcing factor and the advances we identify. Rather, the forcing factors responsible likely changed over time. Our study suggests that ice sheet expansion in Patagonia and New Zealand was driven by underlying orbital parameters, involving a combination of summer intensity, seasonality, and winter duration, but that the precise timing is likely to have been intrinsically linked to migration of the coupled ocean-atmosphere system. Evaluating the various factors likely to have affected the timing of southern mid-latitude glacial advances suggests that late MIS 3 experienced optimum conditions

for glaciers to have advanced. Summer insolation reached a minimum, seasonality was reduced, winter duration was increasing, and sea ice had expanded significantly. This may have induced stratification of the ocean and triggered northward migration of the STF and SAF, bringing cooler temperatures to more of Patagonia and New Zealand and inducing an equatorward shift in the moisture-bearing Southern Westerly Winds system.

Hence, whilst global temperatures did not reach a minimum until MIS 2, summer insolation in the Southern Hemisphere was much higher by that time, and Antarctic sea ice reduced markedly, possibly aided by southward migration of the coupled ocean-atmosphere frontal system as sea ice expansion in the Northern Hemisphere induced a southward shift of the ITCZ. Glacial advances during MIS 2 in Patagonia and New Zealand occurred rapidly with the onset of a prolonged globally cool phase across the gLGM, marked by a discontinuation of hemispheric millennial-scale variability. A consistent offset after 30 ka, in which Patagonian glaciers advanced before those in New Zealand, is unlikely to be an artefact of age calculation but could instead relate either to a latitudinal offset in the timing of changes in seasonality between *ca.* 30 ka and 18 ka, or a lag related to the latitudinal migration of the coupled ocean-atmosphere system. Either way, shifts in the oceanic fronts and atmospheric circulation, as part of a complex climate feedback system, are likely to have been pivotal in determining when mid-latitude glaciers advanced during the last glacial cycle.

Chapter 8.   Conclusions and implications

8.1 Key conclusions

This thesis set out to reconstruct glacial changes of the southernmost ice lobes of the Patagonia Ice Sheet during the Quaternary. Specifically, the aims were to test whether ice advances occurred over timescales of 10^4, 10^5 or 10^6 years and to use this new chronological framework to examine the controls on glacial change. This work has produced a new glacial geomorphological map for the area (Chapter 3); examined the geomorphology of erratic boulder trains used for previous dating (Chapter 4); and applied cosmogenic nuclide dating of outwash depth profiles to test the age of glacial limits (Chapter 5). The thesis also presented a new glacial history for the southernmost ice lobes, against which the timing and nature of ice advances were examined (Chapter 6), and a large dating compilation from across Patagonia and New Zealand to examine possible forcing mechanisms of glacial change (Chapter 8).

8.1.1 Objective 1: Mapping of glacial limits

Mapping of glacial landforms associated with the five southernmost ice lobes showed eleven types of glacial landform: moraine ridges, subdued moraine topography, kettle-kame topography, glacial lineations, irregular and regular hummocky terrain, irregular dissected ridges, an esker, meltwater channels, former shorelines and outwash plains. The geomorphological map reveals the dominance of meltwater landforms (channels, outwash plains and kettle-kame topography) in the study area. It also highlights a difference in the nature of landforms associated with the northern three ice lobes, where limits are marked by numerous clear moraine ridges, compared to those to the south, where hummocky terrain and drift limits prevail. In places, the analysis demonstrated cross-cutting relationships indicative of re-advances.

8.1.2 Objective 2: Use of erratic boulder trains for dating

Erratic boulder trains have been used to provide cosmogenic nuclide dates that have proven critical in the discussion of the timing of glacial advances in the region. Several boulder trains along the southern edge of the BI-SSb lobe have been previously hypothesised to have been deposited in different glacial cycles, even though exposure dating yielded ages within the last glacial cycle. A detailed examination of the boulders in this thesis suggested that they were produced by one or more supraglacial rock avalanches. Rock surface weathering analysis showed little difference in the weathering characteristics between the boulder trains, which is

interpreted to indicate that the EBTs are closer in age than previous work has implied. Thus, while erratic boulder trains can provide useful flow-line indicators and sources of cosmogenic nuclide exposure dating, it is important to understand their formation, transport, and deposition. Importantly, occasional, anomalously old dates should be expected from supraglacial boulder trains caused by pre-exposure prior to and during glacial transport.

8.1.3 Objective 3: Depth profile dating of key limits

Ultimately, testing the age of glacial limits in the region requires new, independent dating to provide robust ages not compromised by post-depositional processes. In light of the new mapping and analysis of the erratic boulder trains, cosmogenic ^{10}Be and ^{26}Al exposure dating of depth-profiles was conducted through outwash associated with the Río Cullen and San Sebastián glacial limits of the BI-SSb lobe, previously hypothesised to date to MIS 12 and 10, respectively. The limits formed more recently than previously thought, giving ages of 45.6 ka (+139.9/-14.3) for the Río Cullen, and 30.1 ka (+45.6/-23.1) for the San Sebastián limits. These dates indicate extensive glaciation in southern Patagonia during MIS 3, prior to the well-constrained, but much less extensive MIS 2 (gLGM) limit that has been dated using cosmogenic dating of boulders and other independent chronological techniques. Whilst the errors from the depth-profile technique are large due to a conservative approach, and large scatter in boulder ages does not allow precise constraint on the timing of deposition of these glacial limits, all of the evidence points towards glacial advances during the last glacial cycle rather than numerous glacial cycles over hundreds of thousands of years.

8.1.4 Objective 4: Reconstructing the regional glacial history

The new age constraints for the BI-SSb lobe warranted further investigation into the timing and nature of ice advances of the five southernmost ice lobes. The geomorphological mapping was used to reconstruct former glacial limits, demarcate flowsets from landform assemblages, reconstruct former proglacial lakes, and evaluate possible glacial landsystems represented in the region. Eight time steps were reconstructed, which highlight the dynamic nature of these ice lobes. There is good evidence for rapid ice flow in the region, and possible surge-like activity, particularly in the Otway and Magellan lobes. Most of the ice lobes re-advanced on at least one occasion and there is evidence for potentially catastrophic drainage of the palaeo-Laguna Blanca proglacial lake. The relative history was used to re-examine published chronological data for the ice lobes, which suggested that the

Magellan, Otway and Skyring lobes likely advanced prior to the gLGM, in a manner similar to the BI-SSb lobe, with similar limits around 30 ka in several of the ice lobes. More extensive limits may have been deposited during the last glacial cycle or during earlier glacial stages in the Quaternary. The evidence for dynamic ice advance and retreat highlights that climatic reconstructions from the glacial geomorphology are not straightforward. However, the similarity in timing elucidated from the available chronological evidence suggests that an underlying external – likely climatic – forcing factor controls glacial advances.

8.1.5   Objective 5: Examining southern mid-latitude glaciation

To examine the possible climatic forcing factors further, a large dataset of previously published [10]Be exposure dates from Patagonia and New Zealand was compiled. This shows that glaciers across a broad range of the southern mid-latitudes advanced at various times during the last glacial cycle. Commonality in the timing of glacial advances implies periods of broad, regional glacial advances driven by similar forcing factors, although this does not mean that all glaciers advanced synchronously. Both regions show a trend for glacial advances, replicated in different glaciers, from at least 45 ka, with advances at *ca.* 41-43 ka, 32-38 ka, 26-27 ka, 18-19 ka and 13-14 ka. Thus, glaciers were advancing well before the gLGM, and indeed by the latter half of MIS 3. The glacial advances were likely driven by underlying orbital parameters, involving a combination of summer intensity, seasonality and winter duration. However, the precise timing is likely to have been linked to the migration of the coupled ocean-atmosphere system. Late MIS 3 may have experienced optimum conditions for glaciers to have advanced: minimum summer insolation, reduced seasonality, increasing winter duration, and expanded sea ice. Ocean stratification and northward migration of the STF and SAF, would have brought cooler temperatures to more of Patagonia and New Zealand and induced an equatorward shift in the moisture-bearing Southern Westerly Wind system.

8.2   Implications

The main implication of this work is that during the last glacial cycle, extensive glacial advances occurred in southernmost South America prior to the gLGM. This is contrary to the established age model for the timing of glacial advances in Patagonia, but is supported by a compilation of dating evidence from the rest of Patagonia and New Zealand, which suggests that glacial advances during MIS 3 may have been a common feature across the southern mid-latitudes. This finding is

important because it suggests that previous work on glacial chronologies around the world may have missed similar advances during the last glacial cycle. It also adds to a growing body of work that shows that glaciers in the southern mid-latitudes advanced prior to the gLGM and did not, therefore, follow global climate trends in the same way as large ice sheets in the Northern Hemisphere. The conclusions and implications of this thesis lead to a number of potential areas for future research.

8.2.1   Further work

8.2.1.1   Dating of the Río Gallegos, Skyring and Otway lobes

The Río Gallegos, Skyring and Otway lobes remain broadly undated. Chapter 6 demonstrated an age of *ca.* 30 ka for a pre-gLGM limit across the Magellan, Otway and Skyring lobes, but the glacial chronology could be significantly extended. An absence of boulders on moraines has likely hindered previous dating attempts, but Chapter 5 highlighted the suitability of depth profiles in outwash for dating glacial limits of the BI-SSb lobe, and this would be worth pursuing for the other southernmost ice lobes if suitable sampling locations can be found.

8.2.1.2   Palaeo-Laguna Blanca drainage

Chapter 6 reconstructed a significant lake drainage event associated with palaeo-Laguna Blanca, first identified by Lovell *et al.* (2012). Given the need for new dates, and the suitability of outwash plains for dating glacial limits in the region, this would be an excellent target. An age from sediments relating to the lake drainage would also help to constrain the timing of the pre-gLGM limits of the Skyring and Otway lobes suggested to have been deposited at *ca.* 30 ka in Chapter 6.

8.2.1.3   Ice thickness constraints

The reconstruction in Chapter 6 provides useful information on glacial extent over time, but cannot say anything about ice thickness. Improved ice thickness estimates would allow palaeoclimatic modelling from the glacial geomorphological record, so this would make a useful addition to our reconstruction. Data on ice thickness would be best provided by identifying and dating trimline evidence, similar to Boex *et al.* (2013) for northern Patagonia.

8.2.1.4   Investigations into possible palaeo-surges

Chapter 6 presented evidence for possible surge-like behaviour of the BI-SSb, Magellan and Otway lobes, but this was based predominantly on discontinuous landform evidence, and none of the lobes display 'ideal' surging landform suites.

This initial, tentative work requires further investigation and would benefit from more detailed sedimentological work to assess features such as glaciotectonised moraines and crevasse-fill ridges. Work on glacial surges has largely been confined to contemporary systems, so palaeo-examples could help to improve our understanding of their triggers in relation to long-term climate and/or topography.

8.2.1.5   Sedimentological work

As mentioned above, the landsystem approach adopted in Chapter 6 was necessarily tentative. This thesis was primarily concerned with glacial chronology and reconstructing broad glacial changes from landforms, but sedimentological work would help to improve our understanding of former glacial dynamics across the region, in a similar manner to the localised work of Benn & Clapperton (2000a; b).

8.2.1.6   Dating pre-gLGM moraines in Patagonia

Chapter 5 demonstrated that glacial limits thought to date from MIS 12 and 10 were deposited during the last glacial cycle. This may not have been anomalous, and similar limits could have been deposited across Patagonia. Indeed, work by Glasser *et al.* (2011) has already suggested the presence of limits of similar age to the BI-SSb lobe in the San Martín Valley. Thus, moraines beyond the gLGM limits in the rest of Patagonia could be targeted for dating to better resolve any regional differences associated with the migration of oceanic and/or atmospheric fronts.

8.2.1.7   MIS 4 in Patagonia

As noted in Chapter 7, the absence of glacial advances during MIS 4 is puzzling given that other palaeoclimatic records indicate significant climate deterioration at this time. Moraine chronologies in Patagonia could be re-examined to establish if MIS 4 moraines have been missed or whether they are truly absent from the southern mid-latitudes.

8.2.1.8   Ice sheet modelling

Modelling of the Patagonian Ice Sheet needs to be updated to reflect our increased understanding of the timing and nature of ice advances. Modelling power has advanced significantly since the last full ice sheet model by Hulton *et al.* (2002), and this thesis has provided a rigorous glacial reconstruction against which ice sheet models can be compared. In this way, our understanding of past climate change in southernmost South America can be improved further.

References

Ackert, R. P., Becker, R. A., Singer, B. S., Kurz, M. D., Caffee, M. W. & Mickelson, D. M. 2008. Patagonian Glacier Response During the Late Glacial–Holocene Transition. *Science*, 321**,** 392-395.

Adamson, D. & Colhoun, E. 1992. Late Quaternary glaciation and deglaciation of the Bunger Hills, Antarctica. *Antarctic Science*, 4**,** 435-446.

Allen, C. S., Pike, J. & Pudsey, C. J. 2011. Last glacial–interglacial sea-ice cover in the SW Atlantic and its potential role in global deglaciation. *Quaternary Science Reviews*, 30**,** 2446-2458.

Anderson, B. & Mackintosh, A. 2006. Temperature change is the major driver of late-glacial and Holocene glacier fluctuations in New Zealand. *Geology*, 34**,** 121-124.

Anderson, R. F., Ali, S., Bradtmiller, L. I., Nielsen, S. H. H., Fleisher, M. Q., Anderson, B. E. & Burckle, L. H. 2009. Wind-Driven Upwelling in the Southern Ocean and the Deglacial Rise in Atmospheric CO2. *Science*, 323**,** 1443-1448.

Anderson, R. S., Dühnforth, M., Colgan, W. & Anderson, L. 2012. Far-flung moraines: Exploring the feedback of glacial erosion on the evolution of glacier length. *Geomorphology*, 179**,** 269-285.

Applegate, P. J., Urban, N. M., Keller, K., Lowell, T. V., Laabs, B. J. C., Kelly, M. A. & Alley, R. B. 2012. Improved moraine age interpretations through explicit matching of geomorphic process models to cosmogenic nuclide measurements from single landforms. *Quaternary Research*, 77**,** 293-304.

Applegate, P. J., Urban, N. M., Laabs, B. J. C., Keller, K. & Alley, R. B. 2010. Modeling the statistical distributions of cosmogenic exposure dates from moraines. *Geoscientific Model Development*, 3**,** 293-307.

Atkins, C. B., Barrett, P. J. & Hicock, S. R. 2002. Cold glaciers erode and deposit: Evidence from Allan Hills, Antarctica. *Geology*, 30**,** 659-662.

Augustinus, P. C., Gore, D. B., Leishman, M. R., Zwartz, D. & Colhoun, E. A. 1997. Reconstruction of ice flow across the Bunger Hills, East Antarctica. *Antarctic Science*, 9**,** 347-354.

Balco, G., Stone, J. O., Lifton, N. A. & Dunai, T. J. 2008. A complete and easily accessible means of calculating surface exposure ages or erosion rates from [10]Be and [26]Al measurements. *Quaternary Geochronology*, 3**,** 174-195.

Ballantyne, C. K., McCarroll, D., Nesje, A. & Dahl, S. O. 1997. Periglacial trimlines, former nunataks and the altitude of the last ice sheet in Wester Ross, northwest Scotland. *Journal of Quaternary Science*, 12**,** 225-238.

Barker, S., Diz, P., Vautravers, M. J., Pike, J., Knorr, G., Hall, I. R. & Broecker, W. S. 2009. Interhemispheric Atlantic seesaw response during the last deglaciation. *Nature*, 457**,** 1097-1102.

Barr, I. D. & Lovell, H. 2014. A review of topographic controls on moraine distribution. *Geomorphology*, 226**,** 44-64.

Barrell, D. J. A. 2011. Chapter 75 - Quaternary Glaciers of New Zealand. *In:* Jürgen Ehlers, P. L. G. & Philip, D. H. (eds.) *Developments in Quaternary Sciences.* Elsevier.

Barrell, D. J. A., Almond, P. C., Vandergoes, M. J., Lowe, D. J. & Newnham, R. M. 2013. A composite pollen-based stratotype for inter-regional evaluation of climatic events in New Zealand over the past 30,000 years (NZ-INTIMATE project). *Quaternary Science Reviews*, 74, 4-20.

Barrows, T. T., Almond, P., Rose, R., Keith Fifield, L., Mills, S. C. & Tims, S. G. 2013. Late Pleistocene glacial stratigraphy of the Kumara-Moana region, West Coast of South Island, New Zealand. *Quaternary Science Reviews*, 74**,** 139-159.

Barrows, T. T., Juggins, S., De Deckker, P., Calvo, E. & Pelejero, C. 2007a. Long-term sea surface temperature and climate change in the Australian–New Zealand region. *Paleoceanography*, 22, PA2215.

Barrows, T. T., Lehman, S. J., Fifield, L. K. & De Deckker, P. 2007b. Absence of Cooling in New Zealand and the Adjacent Ocean During the Younger Dryas Chronozone. *Science*, 318**,** 86-89.

Barrows, T. T., Stone, J. O., Fifield, L. K. & Cresswell, R. G. 2002. The timing of the Last Glacial Maximum in Australia. *Quaternary Science Reviews*, 21**,** 159-173.

Benn, D. I. 2004. Clast morphology. *In:* Evans, D. J. A. & Benn, D. I. (eds.) *A Practical Guide to the study of Glacial Sediments.* Arnold: London.

Benn, D. I. & Ballantyne, C. K. 1994. Reconstructing the transport history of glacigenic sediments: a new approach based on the co-variance of clast form indices. *Sedimentary Geology*, 91**,** 215-227.

Benn, D. I. & Clapperton, C. M. 2000a. Glacial sediment-landform associations and paleoclimate during the last glaciation, Strait of Magellan, Chile. *Quaternary Research*, 54**,** 13-23.

Benn, D. I. & Clapperton, C. M. 2000b. Pleistocene glacitectonic landforms and sediments around central Magellan Strait, southernmost Chile: evidence for fast outlet glaciers with cold-based margins. *Quaternary Science Reviews*, 19**,** 591-612.

Benn, D. I. & Evans, D. J. A. 2010. Glaciers and Glaciation, London, Arnold.

Bennett, M. R., Hambrey, M. J., Huddart, D. & Ghienne, J. F. 1996. The formation of a geometrical ridge network by the surge-type glacier Kongsvegen, Svalbard. Journal of Quaternary Science, 11, 437-449.

Bentley, M. J. & McCulloch, R. D. 2005. Impact of neotectonics on the record of glacier and sea level fluctuations, Strait of Magellan, southern Chile. *Geografiska Annaler Series a-Physical Geography*, 87A**,** 393-402.

Bentley, M. J., Sugden, D. E., Hulton, N. R. J. & McCulloch, R. D. 2005. The landforms and pattern of deglaciation in the Strait of Magellan and Bahia Inútil, southernmost South America. *Geografiska Annaler Series a-Physical Geography*, 87A**,** 313-333.

Berger, A. & Loutre, M. F. 1991. Insolation values for the climate of the last 10 million years. *Quaternary Science Reviews*, 10**,** 297-317.

Blomdin, R., Murray, A., Thomsen, K. J., Buylaert, J.-P., Sohbati, R., Jansson, K. N. & Alexanderson, H. 2012. Timing of the deglaciation in southern Patagonia: Testing the applicability of K-Feldspar IRSL. *Quaternary Geochronology*, 10**,** 264-272.

Blunier, T. & Brook, E. J. 2001. Timing of Millennial-Scale Climate Change in Antarctica and Greenland During the Last Glacial Period. *Science*, 291**,** 109-112.

Bockheim, J., Coronato, A., Rabassa, J., Ercolano, B. & Ponce, J. 2009. Relict sand wedges in southern Patagonia and their stratigraphic and paleo-environmental significance. Quaternary Science Reviews, 28, 1188-1199.

Boex, J., Fogwill, C., Harrison, S., Glasser, N. F., Hein, A., Schnabel, C. & Xu, S. 2013. Rapid thinning of the late Pleistocene Patagonian Ice Sheet followed migration of the Southern Westerlies. *Sci. Rep.*, 3, 1-6.

Bonarelli, G. 1917. Tierra del Fuego y sus turberas. *Anal. del Min. de Agric. de la Nacion.* Buenos Aires.

Boning, C. W., Dispert, A., Visbeck, M., Rintoul, S. R. & Schwarzkopf, F. U. 2008. The response of the Antarctic Circumpolar Current to recent climate change. *Nature Geosci*, 1**,** 864-869.

Boulton, G. S. 1972. Modern Arctic glaciers as depositional models for former ice sheets. *Journal of the Geological Society*, 128**,** 361-393.

Boulton, G. S. 1978. Boulder shapes and grain-size distributions of debris as indicators of transport paths through a glacier and till genesis. *Sedimentology*, 25**,** 773-799.

Boulton, G. S. 1996. Theory of glacial erosion, transport and deposition as a consequence of subglacial sediment deformation. *Journal of Glaciology*, 42**,** 43-62.

Boulton, G. S., van der Meer, J. J. M., Beets, D. J., Hart, J. K. & Ruegg, G. H. J. 1999. The sedimentary and structural evolution of a recent push moraine complex: Holmstrømbreen, Spitsbergen. *Quaternary Science Reviews*, 18**,** 339-371.

Boyd, B. L., Anderson, J. B., Wellner, J. S. & Fernández, R. A. 2008. The sedimentary record of glacial retreat, Marinelli Fjord, Patagonia: Regional correlations and climate ties. *Marine Geology*, 255**,** 165-178.

Breuer, S., Kilian, R., Schörner, D., Weinrebe, W., Behrmann, J. & Baeza, O. 2013. Glacial and tectonic control on fjord morphology and sediment deposition in the Magellan region (53°S), Chile. *Marine Geology*, 346**,** 31-46.

Broecker, W. S. 2003. Does the Trigger for Abrupt Climate Change Reside in the Ocean or in the Atmosphere? *Science*, 300**,** 1519-1522.

Bronk Ramsey, C. 2009. Bayesian Analysis of Radiocarbon Dates. *Radiocarbon*, 51**,** 337-360.

Bujalesky, G., Coronato, A. & Isla, F. 2001. Ambientes glacifluviales y litorales Cuaternarios de la region del Rio Chico, Tierra del Fuego, Argentina. *Revista de la Asociación Geológica Argentina*, 56**,** 73-90.

Buylaert, J. P., Murray, A. S., Gebhardt, A. C., Sohbati, R., Ohlendorf, C., Thiel, C., Wastegård, S. & Zolitschka, B. 2013. Luminescence dating of the PASADO core 5022-1D from Laguna Potrok Aike (Argentina) using IRSL signals from feldspar. *Quaternary Science Reviews*, 71**,** 70-80.

Caldenius, C. C. z. 1932. Las Glaciaciones Cuaternarias en la Patagonia y Tierra del Fuego. *Geografiska Annaler*, 14**,** 1-164.

Calvo, E., Pelejero, C., De Deckker, P. & Logan, G. A. 2007. Antarctic deglacial pattern in a 30 kyr record of sea surface temperature offshore South Australia. *Geophysical Research Letters*, 34**,** L13707.

Caniupán, M., Lamy, F., Lange, C. B., Kaiser, J., Arz, H., Kilian, R., Baeza Urrea, O., Aracena, C., Hebbeln, D., Kissel, C., Laj, C., Mollenhauer, G. & Tiedemann, R. 2011. Millennial-scale sea surface temperature and Patagonian Ice Sheet changes off southernmost Chile (53°S) over the past ~60 kyr. *Paleoceanography*, 26**,** PA3221.

Carrivick, J. L. & Tweed, F. S. 2013. Proglacial lakes: character, behaviour and geological importance. *Quaternary Science Reviews*, 78**,** 34-52.

Carter, L., Cortese, G. 2009. Change in the Southern Ocean: Responding to Antarctica. *PAGES News*, 17**,** 30-32.

Carter, L., McCave, I. N. & Williams, M. J. M. 2008. Circulation and Water Masses of the Southern Ocean: A Review. *In:* Fabio, F. & Martin, S. (eds.) *Developments in Earth and Environmental Sciences.* Elsevier.

Carter, L., Neil, H. L. & Northcote, L. 2002. Late Quaternary ice-rafting events in the SW Pacific Ocean, off eastern New Zealand. *Marine Geology*, 191**,** 19-35.

Černá, B. & Engel, Z. 2011. Surface and sub-surface Schmidt hammer rebound value variation for a granite outcrop. *Earth Surface Processes and Landforms*, 36**,** 170-179.

Chevalier, G., Davies, T. & McSaveney, M. 2009. The prehistoric Mt Wilberg rock avalanche, Westland, New Zealand. *Landslides*, 6**,** 253-262.

Clapperton, C. M. 1989. Asymmetrical drumlins in Patagonia, Chile. *Sedimentary Geology*, 62**,** 387-398.

Clapperton, C. M. 1993. *Quaternary geology and geomorphology of South America*, B.V., Amsterdam, Elsevier Science Publishers.

Clapperton, C. M., Sugden, D. E., Kaufman, D. S. & McCulloch, R. D. 1995. The Last Glaciation in Central Magellan-Strait, southernmost Chile. *Quaternary Research*, 44**,** 133-148.

Clarhäll, A. & Jansson, K. N. 2003. Time perspectives on glacial landscape formation—glacial flow chronology at Lac aux Goélands, northeastern Québec, Canada. *Journal of Quaternary Science*, 18**,** 441-452.

Clark, C. D. 1999. Glaciodynamic context of subglacial bedform generation and preservation. Annals of Glaciology, 28, 23-32.

Clark, C. D. & Stokes, C. R. 2003. Palaeo-ice stream landsystem. *In:* Evans, D. J. A. (ed.) *Glacial Landsystems.* London: Arnold.

Clark, P. U., Dyke, A. S., Shakun, J. D., Carlson, A. E., Clark, J., Wohlfarth, B., Mitrovica, J. X., Hostetler, S. W. & McCabe, A. M. 2009. The Last Glacial Maximum. *Science*, 325**,** 710-714.

Clayton, L. 1964. Karst topography on stagnant glaciers. *Journal of Glaciology*, 5**,** 107-112.

Corliss, B. H. 1983. Quaternary circulation of the Antarctic circumpolar current. *Deep Sea Research Part A. Oceanographic Research Papers*, 30**,** 47-61.

Coronato, A., Ercolano, B., Corbella, H. & Tiberi, P. 2013. Glacial, fluvial and volcanic landscape evolution in the Laguna Potrok Aike maar area, Southern Patagonia, Argentina. *Quaternary Science Reviews*, 71**,** 13-26.

Coronato, A., Martínez, O. & Rabassa, J. 2004. Glaciations in Argentine Patagonia, southern South America. *In:* Ehlers, J. & Gibbard, P. L. (eds.) *Developments in Quaternary Sciences.* Elsevier.

Coronato, A. & Rabassa, J. 2011. Chapter 51 - Pleistocene Glaciations in Southern Patagonia and Tierra del Fuego. *In:* Jürgen Ehlers, P. L. G. & Philip, D. H. (eds.) *Developments in Quaternary Sciences.* Elsevier.

Coronato, A., Roig, C., Rabassa, J., Meglioli, A. 1999. Erratic boulder field of pre-Illinoian age at Punta Sinaí, Tierra del Fuego, southernmost South America. *XV INQUA International Congress.* Durham, South Africa.

Coronato, A. M. J., Coronato, F., Mazzoni, E. & Vázquez, M. 2008. The Physical Geography of Patagonia and Tierra del Fuego. *In:* Rabassa, J. (ed.) *Developments in Quaternary Sciences.* Elsevier.

Crosta, X., Sturm, A., Armand, L. & Pichon, J.-J. 2004. Late Quaternary sea ice history in the Indian sector of the Southern Ocean as recorded by diatom assemblages. *Marine Micropaleontology*, 50**,** 209-223.

Cunningham, W. D. 1993. Strike-slip faults in the southernmost andes and the development of the Patagonian orocline. *Tectonics*, 12**,** 169-186.

Darwin, C. 1841. On the distribution of the erratic boulders and on the contemporaneous unstratified deposits of South America. *Transactions of the Geological Society of London*, 2-6**,** 415-431.

Darwin, C. 1845. *Journal of researches into the natural history and geology of the countries visited during the voyage of H.M.S. Beagle round the world, 1832-36,* London, John Murray.

Darwin, C. 1848. On the Transportal of Erratic Boulders from a lower to a higher level. *Quarterly Journal of the Geological Society*, 4**,** 315-323.

Davies, B. J., Glasser, N. F., Carrivick, J. L., Hambrey, M. J., Smellie, J. L. & Nývlt, D. 2013. Landscape evolution and ice-sheet behaviour in a semi-arid polar environment: James Ross Island, NE Antarctic Peninsula. *Geological Society, London, Special Publications*, 381**,** 353-395.

Davis, J. W. 1880. On a Group of Erratic Boulders at Norber, near Clapham, in Yorkshire. *Proceedings of the Yorkshire Geological and Polytechnic Society*, 7**,** 266-273.

Day, M. & Goudie, A. 1977. Field assessment of rock hardness using the Schmidt hammer. *British Geomorphological Research Group Technical Bulletin*, 18**,** 19-29.

De Muro, S., Di Grande, A., Brambati, A. & Ibba, A. 2014. Geomorphology map of the marine and transitional terraces and raised shorelines of the Península Juan Mazía, Tierra Del Fuego. Straits of Magellan – Chile. *Journal of Maps*, 1-13.

Delaney, K. & Evans, S. 2014. The 1997 Mount Munday landslide (British Columbia) and the behaviour of rock avalanches on glacier surfaces. *Landslides*, 1-18.

Denton, G. H., Anderson, R. F., Toggweiler, J. R., Edwards, R. L., Schaefer, J. M. & Putnam, A. E. 2010. The Last Glacial Termination. *Science*, 328, 1652-1656.

Denton, G. H., Lowell, T. V., Heusser, C. J., Schlüchter, C., Andersen, B. G., Heusser, L. E., Moreno, P. I. & Marchant, D. R. 1999. Geomorphology, Stratigraphy, and Radiocarbon Chronology of LlanquihueDrift in the Area of the Southern Lake District, Seno Reloncaví, and Isla Grande de Chiloé, Chile. *Geografiska Annaler: Series A, Physical Geography*, 81, 167-229.

Desilets, D., Zreda, M. & Prabu, T. 2006. Extended scaling factors for in situ cosmogenic nuclides: New measurements at low latitude. *Earth and Planetary Science Letters*, 246, 265-276.

DiLabio, R. N. W. 1981. Glacial dispersal of rocks and minerals at the south end of Lac Mistassini, Quebec, with special reference to the Icon dispersal train. *Geological Survey of Canada Bulletin*, 323, 46.

DiLabio, R. N. W. 1990. Glacial dispersal trains. *In:* Kujansuu, R. & Saarnisto, M. (eds.) *Glacial Indicator Tracing.* Rotterdam, Netherlands: Balkema Publishers.

Douglass, D. C., Singer, B. S., Kaplan, M. R., Ackert, R. P., Mickelson, D. M. & Caffee, M. W. 2005. Evidence of early Holocene glacial advances in southern South America from cosmogenic surface-exposure dating. *Geology*, 33, 237-240.

Douglass, D. C., Singer, B. S., Kaplan, M. R., Mickelson, D. M. & Caffee, M. W. 2006. Cosmogenic nuclide surface exposure dating of boulders on last-glacial and late-glacial moraines, Lago Buenos Aires, Argentina: Interpretive strategies and paleoclimate implications. *Quaternary Geochronology*, 1, 43-58.

Dunai, T. J. 2001. Influence of secular variation of the geomagnetic field on production rates of in situ produced cosmogenic nuclides. *Earth and Planetary Science Letters*, 193, 197-212.

Dyke, A. S. & Evans, D. J. A. 2003. Ice-marginal terrestrial landsystems: Northern Laurentide and Innuitian ice sheet margins. *In:* Evans, D. J. A. (ed.) *Glacial Landsystems.* London: Hodder Arnold.

Dyke, A. S. & Morris, T. F. 1988. Drumlin Fields, Dispersal Trains, and Ice Streams in Arctic Canada. *The Canadian Geographer*, 32, 86-90.

Ehlers, J., Gibbard, P. L. & Hughes, P. D. (eds.) 2011. *Quaternary Glaciations - Extent and Chronology A Closer Look*.

Engel, Z. 2007. Measurement and age assignment of intact rock strength in the Krkonoše Mountains, Czech Republic. *Zeitschrift für Geomorphologie*, 51, 69-80.

EPICA 2004. Eight glacial cycles from an Antarctic ice core. *Nature*, 429, 623-628.

EPICA 2006. One-to-one coupling of glacial climate variability in Greenland and Antarctica. *Nature*, 444, 195-198.

EPICA 2010. Stable oxygen isotopes of ice core EDML. *PANGAEA*.

Ercolano, B., Mazzoni, E., Vazquez, M. & Rabassa, J. 2004. Drumlins and drumlinoid forms of the Lower Pleistocene in southern Patagonia, Province of Santa Cruz. *Rev. Asoc. Geol. Argent.*, 59, 771-777.

Evans, D. J. A. 2003. *Glacial Landsystems*, Hodder Arnold, London.

Evans, D. J. A. 2003. Ice-marginal terrestrial landsystems: Active temperate glacier margins. *In:* Evans, D. J. A. (ed.) *Glacial Landsystems.* London: Arnold.

Evans, D. J. A. 2007. Glacial Erratics and Till Dispersal Indicators. *In:* Elias, S., A. (ed.) *Encyclopedia of Quaternary Science.* Oxford: Elsevier.

Evans, D. J. A. 2009. Controlled moraines: origins, characteristics and palaeoglaciological implications. *Quaternary Science Reviews*, 28**,** 183-208.

Evans, D. J. A., Archer, S. & Wilson, D. J. H. 1999. A comparison of the lichenometric and Schmidt hammer dating techniques based on data from the proglacial areas of some Icelandic glaciers. *Quaternary Science Reviews*, 18**,** 13-41.

Evans, D. J. A., Clark, C. D. & Rea, B. R. 2008. Landform and sediment imprints of fast glacier flow in the southwest Laurentide Ice Sheet. *Journal of Quaternary Science*, 23**,** 249-272.

Evans, D. J. A. & Rea, B. 1999. Geomorphology and sedimentology of surging glaciers: a land-systems approach. *Annals of Glaciology*, 28**,** 75-82.

Evans, D. J. A. & Rea, B. 2003. Surging glacier landsystem. *In:* Evans, D. J. A. (ed.) *Glacial Landsystems.* London: Arnold.

Evans, D. J. A. & Twigg, D. R. 2002. The active temperate glacial landsystem: a model based on Breiðamerkurjökull and Fjallsjökull, Iceland. *Quaternary Science Reviews*, 21**,** 2143-2177.

Evans, D. J. A., Twigg, D. R., Rea, B. R. & Shand, M. 2007. Surficial geology and geomorphology of the Brúarjökull surging glacier landsystem. *Journal of Maps*, 3**,** 349-367.

Evenson, E. B., Burkhart, P. A., Gosse, J. C., Baker, G. S., Jackofsky, D., Meglioli, A., Dalziel, I., Kraus, S., Alley, R. B. & Berti, C. 2009. Enigmatic boulder trains, supraglacial rock avalanches, and the origin of "Darwin's boulders," Tierra del Fuego. *GSA Today*, 19**,** 4-10.

Fernandez, R. A., Anderson, J. B., Wellner, J. S. & Hallet, B. 2011. Timescale dependence of glacial erosion rates: A case study of Marinelli Glacier, Cordillera Darwin, southern Patagonia. *Journal of Geophysical Research: Earth Surface*, 116**,** F01020.

Ferrari, R., Jansen, M. F., Adkins, J. F., Burke, A., Stewart, A. L. & Thompson, A. F. 2014. Antarctic sea ice control on ocean circulation in present and glacial climates. *Proceedings of the National Academy of Sciences*, 111**,** 8753-8758.

Fischer, H., Fundel, F., Ruth, U., Twarloh, B., Wegner, A., Udisti, R., Becagli, S., Castellano, E., Morganti, A., Severi, M., Wolff, E., Littot, G., Röthlisberger, R., Mulvaney, R., Hutterli, M. A., Kaufmann, P., Federer, U., Lambert, F., Bigler, M., Hansson, M., Jonsell, U., de Angelis, M., Boutron, C., Siggaard-Andersen, M.-L., Steffensen, J. P., Barbante, C., Gaspari, V., Gabrielli, P. & Wagenbach, D. 2007. Reconstruction of millennial changes in dust emission, transport and regional sea ice coverage using the deep EPICA ice cores from the Atlantic and Indian Ocean sector of Antarctica. *Earth and Planetary Science Letters*, 260**,** 340-354.

Fogwill, C. J. 2003. *The application of cosmogenic exposure dating to glacial landforms: Examples from Antarctica and Patagonia.* Ph.D., University of Edinburgh.

Fogwill, C. J. & Kubik, P. W. 2005. A glacial stage spanning the Antarctic Cold Reversal in Torres del Paine (51 degrees S), Chile, based on preliminary cosmogenic exposure ages. *Geografiska Annaler Series a-Physical Geography*, 87A**,** 403-408.

García, J. L., Hall, B. L., Kaplan, M. R., Vega, R. M. & Strelin, J. A. 2014. Glacial geomorphology of the Torres del Paine region (southern Patagonia): Implications for glaciation, deglaciation and paleolake history. *Geomorphology*, 204**,** 599-616.

García, J. L., Kaplan, M. R., Hall, B. L., Schaefer, J. M., Vega, R. M., Schwartz, R. & Finkel, R. 2012. Glacier expansion in southern Patagonia throughout the Antarctic cold reversal. *Geology*, 40**,** 859-862.

Gersonde, R., Abelmann, A., Brathauer, U., Becquey, S., Bianchi, C., Cortese, G., Grobe, H., Kuhn, G., Niebler, H. S., Segl, M., Sieger, R., Zielinski, U. & Fütterer, D. K. 2003. Last glacial sea surface temperatures and sea-ice extent in the Southern Ocean (Atlantic-Indian sector): A multiproxy approach. *Paleoceanography*, 18**,** 1061.

Gersonde, R., Crosta, X., Abelmann, A. & Armand, L. 2005. Sea-surface temperature and sea ice distribution of the Southern Ocean at the EPILOG Last Glacial Maximum—a circum-Antarctic view based on siliceous microfossil records. *Quaternary Science Reviews*, 24**,** 869-896.

Glasser, N. & Jansson, K. 2008. The Glacial Map of southern South America. *Journal of Maps*, 4**,** 175-196.

Glasser, N. F., Harrison, S., Ivy-Ochs, S., Duller, G. A. T. & Kubik, P. W. 2006. Evidence from the Rio Bayo valley on the extent of the North Patagonian Icefield during the Late Pleistocene–Holocene transition. *Quaternary Research*, 65**,** 70-77.

Glasser, N. F., Harrison, S., Schnabel, C., Fabel, D. & Jansson, K. N. 2012. Younger Dryas and early Holocene age glacier advances in Patagonia. *Quaternary Science Reviews*, 58**,** 7-17.

Glasser, N. F. & Jansson, K. N. 2005. Fast-flowing outlet glaciers of the Last Glacial Maximum Patagonian Icefield. *Quaternary Research*, 63**,** 206-211.

Glasser, N. F., Jansson, K. N., Goodfellow, B. W., de Angelis, H., Rodnight, H. & Rood, D. H. 2011. Cosmogenic nuclide exposure ages for moraines in the Lago San Martín Valley, Argentina. *Quaternary Research*, 75**,** 636-646.

Glasser, N. F., Jansson, K. N., Harrison, S. & Kleman, J. 2008. The glacial geomorphology and Pleistocene history of South America between 38 degrees S and 56 degrees S. *Quaternary Science Reviews*, 27**,** 365-390.

Goldie, H. S. 2005. Erratic judgements: re-evaluating solutional erosion rates of limestones using erratic-pedestal sites, including Norber, Yorkshire. *Area*, 37**,** 433-442.

Golledge, N. R., Mackintosh, A. N., Anderson, B. M., Buckley, K. M., Doughty, A. M., Barrell, D. J. A., Denton, G. H., Vandergoes, M. J., Andersen, B. G. & Schaefer, J. M. 2012. Last Glacial Maximum climate in New Zealand inferred from a modelled Southern Alps icefield. *Quaternary Science Reviews*, 46**,** 30-45.

Goudie, A. S. 2006. The Schmidt Hammer in geomorphological research. *Progress in Physical Geography*, 30**,** 703-718.

Graham, D. J., Bennett, M. R., Glasser, N. F., Hambrey, M. J., Huddart, D. & Midgley, N. G. 2007. 'A test of the englacial thrusting hypothesis of "hummocky" moraine formation: case studies from the northwest Highlands, Scotland': Comments. *Boreas*, 36**,** 103-107.

Greenwood, S. L. & Clark, C. D. 2008. Subglacial bedforms of the Irish Ice Sheet. *Journal of Maps*, 4**,** 332-357.

Hahn, A., Kliem, P., Ohlendorf, C., Zolitschka, B. & Rosén, P. 2013. Climate induced changes as registered in inorganic and organic sediment components from Laguna Potrok Aike (Argentina) during the past 51 ka. *Quaternary Science Reviews*, 71**,** 154-166.

Hall, B. L., Porter, C. T., Denton, G. H., Lowell, T. V. & Bromley, G. R. M. 2013. Extensive recession of Cordillera Darwin glaciers in southernmost South America during Heinrich Stadial 1. *Quaternary Science Reviews*, 62**,** 49-55.

Hambrey, M. J. & Huddart, D. 1995. Englacial and proglacial glaciotectonic processes at the snout of a thermally complex glacier in Svalbard. *Journal of Quaternary Science*, 10**,** 313-326.

Harrison, S., Glasser, N., Winchester, V., Haresign, E., Warren, C., Duller, G. A. T., Bailey, R., Ivy-Ochs, S., Jansson, K. & Kubik, P. 2008. Glaciar León, Chilean Patagonia: late-Holocene chronology and geomorphology. *The Holocene*, 18**,** 643-652.

Harrison, S. & Glasser, N. F. 2011. Chapter 54 - The Pleistocene Glaciations of Chile. *In:* Jürgen Ehlers, P. L. G. & Philip, D. H. (eds.) *Developments in Quaternary Sciences.* Elsevier.

Harrison, S., Glasser, N. F., Duller, G. A. T. & Jansson, K. N. 2012. Early and mid-Holocene age for the Tempanos moraines, Laguna San Rafael, Patagonian Chile. *Quaternary Science Reviews*, 31**,** 82-92.

Hart, J. K. & Boulton, G. S. 1991. The interrelation of glaciotectonic and glaciodepositional processes within the glacial environment. *Quaternary Science Reviews*, 10**,** 335-350.

Hein, A. S., Dunai, T. J., Hulton, N. R. J. & Xu, S. 2011. Exposure dating outwash gravels to determine the age of the greatest Patagonian glaciations. *Geology*, 39**,** 103-106.

Hein, A. S., Hulton, N. R. J., Dunai, T. J., Schnabel, C., Kaplan, M. R., Naylor, M. & Xu, S. 2009. Middle Pleistocene glaciation in Patagonia dated by cosmogenic-nuclide measurements on outwash gravels. *Earth and Planetary Science Letters*, 286**,** 184-197.

Hein, A. S., Hulton, N. R. J., Dunai, T. J., Sugden, D. E., Kaplan, M. R. & Xu, S. 2010. The chronology of the Last Glacial Maximum and deglacial events in central Argentine Patagonia. *Quaternary Science Reviews*, 29**,** 1212-1227.

Herman, F., Seward, D., Valla, P. G., Carter, A., Kohn, B., Willett, S. D. & Ehlers, T. A. 2013. Worldwide acceleration of mountain erosion under a cooling climate. *Nature*, 504**,** 423-426.

Heusser, C. J. 1993. Late-glacial of southern South America. *Quaternary Science Reviews*, 12**,** 345-350.

Heusser, C. J. 1995. Three Late Quaternary pollen diagrams from Southern Patagonia and their palaeoecological implications. *Palaeogeography, Palaeoclimatology, Palaeoecology*, 118**,** 1-24.

Heusser, C. J. 2003. *Ice Age Southern Andes: A Chronicle of Paleoecological Events*, Elsevier.

Heusser, C. J., Heusser, L. E., Lowell, T. V., M, A. M. & M, S. M. 2000. Deglacial palaeoclimate at Puerto del Hambre, subantarctic Patagonia, Chile. *Journal of Quaternary Science*, 15**,** 101-114.

Hewitt, K. 1999. Quaternary Moraines vs Catastrophic Rock Avalanches in the Karakoram Himalaya, Northern Pakistan. *Quaternary Research*, 51**,** 220-237.

Hewitt, K. 2009. Rock avalanches that travel onto glaciers and related developments, Karakoram Himalaya, Inner Asia. *Geomorphology*, 103**,** 66-79.

Heyman, J., Stroeven, A. P., Harbor, J. M. & Caffee, M. W. 2011. Too young or too old: Evaluating cosmogenic exposure dating based on an analysis of compiled boulder exposure ages. *Earth and Planetary Science Letters*, 302**,** 71-80.

Hidy, A. J., Gosse, J. C., Pederson, J. L., Mattern, J. P. & Finkel, R. C. 2010. A geologically constrained Monte Carlo approach to modeling exposure ages from profiles of cosmogenic nuclides: An example from Lees Ferry, Arizona. *Geochemistry, Geophysics, Geosystems*, 11**,** Q0AA10.

Hodgson, D. A. & Sime, L. C. 2010. Palaeoclimate: Southern westerlies and CO2. *Nature Geosci*, 3**,** 666-667.

Hubbard, A., Hein, A. S., Kaplan, M. R., Hulton, N. R. J. & Glasser, N. 2005. A modelling reconstruction of the last glacial maximum ice sheet and its

deglaciation in the vicinity of the Northern Patagonian Icefield, South America. *Geografiska Annaler Series a-Physical Geography*, 87A**,** 375-391.

Huddart, D. 2002. Norber Erratics. *In:* Huddart, D. & Glasser, N. (eds.) *Quaternary of Northern England.* Peterborough: JNCC.

Hughes, P. D., Gibbard, P. L. & Ehlers, J. 2013. Timing of glaciation during the last glacial cycle: evaluating the concept of a global 'Last Glacial Maximum' (LGM). *Earth-Science Reviews*, 125**,** 171-198.

Hulton, N., Sugden, D., Payne, A. & Clapperton, C. 1994. Glacier Modeling and the Climate of Patagonia during the Last Glacial Maximum. *Quaternary Research*, 42**,** 1-19.

Hulton, N. R. J., Purves, R. S., McCulloch, R. D., Sugden, D. E. & Bentley, M. J. 2002. The Last Glacial Maximum and deglaciation in southern South America. *Quaternary Science Reviews*, 21**,** 233-241.

Huybers, P. & Denton, G. 2008. Antarctic temperature at orbital timescales controlled by local summer duration. *Nature Geosci*, 1**,** 787-792.

Ivy-Ochs, S., Schlüchter, C., Kubik, P. W. & Denton, G. H. 1999. Moraine Exposure Dates Imply Synchronous Younger Dryas Glacier Advances in the European Alps and in the Southern Alps of New Zealand. *Geografiska Annaler: Series A, Physical Geography*, 81**,** 313-323.

Jackson, L. E. & Duk-Rodkin, A. 1996. Quaternary geology of the ice-free corridor: glacial controls on the peopling of the New World. *In:* Akazawa, T. & Szathmary, E. (eds.) *Prehistoric Mongoloid Dispersals.* Oxford: Oxford University Press.

Jackson, L. E. & Little, E. C. 2004. A single continental glaciation of Rocky Mountain Foothills, south-western Alberta, Canada. *In:* Ehlers, J. & Gibbard, P. L. (eds.) *Developments in Quaternary Sciences.* Elsevier.

Jackson, L. E., Phillips, F. M. & Little, E. C. 1999. Cosmogenic ^{36}Cl dating of the maximum limit of the Laurentide Ice Sheet in southwestern Alberta. *Canadian Journal of Earth Sciences*, 36**,** 1347-1356.

Jackson, L. E., Phillips, F. M., Shimamura, K. & Little, E. C. 1997. Cosmogenic ^{36}Cl dating of the Foothills erratics train, Alberta, Canada. *Geology*, 25**,** 195-198.

Jamieson, S. S. R., Hulton, N. R. J. & Hagdorn, M. 2008. Modelling landscape evolution under ice sheets. *Geomorphology*, 97**,** 91-108.

Jibson, R. W., Harp, E. L., Schulz, W. & Keefer, D. K. 2006. Large rock avalanches triggered by the M 7.9 Denali Fault, Alaska, earthquake of 3 November 2002. *Engineering Geology*, 83**,** 144-160.

Johnson, M. & Clayton, L. 2003. Supraglacial landsystems in lowland terrain. *In:* Evans, D. J. A. (ed.) *Glacial Landsystems.* London: Arnold.

Kaiser, J. & Lamy, F. 2010. Links between Patagonian Ice Sheet fluctuations and Antarctic dust variability during the last glacial period (MIS 4-2). *Quaternary Science Reviews*, 29**,** 1464-1471.

Kaiser, J., Lamy, F. & Hebbeln, D. 2005. A 70-kyr sea surface temperature record off southern Chile (Ocean Drilling Program Site 1233). *Paleoceanography*, 20**,** PA4009.

Kaplan, M. R., Ackert, R. P., Singer, B. S., Douglass, D. C. & Kurz, M. D. 2004. Cosmogenic nuclide chronology of millennial-scale glacial advances during O-isotope stage 2 in Patagonia. *Geological Society of America Bulletin*, 116**,** 308-321.

Kaplan, M. R., Coronato, A., Hulton, N. R. J., Rabassa, J. O., Kubik, P. W. & Freeman, S. P. H. T. 2007. Cosmogenic nuclide measurements in southernmost South America and implications for landscape change. *Geomorphology*, 87**,** 284-301.

Kaplan, M. R., Douglass, D. C., Singer, B. S. & Caffee, M. W. 2005. Cosmogenic nuclide chronology of pre-last glacial maximum moraines at Lago Buenos Aires, 46°S, Argentina. *Quaternary Research*, 63**,** 301-315.

Kaplan, M. R., Fogwill, C. J., Sugden, D. E., Hulton, N., Kubik, P. W. & Freeman, S. P. H. T. 2008a. Southern Patagonian glacial chronology for the Last Glacial period and implications for Southern Ocean climate. *Quaternary Science Reviews*, 27**,** 284-294.

Kaplan, M. R., Hein, A. S., Hubbard, A. & Lax, S. M. 2009. Can glacial erosion limit the extent of glaciation? *Geomorphology*, 103**,** 172-179.

Kaplan, M. R., Moreno, P. I. & Rojas, M. 2008b. Glacial dynamics in southernmost South America during Marine Isotope Stage 5e to the Younger Dryas chron: a brief review with a focus on cosmogenic nuclide measurements. *Journal of Quaternary Science*, 23**,** 649-658.

Kaplan, M. R., Schaefer, J. M., Denton, G. H., Barrell, D. J. A., Chinn, T. J. H., Putnam, A. E., Andersen, B. G., Finkel, R. C., Schwartz, R. & Doughty, A. M. 2010. Glacier retreat in New Zealand during the Younger Dryas stadial. *Nature*, 467**,** 194-197.

Kaplan, M. R., Schaefer, J. M., Denton, G. H., Doughty, A. M., Barrell, D. J. A., Chinn, T. J. H., Putnam, A. E., Andersen, B. G., Mackintosh, A., Finkel, R. C., Schwartz, R. & Anderson, B. 2013. The anatomy of long-term warming since 15 ka in New Zealand based on net glacier snowline rise. *Geology*, 41**,** 887-890.

Kaplan, M. R., Strelin, J. A., Schaefer, J. M., Denton, G. H., Finkel, R. C., Schwartz, R., Putnam, A. E., Vandergoes, M. J., Goehring, B. M. & Travis, S. G. 2011. In-situ cosmogenic ^{10}Be production rate at Lago Argentino, Patagonia: Implications for late-glacial climate chronology. *Earth and Planetary Science Letters*, 309**,** 21-32.

Kelley, S. E., Kaplan, M. R., Schaefer, J. M., Andersen, B. G., Barrell, D. J. A., Putnam, A. E., Denton, G. H., Schwartz, R., Finkel, R. C. & Doughty, A. M. 2014. High-precision ^{10}Be chronology of moraines in the Southern Alps indicates synchronous cooling in Antarctica and New Zealand 42,000 years ago. *Earth and Planetary Science Letters*, 405**,** 194-206.

Kerr, A. & Sugden, D. 1994. The sensitivity of the south chilean snowline to climatic change. *Climatic Change*, 28**,** 255-272.

Kilian, R., Baeza, O., Breuer, S., Ríos, F., Arz, H., Lamy, F., Witrz, J., Baque, D., Korf, P., Kremer, K., Ríos, C., Mutschke, E., Simon, M., De Pol-Holz, R., Arevalo, M., Wörner, G., Schneider, C. & Casassa, G. 2013. Evolución paleogeográfica y paleoecológica del Sistema de fiordos del Seno Skyring y Seno Otway en la region de Magallanes durante el Tardiglacial y Holoceno. *Anales Instituto Patagonia (Chile)*, 41**,** 5-26.

Kilian, R. & Lamy, F. 2012. A review of Glacial and Holocene paleoclimate records from southernmost Patagonia (49–55°S). *Quaternary Science Reviews*, 53**,** 1-23.

Kilian, R., Schneider, C., Koch, J., Fesq-Martin, M., Biester, H., Casassa, G., Arévalo, M., Wendt, G., Baeza, O. & Behrmann, J. 2007. Palaeoecological constraints on late Glacial and Holocene ice retreat in the Southern Andes (53°S). *Global and Planetary Change*, 59**,** 49-66.

Kirkbride, M. P. 2005. Boulder edge-roundness as an indicator of relative age: A lochnagar case study. *Scottish Geographical Journal*, 121**,** 219-236.

Kirkbride, M. P. & Winkler, S. 2012. Correlation of Late Quaternary moraines: impact of climate variability, glacier response, and chronological resolution. *Quaternary Science Reviews*, 46**,** 1-29.

Kjær, K. H. & Krüger, J. 2001. The final phase of dead-ice moraine development: processes and sediment architecture, Kötlujökull, Iceland. *Sedimentology*, 48**,** 935-952.

Kleman, J., Hättestrand, C., Stroeven, A. P., Jansson, K., De Angelis, H. & Borgström, I. 2006. Reconstruction of palaeo-ice sheets - inversion of their

glacial geomorphological record. *In:* Knight, P. (ed.) *Glaciology and Earth's Changing Environment.* Blackwell.

Klepeis, K. A. 1994. Relationship between uplift of the metamorphic core of the southernmost Andes and shortening in the Magallanes foreland fold and thrust belt, Tierra del Fuego, Chile. *Tectonics*, 13**,** 882-904.

Kliem, P., Buylaert, J. P., Hahn, A., Mayr, C., Murray, A. S., Ohlendorf, C., Veres, D., Wastegård, S. & Zolitschka, B. 2013a. Magnitude, geomorphologic response and climate links of lake level oscillations at Laguna Potrok Aike, Patagonian steppe (Argentina). *Quaternary Science Reviews*, 71**,** 131-146.

Kliem, P., Enters, D., Hahn, A., Ohlendorf, C., Lisé-Pronovost, A., St-Onge, G., Wastegård, S. & Zolitschka, B. 2013b. Lithology, radiocarbon chronology and sedimentological interpretation of the lacustrine record from Laguna Potrok Aike, southern Patagonia. *Quaternary Science Reviews*, 71**,** 54-69.

Knechtel, M. M. 1942. Snake Butte boulder train and related glacial phenomena, north-central Montana. *Geological Society of America Bulletin*, 53**,** 917-936.

Kohfeld, K. E., Graham, R. M., de Boer, A. M., Sime, L. C., Wolff, E. W., Le Quéré, C. & Bopp, L. 2013. Southern Hemisphere westerly wind changes during the Last Glacial Maximum: paleo-data synthesis. *Quaternary Science Reviews*, 68**,** 76-95.

Krüger, J. 1987. Traek af et glaciallandskabs udvikling ved nordranden af Myrdalsjökull, Iceland. *Dansk Geologisk Foreningens*, Arsskrift for 1986**,** 49-65.

Kujansuu, R. & Saarnisto, M. 1990. *Glacial Indicator Tracing*, Rotterdam, Netherlands, Balkema Publishers.

Labeyrie, L., Labracherie, M., Gorfti, N., Pichon, J. J., Vautravers, M., Arnold, M., Duplessy, J.-C., Paterne, M., Michel, E., Duprat, J., Caralp, M. & Turon, J.-L. 1996. Hydrographic changes of the Southern Ocean (southeast Indian Sector) Over the last 230 kyr. *Paleoceanography*, 11**,** 57-76.

Lal, D. 1991. Cosmic ray labeling of erosion surfaces: in situ nuclide production rates and erosion models. *Earth and Planetary Science Letters*, 104**,** 424-439.

Lamy, F., Kaiser, J., Arz, H. W., Hebbeln, D., Ninnemann, U., Timm, O., Timmermann, A. & Toggweiler, J. R. 2007. Modulation of the bipolar seesaw in the Southeast Pacific during Termination 1. *Earth and Planetary Science Letters*, 259**,** 400-413.

Lamy, F., Kaiser, J., Ninnemann, U., Hebbeln, D., Arz, H. W. & Stoner, J. 2004. Antarctic Timing of Surface Water Changes off Chile and Patagonian Ice Sheet Response. *Science*, 304**,** 1959-1962.

Larsen, S. H., Davies, T. R. H. & McSaveney, M. J. 2005. A possible coseismic landslide origin of late Holocene moraines of the Southern Alps, New Zealand. *New Zealand Journal of Geology and Geophysics*, 48**,** 311-314.

Lawson, T. J. 1990. Former ice movement in Assynt, Sutherland, as shown by the distribution of glacial erratics. *Scottish Journal of Geology*, 26**,** 25-32.

Lawson, T. J. 1995. Boulder Trains as indicators of former ice flow in Assynt, N.W. Scotland. *Quaternary Newsletter*, 75**,** 15-21.

Lifton, N. A., Bieber, J. W., Clem, J. M., Duldig, M. L., Evenson, P., Humble, J. E. & Pyle, R. 2005. Addressing solar modulation and long-term uncertainties in scaling secondary cosmic rays for in situ cosmogenic nuclide applications. *Earth and Planetary Science Letters*, 239**,** 140-161.

Lisé-Pronovost, A., St-Onge, G., Gogorza, C., Haberzettl, T., Jouve, G., Francus, P., Ohlendorf, C., Gebhardt, C. & Zolitschka, B. 2015. Rock-magnetic proxies of wind intensity and dust since 51,200 cal BP from lacustrine sediments of Laguna Potrok Aike, southeastern Patagonia. *Earth and Planetary Science Letters*, 411**,** 72-86.

Lisé-Pronovost, A., St-Onge, G., Gogorza, C., Haberzettl, T., Preda, M., Kliem, P., Francus, P. & Zolitschka, B. 2013. High-resolution paleomagnetic secular variations and relative paleointensity since the Late Pleistocene in southern South America. *Quaternary Science Reviews*, 71**,** 91-108.

Lisé-Pronovost, A., St-Onge, G., Gogorza, C., Jouve, G., Francus, P. & Zolitschka, B. 2014. Rock-magnetic signature of precipitation and extreme runoff events in south-eastern Patagonia since 51,200 cal BP from the sediments of Laguna Potrok Aike. *Quaternary Science Reviews*, 98**,** 110-125.

Lisiecki, L. E. & Raymo, M. E. 2005. A Pliocene-Pleistocene stack of 57 globally distributed benthic δ^{18}O records. *Paleoceanography*, 20**,** PA1003.

Lovell, H., Stokes, C. R. & Bentley, M. J. 2011. A glacial geomorphological map of the Seno Skyring-Seno Otway-Strait of Magellan region, southernmost Patagonia. *Journal of Maps*, 7**,** 318-339.

Lovell, H., Stokes, C. R., Bentley, M. J. & Benn, D. I. 2012. Evidence for rapid ice flow and proglacial lake evolution around the central Strait of Magellan region, southernmost Patagonia. *Journal of Quaternary Science*, 27**,** 625-638.

Lukas, S. 2005. A test of the englacial thrusting hypothesis of 'hummocky' moraine formation: case studies from the northwest Highlands, Scotland. *Boreas*, 34**,** 287-307.

Lukas, S. 2007. 'A test of the englacial thrusting hypothesis of "hummocky" moraine formation: case studies from the northwest Highlands, Scotland': Reply to comments. *Boreas*, 36**,** 108-113.

Marangunic, C. & Bull, C. 1968. The landslide on the Sherman Glacier. *The Great Alaska Earthquake of 1964–Hydrology, Pt. A.* Washington, DC: National Academy of Sciences.

Markgraf, V. 1993. Paleoenvironments and paleoclimates in Tierra del Fuego and southernmost Patagonia, South America. *Palaeogeography, Palaeoclimatology, Palaeoecology*, 102**,** 53-68.

Martinez-Garcia, A., Rosell-Mele, A., Jaccard, S. L., Geibert, W., Sigman, D. M. & Haug, G. H. 2011. Southern Ocean dust-climate coupling over the past four million years. *Nature*, 476**,** 312-315.

Martínez, O., Coronato, A. & Rabassa, J. 2011. Chapter 52 - Pleistocene Glaciations in Northern Patagonia, Argentina: An Updated Review. *In:* Jürgen Ehlers, P. L. G. & Philip, D. H. (eds.) *Developments in Quaternary Sciences.* Elsevier.

Massaferro, J. & Larocque-Tobler, I. 2013. Using a newly developed chironomid transfer function for reconstructing mean annual air temperature at Lake Potrok Aike, Patagonia, Argentina. *Ecological Indicators*, 24**,** 201-210.

Matthews, J. A. & Owen, G. 2010. Schmidt hammer exposure-age dating: developing linear age-calibration curves using Holocene bedrock surfaces from the Jotunheimen–Jostedalsbreen regions of southern Norway. *Boreas*, 39**,** 105-115.

McCarroll, D. 1991. The schmidt hammer, weathering and rock surface roughness. *Earth Surface Processes and Landforms*, 16**,** 477-480.

McCarroll, D. & Nesje, A. 1993. The vertical extent of ice sheets in Nordfjord, western Norway: measuring degree of rock surface weathering. *Boreas*, 22**,** 255-265.

McCarroll, D. & Nesje, A. 1996. Rock Surface Roughness as an Indicator of Degree of Rock Surface Weathering. *Earth Surface Processes and Landforms*, 21**,** 963-977.

McColl, S. T. & Davies, T. R. 2011. Evidence for a rock-avalanche origin for 'The Hillocks' "moraine", Otago, New Zealand. *Geomorphology*, 127**,** 216-224.

McCulloch, R. D. & Bentley, M. J. 1998. Late glacial ice advances in the Strait of Magellan, southern Chile. *Quaternary Science Reviews*, 17**,** 775-787.

McCulloch, R. D., Bentley, M. J., Purves, R. S., Hulton, N. R. J., Sugden, D. E. & Clapperton, C. M. 2000. Climatic inferences from glacial and palaeoecological evidence at the last glacial termination, southern South America. *Journal of Quaternary Science*, 15**,** 409-417.

McCulloch, R. D., Bentley, M. J., Tipping, R. M. & Clapperton, C. M. 2005a. Evidence for late-glacial ice dammed lakes in the central Strait of Magellan and Bahia Inutil, southernmost South America. *Geografiska Annaler Series a-Physical Geography*, 87A**,** 335-362.

McCulloch, R. D. & Davies, S. J. 2001. Late-glacial and Holocene palaeoenvironmental change in the central Strait of Magellan, southern Patagonia. *Palaeogeography Palaeoclimatology Palaeoecology*, 173**,** 143-173.

McCulloch, R. D., Fogwill, C. J., Sugden, D. E., Bentley, M. J. & Kubik, P. W. 2005b. Chronology of the last glaciation in central Strait of Magellan and Bahia Inutil, southernmost South America. *Geografiska Annaler Series a-Physical Geography*, 87A**,** 289-312.

McGee, D., Broecker, W. S. & Winckler, G. 2010. Gustiness: The driver of glacial dustiness? *Quaternary Science Reviews*, 29**,** 2340-2350.

McGlone, M. S., Turney, C. S. M., Wilmshurst, J. M., Renwick, J. & Pahnke, K. 2010. Divergent trends in land and ocean temperature in the Southern Ocean over the past 18,000 years. *Nature Geosci*, 3**,** 622-626.

Meglioli, A. 1992. *Glacial Geology and Chronology of southernmost Patagonia and Tierra del Fuego, Argentina and Chile.* Ph.D., Lehigh.

Mercer, J. H. 1976. Glacial history of southernmost South America. *Quaternary Research*, 6**,** 125-166.

Montgomery, D. R. 2002. Valley formation by fluvial and glacial erosion. *Geology*, 30**,** 1047-1050.

Moreno, P. I., Francois, J. P., Moy, C. M. & Villa-Martínez, R. 2010. Covariability of the Southern Westerlies and atmospheric CO_2 during the Holocene. *Geology*, 38**,** 727-730.

Moreno, P. I., François, J. P., Villa-Martínez, R. P. & Moy, C. M. 2009a. Millennial-scale variability in Southern Hemisphere westerly wind activity over the last 5000 years in SW Patagonia. *Quaternary Science Reviews*, 28**,** 25-38.

Moreno, P. I., Jacobson, G. L., Lowell, T. V. & Denton, G. H. 2001. Interhemispheric climate links revealed by a late-glacial cooling episode in southern Chile. *Nature*, 409**,** 804-808.

Moreno, P. I., Kaplan, M. R., Francois, J. P., Villa-Martinez, R., Moy, C. M., Stern, C. R. & Kubik, P. W. 2009b. Renewed glacial activity during the Antarctic cold reversal and persistence of cold conditions until 11.5 ka in southwestern Patagonia. *Geology*, 37**,** 375-378.

Moreno, P. I., Vilanova, I., Villa-Martínez, R., Garreaud, R. D., Rojas, M. & De Pol-Holz, R. 2014. Southern Annular Mode-like changes in southwestern Patagonia at centennial timescales over the last three millennia. *Nature Communications*, 5.

Moreno, P. I., Villa-Martínez, R., Cárdenas, M. L. & Sagredo, E. A. 2012. Deglacial changes of the southern margin of the southern westerly winds revealed by terrestrial records from SW Patagonia (52°S). *Quaternary Science Reviews*, 41**,** 1-21.

Mountjoy, E. W. 1958. Jasper area Alberta, a source for the Foothills erratics train. *Canadian Petroleum Geology Bulletin*, 6**,** 218-226.

Murray, D. S., Carlson, A. E., Singer, B. S., Anslow, F. S., He, F., Caffee, M., Marcott, S. A., Liu, Z. & Otto-Bliesner, B. L. 2012. Northern Hemisphere forcing of the last deglaciation in southern Patagonia. *Geology*, 40**,** 631-634.

Natland, M., Gonzalez, P., Canon, A. & Ernst, M. 1974. Geology and paleontology of Magellanes Basin: A system of stages for correlation of Magellanes Basin sediments. *Geological Society of America Memoir*, 139**,** 3-57.

Nelson, E. P., Dalziel, I.W.D., Milnes, A.G. 1980. Structural geology of the Cordillera Darwin; collisional-style orogenesis in the southernmost Chilean Andes. *Eclogae Geologicae Helvetiae*, 73**,** 727–751.

Nesje, A., McCarroll, D. & Dahl, S. O. 1994. Degree of rock surface weathering as an indicator of ice-sheet thickness along an east—west transect across southern Norway. *Journal of Quaternary Science*, 9**,** 337-347.

Nishiizumi, K., Imamura, M., Caffee, M. W., Southon, J. R., Finkel, R. C. & McAninch, J. 2007. Absolute calibration of 10Be AMS standards. *Nuclear Instruments and Methods in Physics Research Section B: Beam Interactions with Materials and Atoms*, 258**,** 403-413.

Nordenskjöld , O. 1899. *Geologie, Geographie und Anthropologie. Schwedischen Expedition nach den Magellanslandern*, Stockholm, Norstedt and Soner.

Ó Cofaigh, C., Evans, D. J. A. & England, J. 2003. Ice-marginal terrestrial landsystems: Sub-polar glacier margins of the Canadian and Greenland High Arctic. *In:* Evans, D. J. A. (ed.) *Glacial Landsystems.* London: Arnold.

Pahnke, K., Zahn, R., Elderfield, H. & Schulz, M. 2003. 340,000-Year Centennial-Scale Marine Record of Southern Hemisphere Climatic Oscillation. *Science*, 301**,** 948-952.

Pelejero, C., Calvo, E., Barrows, T. T., Logan, G. A. & De Deckker, P. 2006. South Tasman Sea alkenone palaeothermometry over the last four glacial/interglacial cycles. *Marine Geology*, 230**,** 73-86.

Peltier, W. R. 2004. Global glacial isostasy and the surface of the ice-age earth: The ICE-5G (VM2) Model and GRACE. *Annual Review of Earth and Planetary Sciences*, 32**,** 111-149.

Pendall, E., Markgraf, V., White, J. W. C., Dreier, M. & Kenny, R. 2001. Multiproxy Record of Late Pleistocene–Holocene Climate and Vegetation Changes from a Peat Bog in Patagonia. *Quaternary Research*, 55**,** 168-178.

Porter, S., Clapperton, C. & Sugden, D. 1992. Chronology and dynamics of deglaciation along and near the Strait of Magellan, southernmost South America. *SGU series Ca. Research paper***,** 233-239.

Porter, S. C. 1990. Character and ages of Pleistocene Drifts in a transect across the Strait of Magellan. *Quaternary of South America and Antarctica Peninsula*, 7**,** 35-49.

Price, R. J. 1970. Moraines at Fjallsjökull, Iceland. *Arctic and Alpine Research*, 2**,** 27-42.

Price, R. J. 1973. *Glacial and fluvioglacial landforms*, Edinburgh, Oliver and Boyd.

Putnam, A. E., Denton, G. H., Schaefer, J. M., Barrell, D. J. A., Andersen, B. G., Finkel, R. C., Schwartz, R., Doughty, A. M., Kaplan, M. R. & Schluchter, C. 2010a. Glacier advance in southern middle-latitudes during the Antarctic Cold Reversal. *Nature Geosci*, 3**,** 700-704.

Putnam, A. E., Schaefer, J. M., Barrell, D. J. A., Vandergoes, M., Denton, G. H., Kaplan, M. R., Finkel, R. C., Schwartz, R., Goehring, B. M. & Kelley, S. E. 2010b. In situ cosmogenic ^{10}Be production-rate calibration from the Southern Alps, New Zealand. *Quaternary Geochronology*, 5**,** 392-409.

Putnam, A. E., Schaefer, J. M., Denton, G. H., Barrell, D. J. A., Andersen, B. G., Koffman, T. N. B., Rowan, A. V., Finkel, R. C., Rood, D. H., Schwartz, R., Vandergoes, M. J., Plummer, M. A., Brocklehurst, S. H., Kelley, S. E. & Ladig, K. L. 2013a. Warming and glacier recession in the Rakaia valley, Southern Alps of New Zealand, during Heinrich Stadial 1. *Earth and Planetary Science Letters*, 382**,** 98-110.

Putnam, A. E., Schaefer, J. M., Denton, G. H., Barrell, D. J. A., Birkel, S. D., Andersen, B. G., Kaplan, M. R., Finkel, R. C., Schwartz, R. & Doughty, A. M.

2013b. The Last Glacial Maximum at 44°S documented by a [10]Be moraine chronology at Lake Ohau, Southern Alps of New Zealand. *Quaternary Science Reviews*, 62**,** 114-141.

Putnam, A. E., Schaefer, J. M., Denton, G. H., Barrell, D. J. A., Finkel, R. C., Andersen, B. G., Schwartz, R., Chinn, T. J. H. & Doughty, A. M. 2012. Regional climate control of glaciers in New Zealand and Europe during the pre-industrial Holocene. *Nature Geosci*, 5**,** 627-630.

Rabassa, J. 2008. Late Cenozoic Glaciations in Patagonia and Tierra del Fuego. *In:* Rabassa, J. (ed.) *Developments in Quaternary Sciences.* Elsevier.

Rabassa, J., Bujalesky, G.G., Meglioli, A., Coronato, A., Gordillo, S., Roig, C., Salemme, M. 1992. The Quaternary of Tierra del Fuego, Argentina: the status of our knowledge. *Sveriges Geologiska Undersokning Ser. CA*, 81**,** 249-256.

Rabassa, J. & Clapperton, C. M. 1990. Quaternary glaciations of the southern Andes. *Quaternary Science Reviews*, 9**,** 153-174.

Rabassa, J., Coronato, A., Bujalesky, G., Salemme, M., Roig, C., Meglioli, A., Heusser, C., Gordillo, S., Roig, F., Borromei, A. & Quattrocchio, M. 2000. Quaternary of Tierra del Fuego, Southernmost South America: an updated review. *Quaternary International*, 68-71**,** 217-240.

Rabassa, J., Coronato, A. & Martínez, O. 2011. Late Cenozoic glaciations in Patagonia and Tierra del Fuego: an updated review. *Biological Journal of the Linnean Society*, 103**,** 316-335.

Rabassa, J., Coronato, A. M. & Salemme, M. 2005. Chronology of the Late Cenozoic Patagonian glaciations and their correlation with biostratigraphic units of the Pampean region (Argentina). *Journal of South American Earth Sciences*, 20**,** 81-103.

Rabassa, J., Tonni, E. P. & Carlini, A. 2009. The Ensenadan Stage/Age in southern South America. *Quaternary International*, 210**,** 1-3.

Rae, A. C., Harrison, S., Mighall, T. & Dawson, A. G. 2004. Periglacial trimlines and nunataks of the Last Glacial Maximum: the Gap of Dunloe, southwest Ireland. *Journal of Quaternary Science*, 19**,** 87-97.

Raedecke, L. D. 1978. Formas del terreno y depositos cuaternarios Tierra del Fuego central, Chile. *Revista Geologica De Chile*, 5**,** 3–31.

Rasmussen, S. O., Andersen, K. K., Svensson, A. M., Steffensen, J. P., Vinther, B. M., Clausen, H. B., Siggaard-Andersen, M. L., Johnsen, S. J., Larsen, L. B., Dahl-Jensen, D., Bigler, M., Röthlisberger, R., Fischer, H., Goto-Azuma, K., Hansson, M. E. & Ruth, U. 2006. A new Greenland ice core chronology for the last glacial termination. *J. Geophys. Res.*, 111**,** D06102.

Recasens, C., Ariztegui, D., Gebhardt, C., Gogorza, C., Haberzettl, T., Hahn, A., Kliem, P., Lisé-Pronovost, A., Lücke, A., Maidana, N., Mayr, C., Ohlendorf, C., Schäbitz, F., St-Onge, G., Wille, M., Zolitschka, B. & Team, S. 2012. New insights into paleoenvironmental changes in Laguna Potrok Aike, southern Patagonia, since the Late Pleistocene: The PASADO multiproxy record. *The Holocene*, 22**,** 1323-1335.

Reimer, P. J., Bard, E., Bayliss, A., Beck, J. W., Blackwell, P. G., Bronk Ramsey, C., Buck, C. E., Cheng, H., Edwards, R. L., Friedrich, M., Grootes, P. M., Guilderson, T. P., Haflidason, H., Hajdas, I., Hatté, C., Heaton, T. J., Hoffmann, D. L., Hogg, A. G., Hughen, K. A., Kaiser, K. F., Kromer, B., Manning, S. W., Niu, M., Reimer, R. W., Richards, D. A., Scott, E. M., Southon, J. R., Staff, R. A., Turney, C. S. M. & van der Plicht, J. 2013. *IntCal13 and Marine13 Radiocarbon Age Calibration Curves 0–50,000 Years cal BP*.

Reznichenko, N. V., Davies, T. R. H. & Alexander, D. J. 2011. Effects of rock avalanches on glacier behaviour and moraine formation. *Geomorphology*, 132**,** 327-338.

Roberts, D. H., Dackombe, R. V. & Thomas, G. S. P. 2007. Palaeo-ice streaming in the central sector of the British—Irish Ice Sheet during the Last Glacial Maximum: evidence from the northern Irish Sea Basin. *Boreas*, 36**,** 115-129.

Rodbell, D. T., Smith, J. A. & Mark, B. G. 2009. Glaciation in the Andes during the Lateglacial and Holocene. *Quaternary Science Reviews*, 28**,** 2165-2212.

Rodés, Á., Pallàs, R., Braucher, R., Moreno, X., Masana, E. & Bourlés, D. L. 2011. Effect of density uncertainties in cosmogenic 10Be depth-profiles: Dating a cemented Pleistocene alluvial fan (Carboneras Fault, SE Iberia). *Quaternary Geochronology*, 6**,** 186-194.

Rodés, Á., Pallàs, R., Ortuño, M., García-Melendez, E. & Masana, E. 2014. Combining surface exposure dating and burial dating from paired cosmogenic depth profiles. Example of El Límite alluvial fan in Huércal-Overa basin (SE Iberia). *Quaternary Geochronology*, 19**,** 127-134.

Roed, M. A., Mountjoy, E. W. & Rutter, N. W. 1967. The Athabasca Valley Erratics Train, Alberta and Pleistocene ice movements across the continental divide. *Canadian Journal of Earth Sciences*, 4**,** 625-632.

Rother, H., Fink, D., Shulmeister, J., Mifsud, C., Evans, M. & Pugh, J. 2014. The early rise and late demise of New Zealand's last glacial maximum. *Proceedings of the National Academy of Sciences*, 111**,** 11630-11635.

Rutter, N., Schnack, E. J., Rio, J. d., Fasano, J. L., Isla, F. I. & Radtke, U. 1989. Correlation and dating of Quaternary littoral zones along the Patagonian coast, Argentina. *Quaternary Science Reviews*, 8**,** 213-234.

Ryan, M. T., Dunbar, G. B., Vandergoes, M. J., Neil, H. L., Hannah, M. J., Newnham, R. M., Bostock, H. & Alloway, B. V. 2012. Vegetation and climate in Southern Hemisphere mid-latitudes since 210 ka: new insights from marine and terrestrial pollen records from New Zealand. *Quaternary Science Reviews*, 48**,** 80-98.

Sagredo, E. A., Moreno, P. I., Villa-Martinez, R., Kaplan, M. R., Kubik, P. W. & Stern, C. R. 2011. Fluctuations of the Última Esperanza ice lobe (52°S), Chilean Patagonia, during the last glacial maximum and termination 1. *Geomorphology*, 125**,** 92-108.

Salonen, V.-P. 1986. *Glacial transport distance distributions of surface boulders in Finland*, Geologian tutkimuskeskus.

Sánchez, J. S., Mosquera, D. F. & Romaní, J. R. V. 2009. Assessing the age-weathering correspondence of cosmogenic [21]Ne dated Pleistocene surfaces by the Schmidt Hammer. *Earth Surface Processes and Landforms*, 34**,** 1121-1125.

Schäbitz, F., Wille, M., Francois, J.-P., Haberzettl, T., Quintana, F., Mayr, C., Lücke, A., Ohlendorf, C., Mancini, V., Paez, M. M., Prieto, A. R. & Zolitschka, B. 2013. Reconstruction of palaeoprecipitation based on pollen transfer functions – the record of the last 16 ka from Laguna Potrok Aike, southern Patagonia. *Quaternary Science Reviews*, 71**,** 175-190.

Schaefer, J. M., Denton, G. H., Barrell, D. J. A., Ivy-Ochs, S., Kubik, P. W., Andersen, B. G., Phillips, F. M., Lowell, T. V. & Schlüchter, C. 2006. Near-Synchronous Interhemispheric Termination of the Last Glacial Maximum in Mid-Latitudes. *Science*, 312**,** 1510-1513.

Schomacker, A. 2008. What controls dead-ice melting under different climate conditions? A discussion. *Earth-Science Reviews*, 90**,** 103-113.

Schomacker, A., Benediktsson, Í. Ö. & Ingólfsson, Ó. 2014. The Eyjabakkajökull glacial landsystem, Iceland: Geomorphic impact of multiple surges. *Geomorphology*, 218**,** 98-107.

Seidov, D. & Maslin, M. 2001. Atlantic ocean heat piracy and the bipolar climate see-saw during Heinrich and Dansgaard–Oeschger events. *Journal of Quaternary Science*, 16**,** 321-328.

Shakesby, R. A., Matthews, J. A., Karlén, W. & Los, S. O. 2011. The Schmidt hammer as a Holocene calibrated-age dating technique: Testing the form of the R-value-age relationship and defining the predicted-age errors. *The Holocene*, 21**,** 615-628.

Shane, P. & Sandiford, A. 2003. Paleovegetation of marine isotope stages 4 and 3 in northern new zealand and the age of the widespread rotoehu tephra. *Quaternary Research*, 59**,** 420-429.

Sharp, M. 1984. Annual moraine ridges, at Skalafellsjökull, south-east Iceland. *Journal of Glaciology*, 30**,** 89-93.

Sharp, M. 1985a. " Crevasse-Fill" Ridges: A Landform Type Characteristic of Surging Glaciers? *Geografiska Annaler. Series A. Physical Geography***,** 213-220.

Sharp, M. 1985b. Sedimentation and stratigraphy at Eyjabakkajökull—An Icelandic surging glacier. *Quaternary Research*, 24**,** 268-284.

Shugar, D. H. & Clague, J. J. 2011. The sedimentology and geomorphology of rock avalanche deposits on glaciers. *Sedimentology*, 58**,** 1762-1783.

Shulmeister, J., Davies, T. R., Evans, D. J. A., Hyatt, O. M. & Tovar, D. S. 2009. Catastrophic landslides, glacier behaviour and moraine formation – A view from an active plate margin. *Quaternary Science Reviews*, 28**,** 1085-1096.

Shulmeister, J., Fink, D. & Augustinus, P. C. 2005. A cosmogenic nuclide chronology of the last glacial transition in North-West Nelson, New Zealand—new insights in Southern Hemisphere climate forcing during the last deglaciation. *Earth and Planetary Science Letters*, 233**,** 455-466.

Shulmeister, J., Fink, D., Hyatt, O. M., Thackray, G. D. & Rother, H. 2010. Cosmogenic ^{10}Be and ^{26}Al exposure ages of moraines in the Rakaia Valley, New Zealand and the nature of the last termination in New Zealand glacial systems. *Earth and Planetary Science Letters*, 297**,** 558-566.

Shulmeister, J., Goodwin, I., Renwick, J., Harle, K., Armand, L., McGlone, M. S., Cook, E., Dodson, J., Hesse, P. P., Mayewski, P. & Curran, M. 2004. The Southern Hemisphere westerlies in the Australasian sector over the last glacial cycle: a synthesis. *Quaternary International*, 118–119**,** 23-53.

Sikes, E. L., Howard, W. R., Samson, C. R., Mahan, T. S., Robertson, L. G. & Volkman, J. K. 2009. Southern Ocean seasonal temperature and Subtropical Front movement on the South Tasman Rise in the late Quaternary. *Paleoceanography*, 24**,** PA2201.

Sime, L. C., Kohfeld, K. E., Le Quéré, C., Wolff, E. W., de Boer, A. M., Graham, R. M. & Bopp, L. 2013. Southern Hemisphere westerly wind changes during the Last Glacial Maximum: model-data comparison. *Quaternary Science Reviews*, 64**,** 104-120.

Singer, B. S., Ackert, R. P. & Guillou, H. 2004a. ^{40}Ar/^{39}Ar and K-Ar chronology of Pleistocene glaciations in Patagonia. *Geological Society of America Bulletin*, 116**,** 434-450.

Singer, B. S., Brown, L. L., Rabassa, J. & Guillou, H. 2004b. ^{40}Ar/^{39}Ar ages of Late Pliocene and Early Pleistocene Geomagnetic and Glacial Events in Southern Argentina. *AGU Geophysical Monograph Timescales of the Internal Geomagnetic Field.*

Sosio, R., Crosta, G. B., Chen, J. H. & Hungr, O. 2012. Modelling rock avalanche propagation onto glaciers. *Quaternary Science Reviews*, 47**,** 23-40.

Stahl, T., Winkler, S., Quigley, M., Bebbington, M., Duffy, B. & Duke, D. 2013. Schmidt hammer exposure-age dating (SHD) of late Quaternary fluvial terraces in New Zealand. *Earth Surface Processes and Landforms*, 38**,** 1838-1850.

Stalker, A. M. 1956. The erratics train, foothills of Alberta. *Geological Survey of Canada Bulletin*, 37**,** 31.

Stalker, A. M. 1976. Megablocks, or the enormous erratics of the Albertan Prairies. *Geological Survey of Canada, Paper*, 76-1C**,** 185-188.

Stenni, B., Buiron, D., Frezzotti, M., Albani, S., Barbante, C., Bard, E., Barnola, J. M., Baroni, M., Baumgartner, M., Bonazza, M., Capron, E., Castellano, E., Chappellaz, J., Delmonte, B., Falourd, S., Genoni, L., Iacumin, P., Jouzel, J., Kipfstuhl, S., Landais, A., Lemieux-Dudon, B., Maggi, V., Masson-Delmotte, V., Mazzola, C., Minster, B., Montagnat, M., Mulvaney, R., Narcisi, B., Oerter, H., Parrenin, F., Petit, J. R., Ritz, C., Scarchilli, C., Schilt, A., Schupbach, S., Schwander, J., Selmo, E., Severi, M., Stocker, T. F. & Udisti, R. 2011. Expression of the bipolar see-saw in Antarctic climate records during the last deglaciation. *Nature Geosci*, 4**,** 46-49.

Stern, C. R., Moreno, P. I., Villa-Martínez, R., Sagredo, E. A., Prieto, A. & Labarca, R. 2011. Evolution of ice-dammed proglacial lakes in Última Esperanza, Chile: implications from the late-glacial R1 eruption of Reclús volcano, Andean Austral Volcanic Zone. *Andean geology*, 38**,** 82-97.

Stokes, C. R. & Clark, C. D. 1999. Geomorphological criteria for identifying Pleistocene ice streams. *Annals of Glaciology*, 28**,** 67-74.

Stokes, C. R. & Clark, C. D. 2004. Evolution of late glacial ice-marginal lakes on the northwestern Canadian Shield and their influence on the location of the Dubawnt Lake palaeo-ice stream. Palaeogeography, Palaeoclimatology, Palaeoecology, 215, 155-171.

Stokes, C. R., Spagnolo, M. & Clark, C. D. 2011. The composition and internal structure of drumlins: Complexity, commonality, and implications for a unifying theory of their formation. *Earth-Science Reviews*, 107**,** 398-422.

Stone, J. O. 2000. Air pressure and cosmogenic isotope production. *J. Geophys. Res.*, 105**,** 23753-23759.

Storrar, R. & Stokes, C. R. 2007. A Glacial Geomorphological Map of Victoria Island, Canadian Arctic. *Journal of Maps*, 3**,** 191-210.

Strelin, J. A., Denton, G. H., Vandergoes, M. J., Ninnemann, U. S. & Putnam, A. E. 2011. Radiocarbon chronology of the late-glacial Puerto Bandera moraines, Southern Patagonian Icefield, Argentina. *Quaternary Science Reviews*, 30**,** 2551-2569.

Sugden, D. E., Bentley, M. J., Fogwill, C. J., Hulton, N. R. J., McCulloch, R. D. & Purves, R. S. 2005. Late-glacial glacier events in southernmost South America: A blend of 'northern'and 'southern' hemispheric climatic signals? *Geografiska Annaler Series a-Physical Geography*, 87A**,** 273-288.

Sugden, D. E., Hulton, N. R. J. & Purves, R. S. 2002. Modelling the inception of the Patagonian icesheet. *Quaternary International*, 95–96**,** 55-64.

Sugden, D. E., McCulloch, R. D., Bory, A. J. M. & Hein, A. S. 2009. Influence of Patagonian glaciers on Antarctic dust deposition during the last glacial period. *Nature Geoscience*, 2**,** 281-285.

Suggate, R. P. & Almond, P. C. 2005. The Last Glacial Maximum (LGM) in western South Island, New Zealand: implications for the global LGM and MIS 2. *Quaternary Science Reviews*, 24**,** 1923-1940.

Sumner, P. & Nel, W. 2002. The effect of rock moisture on Schmidt hammer rebound: tests on rock samples from Marion Island and South Africa. *Earth Surface Processes and Landforms*, 27**,** 1137-1142.

Sutherland, R., Kim, K., Zondervan, A. & McSaveney, M. 2007. Orbital forcing of mid-latitude Southern Hemisphere glaciation since 100 ka inferred from cosmogenic nuclide ages of moraine boulders from the Cascade Plateau, southwest New Zealand. *Geological Society of America Bulletin*, 119**,** 443-451.

Teller, J. 2003. Subaquatic landsystems: large proglacial lakes. *In:* Evans, D. J. A. (ed.) *Glacial Landsystems.* London: Arnold.

Thackray, G. D., Shulmeister, J. & Fink, D. 2009. Evidence for expanded Middle and Late Pleistocene glacier extent in northwest Nelson, New Zealand. *Geografiska Annaler: Series A, Physical Geography*, 91, 291-311.

Ton-That, T., Singer, B., Morner, N. A. & Rabassa, J. 1999. Datacion por el metodo ^{40}Ar/^{39}Ar de lavas basalticas y geologia del Cenozoico Superior en la region del Lago Buenos Aires, provincia de Santa Cruz, Argentina. *Asociacion Geologica Argentina, Revista*, 54, 333-352.

Tovar, S. D., Shulmeister, J. & Davies, T. R. 2008. Evidence for a landslide origin of New Zealand/'s Waiho Loop moraine. *Nature Geosci*, 1, 524-526.

Vandergoes, M. J., Newnham, R. M., Denton, G. H., Blaauw, M. & Barrell, D. J. A. 2013. The anatomy of Last Glacial Maximum climate variations in south Westland, New Zealand, derived from pollen records. *Quaternary Science Reviews*, 74, 215-229.

Vandergoes, M. J., Newnham, R. M., Preusser, F., Hendy, C. H., Lowell, T. V., Fitzsimons, S. J., Hogg, A. G., Kasper, H. U. & Schluchter, C. 2005. Regional insolation forcing of late Quaternary climate change in the Southern Hemisphere. *Nature*, 436, 242-245.

Veres, D., Bazin, L., Landais, A., Toyé Mahamadou Kele, H., Lemieux-Dudon, B., Parrenin, F., Martinerie, P., Blayo, E., Blunier, T., Capron, E., Chappellaz, J., Rasmussen, S. O., Severi, M., Svensson, A., Vinther, B. & Wolff, E. W. 2013. The Antarctic ice core chronology (AICC2012): an optimized multi-parameter and multi-site dating approach for the last 120 thousand years. *Clim. Past*, 9, 1733-1748.

Vincent, P. J., Wilson, P., Lord, T. C., Schnabel, C. & Wilcken, K. M. 2010. Cosmogenic isotope (^{36}Cl) surface exposure dating of the Norber erratics, Yorkshire Dales: Further constraints on the timing of the LGM deglaciation in Britain. *Proceedings of the Geologists' Association*, 121, 24-31.

Walther, A., Rabassa, J., Coronato, A., Tassone, A. & Vilas, J. F. 2007. Paleomagnetic study of glacigenic sediments from Tierra del Fuego. *GEOSUR abstract volume.*

Wang, Z., Kuhlbrodt, T. & Meredith, M. P. 2011. On the response of the Antarctic Circumpolar Current transport to climate change in coupled climate models. *J. Geophys. Res.*, 116, C08011.

Ward, B. C., Bond, J. D. & Gosse, J. C. 2007. Evidence for a 55–50 ka (early Wisconsin) glaciation of the Cordilleran ice sheet, Yukon Territory, Canada. *Quaternary Research*, 68, 141-150.

Wastegård, S., Veres, D., Kliem, P., Hahn, A., Ohlendorf, C. & Zolitschka, B. 2013. Towards a late Quaternary tephrochronological framework for the southernmost part of South America – the Laguna Potrok Aike tephra record. *Quaternary Science Reviews*, 71, 81-90.

White, K., Bryant, R. & Drake, N. 1998. Techniques for measuring rock weathering: application to a dated fan segment sequence in southern Tunisia. *Earth Surface Processes and Landforms*, 23, 1031-1043.

Whittaker, T. E., Hendy, C. H. & Hellstrom, J. C. 2011. Abrupt millennial-scale changes in intensity of Southern Hemisphere westerly winds during marine isotope stages 2–4. *Geology*, 39, 455-458.

Williams, P. W. 1996. A 230 ka record of glacial and interglacial events from Aurora Cave, Fiordland, New Zealand. *New Zealand Journal of Geology and Geophysics*, 39, 225-241.

Williams, P. W., McGlone, M., Neil, H. & Zhao, J.-X. 2015. A review of New Zealand palaeoclimate from the Last Interglacial to the global Last Glacial Maximum. *Quaternary Science Reviews*, 110, 92-106.

Wilson, P., Barrows, T. T., Lord, T. C. & Vincent, P. J. 2012. Surface lowering of limestone pavement as determined by cosmogenic (^{36}Cl) analysis. *Earth Surface Processes and Landforms*, 37, 1518-1526.

Wilson, P., Bentley, M. J., Schnabel, C., Clark, R. & Xu, S. 2008. Stone run (block stream) formation in the Falkland Islands over several cold stages, deduced from cosmogenic isotope (^{10}Be and ^{26}Al) surface exposure dating. *Journal of Quaternary Science*, 23**,** 461-473.

Wolff, E. W., Barbante, C., Becagli, S., Bigler, M., Boutron, C. F., Castellano, E., de Angelis, M., Federer, U., Fischer, H., Fundel, F., Hansson, M., Hutterli, M., Jonsell, U., Karlin, T., Kaufmann, P., Lambert, F., Littot, G. C., Mulvaney, R., Röthlisberger, R., Ruth, U., Severi, M., Siggaard-Andersen, M. L., Sime, L. C., Steffensen, J. P., Stocker, T. F., Traversi, R., Twarloh, B., Udisti, R., Wagenbach, D. & Wegner, A. 2010a. Changes in environment over the last 800,000 years from chemical analysis of the EPICA Dome C ice core. *Quaternary Science Reviews*, 29**,** 285-295.

Wolff, E. W., Chappellaz, J., Blunier, T., Rasmussen, S. O. & Svensson, A. 2010b. Millennial-scale variability during the last glacial: The ice core record. *Quaternary Science Reviews*, 29**,** 2828-2838.

Wolff, E. W., Fischer, H., Fundel, F., Ruth, U., Twarloh, B., Littot, G. C., Mulvaney, R., Röthlisberger, R., de Angelis, M., Boutron, C. F., Hansson, M., Jonsell, U., Hutterli, M. A., Lambert, F., Kaufmann, P., Stauffer, B., Stocker, T. F., Steffensen, J. P., Bigler, M., Siggaard-Andersen, M. L., Udisti, R., Becagli, S., Castellano, E., Severi, M., Wagenbach, D., Barbante, C., Gabrielli, P. & Gaspari, V. 2006. Southern Ocean sea-ice extent, productivity and iron flux over the past eight glacial cycles. *Nature*, 440**,** 491-496.

Wolff, E. W., Fischer, H. & Rothlisberger, R. 2009. Glacial terminations as southern warmings without northern control. *Nature Geosci*, 2**,** 206-209.

Zhu, J., Lücke, A., Wissel, H., Mayr, C., Enters, D., Ja Kim, K., Ohlendorf, C., Schäbitz, F. & Zolitschka, B. 2014. Climate history of the Southern Hemisphere Westerlies belt during the last glacial–interglacial transition revealed from lake water oxygen isotope reconstruction of Laguna Potrok Aike (52° S, Argentina). *Clim. Past*, 10**,** 2153-2169.

Zolitschka, B., Anselmetti, F., Ariztegui, D., Corbella, H., Francus, P., Lücke, A., Maidana, N. I., Ohlendorf, C., Schäbitz, F. & Wastegård, S. 2013. Environment and climate of the last 51,000 years – new insights from the Potrok Aike maar lake Sediment Archive Drilling prOject (PASADO). *Quaternary Science Reviews*, 71**,** 1-12.

Zolitschka, B., Anselmetti, F., Ariztegui, D., Corbella, H., Francus, P., Ohlendorf, C., Schabitz, F., PASADO Scientific Drilling Team 2009. The Laguna Potrok Aike Scientific Drilling Project PASADO (ICDP Expedition 5022). *Scientific Drilling.*